RESEARCH & REVIEWS IN ENGINEERING - II

DECEMBER, 2021

EDITORS

ASSOC. PROF. DR. SELAHATTIN BARDAK

ASSIST. PROF. DR. NESLI AYDIN

ASSIST. PROF. DR. YALÇIN BOZTOPRAK

gece kitaplığı

İmtiyaz Sahibi / Publisher • Yaşar Hız

Genel Yayın Yönetmeni / Editor in Chief • Eda Altunel

Editörler/ Editors • Assoc. Prof. Dr. Selahattin Bardak

Assist. Prof. Dr. Nesli Aydın

Assist. Prof. Dr. Yalçın Boztoprak

Kapak & İç Tasarım / Cover & Interior Design • Gece Kitaplığı

Birinci Basım / First Edition • © Aralık 2021

ISBN • 978-625-8075-45-8

Gece Kitaplığı / Gece Publishing
Türkiye Adres / Turkey Address: Kızılay Mah. Fevzi Çakmak 1.
Sokak Ümit Apt. No: 22/A Çankaya / Ankara / TR
Telefon / Phone: +90 312 384 80 40
web: www.gecekitapligi.com
e-mail: gecekitapligi@gmail.com

Baskı & Cilt / Printing & Volume
Sertifika / Certificate No: 47083

Research & Reviews in Engineering - II

December, 2021

Editors
Assoc. Prof. Dr. Selahattin Bardak
Assist. Prof. Dr. Nesli Aydın
Assist. Prof. Dr. Yalçın Boztoprak

CONTENTS

Chapter 1

ELECTRONIC EVOLUTION OF FIREARMS; PAST AND FUTURE

Faruk GÜNER[1]
Hilmi ZENK[2]

1 Faruk Güner Dr.Öğr.Üyesi Giresun Üniversitesi / Orcid 0000-0002-3438-0553
2 Hilmi Zenk Dr.Öğr.Üyesi / Giresun Üniversitesi / Orcid 0000-0002-1653-8580

1. Introduction

Personal weapons are a concept that has existed since the day human beings were in the world. The first personal weapon can be considered a piece of stone. This piece of stone first turned into a piece of shaped stone, then into shaped metal, and then into firearms over a long period of time. Although using a gun is a concept far outside of our daily life, it is a subject that is studied frequently and openly in academic terms and is not transparent at all. The basic nature of a general academic project is to benefit people, protect the environment and make life easier. When the subject comes to weapons, another person must be killed to protect the others. This is not a wish which people would like to live, but it has been the subject of all wars those have shaped history.

All the work done by scientists has been tried to be turned into a weapon in some way. The best example of this phemone is the splitting of the atom. Scientists trying to understand the atomic structure have expressed the energy that emerges as a result of the splitting of the atom. Other scientists have combined this with radioactivity to create nuclear weapons, the most destructive weapons in human history. Peace is actually a period when people with bigger weapons silence other people and prepare for another war. People with big weapons in their hands, that is, countries with nuclear power today, establish a serious superiority over other countries. We live in a world where there has been no major war since World War II. Unfortunately, this situation is not permanent. Osman Pamukoğlu, one of the important military identities raised by Turkey, recently wrote interesting facts about the inevitability of war are presented to the readers in his book titled "World War III-When It Will Come Out and Who It Will Be Between".

A generally accepted definition could be made about the milestones of mankind in the history untill the French Revolution of 1789. Although definitions such as "democracy age", "information age", "computer age" are made for the aftermath of the French Revolution, it is actually the "electric age" that should be defined. Electricity has now become indispensable in all areas of life. In order turn an engineering product into an industrial product it must make life easier, increase safety and efficiency. In order to achieve these goals, electrical and electronic engineering must be included in the product. Even though the industry is moving towards the fact that software engineering is necessary, where electronics are not enough, it is also clear that software will not work without electricity. From this point of view, it is not difficult to predict that the future of personal firearms will also pass through electronic circuits. In this book section, it has been tried to explain the electrical and electronic features and the direction of the features that have been revealed in personal firearms in the future.

2. Past

The concept of firearm emerged with the discovery of gunpowder by the Chinese in 904-905. According to some interpretations, Chinese alchemists made this discovery to produce fireworks rather than weapons. As mentioned in the introduction, it is inevitable that all discoveries will evolve to serve military purposes. After this discovery, different cannons and hand guns were developed. However, even the transformation of these weapons into automatic weapons took a long time. Some Fitilli tüfek studies point out that the cannons produced in the early periods were insufficient to demolish the walls of the castles. At this point, only discovering gunpowder should not be enough, while it took a long time to produce an effective weapon by the desired power. The oldest evidence of firearms is the first rifle in handball format which was produced in China in the 10th century. However, it emerged at the end of the 14th century as the structure closest to the current format as we know it and its working principle.

The nomenclature as hand cannon was made in Europe for the weapons carried by Chinese traders from Asia to Europe. In this weapon, the braided fuse was caught in the "contact hole" on the barrel, the gunpowder would start to burn and the bullet would be fired. The first step of the transition from these primitive weapons to modern automatic, semi-automatic rifles or pistols was matchlocks that emerged in the 1400s. Until the matchlock, guns did not have trigger-like mechanisms. When firing, one hand held the flaming string that would fire the gunpowder, so the weapon would stabilize with one hand, which would definitely negatively affect its accuracy. With the mathlock-gun, the vice or arm called the serpentine under the gun was pulled, the wick was approached to the contact hole and the gun was fired. As both hands remained on the gun when the gunpowder was fired, the hit success rate increased. During its period, this invention achieved important military successes. The firing rate was slow since the matchlock guns were loaded from the barrel. The rate of fire was increased with the method called salvo fire tactic developed by the Japanese and Dutch soldiers. In this method, the soldiers line up in two rows and shoot. While the front soldier takes aim and fires, the second line of soldiers does the loading work. When the first line of soldiers fire, they move to the back and starts to load his gun. In the meantime, the soldier behind initially fires and the cycle continues.

In 1544, easily transportable short-barreled pistols began to be produced. More shorter barrel weapons could only be produced in the 15th and 16th centuries, with the design of flint-springed models of these weapons. This innovation, which started to be used widely in the 17th century and will reign for 200 years, was flintlock guns. The gunpowder

ignition problem in mathlock-gun is eliminated in flintlock guns with the principle of crushing the gunpowder to produce sparks. This principle gave a significant advantage as it accelerated shooters very much.

Engineers didn't just try to increase the rate of fire to increase firepower. In order to increase the firepower, first multi-barreled guns were produced, and then automatic firearms were tried to be produced. It begins with the invention of guns called revolvers, known as the first rapid-fire gun, in the 1800s. Although this type of weapon is technically classified as a rotary mechanism weapon, they are also called revolvers. The idea of grooving the barrel, the next big step in weapon technology, was introduced in the 19th century. The recess and protrusion structures, called groove sets, increased the target accuracy and terminal ballistic effects on the target. At the end of the 19th century, after the six fires and groove set steps, shelled bullets with a primary igniter were produced. While the production of sleeved bullets paved the way for the emergence of different serial firing mechanisms in the 20th century, it paved the way for the production of automatic and semi-automatic personal firearms.

3. Current Situation

During the period of two great wars, namely world wars, personal firearms showed significant mechanical developments for both individual and military use. At this point, weapons that are light, have high firepower, fully automatic, easy to clean, mass-produced, long range, suitable for different climatic conditions and offering high security measures to the user have been produced. After this point, it becomes increasingly difficult to experience mechanical, metallurgical or chemical developments and very long studies are needed. In the next step, weapons supported by electronic capabilities, called "smart weapons", came to the fore. Personal weapons, which are called smart weapons by evolving electronically, initially aim to offer limited use by identifying with the authorized user for firing the weapon. Personalized gun advocates argue that many lives can be saved thanks to the gun's authorized user feature. The concept of an electronically personalized weapon was first introduced in 1990 after a criminal used a police officer's weapon against a police officer. In addition, many reasons such as the increase in murders committed with smuggled weapons, the deaths caused by guns by children left unattended, the guns owned by their families and the students who have guns in schools have revealed the need for personalized guns. According to a study published in the journal Injury Epidemiology in 2015, approximately 110 children die from unintentional fire every year, and according to data from disease control centers, between 14,000 and 19,000 people are injured in firearm accidents each year.

Another study shows that the majority of suicides with guns in America are committed with weapons belonging to family elders. According to the same study, 82% of young people who attempted suicide were with weapons belonging to their families, and 84% of accidental deaths occurred in the home or car of the victims' families. In addition, between 2005 and 2010 almost 1.5 million weapons were stolen and became out of control. If the use of smart weapons had been widespread, could these deaths have been prevented?

Today, we can classify the weapons that we can call smart weapons or personal weapons under two general headings. The first of these is radio frequency-based technology (Radio Frequency Identification-RFID) weapons, and the other is weapons using technology based on biometric features. In RFID weapons, the trigger mechanism is opened to use with the radio frequency sent by an object carried by the shooter. Biometric weapons open the trigger mechanism with the approval of the finger or palm reader, which is usually on the handle of the weapon.

Electronically evolved personal weapons have been in business for nearly 25 years. The development of the society slowed down due to the political pressures of the anti-gun and human rights defender. On the other hand, the thought that the sales figures would be low due to an increase in costs constantly delayed the decision of the manufacturers to invest. In the report published annually by the Stockholm International Peace Research Institute, an independent research organization, the United States of America (USA), which is an important producer and consumer in the world market in the arms industry, also carried out pioneering studies in the field of smart weapons. Although many designs are no more than prototypes, successful commercial products exist. For example, the two major US arms manufacturers Colt and Smith & Wesson agreed to manufacture a smart gun in aim to avoid deaths from accidental shooting in 2000. Also, the US government encouraged and sponsored the Project. They said that they gave up on the deal due to boycotts by gun manufacturers and opposition groups and that they had no such plans.

We can list some examples worth examining around the world as follows;

Germany's Armatix company has developed the intelligent system consisting of iP1 and iW1. Those were the two main parts of the .22 caliber gun where the iP1 is a pistol which was activated by the iW1, a wrist-worn device that communicates using radio frequency identification. An intelligent system pistol will only fire if it is within range of this watch. This smart weapon is one of the first examples of smart weapons to find a place in many markets. One of the disadvantages of electronic weapons is

the possibility of hacking. In 2017, this weapon produced by the Armatix company was hacked by malicious people and an attempt was made to discredit the weapon and the trust of the weapon began to be questioned.

In this weapon, Armatix company developed a design that gives authorization to the user by communicating with a wrist-mounted transponder (iW1) between the watch. The use of RFID offers a safer system to outside interference. The wrist-worn transponder is also a watch. The transponder becomes personalized by requiring a five-digit PIN code to be entered before transmitting the signal. PIN code is entered with the help of the keys on the watch. If an in correct PIN code entered, the watch displays "FAIL" comment on its screen. Otherwise when the PIN code is correct, "GOOD" will appear on the screen of the watch. The authorization time must be remained by the user over the watch. Then a signal sent from the watch to the gun in order to set a specified time period fot firing. The gun will be disabled when the set time expires. The user may be manually disabled the gun before the specified time runs out. The gun will also be disabled if the distance get bigger than the gun-watch communication range. It will automatically reactivate when brought back to the standard 15 inch activation distance found in the gun's software. When the batteries are first inserted into the system, the clock synchronizes with the gun within a few seconds and the LED screen on the firearm displays colors with different meanings. Blue indicates that the magazine is not inserted, Red indicates that the weapon is not ready due to an unauthorized user or out of sync, Green indicates that the weapon is ready to fire, and a flashing indicator indicates that the battery level is low. The gun was allowed to be offered for sale in 2013 by passing the US gun regulations.

Figure 1 Armatix iP1 Weapon and iW1 watch and other equipment

In 1998, iGun Technology Corporation developed a shotgun, the M-2000. It can be considered as the first prototype which was ready to be presented as a commercial product in the hunting weapons market. The two-stage trigger guard system consists of a ring worn on the finger on one side and the receiver unit on the shot gun. The user wears a ring with a passive RFID tag embedded in the electronics circuit. The ring is energized by the RFID reader located in the pistol grip and the ring generates a code. When the signal that the rifle is held in the normal position is received by the code from the ring, the trigger fires.

Figure 2. M2000 rifle and signal transmitter ring manufactured by iGun Technology Corporation

Another electronic evolution in personal weapons is that weapons can be fired thanks to fingerprint sensors. Kai Kloepfer, a young entrepreneur from the USA, invented a gun with a fingerprint sensor at a young age and made it possible to fire the gun only if the fingerprint matched.

Figure 3. Kai Kloepfer's smart gun prototype

In 1997, the gun manufacturer Colt's Manufacturing Company tried to communicate between the gun and a wristband on the authorized user using RFID. The communication process begins with the user grasping the device. There is a switch located inside the pistol grip that starts the action when pressed. By pressing the grip switch, it sends a signal to the wristband that the gun owner should carry, on which there is a transceiver unit. When a signal is received on the wristband, the wristband sends a specially produced response code according to the weapon. If the code sent is authorized, a miniature motor is activated and a locking pin dislodges from the trigger mechanism, allowing the gun to fire by the user.

They found that in the authorization method used, when the trigger mechanism was intervened by an unauthorized user, the mechanism was damaged due to force. Therefore, a new prototype was designed, consisting of main modification. The new prototype consist a much smaller transponder in order to minimize the whole volüme of the gun. A power supply added to the system to meet the guns energy needs. The RFID unit on the grip modüle changed a new and better communicable RFID unit. Also a laser aiming device mounted on the gun to get a better hit accuracy.

Inside the gun improved blocking for the trigger mechanism desingned. Finally, a small identification screen added to system to make the gun comfortable. $1,000,000 was spent developing this prototype. In order to improve the trigger mechanism of the new prototype developed, in the previous prototype; A new blocking bar on the trigger path replaced by the trigger mechanism which consists of a DC motor and lead screw assembly. However, this new prototype produced could not pass the tests due to the durability problems of the teetic mechanism, the problems experienced in the grip module and software programs. Despite all these negativities, these studies have shown that it is possible to integrate a transmitter technology into the watch and a signal receiving actuator inside the gun grip.

Figure 4. Prototype and Working Principle Developed by Colt's Manufacturing Company

Biometric technologies use individual physiological characteristics to identify the authorized user of the weapon. These physiological features can be many personal features such as fingerprint, face, voice, vascular map. However, not all of this biometric data can be easily used to allow the use of a smart weapon. Between 2000 and 2005, the Smith & Wesson company worked on approaches such as tissue spectroscopy for authentication, including PIN codes, biometric fingerprints, and skin. In the first phase of their work, it was aimed to design an electronic ignition and authentication system that requires pin code verification. Then, studies were carried out to develop a fingerprint reading system that does not integrate the authentication process into the weapon, and to authorize weapons with biometric data.

Figure 5. A biometrically controlled prototype developed by Smith & Wesson

New Jersey Institute of Technology officials; In 2008, they developed a smart weapon using pressure sensors, assuming that the pressure and grip that a person applies while pulling the trigger is a biometric situation specific to the user. In the weapon design called Child Safe Personalized Weapon, the pressure sensors placed on both sides of the gun handle consist of piezoelectric materials that convert the mechanical energy applied by the user. This unique grip-based design applied is called Dynamic grip recognition (DGR). In the first design, there was a special microprocessor supporting digital signal processing in the grip region, system control functions, micro electromechanical (MEMS) systems for trigger motion detection, a 3.7 V and 600 mA battery. The biggest disadvantage of the design was that it was only authorized by the user and did not include an electronic control of gun safety.

After the first prototype was unveiled in 2004, a second prototype was built in 2008. The prototype is intended to disable the weapon in unauthorized use. They used the solenoid-based inhibition mechanism in their design. They also revealed a prototype design of the Baretta M9, which can fire with integrated DGR hardware in support of a rechargeable lithium-ion battery. Due to the high electricity consumption of the solenoid-based inhibition mechanism, the battery was consumed at low number of shots. To solve the problem, a spring made of a new generation shape memory material called nitinol was used. In the following years, additional electronic equipment such as increasing the number of sensors and face recognition are tried to be added to the system.

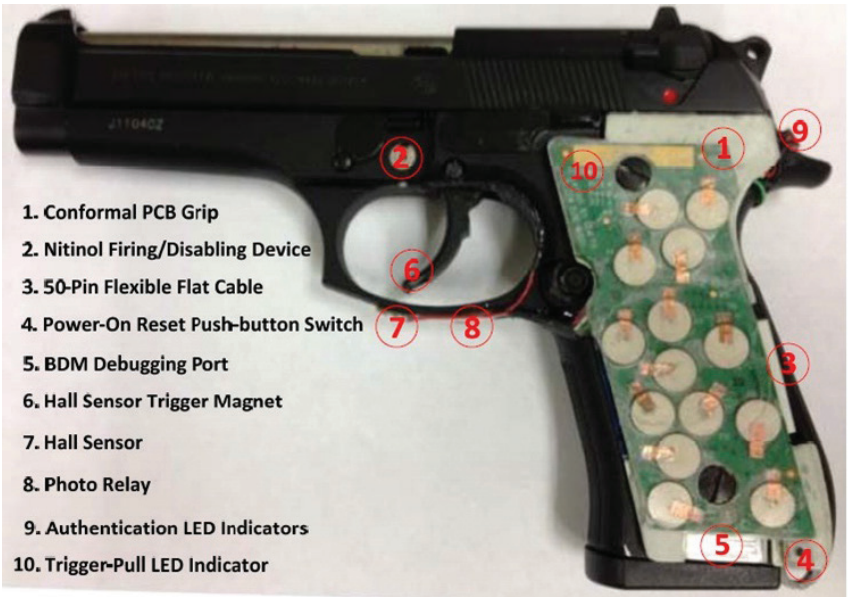

Figure 6 Child Safe Personalized Weapon Protype developed by the New Jersey Institute

American-based company called Secure Gun Technology (SGT) developed a shotgun prototype in 2013 with an authorization system used with fingerprint identification sensor module technology. This sensor module used in the design features image-based technology that looks at the patterns of a hand or finger. This module operated in the visible or near infrared spectrum and the system compares the optical data of a registered user with that of the person holding the gun.

The SGT system was designed to be authoritative as long as it held a handgun. If the authorized user lifted his hand from the grip for more than one second, the system was deauthorizing. There was no need to keep the finger on the scanner after the initial authorization was obtained. Using a split firing pin design that allowed the hammer to drop if an unqualified person used the gun, it would disable the firing pin and prevent the shotgun from working.

Kodiak Industries officials initially considered designing a biometrically activated firearm in 2012, called the Intelligun. He wanted to integrate the 1911-style 45 caliber gun with a fingerprint-based locking system that could be unlocked immediately by the authorized user, which had not been done until then, and to patent this design.

The Intelligun consists of a protected, sealed handle and mainspring. In this design, instead of the standard handle and mainspring, they considered a design that includes special security screws to prevent

tampering with the system. The unit is supposed to be water resistant and chemical resistant. They considered adding a fingerprint sensor, which when integrated into this design did not drastically change the main parts of the gun. The total weight of the add-on component weighs less than a tenth of the total weight of a firearm.

The system opens with the help of the pressure sensor when the gun is gripped by hand. The finger registered in the system is read with the help of the sensor and compared with the authorized person list. If the user is found to be authorized, it can fire. If it is detected that the user is not authorized three times while holding the weapon, the weapon will switch to high security mode and the administrator who has introduced the weapon to the system makes it operational again. In the unit integrated into the gun, there is a button that can emit three different LED lights (red, yellow, green) showing the system status, battery life and operating information. In addition, the lithium-ion battery in the system has a life of approximately one year and can be charged via a standard micro USB port.

Identilock which is recently designed in the USA, has presented a biometric gun safety system that requires the user to touch the fingerprint reader before activating the trigger of the firearm. The unlocking process takes less than a second in this activation system. When the gun is unlocked the trigger guard falls harmlessly to the ground. If a problem occurs with the unlocking system or the battery runs out a physical key can be used to activate the trigger. Manufacturer used a USB chargable battery which has a half year life with a two hours charge.

Figure 8 Personal Weapon with Next-Gen Identylock Design

4. Future Innovations

When we look at the history of personal weapons, it is clear that important works have been achieved and great progress has been made in the last 25 years. Our personal predictions about which direction the future will take are limited only by our imagination. An important part of the technological products are put forward by the scientists who are displayed in the cinema and aim to make someone's dreams come true.

The laser weapons we see in many science fiction movies will be innovations we will see in the near future. Significant work is being carried out on the design of weapons of different sizes using laser beams or sound waves. Especially large-scale weapons using laser beams have been produced, but it is estimated that it will take a long time for these weapons to be reduced to the size of personal weapons. In order to experience this progress, it is necessary to introduce material technology that will reduce the size of electronic circuit elements.

A different perspective to the future perspective is being developed over unmanned aerial vehicles (drone). Existing armed drones provide fire support against a few enemy elements. On the other hand, the effective

range of long-range sniper rifles that can be used by an infantryman can be a maximum of 2000m. In the future, the aiming capability of drone support has been improved and it will be possible to shoot at targets out of sight. The drone can provide information to the weapon, such as an artillery support team, so that it can be correctly positioned and fired. The drone may not extend the shooter's effective range longer distances without a direct target.

Another approach to drone use is based on another technology developed by DARPA. DARPA stands for The Defense Advanced Research Projects Agency, which is a government agency under the US Department of Defense and responsible for developing new technologies for use by the US military. One of the many works that this company has done is the directional gun bullet. Using a drone as a guide to a steerable gun bullet is a viable idea.

Today, the position of the target can be followed up to the last moment by using marking technology in missile and rocket shots. This technology can be done with satellite support, and the mission of the satellite can be made locally by using drone support for long-range or short-range weapons. In order for such a development to be experienced, first of all, bullet technology must be developed. If artificial intelligence is integrated into such a system, it may be sufficient for the user to simply have the weapon ready. Firepower is obtained by giving the command necessary for the firing of the ready-made weapon by the system. The problem of controlling this technology is a separate and important discussion of the human being, who had such a dream about 30 years ago in the movie Terminator. The most important deficiency of systems designed to use fewer or no people in terms of human safety is the ability to make decisions. The development of artificial intelligence that can fulfill this capability is again the problem of electronics and software engineering. In the solution of the problem, it is aimed that the machines follow the practices taught in a certain situation. As a result, people can make wrong decisions. The real problem with artificial intelligence is that the possibility of getting out of control one day is really on the table.

In the coming years, with the development of artificial intelligence, our personal weapon can turn into one of our smart home items such as a robot vacuum cleaner with the help of an application we download to your phone. After matching the downloaded application and the weapon, all information such as the location of our weapon and the number of bullets in the magazine can be seen and controlled with the application. This control can be managed via the GSM/GPRS module. In case of theft of a GSM/GPRS controlled weapon, the location information will be obtained continuously and it will be possible to prevent the use of the weapon. At

the same time, by imposing a shooting ban at the defined locations, attacks on places where people live collectively, such as military institutions, government institutions, health institutions and educational institutions, will be prevented.

Today, three-dimensional printers are constantly showing themselves in new areas. The first examples produced with 3D printers in the arms industry appeared about 20 years ago. Although these single-shot guns are thought of as models produced for the purpose of committing murder at short range without the rifle set form, the future may be different. If it is possible to process metal materials with 3D printers or if existing polymer-based materials are brought to the strength to shoot multiple shots, the place of personal weapons produced by this method in our lives may increase. Using the method will make the weapons lighter, so it will be advantageous to add different electronic equipment.

The next electronic evolution of personal firearms could be effective enough to change the firearm name. Electromagnetic ball systems called "railgun" work by using the behavior of magnetism, namely Lorentz forces. In these systems, a steel core, which acts as a bullet, is placed in the gun. The working structure of the system is similar to a simple solenoid valve. The magnetic field formed on the coil, which is energized in the solenoid valve, exerts a force on the core, which acts as an on-off valve in the valve. The core moves with the effect of this force. With the same logic, Railgun systems aim to create a magnetic field and direct the core, which it uses as a bullet, to the target at a very high speed. A large energy source is needed for the magnetic field required in the system. Although this electrical energy can be supplied from batteries, the minimum battery capacity required is still too bulky for a personal weapon. In the future, it will be possible to talk about fireless personal pistols by reducing the need for electrical energy and increasing the battery capacity.

The development of technology, especially in the field of software, is eye-catching. It is also clear that this rapid change will perfect the electronic evolution of personal firearms. Over time fingerprint sensors, RFID or biometric systems will be perfected in terms of speed security target accuracy. It will cause high costs in the beginning, but the increase in mass production over time will reduce the costs with the development of material technology.

A gun is a cold object for some, a necessity for others. As there will always be those who think that a gun is a necessity and therefore demand rights, there will also be those who are against guns and demand rights and freedoms to restrict access to guns. In fact, there are points on which both sides agree with each other in this debate. According to a study conducted

in Pittsburgh, USA in 2008, most of the firearms used in gun crimes did not belong to the perpetrator, and a survey conducted in Chicago, USA in 2015, revealed that 40% of inmates obtained their guns from the black market or theft. In this case, the group that is against personal armament says that the main source of these events is the possession of firearms by individuals. No firearm owner buys a gun with the foresight that his gun will be stolen and involved in a crime. The vast majority of people who buy guns take this action out of security concerns. It has become inevitable to take a precaution against the events. One such measure is the further electronic "personalization" of personal weapons. Since electronically personalized weapons are weapons that only allow the owner to use the weapon, uncontrolled actions will be prevented.

Political reasons and the attitudes of arms dealers are the main reasons why personal smart weapons are not used more widely. Death threats and intimidation by classical arms dealers against smart weapons manufacturers have slowed down the electronic evolution of weapons considerably. Due to these attitudes of arms dealers, many investors withdrew their support from the projects, and therefore these projects that could not be realized remained as prototypes. Another reason is the questioning of the reliability of smart weapons technology. Devices with electronic equipment can give sensitive responses. For example, a capacitive detector may be adversely affected by moisture on a human finger, extreme temperatures may reduce the thermal imaging reliability of the weapon, fingerprint reading systems may be affected by paint, dirt or gloves. Likewise, rings, necklaces, such personal belongings used in RFID weapons. Even if the vehicles are inside the house, when you are not with you, the weapon will be unusable during an emergency. Another questionable issue in RFID weapons is the possibility of taking control of the weapon by hackers.

In addition, both technologies bring battery problems. Another feature that is not liked by the users of electronic weapons is that the weapon does not allow more than one user. When a need arises for a weapon to be used by a family, a law enforcement agency or soldiers, these weapons remain incomplete, thus limiting the sale of weapons. In addition, it is obvious that the maintenance of these weapons will be different from the existing weapons. This situation limits the use of smart weapons. Considering that the guns should work without any trouble every time, there is still a distrust of electronically equipped weapons due to these problems.

It is an acceptable fact that we need this technology for a safer world future. But another fact that has to be accepted is that it is impossible to fully trust these weapons as a result of the current state of smart weapons. Because there are many conditions that must be fulfilled before firing the smart weapon, and there are many reasons that can cause the system

to fail. While the issues that people who use traditional weapons should worry about before using the guns are more or less clear, they will have to worry about many issues such as batteries, electronics, software, grip safety, fall safety, losing watch or ring, not reading fingerprints in smart guns. Worry is one of the last things you should have before using the gun.

5. References

Armatix iP1 Limited Edition Set. (2021, November). Armatix-SimonsVoss Technologies AG. http://www.armatix.us/iP1-Limited-Edition.804.0.html?&L=7

Arquebus. (2021). Https://En.Wikipedia.Org/Wiki/Arquebus.

Aydın, Ö. (2019). *Freedom And Individualistic Armament From The Point of Security*.

Chase, K. (2008). *Firearms: A Global History to 1700*. Cambridge University Press.

Darıcılı, A. B. (2021). New threat in individual armament: 3D printed weapons. *Anadolu Ajansı*.

Delgado, M. (2021). *Urban Gun Violence*. Oxford University Press. https://doi.org/10.1093/oso/9780197515518.001.0001

Firearm. (2021, November). Https://En.Wikipedia.Org/Wiki/Firearm.

Gammon, K. (2016, February 8). *The Tech Behind Smart Guns*. American Institute of Physics.

Gobinet, P. (2013, June 17). Personalized Firearms and Electronic Safety Devices: Perspectives. *Smart Technology in SALW Control: Civilian Protection, the UN-POA, and Transfer Control (SmartCon)*.

Greene, M. (2013). *A Review of Gun Safety Technologies*.

Güner, F. (2019). *Hafif Silahlar ve Balistik*. Nobel Yayın.

Güner, F. (2020). Numerical Investigation of AISI 4140 Powder High Relative Density Compaction In Terms of Compaction Velocity. *Mechanics*, *26*(1), 5–11. https://doi.org/10.5755/j01.mech.26.1.22862

Hayes, J. (2016). Smart Gun Technology. *Homeland Defense & Security Information Analysis Centre*, *3*(3).

Heubl, B. (2020, June). Will smart guns hit their target this time? *Https://Eandt.Theiet.Org/Content/Articles/2020/06/Us-Smart-Gun-Tech-Start-Ups-to-Bring-Personalised-Weapons-to-Market/*.

Identilock Security System Ready In The Blink of An Eye. (n.d.). Identilock. Retrieved November 28, 2021, from https://getidentilock.com/

Invention and Historical Development of the Pistol. (2014). Https://Bilgi.Sitesi.Web.Tr/Tabancanin-Icadi-ve-Tarihsel-Gelisimi.Html.

Kara, Bu. (2021). The invention and historical development of the firearm. *Https://Ungo.Com.Tr/2021/03/Atesli-Silahin-Icadi-ve-Tarihi-Gelisimi/*.

Narayana, V., Nikhil, N., Reddy, K., Mohammed, S. & Kurup, S. (2017). Design of Smart Gun Employing Biometric Security. *International Journal Of Electrical, Electronics And Data Communication*, *5*(5).

Nguyen, N. (2021, November 26). *Here's What's Up With "Smart Guns" — And Why You Can't Buy One In The US*. Https://Www.Buzzfeednews.Com/Article/Nicolenguyen/What-Is-Smart-Gun-Technology/.

Pamukoğlu, O. (2019). *III.World War*. Inkilap Kitabevi.

Radio Frequency Identification (RFID) Guns. (n.d.). Smart Tech Challenges Foundation. Retrieved November 28, 2021, from https://smarttechfoundation.org/smart-firearms-technology/rfid-guns/

Sebastian, D. (2016). The Conversation: What Makes a "Smart Gun" Smart? *SCIENTIFIC AMERICAN*.

Shen, J., Fan, S., Ji, Y., Zhu, Q. & Duan, J. (2020). Aerodynamics analysis of a hypersonic electromagnetic gun launched projectile. *Defence Technology*, *16*(4), 753–761. https://doi.org/10.1016/j.dt.2020.01.008

Stevenson, D. (2020). Smart Guns, the Law, and the Second Amendment. *Penn State Law Review*, *124*(3).

Chapter 2

BIOLOGICAL CONTROL

Sevcan AYTAÇ KORKMAZ[1]
Veysel ÇAKIR [2]

1 Fırat University Electronic Technology Department Elazığ, Turkey
2 Fırat University Biotechnology Department Elazığ, Turkey

Introduction

The growing risks, some pathogens(toxins), pesticides, drugs, heavy metals have been realised recently, owing to haphazard agriculture and animal husbandry areas having critical health effects from the point of causing diseases [3]. The more the quality and safety is challenged, the more strong equipments are needed to create a product of typical parameters. *Despite* traditional detection techniques are convenient, they spend a lot of time and to need serious protocol with an eleborate procedure and qualified personnel. *For instance,* traditional detection techniques and standard pathogen detection *techniques* such as culture counting and colony counting might take up a few days. Furthermore, physicochemical methods like liquid chromatography–tandem mass spectrometry (LCMS/MS), for contamination testing such as toxins, veterinary drug residues, heavy metals tend to be expensive, complicated to perform and to spend time [4]. But, chromatography and spectrometry can procure more safe and conclusive datas still a higher through put with less operator training are needed by screening tests [1].

A rapid method of screening these hazards in the bulk material handling industry to provide food safety and foood quality could be the answer. In this conditions, in growing meat industry rapidly, for methods of quality control and safety of meat and meat products can become the biosensor an effective alternative. They have some advantages such as high degree of sensitivity and specificity of detection where minimum sample preparation is there, cost-effectiveness, miniaturization and portability for real time monitoring [5]. Furthermore, HACCP system can be used to verify that is a given process is under control, since the sensitivity of high biosensor lets the detection of pathogenic microorganisms, pesticides and another contaminants in minutes or hours [1,6].

Biosensors can be described as an analytical instrument, which transforms a biological answer into an electrical signal and comes out of two main components: a bioreceptor or biorecognition element, which recognizes the target analyte and a transducer, which transforms the recognition event into a quantifiable electrical signal [7]. Therefore, biosensors can be classified on the main of type of biocomponent involved, mechanism or mode of signal transduction etc [8]. The recognition elements can be systems containing enzymes, cell receptors, microorganisms, antigens, antibodies and nucleic acids. The transduction elements are usually electrochemical, optical or piezoelectric, and the electrical signals when based on a change in the measured current are amperometric; when change in the measured voltage between the electrodes are potentiometric and when a change in the functions to charge of transport, so then they are conductometric. The optical sensors are usually predicated on the

absorbance principle, fluorescence, chemiluminescence, surface plasmon resonance etc. The sensors predicated on mass produce a mass dependent signal for the analyte that interact with the sensors and give information regarding analyte presence [1].

Even though the first progress in the biosensors was aimed to use in the medical diagnostic equipments, afterwards the principles of detection and quantification of biological molecules started to find its way in the food industry too. While biosensors can be uncomplicatedly applied for meat sample with the least processing methods such as mincing or homogenization, beginning enrichment activities may not be needed for pathogen or toxin detection, saving the analyses time. Even though little commercialization of the instrument has been done in the meat industry unlike the fields like medical diagnostics but with the increasing load of bulk handling it is going to be hard to continue the safety of products and the quality of products without a faster screening instruments like biosensor. This article envisages to discuss the possible area of the emerging instrument in the meat industry about ensure the quality and the safety of meat products [1].

Food biotechnology, together with use of plants and animals directly, is related the application of (live) food microorganisms, like yeasts, fungi, bacilli and lactic acid bacteria, in industrial areas. Basic purposes are increased production of ingredients and improved properties of starter cultures, such as reproducible growth characteristics, enhanced flavour formation and proteolytic activities or better autolytic properties. Investigation of the effect of food microorganisms on human health is also an essential area, for example, in prebiotics and probiotics research [9-10]. On the other part, attention are needed since the prevention of food-spoilage and pathogenic microbes. Food biotechnology' purpose are both directed towards improving food production and meet the requests by consumer for safe, natural, fresh, tasteful and convenient products [9,11].

The research programs that is for improvement of industrial activities of microorganisms used in fermentation progress were focussed in the beginning on microbial strain selection then classical mutagenesis, finaally followed by more directed approaches using genetic engineering. These approaches' essential advantages are that they are time-consuming, side-effects being in the selected or constructed strains are difficult to estimate and value, and the full range of engineering possibilities can not be exploited due to lack of knowledge of inter-related regulatory and metabolic processes going on in a cell. Moreover, the consumer population's part is worried seriously about the safety of the novel foods, and if undesirable spread of genetically modified microorganisms in environment can be controlled. Functional genomics can exactly provide solutions in the last two fields.

Several criteria and options for safe biotechnology and for risk-assessment procedures for the environmental application of microorganisms have been discussed recently [9,12].

Within future decade, reaching various industrial aims will be possible for application of functional genomics programs on food microorganisms. For instance, to designate side-effects of genetic alterations on functionality in products, to occur wanted pleiotropic effects by specific regulatory mutations, to predict and develop stress responses, to develop novel antimicrobial systems, and to direct metabolic engineering efforts. Likewise, it will enable the identification of novel (enzyme) activities, the performance of high-throughput mutation analyses in strains of interest and the improvement of quick identification analyses for food spoilage or pathogenic microorganisms. The review provides an check of current improvements in high throughput technology and discusses their practicality about food biotechnology [9].

Riboflavin, also known as 7,8-dimethyl-10-[(2S,3S,4R)-2,3,4,5-tetrahydroxy pentyl]benzo[g]pteridine-2,4-dione, vitamin B2 is a water soluble vitamin naturally synthesized by plants and some microorganisms. It is an important micronutrient for animal and human diets, as it is not synthesized by higher animals. The product riboflavin that is used applications in small amounts as the colouring agent E101 or as a nutritional additive in animal feedstuffs besides as an additive in food [15-16]. In the beginning, riboflavin was fundamentally chemically synthesised for the production of very pure material. Biotechnological improvements have consequence in microbiological processes that can compete with the chemical synthesis and in our times commercial production of vitamin B2 is commonly done by fermentation.

In most instances, riboflavin's microbial synthesis involves genetically engineered selected strains of Escherichia (E.) coli, Bacillus (B.) subtilis, Ashbya (A.) gossypii, and Candida (C.) famata [16]. Genetically modified strains of E. coli and B. Subtilis are potentially the best known [17] within genetically modified micro-organisms (GMMs) as in these bacteria the riboflavin biosynthetic pathway has been studied in detail [18]. B. subtilis is an aerobic endospore forming bacterium prevalently found in nature and it has not a pathogenic or toxigenic potential. The large-scale fermentation production of speciality chemicals of enzymes used in food production processes, and of several traditional ways of food preparation are used in direction of experiences about safe [15].

All the time, non-sporulating derivatives of the B. subtilis strain 168 were genetically modified (GM), it always carry natural mutations inducing riboflavin overproduction. Introduction of different plasmids

harbouring both a recombinant B. subtilis riboflavin biosynthetic operon under the control of a strong promoter and antibiotic resistance genes as selection markers (like; cat, tet, ermAM), resulted in genetically modified B. subtilis strains with multiple copies of the rib operon (rib operon, also known as ribDEAHT operon, i.e. including the ribD, ribE, ribA, ribH, ribT genes). These strains can enhance riboflavin expression by 10 - 25 times the size [15,19-22].

In the last product, additives produced with GMM are show that neither the production strain nor its recombinant DNA can be detected according to EFSA guidance [22]. In September 2014, it was notified in RASFF (the European Rapid Alert System for Food and Feed) that a German official enforcement laboratory in Hesse detected viable GM B. subtilis spores in a consignment of vitamin B2 feed additive (80% feed grade) imported from China [15,23].

In April 2015, the Belgian official control laboratory published a report which about the genome sequence of a GM subtilis strain [24] This strain (isolate 2014-3557) was identified by a French competent authority in many vitamin B2 (riboflavin, 80% feed grade) imported to France from China. On basis of NGS (Next Generation Sequencing) result of a Belgian institution a TaqMan qPCR method (identified VitB2 - UGM) for specific detection of this EUunauthorized GM riboflavin overproducing B. subtilis was developed [24]. In addition to this, a junction between the riboflavin biosynthesis genes and the vector backbone are targeted by the TaqMan qPCR method. It remains unsolved if the aimed sequence is integrated into the bacterial genome or present on a plasmid. For the latter situation, the detection may fail if the plasmid is lost and the corresponding target sequence is therefore missing. Also, the comprehensive molecular characterization of the GM strains' genome and plasmids have not been reported by the authors [15].

In [15] review, microbiological and molecular analyses of the GM B. subtilis strain that is found in Germany in 2014 are presented. DNA is extracted from two independent isolates to characterize in detail the genome of these riboflavin-overproducing GM B. subtilis strains, and to reconstruct the putative plasmids present for performed whole genome sequencing (WGS). Later on, construct and event specific PCR based methods for its detection in food and feed were improved and applied [15].

DAS-444Ø6-6 soybean was genetically engineered (GE) by use applications of three varied herbicides. Expression of the aryloxyalkanoate dioxygenase 12 (AAD-12) enzyme provides tolerance to 2,4-dichlorophenoxyacetic acid (2,4-D) by catalyzing its degradation, expression of the phosphinothricin acetyltransferase (PAT) enzyme

inactivates glufosinate ammonium by acetylation of the l-isomer into *N*-acetyl-l-glufosinate ammonium, and expression of the double-mutated maize 5-enolpyruvyl shikimate-3-phosphate synthase (2mEPSPS) enzyme provides tolerance to glyphosate by replacing the function of the native soybean EPSPS enzyme (which is inactivated by glyphosate to control weeds/plants) [26]. These properties offer producers multiple additional choices for herb control in soybean [25-26]. The evidence's weight determines the food and feed safety of a genetically engineered crop [27-29]. This evidence has knowlegde that is whole past of safety for the expressed proteins and/or the source organism about its identify. While assessing safety, certain properties of the expressed protein provide important evidence to consider. These traits include mode of action, amino acid sequence similarity to proteins with whole past of safe use and to those known to be allergenic or toxic, stability to standard food processing and cooking procedures and digestive stability. For some proteins, these properties are enough to robustly evaluate safety [30]. In addition, toxicity can be empirically evaluated in vivo via high-dose animal works with purified protein.

Unless a feedst uff in genetically engineered proteins remain spoilage whole-food animal-feeding works might provide benefit in term of the safety assessment for proteins that cannot be purified in an active form, and for which high margins of exposure can be obtained relative to actual exposure under standard use [31]. In practice, whole-food feeding works are usually used to investigate unwanted compositional changes within the genetically engineered crop that might not be detected in works that directly analyze the composition of the edible portion of the crop [31]. The large part of information shows that adverse unintended compositional changes in GE crops are a lower risk compared with traditionally bred crops, composition works are nearly globally wanted for all new GE events, and whole-food animal works are wanted by some regulatory authorities that assess GE crop safety [31,32]

In our review, the weight of evidence for the safety of DAS-444Ø6-6 soybean based on: 1) the intended genetically engineered properties and 2) potential unintended adverse impact of the genetically engineered proteins (or the transgenesis process) on endogenous plant metabolic pathways. The approved GE crops that have been assessed universally for safety expresses proteins; the PAT and 2mEPSPS proteins. For the 2mEPSPS protein, these crops include GA21 maize, FG72 soybean, and Glytol cotton; for the PAT protein, these crops include T25 maize, A5547-127 soybean, and 281-24-236 cotton [33-34]. Thus, the PAT and 2mEPSPS proteins are not among the novel food or feed risks [35-36]. For all of these datas, the present safety assessment focuses on the AAD-12 protein and any potential

unexpected impacts in the DAS-444Ø6-6 soybean event originating from transgenesis or the AAD-12 enzyme. It must not ignore that the AAD-12 protein is also expressed by event DAS-68416-4 soybean [25].

Conclusion

In last decade, biosensor technology has attracted attention, for it is a promising instrument to lower detection limit with quick analysis time at relatively low cost. In spite of the fact that conventional detection tecniques are critical, they delay behind the analytical tecniques despitedetection time. Biosensor usage in quick detection of contaminants can lead to release of products within hours or even minutes, rather than holding them since a few days. It can also be a well instrument for screening a big thorough put of samples and going for confirmation only for tiny number. The multiplexing a new and more advanced approach with the potential of detecting a num ber of pathogens, toxins, pesticides etc. have give to thanks to the raised use of array and multiple channel systems. Finally, the development of detection technique which is more reliable, rapid, accurate, simple, sensitive, selective and cost effective must be provided [1].

Food biotechnology will gain advantage from a functional genomics approach greatly; to constitute novel opportunities to ensure the safety of foods, to develop the quality of fermented products and to substantiate health claims related to the ingestion of specific microbes. Also, the better understanding of secretion processes, stress-responses and complex regulatory mechanisms will optimize industrial production of ingredients. Exciting new technologies for life sciences are being developed with incredible speed. Transcriptome and proteome research have some blanks which are being bridged by inventions recently, such as the synthesis of double-stranded oligonucleotide arrays for parallel investigations of DNA protein interactions [13]. While a study on the *S. cerevisiae* ribosome showed recently, advances in mass spectroscopy provide direct analysis of protein complexes, The procedure can identify more than 100 proteins in a single run, hence providing the simultaneous analysis of all components of huge macromolecular complexes [14]. Absolutely, these and other novel methods in genomics will profoundly change the nature of food biotechnology in the future millennium [9].

The value of the use of NGS approaches have been described; enforcement authorities and official control laboratories by assisting food/feed competent, the presence of GMMs in biotechnological products in their researches. The approach defined in the review showed to provide a detailed molecular characterization of an unknown GMM and thus facilitated the risk assessment and together the imprevement of specific PCR methods for its detection [15].

Nonetheless, the study showed that the bioinformatics analysis of the data produced by NGS is still a challenging task and would require the development of adapted bioinformatics instruments in order to be implemented for routine data analysis and management in the frame of GMO characterization and detection. The research of the GM B. subtilis strain showed at the same time, that indepth literature review is fundamental to interpret the series data and to fully understand and characterize the sample, specially if completely unknown [15].

In the [25] are current or past worker of Dow AgroSciences LLC, which develops and markets transgenic seed. Dow AgroSciences LLC and MS Technologies™ are co-developing DAS-444Ø6-6 soybean. In the [25] demand the elimination of animal studies where datas are unlikely to meaningfully contribute to safety assessment [25].

Reference

[1] Singh, P. K., Jairath, G., Ahlawat, S. S., Pathera, A., & Singh, P. (2016). Biosensor: an emerging safety tool for meat industry. *Journal of food science and technology*, *53*(4), 1759-1765.

[2] Ferreira S, De Souza MB, Trierweiler JO, Broxtermann O, Folly ROM, Hitzmann B (2003) Aspects concerning the use of biosensors for process control: experimental and simulation investigations. Comput Chem Eng 27:1165–1173

[3] Kim SJ, Gobi KV, Iwasaka H, Tanaka H, Miura N (2007) Novel miniature SPR immunosensor equipped with all-in-one multimicrochannel sensor chip for detecting low-molecular-weight analytes. Biosens Bioelectron 23:701–707

[4] McGrath TF, Elliott CT, Fodey TL (2012) Biosensors for the analysis of microbiological and chemical contaminants in food. Anal Bioanal Chem 403:75–92

[5] Singh A, Poshtiban S, Evoy S (2013) Recent advances in bacteriophage based biosensors for food-borne pathogen detection. Sensors 13: 1763–1786

[6] Luo J, Liu X, Tian Q, Yue W, Zeng J, Chen G, Cai X (2009) Disposable bioluminescence-based biosensor for detection of bacterial count in food. Anal Biochem 394(1):1–6

[7] Velusamy V, Arshak K, Korostynska O, Oliwa K, Adley C (2010) An overview of foodborne pathogen detection: in the perspective of biosensors. Biotechnol Adv 28:232–254

[8] Lavecchia T, Tibuzzi A, Giardi MT (2010) Biosensors for Functional Food Safety and Analysis. In Bio-Farms for Nutraceuticals: Functional Food and Safety Control by Biosensors edtd. Maria Teresa Giardi, Giuseppina Rea and Bruno Berra. chapter 20 Landes Bioscience and Springer Science + Business Media.

[9] Kuipers, O. P. (1999). Genomics for food biotechnology: prospects of the use of high-throughput technologies for the improvement of food microorganisms. Current opinion in biotechnology, 10(5), 511-516.

[10] Ricke SC, Pillai SD: Conventional and molecular methods for understanding probiotic bacteria functionality in gastrointestinal tracts. Crit Rev Microbiol 1999, 25:19-38.

[11] Richardson DP: Functional foods — shades of grey: an industry perspective. Nutr Rev 1996, 54:174-185.

[12] Doblhoff-Dier O, Bachmayer H, Bennett A, Brunius G, Bürki K, Cantley M, Collins C, Crooy P, Elmquist A, Frontali-Botti C et al.: Safe biotech-

nology 9: values in risk assessment for the environmental application of microorganisms. Trends Biotechnol 1999, 17:307-311.

[13] Bulyk ML, Gentalen E, Lockhart DJ, Church GM: Quantifying DNA protein interactions by double-stranded DNA arrays. Nat Biotechnol 1999, 17:573-577.

[14] Link AJ, Eng J, Schieltz DM, Carmack E, Mize GJ, Morris DR, Garvik BM, Yates JR: Direct analysis of protein complexes using mass spectroscopy. Nat Biotechnol 1999, 17:676-682.

[15] Paracchini, V., Petrillo, M., Reiting, R., Angers-Loustau, A., Wahler, D., Stolz, A., ... & Pecoraro, S. (2017). Molecular characterization of an unauthorized genetically modified Bacillus subtilis production strain identified in a vitamin B2 feed additive. Food chemistry, 230, 681-689.

[16] Abbas, C. A., & Sibirny, A. A. (2011). Genetic control of biosynthesis and transport of riboflavin and flavin nucleotides and construction of robust biotechnological producers. Microbiology and Molecular Biology Reviews, 75(2), 321–360.

[17] Burgess, C. M., Smid, E. J., & van Sinderen, D. (2009). Bacterial vitamin B2, B11 and B12 overproduction: An overview. International Journal of Food Microbiology, 133 (1–2), 1–7.

[18] Bacher, A., Eberhardt, S., Eisenreich, W., Fischer, M., Herz, S., Illarionov, B., ... Richter, G. (2001). Biosynthesis of riboflavin. Vitamins and Hormones, 61, 1–49.

[19] Mander, L., & Liu, H. W. (2010). Comprehensive Natural Products II: Chemistry and Biology: 10 Volume Set (Vol. 7 chapter 7.04.5.2 ‘‘Riboflavin Pathway Engineering”). Elsevier Science & Technology.

[20] Perkins, B. J., Sloma, A., Hermann, T., Theriault, K., Zachgo, E., Erdenberger, T., ... Pero, J. (1999). Genetic engineering of Bacillus subtilis for the commercial production of riboflavin. Journal of Industrial Microbiology and Biotechnology, 22(1), 8–18.

[21] Smolke, C. (2009). Riboflavin pathway engineering. In The metabolic pathway engineering handbook: Fundamentals. CRC Press.

[22] EFSA (2011). Guidance on the risk assessment of genetically modified microorganisms and their products intended for food and feed use. EFSA Journal, 9(6), 2193.

[23] RASFF (2014). Unauthorised genetically modified (Bacillus subtilis) bacteria in vitamin B2 from China, via Germany (Accessed 08.03.2017) https://webgate.ec. europa.eu/rasff-window/portal/?event=notificationDetail&NOTIF_REFERENCE= 2014.1249.

[24] Barbau-Piednoir, E., De Keersmaecker, S. C., Wuyts, V., Gau, C., Pirovano, W., Costessi, A., ... Roosens, N. H. (2015). Genome sequence of EU-unauthorized genetically modified Bacillus subtilis strain 2014–3557

overproducing riboflavin, isolated from a vitamin B2 80% feed additive. Genome Announcements, 3(2).

[25] Herman, R. A., Ekmay, R. D., Schafer, B. W., Song, P., Fast, B. J., Papineni, S., ... & Juberg, D. R. (2018). Food and feed safety of DAS-444Ø6-6 herbicide-tolerant soybean. Regulatory Toxicology and Pharmacology, 94, 70-74.

[26] Lepping et al., 2013 M.D. Lepping, et al.Compositional equivalence of DAS-444Ø6-6 (AAD-12 + 2mEPSPS + PAT) herbicide-tolerant soybean and nontransgenic soybean J. Agric. Food Chem., 61 (2013), pp. 11180-11190

[27] OECD, 1993 OECDSafety Evaluation of Foods Derived by Modern Biotechnology: Concepts and Principles (1993)

[28] Hammond et al., 2013 B. Hammond, et al.Toxicological evaluation of proteins introduced into food crops Crit. Rev. Toxicol., 43 (2013), pp. 25-42

[29] Herman et al., 2015 R.A. Herman, et al.Percent amino-acid identity thresholds are not necessarily conservative for predicting allergenic cross-reactivity Food Chem. Toxicol., 81 (2015), pp. 141-142

[30] Delaney et al., 2008 B. Delaney, et al.Evaluation of protein safety in the context of agricultural biotechnology Food Chem. Toxicol., 46 (2008), pp. S71-S97

[31] Herman and Ekmay, 2014 R.A. Herman, R. Ekmay Do whole-food animal feeding studies have any value in the safety assessment of GM crops? Regul. Toxicol. Pharmacol., 68 (2014), pp. 171-174

[32] Herman and Price, 2013 R.A. Herman, W.D. Price Unintended compositional changes in genetically modified (GM) crops: 20 years of research J. Agric. Food Chem., 61 (2013), pp. 11695-11701

[33] CERA - ILSI Research Foundation, 2016b CERA - ILSI Research FoundationA Review of the Food and Feed Safety of the PAT Protein (2016)

[34] CERA - ILSI Research Foundation, 2016a CERA - ILSI Research FoundationA Review of the Food and Feed Safety of the EPSPS Protein (2016) Herouet-Guicheney et al., 2009

[35] C. Herouet-Guicheney, et al.Safety evaluation of the double mutant 5-enol pyruvylshikimate-3-phosphate synthase (2mEPSPS) from maize that confers tolerance to glyphosate herbicide in transgenic plants Regul. Toxicol. Pharmacol., 54 (2009), pp. 143-153

[36] Hérouet et al., 2005 C. Hérouet, et al. Safety evaluation of the phosphinothricin acetyltransferase proteins encoded by the pat and bar sequences that confer tolerance to glufosinate-ammonium herbicide in transgenic plants Regul. Toxicol. Pharmacol., 41 (2005), pp. 134-149

Chapter 3

HEXAROTOR LATERAL FLIGHT CONTROL USING DEEP NEURAL NETWORK AND MORPHING

Oguz KOSE[1]

Tugrul OKTAY[2]

1 Asst. Prof. Oguz KOSE, * Gumushane University, School of Applied Sciences, Department of Aviation Management, Gumushane, Turkey, oguzkose24@gmail.com, (ORCID: 0000-0002-8069-8749)

2 Prof. Tugrul OKTAY, Erciyes University, Departmant of Aeronautical Engineering, Kayseri, Turkey, tugruloktay52@gmail.com, (ORCID: 0000-0003-4860-2230)

Introduction

Studies on UAVs have increased rapidly in recent years. UAVs have been a source of information gathering in many areas such as military operations, weather, traffic control, search and rescue[1]. In the early days, research was limited to quadrotor UAVs known as quadrotors[2]. Recently, however, research has focused on UAVs known as hexarotors because they have many advantages over quadrotor. For example, the hexarotor provides longer flight time, and can carry more payloads compared to the quadrotor.

The contributions of this work are: developing the hexarotor UAV linear mathematical model accurately and in detail. Drawing the hexarotor full model and morphing states in Solidworks program in accordance with the derived model. To apply the control algorithm in accordance with the model and to determine the parameters of the deep neural network and control algorithm. To analyze the effect on flight by performing hexarotor simulations with the obtained parameters in Matlab/Simulink environment.

The paper remainder is organized as follows. In the next Section the mathematical formulation, the dynamic model of the hexarotor and morphing are described. In section III, PID control algorithm and deep neural network are presented. In section IV, the simulation results performed with the proposed method are given and in the last part the effect of the results on the flight is discussed.

Hexarotor Model and Morphing

The Hexarotor is a 6 rotor helicopter. The thrust or upward force is provided by 6 rotors. Other movements can be controlled by changing the speed of the motors. A hexarotor has 6 rotors arranged clockwise and counterclockwise, working together to provide upward thrust, eliminating the need for countermeasures[3].

Leonhard Euler described the Euler angles. These angles define the angular orientation of the fixed body relative to a reference frame. The Euler angles for the hexarotor are roll(ϕ), pitch(θ), and yaw(ψ). In this study, the roll motion is discussed for

the hexarotor. Roll motion is defined as the state of the hexarotor blades not being parallel to the ground. The schematic of the hexarotor is presented below.

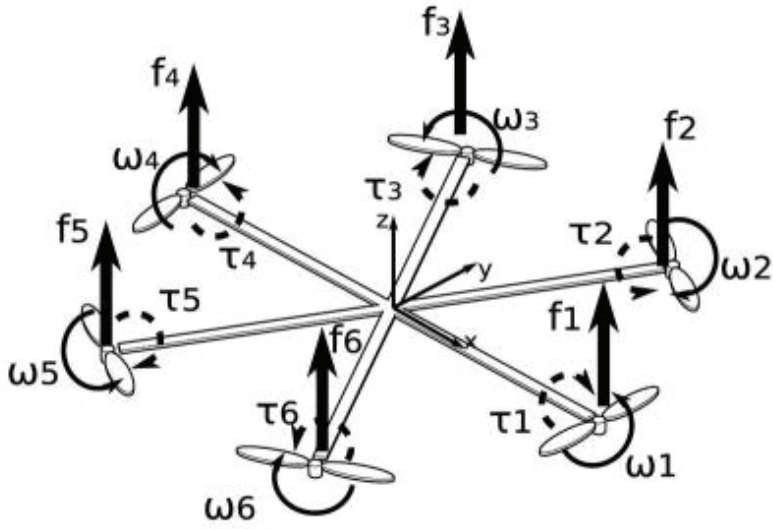

Figure 1. Schematic of the Hexarotor

In the inertial frame, the linear position vector and rotational position vector can be defined through $X = [x \quad y \quad z]$ and $\eta = [\phi \quad \theta \quad \psi]$. Hexarotor is a system with non-linear dynamics. Using various techniques, non-linear dynamics are converted to linear dynamics. The linear equations used in this study are given in the equations below.

$$\ddot{x} = g\theta \tag{1}$$

$$\ddot{y} = -g\phi \tag{2}$$

$$\ddot{z} = -g + \frac{U_1}{m} \tag{3}$$

$$\ddot{\phi} = \frac{U_2}{I_x} \tag{4}$$

$$\ddot{\theta} = \frac{U_3}{I_y} \tag{5}$$

$$\ddot{\psi} = \frac{U_4}{I_z} \tag{6}$$

In these equations, m mass, I_x, I_y and I_z moment of inertia, U_1, U_2, U_3, U_4 represent the control inputs. In lateral flight, the U_2 input will be used.

$$U_2 = \frac{bl\sqrt{3}}{2}(-\omega_5^2 + \omega_3^2 + \omega_2^2 - \omega_6^2) \tag{7}$$

$$\omega_G = -\omega_1 + \omega_2 - \omega_3 + \omega_4 - \omega_5 + \omega_6 \tag{8}$$

In this study, since the lateral movement is controlled, the variable $\ddot{\phi}$ is kept under control.

In general, morphing can be characterized based on the characteristic of hexarotor variable geometric arms. In the morphing state, it can generally be accomplished by shortening and lengthening the arm lengths. Morphing can affect both its mission and mission change on the UAV[4]. Morphing is a newly introduced developmental feature in UAVs. With morphing, a hexarotor can provide flight in the desired type of mission, more efficient and efficient flight can be achieved, more payloads can be carried and battery savings can be achieved by changing the hexarotor arm length according to the battery status.

In this study, a hexarotor was morphed and the effect of morphing states on lateral flight was investigated. Since changes (elongation and shortening) occur on the hexarotor arm lengths with morphing, it will have effect on the aerodynamic structure. Since the distances to the hexarotor rotation axis change with morphing, there will also be changes on the moments of inertia. Changes on the moment of inertia directly affect the equations of motion. The following figure shows the hexarotor initial state and morphing state.

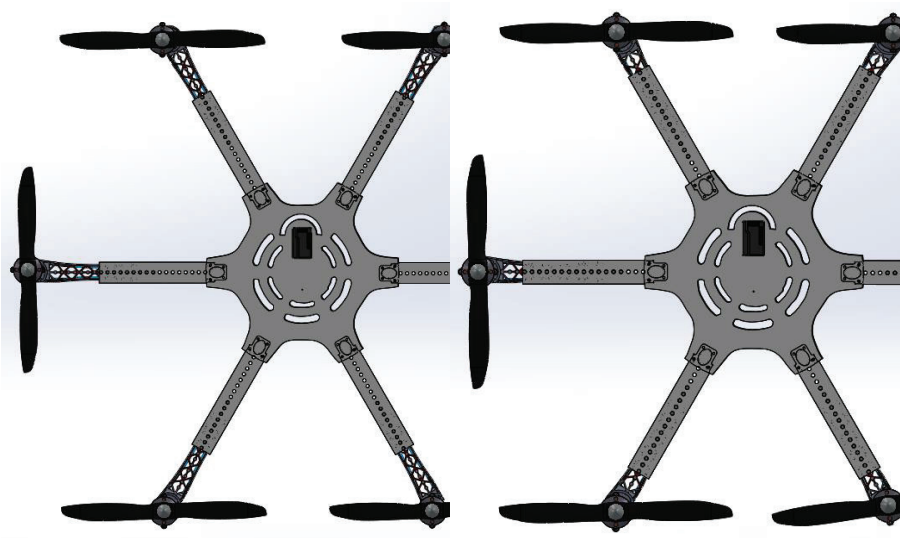

(a) (b)

Figure 2. (a) Hexarotor, (b) Hexarotor morphing

The hexarotor has one fixed outer arm on each arm and an inner arm that moves within the hexarotor outer arm. The hexarotor inner arm performs the morphing process by moving back and forth inside the outer arm. Hexarotor arms extend or shorten by 1.5 cm with each morphing step, so each morphing step is 1.5 cm. Hexarotor starts its flight with an arm length of 41.4 cm in its initial state. Hexarotor arms reach 51.9 cm in length when fully extended, and 30.9 cm when fully extended. In the hexarotor initial state, the inner arms are positioned at the midpoint of the outer arms, as there may be a case of shortening the arms in the initial state. The mass does not change in its initial and morphing states and is 1812 g. Hexarotor mass includes equipment such as controller, battery, GPS, GPS foot, ESC, motor, hexarotor body.

In the morphing state, there will be a change in the moment of inertia as the distances of the arm lengths from the hexarotor center of mass, which is the axis of rotation, change[5]. The moment of inertia on the x, y and z axes can be written as follows.

$$I = \begin{bmatrix} I_x & 0 & 0 \\ 0 & I_y & 0 \\ 0 & 0 & I_z \end{bmatrix} \tag{9}$$

Control System and Deep Neural Networks

In this study, PID control is used to control the hexarotor. PID control is a control algorithm used in linear systems today[6]. As shown in the figure, the PID control uses the tuning parameters K_p, K_i and K_d, and it is easy to adjust for the linear system with these parameters. The PID algorithm is preferred due to its simplicity of construction. However, the PID algorithm can give bad results in extremely non-linear structures such as quadrotor and hexarotor, so the model to be controlled should either be simplified or linearized[7].

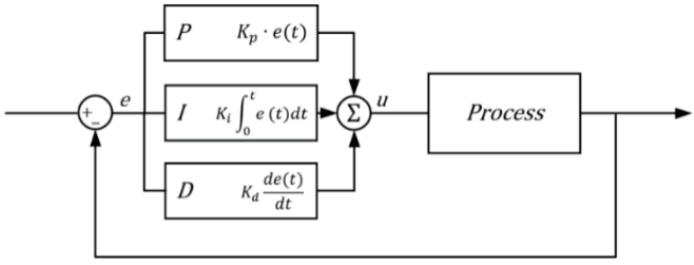

Figure 3. PID structure

The PID control equation form is as follows.

$$u(t) = K_p\, e(t) + K_i \int_0^t (t)d(t) + K_d\, de(t)/d(t) \qquad (10)$$

With advances in hardware and big data, more advanced computational methods have become popular[8]. At the intersection of statistics, mathematics, and computer science, machine learning is gaining momentum by designing algorithms that iteratively improve their own behavior. Deep neural network applications is a subfield of machine learning devoted to creating algorithms that explain and learn from high and low level data abstractions that traditional machine learning algorithms often fail to do[9]. Deep learning algorithms not only have the ability to predict and classify, but they can also learn different levels of complexity. An example of this is that a neural network has

eyelashes, faces, people, etc. It is found in image recognition on which recognition is built.

The structure of deep learning models is usually such that they have layers of nonlinear units that process data or neurons, and the multiple layers in these models process different levels of abstraction of the data[10]. The figure below shows a visualization of the layers of neural networks.

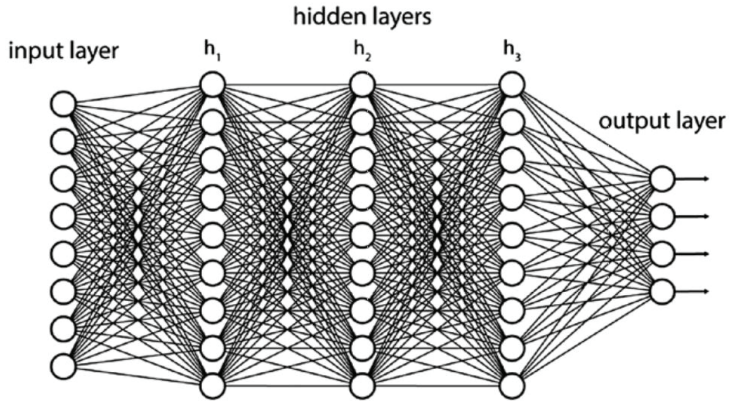

Figure 4. Layered node structure

Deep neural networks are distinguished by having many hidden layers, called "hidden" because it is not obvious what the inputs and outputs of these neurons are beyond knowing that they are the outputs of the previous layer.

In this paper, hexarotor moments of inertia (I_x, I_y, and I_z) and PID control parameters (K_p, K_i and K_d) were determined by deep neural network for lateral flight. Since the hexarotor arm length changes in each morphing state, the hexarotor moment of inertia and PID control parameters also change accordingly. It is difficult to find every time with analytical methods. For this, 15 models of hexarotor have been drawn, including initial and morphing states. Moments of inertia were taken from these models and PID coefficients were determined. The data of 15 models were used for deep neural network training. 70% of the data is used for training and 30% for validation. Deep neural network has 2 hidden layers. While there are 10 neurons in the 1st hidden layer, there are

5 neurons in the 2nd hidden layer. Deep neural network structure is shown below.

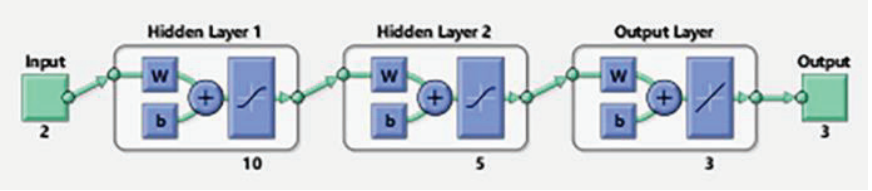

Figure 5. Deep Neural Network structure

In this study, the algorithm created runs 5 iterations and 6 iterations are taken into account, including the initial state. At each iteration, the algorithm randomly predicts a value between -100 and +100. This value determines whether the arm is extended or shortened. Values between 0 and -100 give the value that the arm should shorten as a percentage, while values between 0 and +100 give the amount that the arm should lengthen in percent. In its initial state, the hexarotor inner arms are positioned at the midpoint of the outer arms and are 41.4 cm long. Here is the amount of 10.5 cm lengthening and shortening of the arm. In addition, when the arm is shortened, the amount of elongation increases and when it is extended, the amount of shortening increases. In the next iteration, the elongation and shortening of the arm are calculated over the new values. For example, if +50 is predicted by the algorithm in the first iteration, the new values will be as follows.

- $Random\ Value = 50$
- $Arm_{Elongation} = 10.5$
- $Arm_{Shortening} = 10.5$
- $Arm_{Length} = 30.9$
- $New\_Arm_{Shortening} = Arm_{Elongation} + (Arm_{Shortening} * Random\ Value/100)$
- $New\_Arm_{Elongation} = Arm_{Elongation} - (Arm_{Elongation} * Random\ Value/100)$
- $Arm_{Length} = Arm_{Length} + New\_Arm_{Elongation}$
- $[Moment\ of\ Inertia,\ PID\ Coefficient] = Deeep\_Neural\_Network(Arm_{Length})$

The new arm length(Arm_{Length}) found by the algorithm is sent into the deep neural network. By providing learning with 15 previously defined data, the moment of inertia and PID control parameter of the new arm length are obtained. In each iteration, these operations are repeated to find new values for each morphing state. Thus, the most appropriate moment of inertia and PID coefficients are obtained for each hexarotor morphing state.

Result and Discussion

The values determined randomly by the algorithm are shown in the figure below.

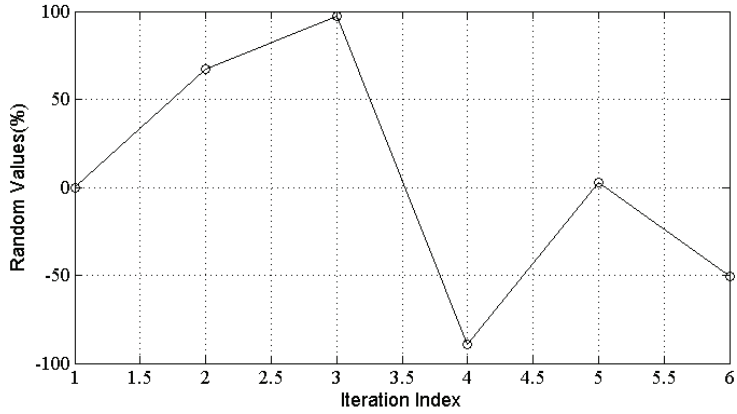

Figure 6. Random values

The variation of hexarotor arm lengths according to random values is shown in the figure below.

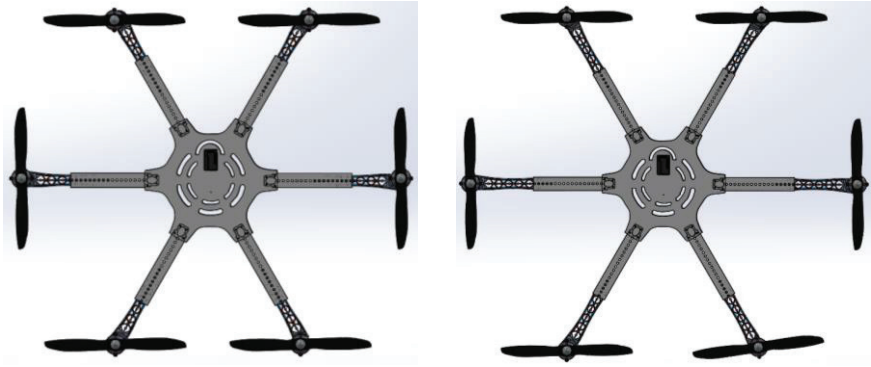

(a) (b)

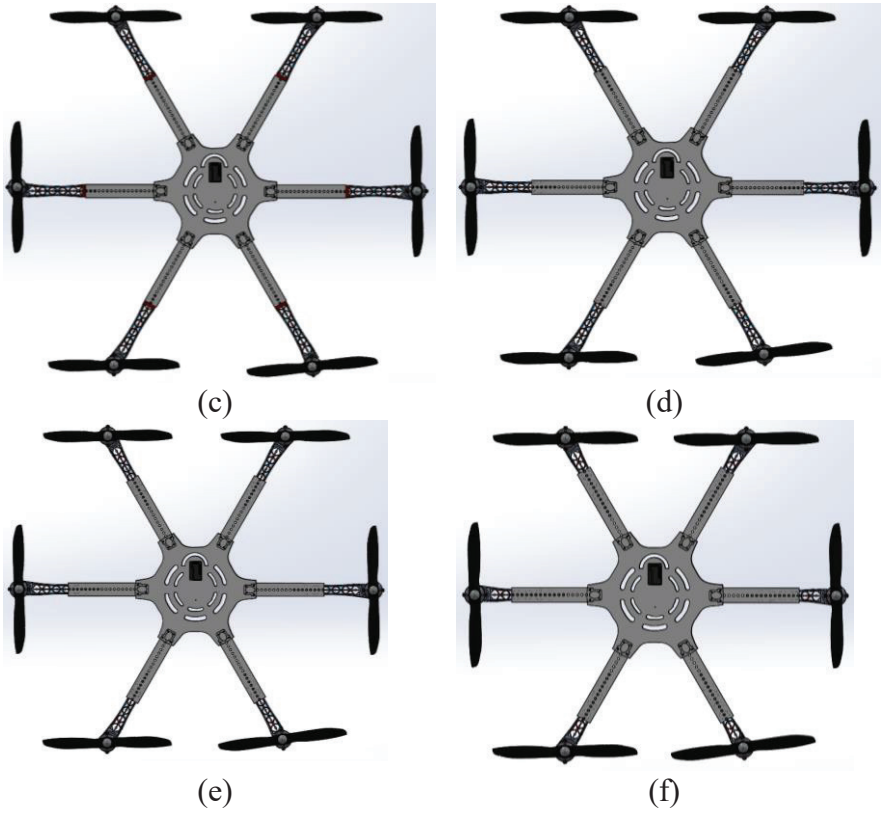

Figure 7. Hexarotor arm change

The new arm lengths calculated according to the random values are shown in the figure below.

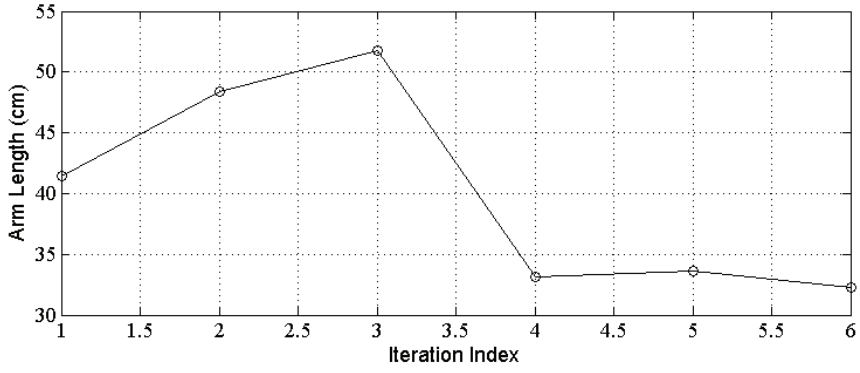

Figure 8. Arm length according to random values

The graph showing the remaining elongation and shortening at the end of each iteration is shown below.

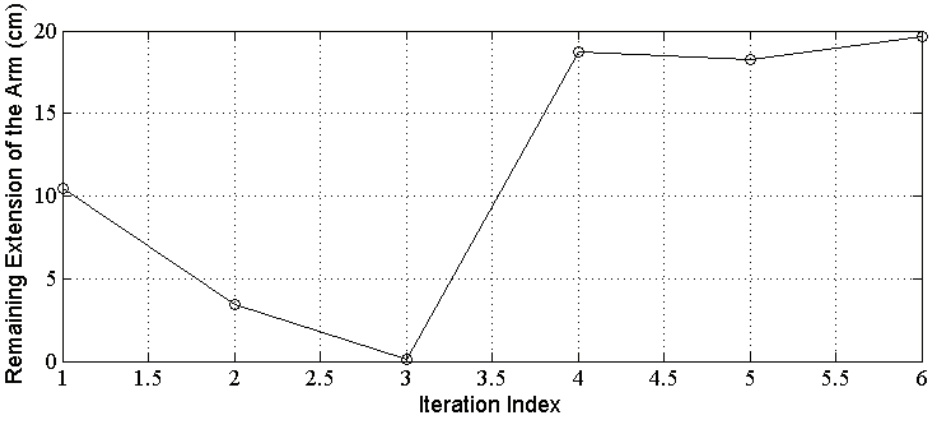

(a)

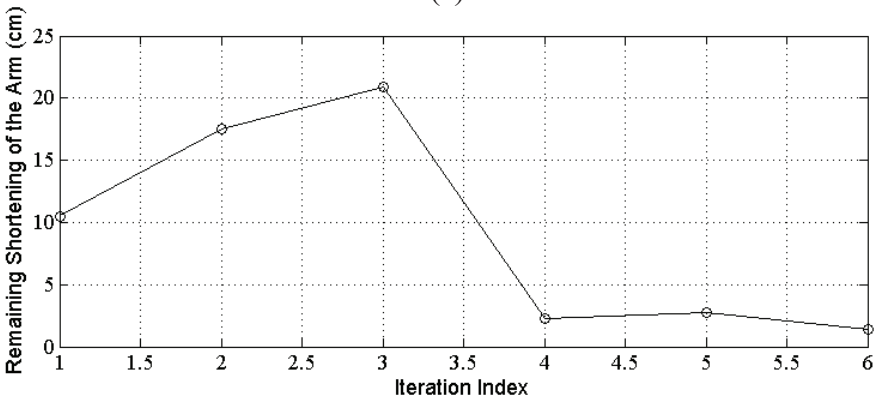

(b)

Figure 9. (a) Extension, (b) Shortening

In each iteration, the arm length is redetermined according to the random value and the arm length is get to the Deep Neural Network function. The function performs the learning process according to the previously determined data and determines the new moment of inertia and PID coefficients according to the incoming arm length value. Moment of inertia and PID control parameter obtained in each iteration are shown in the figure below.

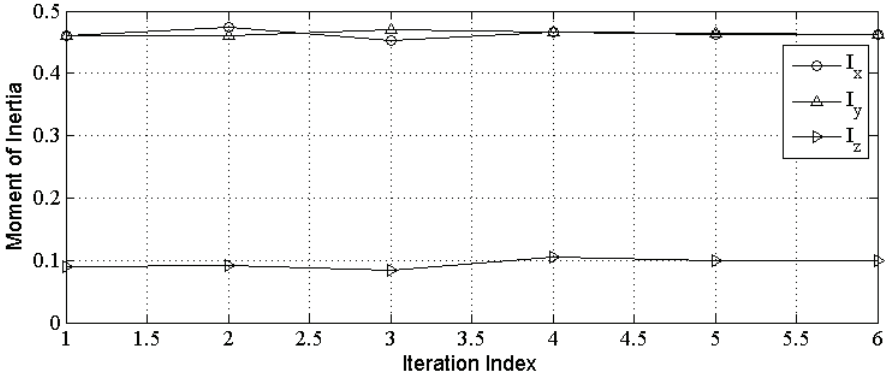

(a)

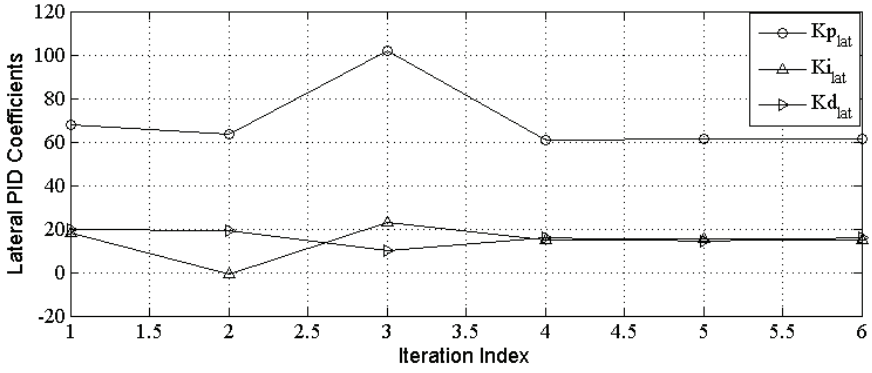

(b)

Figure 10. (a) Moment of inertia, (b) PID control parameter

Lateral flight simulations were performed in Matlab/Simulink environment according to the moment of inertia and PID control paratmeter obtained from the Deep Neural Network function. Flight simulations for each iteration are given in the figure below.

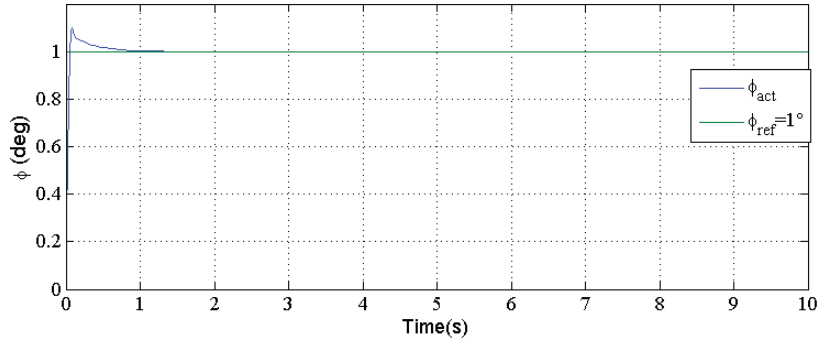

(a)

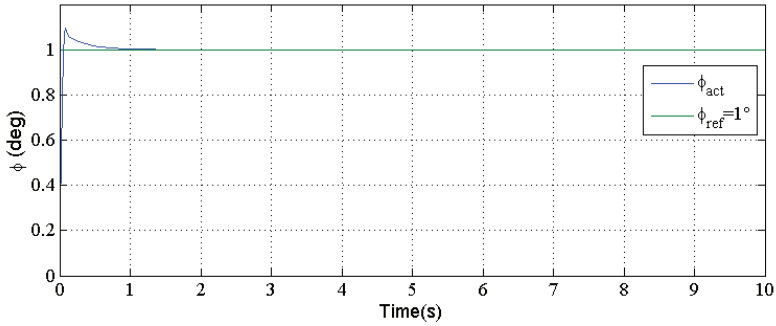

(b)

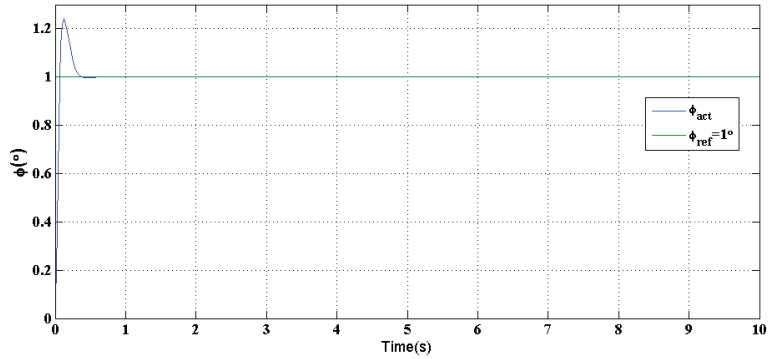

(c)

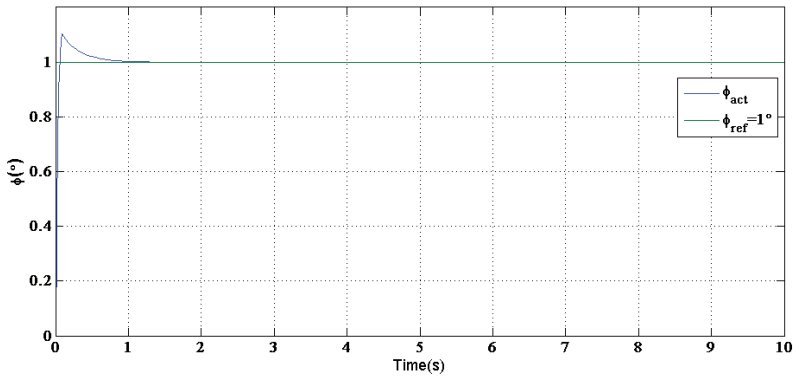

(d)

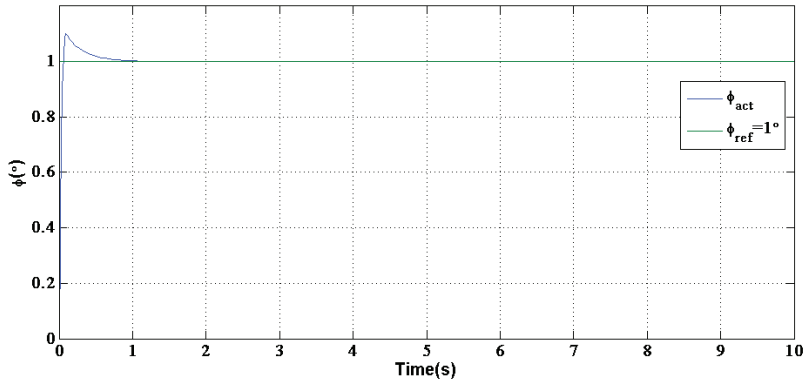

(e)

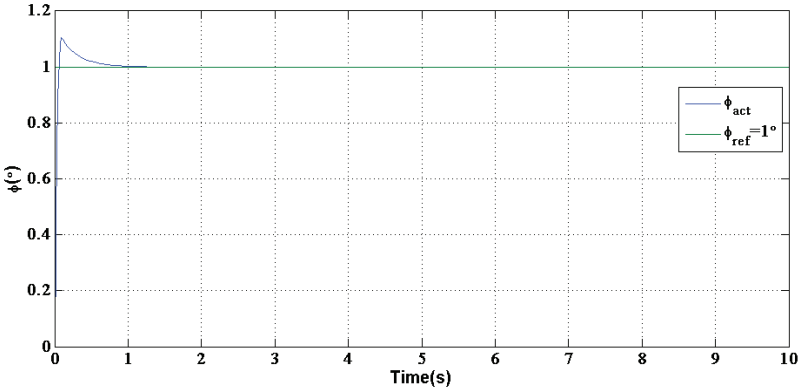

(f)

Figure 11. Simulation result

Conclusions

This article discusses the effect on hexarotor sideways flight. The Hexarotor mathematical model was created using the Newton-Euler approach. However, since it is difficult to apply a control algorithm to the non-linear model, the mathematical model has been converted to linear equations. In the case of morphing, there will be a change in the moment of inertia as the hexarotor arm lengths change and the distance from the rotation axis changes. Since hexarotor structural changes occur with morphing, the PID coefficients, which are the control algorithms, need to be updated in every morphing situation. Updating both the moment of inertia and the PID coefficients according to the morphing state is difficult to obtain with analytical methods. In this part, Deep Neural Network is used as a solution. 15 models were drawn in Solidworks

program for Deep Neural Network. Moments of inertia were obtained from these models. In addition, the control algorithm PID coefficients were determined separately for 15 models. Obtained parameters were used for Deep Neural Network training. 70% of the data was used for training and the remaining 30% was used for validation. Moment of inertia and PID coefficients are simulated for lateral flight in Matlab/Simulink environment according to the amount of extension or shortening determined randomly. In the simulations, it was observed that the morphing state had an effect on the lateral flight. The effect was determined by both the simulation results and the design performance criteria.

	1	**2**	**3**	**4**	**5**	**6**
Rise time	0.0309 sec	0.0206 sec	0.0455 sec	0.0379 sec	0.0411 sec	0.0381 sec
Settling time	0.452 sec	0.201 sec	0.308 sec	0.501 sec	0.498 sec	0.498 sec
Overshoot	10.2 %	13.7 %	24.5 %	10.2 %	11.4 %	10.4 %

References

[1] M. Walid, N. Slaheddine, A. Mohamed, and B. Lamjed, "Modelling, identification and control of a quadrotor UAV," *2018 15th Int. Multi-Conference Syst. Signals Devices, SSD 2018*, no. October, pp. 1017–1022, 2018, doi: 10.1109/SSD.2018.8570512.

[2] O. Kose and T. Oktay, "Investigation of the Effect of Differential Morphing on Forward Flight by Using PID Algorithm in Quadrotors," *J. Aviat.*, vol. 4, no. 1, pp. 15–21, 2020.

[3] D.-K. Le and T.-K. Nam, "A study on the modeling of a hexacopter," *J. Korean Soc. Mar. Eng.*, vol. 39, no. 10, pp. 1023–1030, Dec. 2015, doi: 10.5916/jkosme.2015.39.10.1023.

[4] M. a Erbil, S. D. Prior, M. Karamanoglu, S. Odedra, C. Barlow, and D. Lewis, "Reconfigurable Unmanned Aerial Vehicles," *Cormorant*, no. June 2014, pp. 7–11, 2009.

[5] T. Oktay and O. Kose, "Simultaneous quadrotor autopilot system and collective morphing system design," *Aircr. Eng. Aerosp. Technol.*, vol. 92, no. 7, pp. 1093–1100, 2020, doi: 10.1108/AEAT-01-2020-0026.

[6] T. Oktay and S. Coban, "Simultaneous longitudinal and lateral flight control systems design for both passive and active morphing TUAVs," *Elektron. ir Elektrotechnika*, vol. 23, no. 5, pp. 15–20, 2017, doi: 10.5755/j01.eie.23.5.19238.

[7] O. Kose and T. Oktay, "Investigation of the Effect of Differential Morphing on Lateral Flight by Using PID Algorithm in Quadrotors," *Eur. J. Sci. Technol.*, no. 18, pp. 636–644, 2020, doi: 10.31590/ejosat.702727.

[8] H. Zhang, C. Cao, L. Xu, and T. A. Gulliver, "A UAV Detection Algorithm Based on an Artificial Neural Network," *IEEE Access*, vol. 6, pp. 24720–24728, 2018, doi: 10.1109/ACCESS.2018.2831911.

[9] S. Back, G. Cho, J. Oh, X. T. Tran, and H. Oh, "Autonomous UAV Trail Navigation with Obstacle Avoidance Using Deep Neural Networks," *J. Intell. Robot. Syst. Theory Appl.*, vol. 100, no. 3–4, pp. 1195–1211, 2020, doi: 10.1007/s10846-020-01254-5.

[10] Z. Fan, J. Lu, M. Gong, H. Xie, and E. D. Goodman, "Automatic Tobacco Plant Detection in UAV Images via Deep Neural Networks," *IEEE J. Sel. Top. Appl. Earth Obs. Remote Sens.*, vol. 11, no. 3, pp. 876–887, 2018, doi: 10.1109/JSTARS.2018.2793849.

Chapter 4

VARIATION OF ELECTRICAL RESISTIVITY PROPERTIES OF BULK $BI_{2.1}SR_{2.0}CA_{1.1}CU_{2.0}O_Y$ SUPERCONDUCTING MATERIALS

Asaf Tolga ULGEN[1]

Mahir GULEN[2]

Yusuf ZALAOGLU[3]

1 Assoc.Prof, Sirnak University, Department of Electric-Electronic Engineering, Sirnak–Turkey, 73000 Orcid ID 0000-0002-7112-5607

2 Dr. Bartın University, Department of Mechanical Engineering, Bartın-Turkey, 74110 Orcid ID 0000-0002-6001-8494

3 Assoc. Prof, Osmaniye Korkut Ata University, Department of Physics, Osmaniye–Turkey Orcid: 0000-0003-2191-8112

1. Introduction

Increase in people's understanding of global energy consumption gradually rises depending upon the technological developments and population growth rate. That's exactly why, we require new scientific approaches to overcome the problematic concepts; namely, the energy production and consumption, energy protection, energy conservation, resource conservation and electricity demand. Of the scientific approaches, the energy management founded on the efficient use of energy (do more work with existing same energy or do the same work with less energy) is a newfound science and is used to balance between the energy production and energy consumption with the aid of three main objectives: These are the resource conservation, energy conservation, climate protection and cost savings, respectively. On this basis, the energy management policy based on the efficient energy use is aimed to logically decrease the required energy amount in the production and services so that the human beings can improve the energy efficiency as much as possible and especially protect the climate change [1]. That is to say, the scientific approaches associated with the energy production and consumption are related to the energy management, energy efficiency, energy protection, resource conservation and environmental management.

Particularly, the efficient use of energy takes an important place in the electricity and power systems. Accordingly, the energy loses related to the ohmic resistivity or energy dissipation play a crucial role in the energy consumption problems. In this regard, the uses of superconducting materials (especially type-II ceramic compounds with superior features such as larger current and magnetic field carrying ability, lower power consumption and energy losses) provides a serious motivation on the energy management policy. In other words, preference of superconducting ceramic compounds with very higher critical transition temperatures, thermodynamic stability, magnetic field and current carrying ability in the usage of metallurgical, electro-optic, network system, future cryo/refrigeration, spintronics, power transmission cable, innovative energy infrastructure, medical diagnosis, hydrogen society, sensitive process control, nuclear and particle physics, heavy-industrial technology and advanced engineering application

fields [2–8] seems to be a global solution to limit the energy consumption and ecological problems. Even, the scientists have extensively studied on the materials sciences in all areas to overcome the energy management policy and human health [9–16].

As for the superconducting materials preferred in the application fields, the dc electrical properties become a leader to determine that where the superconducting material can be used. Thus, in the current work, the influence of various cadmium molar addition amount ($0.0 \leq x \leq 0.30$) on the basic dc electrical resistivity properties including the dc electrical resistivity at room temperature (ρ_{300K}), electrical resistivity at 90 K (ρ_{90K}), residual resistivity (abbreviated as ρ_{res}), residual resistivity ratio (shown as *RRR*) and $\Delta\rho$ (subtraction of ρ_{300K} and ρ_{90K}) for the bulk $Bi_{2.1}Sr_{2.0}Ca_{1.1}Cu_{2.0}O_y$ superconducting ceramic structure is thoroughly examined by using the temperature-dependent dc resistivity tests (ρ-T). According to the experimental measurement results gathered, it is obtained that the cadmium impurity addition damages seriously the main conduction properties of $Bi_{2.1}Sr_{2.0}Ca_{1.1}Cu_{2.0}O_y$ (Bi-2212) superconducting ceramic material.

2. Experimental details for Cadmium Added $Bi_{2.1}Sr_{2.0}Ca_{1.1}Cu_{2.0}O_y$ Superconducting Compounds

In the present study, the bulk $Bi_{2.1}Sr_{2.0}Ca_{1.1}Cu_{2.0}Cd_xO_y$ ceramic compounds are prepared within the different cadmium molar ratios between $0.0 \leq x \leq 0.30$ by the conventional solid-state reaction method. For the production of $Bi_{2.1}Sr_{2.0}Ca_{1.1}Cu_{2.0}Cd_xO_y$ materials, the high purity oxide and carbonate chemicals such as CdO, $SrCO_3$, CuO, Bi_2O_3, and $CaCO_3$ are used. Initially, all the chemicals are separately weighed by the electronic balance to produce the superconducting materials within the required stoichiometric ratios. Thus, a total of approximately 3 mg of chemicals is obtained.

The mixture of powder is further ground by a grinder in an agate mortar for 1 hour in atmospheric pressure conditions. The homogenous mixed chemicals are subjected to the pre-heating calcination processes at the temperature of 800 °C for 36 hours in the furnace with the heating rate of 5 °C/min. After right, the samples calcined are cooled down the room temperature with the cooling rate of 5 °C/min. The mixture of powders is removed from the furnace

and is separately re-ground by a grinder for 1 hour in the agate mortar. The re-milled powder is pelletized into the solid bars with sizes of 1.5x0.5x0.2 cm^3 by means of 300 MPa force in the normal atmospheric pressure conditions so that the interaction between the superconducting grains can be improved as much as possible, and the opening between layers, defects and voids can be extensively reduced in the crystal system. The pelletized samples are exposed to the sintering process at the temperature of 850 °C for 24 h duration. The bulk $Bi_{2.1}Sr_{2.0}Ca_{1.1}Cu_{2.0}Cd_xO_y$ ceramic compounds produced within the different molar ratios including x=0, 0.01, 0.03, 0.05, 0.07, 0.10 and 0.30 will hereafter be displayed as the pure and Cd-1, Cd-2, Cd-3, Cd-4, Cd-5 and Cd-6, respectively.

The role of cadmium foreign impurity on the main dc electrical resistivity properties of bulk $Bi_{2.1}Sr_{2.0}Ca_{1.1}Cu_{2.0}Cd_xO_y$ ($0.0 \leq x \leq 0.3$) superconducting samples is experimentally investigated by the conventional four-probe method in the temperature intervals 35 K-180 K in the He closed-cycle cryostat system. During the electrical resistivity versus temperature measurements 5 mA current is applied on the sample surfaces and the measurement signals are taken within the accuracy of ± 0.01 mΩ.cm by means of the programmable nano-voltmeter and current source. Besides, the experimental data are monitored by Labview software program. The experimental findings enable us to define the differentiation of main electrical resistivity quantities such as the dc electrical resistivity at room temperature (ρ_{300K}), electrical resistivity at 90 K (ρ_{90K}), residual resistivity (ρ_{res}), residual resistivity ratio (RRR) and $\Delta\rho$ for the bulk $Bi_{2.1}Sr_{2.0}Ca_{1.1}Cu_{2.0}O_y$ superconducting ceramic structure with the cadmium addition level.

3. Results and discussion

3.1. Variation of Electrical Resistivities of $Bi_{2.1}Sr_{2.0}Ca_{1.1}Cu_{2.0}Cd_xO_y$ Ceramic Compounds with Different Cadmium Impurity Addition Level

In the current study, the change of main electrical resistivity quantities including ρ_{300K}, ρ_{90K}, ρ_{res}, RRR and $\Delta\rho$ parameters as a function of cadmium impurity addition level for the solid $Bi_{2.1}Sr_{2.0}Ca_{1.1}Cu_{2.0}Cd_xO_y$ superconducting ceramic compounds is extensively explored by the temperature-dependent resistivity

measurements executed at the temperature range of 35 K-180 K. All the experimental curves are graphically depicted in Fig.1 a-g.

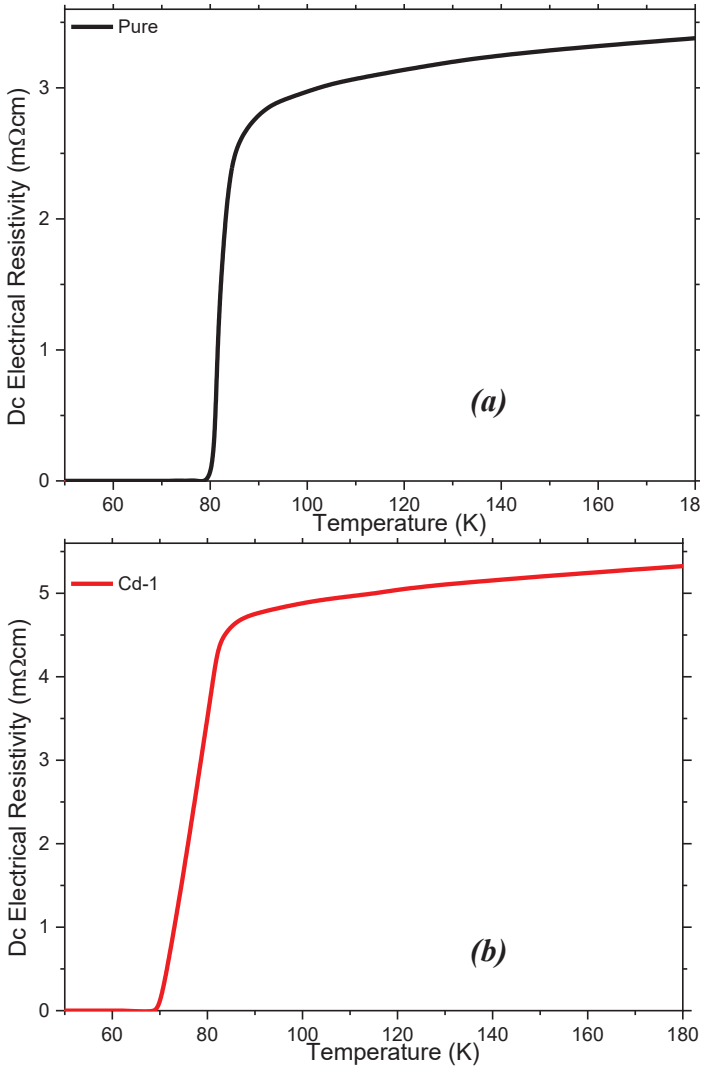

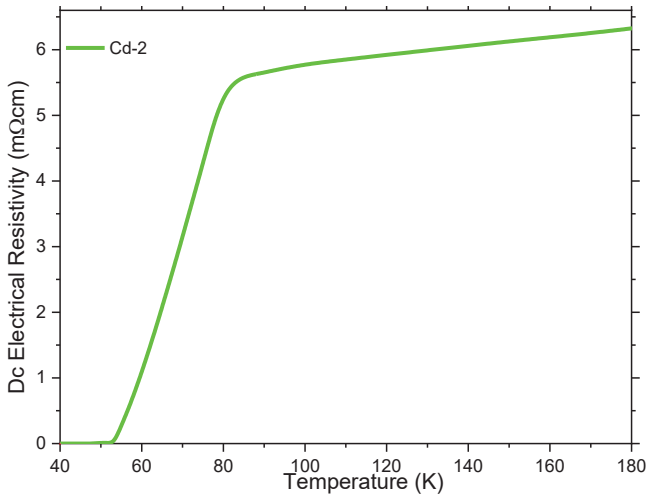
Cd-2
Dc Electrical Resistivity (mΩcm)
Temperature (K)
0
1
2
3
4
5
6
40
60
80
100
120
140
160
180

(c)

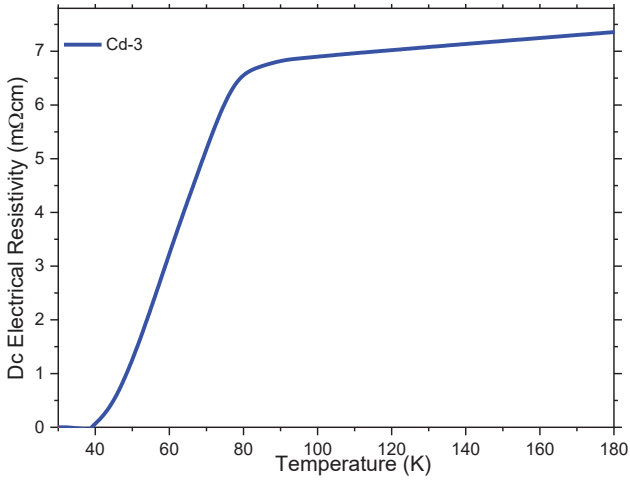
Cd-3
Dc Electrical Resistivity (mΩcm)
Temperature (K)
0
1
2
3
4
5
6
7
40
60
80
100
120
140
160
180

(d)

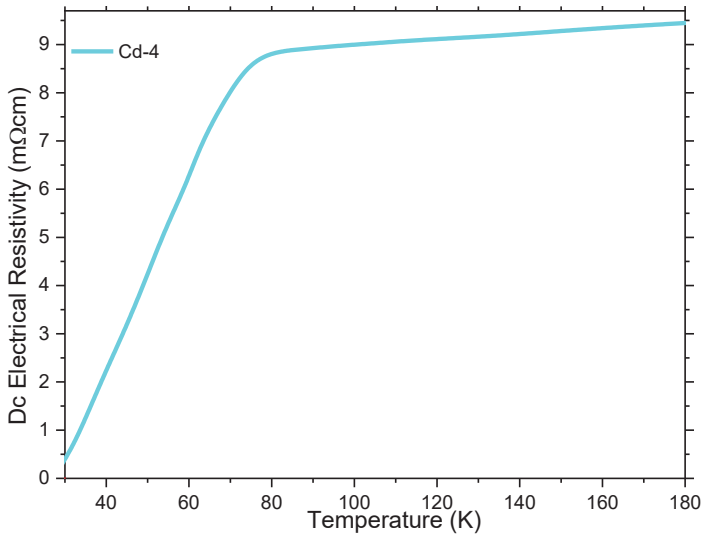
Cd-4
Dc Electrical Resistivity (mΩcm)
Temperature (K)
0
1
2
3
4
5
6
7
8
9
40
60
80
100
120
140
160
180

(f)

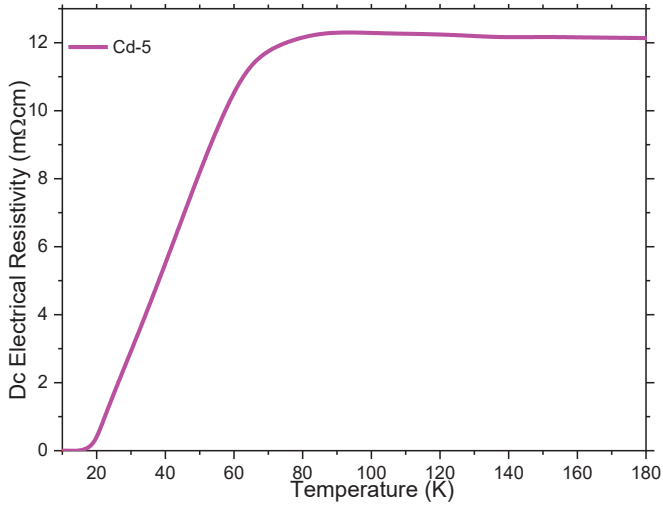
Cd-5
Dc Electrical Resistivity (mΩcm)
Temperature (K)
0
2
4
6
8
10
12
20
40
60
80
100
120
140
160
180

(f)

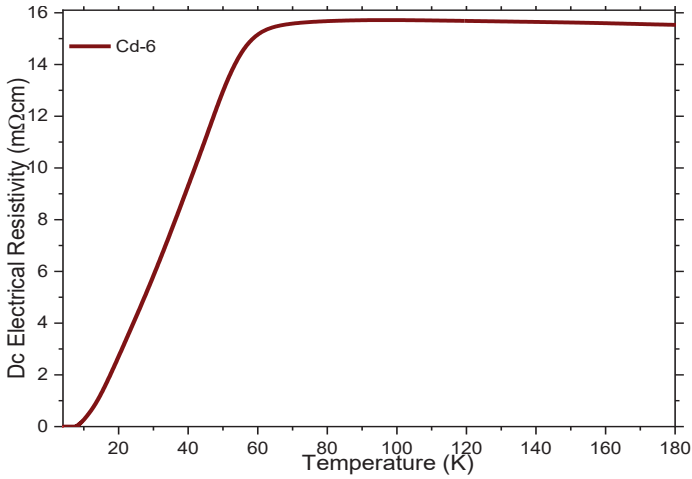

(g)

Figure 1 Variation of dc electrical resistivities of (a) pure, (b) Cd-1, (c) Cd-2, (d) Cd-3, (e) Cd-4, (f) Cd-5 and (g) Cd-6 superconducting materials.

It is obvious from the figure that the dc electrical resistivity curves are found to strongly depend on the cadmium foreign impurity addition level. In this context, it is apparent that the foreign cadmium elements are successfully introduced into the solid $Bi_{2.1}Sr_{2.0}Ca_{1.1}Cu_{2.0}O_y$ superconducting ceramic compound. Moreover, one can see that there seems a change in the main characteristic metallic-like feature. Namely, the polycrystalline $Bi_{2.1}Sr_{2.0}Ca_{1.1}Cu_{2.0}Cd_xO_y$ superconducting materials present the main metallic-like property above the onset critical transition temperature up to the certain cadmium addition level of x=0.07 after which the Cd-5 and Cd-6 sample exhibits the typical insulator behavior. This is because, the increment in the cadmium impurity addition level damages seriously on the main crystal structure of bulk $Bi_{2.1}Sr_{2.0}Ca_{1.1}Cu_{2.0}O_y$ superconducting materials due to the induced permanent crystallinity problems such as the internal/structural defects, edge/screw dislocations, lattice strains, porosity, microscopic/macroscopic cracks, grain boundaries, stacking faults, voids, pores, impurity residues and grain boundary interaction problems in the crystal system [17–19]. Moreover, it is to be mentioned here that the presence of cadmium impurity in the Bi-2212 superconducting matrix leads to remarkably decrease the formation of super-electrons and mobile hole carrier concentrations [20, 21]. Besides, it can be discussed that the existence of cadmium

foreign impurity degrades seriously the logarithmic distribution for the active, dynamic and effective electronic density of states at the vicinity of Fermi energy level [22, 23].

3.2. Room temperature resistivity findings

As for the numerical values, the variation of dc electrical resistivity at room temperature (ρ_{300K}) with the cadmium foreign impurity level takes the first place in this study. One can see all the numerical ρ_{300K} values in Table 1 (deduced from Fig. 1. a-g). It is obvious from the table that there seems a similar trend with the metallic characteristic behavior (constantly decrement trend). Namely, the ρ_{300K} values are found to increase systematically from 3.709 m.Ωcm (for the pure sample) until the value of 15.290 m.Ωcm (for the Cd-6 sample with the maximum cadmium addition level inserted in the superconducting lattice) with the increment in the cadmium foreign impurity level. On this basis, the other cadmium added Bi-2212 compounds display the moderate ρ_{300K} values changing between 5.924 m.Ωcm and 12.221 m.Ωcm. This means that the enhancement of cadmium foreign impurity level in the bulk $Bi_{2.1}Sr_{2.0}Ca_{1.1}Cu_{2.0}O_y$ superconducting system results in both the dramatic degradation in the mobile hole carrier concentrations and increase in the formation of permanent crystallinity problems in the crystal system.

3.3. Effect of Cadmium addition on Residual Resistivity Parameter

In this part of chapter, the approach of Matthiessen's rule is used to determine the change in the residual resistivity parameters of polycrystalline $Bi_{2.1}Sr_{2.0}Ca_{1.1}Cu_{2.0}Cd_xO_y$ superconducting materials with the aid of dc electrical resistivity curves given in Fig. 1.a-g [24]. Namely,

$$\rho(T) = \rho_i(T) + \rho_{res} \quad (1)$$

in the relation, $\rho(T)$ resistivity value is in attribution to total resistivity given at any temperature when $\rho_i(T)$ parameter depends on the temperature. Similarly, the ρ_{res} value presents the residual resistivity and is a temperature independent parameter. In other

words, the ρ_{res} parameter depends on the main crystallinity problems in the crystal system [25]. Accordingly, the parameter is inferred from the dc electrical graphs using the data extrapolation approach. One can see the differentiation of ρ_{res} parameters with the cadmium impurity addition level of bulk $Bi_{2.1}Sr_{2.0}Ca_{1.1}Cu_{2.0}O_y$ ceramic compounds in Table 1. According to the data provided in Table 1, it is clear that the increment of cadmium impurity level causes to increase considerably the ρ_{res} parameters due the rapid enhanced main structural crystallinity problems. Numerically, the un-added compound possesses the minimum ρ_{res} value of 2.578 m.Ωcm while the maximum ρ_{res} value of 15.936 m.Ωcm is noted for the Cd-6 superconducting sample.

The other materials exhibit the moderate values varying from 4.632 m.Ωcm (for the Cd-1 material) until the value of 12.405 m.Ωcm (for the Cd-5 sample). Interestingly, it can be noted here that there appears a dramatic increment in the residual resistivity beyond the cadmium addition level of x=0.07 (Fig. 2).

Table 1. Variation of dc electrical resistivity quantities for pure and cadmium added bulk Bi-2212 ceramic compounds

Materials	ρ_{300K} ***(mΩcm)***	ρ_{res} ***(mΩcm)***	ρ_{90K} ***(mΩcm)***	$\Delta\ \rho\ (\rho_{300K} - \rho_{90K})$ ***(mΩcm)***	***RRR*** (ρ_{300K}/ρ_{90K})
Pure	3.709	2.578	2.835	0.874	1.308
Cd-1	5.924	4.632	4.752	1.172	1.247
Cd-2	7.099	5.161	5.775	1.324	1.229
Cd-3	8.267	6.265	6.874	1.393	1.203
Cd-4	10.311	8.532	8.762	1.549	1.177
Cd-5	12.221	12.405	12.298	-0.077	0.994
Cd-6	15.290	15.936	15.741	-0.451	0.971

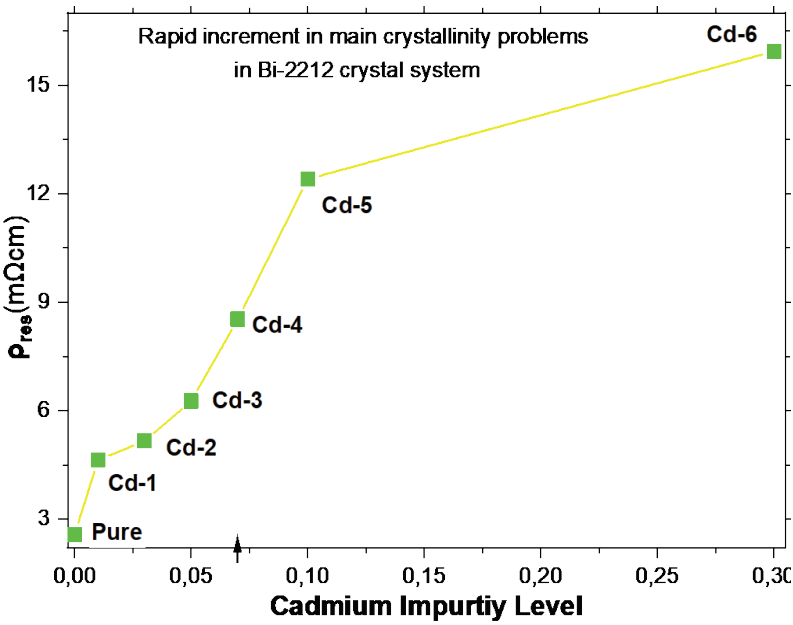

Figure 2 Variation of residual resistivity with cadmium addition level for polycrystalline $Bi_{2.1}Sr_{2.0}Ca_{1.1}Cu_{2.0}Cd_xO_y$ superconducting materials.

3.4. Change of ρ_{90K} Parameter with Cadmium Addition Level

The dc electrical resistivity at 90 K is directly associated with the impurity scattering and formation of lattice strains in the crystal structure for the bulk Bi-2212 superconducting crystal system. The ρ_{90K} parameter is semi-empirically deduced from the transition of intragranular regions from the superconducting state into the normal state. We depict all the computations related to ρ_{90K} parameters of bulk $Bi_{2.1}Sr_{2.0}Ca_{1.1}Cu_{2.0}Cd_xO_y$ ceramic compounds in Table 1. As seen from the table, the ρ_{90K} parameter for the Bi-2212 superconducting system is observed to harshly increase depending on the cadmium impurity addition level. Numerically, the un-added material has the smallest ρ_{90K} value of 2.835 m.Ωcm; on the other hand, the Cd-6 sample with the largest dopant obtains the highest ρ_{90K} value of 15.741 m.Ωcm. The other ones possess the moderate ρ_{90K} values varying between 4.752 m.Ωcm and 12.298 m.Ωcm. Thus, it can be discussed that the increment in the cadmium impurity in the bulk Bi-2212 superconducting crystal structure

leads to dramatically increase the impurity scattering and lattice strains.

3.5. Effect of Cadmium Impurities on RRR Parameters of Bi-2212 Crystal System

This part of chapter focuses directly on the Bi-2212 material quality [26] defining the residual resistivity ratio depending on the ratio between two valuable resistivity results (ρ_{300K} and ρ_{90K}). One can see all the calculations about the *RRR* values in Table 1. It is apparent from the table that the material quality (*RRR* parameter) is found to be affected by the cadmium impurity addition level. The pure sample possesses the highest *RRR* value of 1.308 whereas the smallest *RRR* value of 0.971 ascribes to the bulk Cd-6 superconducting sample. Besides, the Cd-1, Cd-2, Cd-3, Cd-4 and Cd-5 compounds exhibit the *RRR* values of 1.247, 1.229, 1.203, 1.177 and 0.994, respectively. All the findings show clearly that the increment trend in the cadmium impurity addition level damages seriously on the Bi-2212 material quality.

3.6. Δρ parameter findings

$\Delta\rho$ parameter is another parameter that is interested in the formation of structural crystallinity disorders and defects in the Bi-2212 superconducting crystal system. The parameter is known to depend sensitively on the dopant mechanism and preparation condition. Mathematically, the parameter of $\Delta\rho$ is determined from the differentiation between ρ_{300K} and ρ_{90K} parameters. One can see the effect of cadmium impurity addition on the $\Delta\rho$ parameters of $Bi_{2.1}Sr_{2.0}Ca_{1.1}Cu_{2.0}O_y$ superconducting system in Table 1. It is visible form the table that the $\Delta\rho$ value is strongly changed depending on the dopant addition level. On this basis, the $\Delta\rho$ parameter is found to increase monotonously from 0.879 m.Ωcm (for the pure sample) to 1.549 m.Ωcm (for the Cd-4 sample) up to the cadmium addition level of x=0.07 beyond which the value is observed to be negative (-0.077 m.Ωcm for the Cd-5 sample and -0.451 m.Ωcm for the bulk Cd-6 compound). This is attributed to the fact that the critical cadmium addition level of x=0.07 totally damages on the structural crystallinity quality (depending on the increment in the disorders and defects) in the Bi-2212

superconducting crystal system. To sum up, all the experimental measurement results reveal that the presence of cadmium impurity addition harms seriously the main electrical resistivity results.

4. Conclusion

In the present work, a strong relationship between the main electrical resistivity and permanent structural crystallinity problems is developed for the solid $Bi_{2.1}Sr_{2.0}Ca_{1.1}Cu_{2.0}O_y$ superconducting ceramic compounds with the assistant of temperature-dependent electrical resistivity measurements exerted in the temperature intervals of 35 K-180 K. The polycrystalline Bi-2212 materials are prepared by the standard solid-state reaction method at the temperature of 850 °C for 24 h sintering time. The experimental electrical resistivity curves allow us to define the role of cadmium impurity addition level on the dc electrical resistivity at room temperature, electrical resistivity at 90 K, residual resistivity, residual resistivity ratio and $\Delta\rho$ for the bulk $Bi_{2.1}Sr_{2.0}Ca_{1.1}Cu_{2.0}O_y$ superconducting ceramic structure. the experimental findings show that all the characteristic electrical resistivity parameters are observed to significantly depend on the cadmium impurity level. This fact illustrates that the cadmium impurities are successfully entered into the solid $Bi_{2.1}Sr_{2.0}Ca_{1.1}Cu_{2.0}O_y$ superconducting ceramic matrix. Moreover, it is observed that the dc electrical resistivity quantities are found to reduce significantly due to the induced permanent structural crystallinity problems in the Bi-2212 crystal matrix. It is to be mentioned here that there is a critical addition point such as x=0.07 above which the cadmium added Bi-2212 superconducting materials exhibit the typical insulator behavior. Similarly, after the critical addition level there appears a dramatic change in the residual resistivity and $\Delta\rho$ parameters. Namely, after the certain cadmium addition level of x=0.07 much more permanent structural crystallinity problems appear in the crystal structure, and it can be added that the Cd-6 sample with the maximum cadmium addition level inserted in the superconducting lattice is noticed to be the worst material.

Acknowledgement: This work was supported by the Sirnak University Scientific Research Project Coordination Unit (Project Number: 2019.FNAP.06.02.01)

References

[1] A.T. Ulgen, T. Turgay, C. Terzioglu, G. Yildirim, M. Oz, Role of Bi/Tm substitution in Bi-2212 system on crystal structure quality, pair wave function and polaronic states, J. Alloy. Compd. 764 (2018) 755–766.
[2] H.H. Xu, L. Cheng, S.B. Yan, D.J. Yu, L.S. Guo, X. Yao, Recycling failed bulk YBCO superconductors using the NdBCO/YBCO/MgO film-seeded top-seeded melt growth method,
J. Appl. Phys. 111 (2012) 103910.
[3] K.Y. Choi, I.S. Jo, S.C. Han, Y.H. Han, T.H. Sung, M.H. Jung, G.S. Park, S.I. Lee, High and uniform critical current density for large-size $YBa_2Cu_3O_{7-\delta}$ single crystals, Curr. Appl. Phys. 11 (2011) 1020–1023.
[4] G. Yildirim, Determination of optimum diffusion annealing temperature for Au surface-layered Bi-2212 ceramics and dependence of transition temperatures on disorders, J. Alloy. Compd. 699 (2017) 247–255.
[5] T.A. Coombs, A finite element model of magnetization of superconducting bulks using a solid-state flux pump, IEEE T. Appl. Supercond. 21 (2011) 3581–3586.
[6] F.N. Werfel, U. Floegel-Delor, R. Rothfeld, T. Riedel, B. Goebel, D. Wippich, P. Schirrmeister, Superconductor bearings, flywheels and transportation, Supercond. Sci. Technol. 25 (2012) 014007.
[7] W. Buckel, R. Kleiner, Superconductivity: Fundamentals and Applications, 2nd ed., Wiley-VCH Verlag, Weinheim, (2004).
[8] A.T. Ulgen, G. Yildirim, Gece Kitapligi, Change in Key Mechanical Design Quantities of Bi-2212 Superconducting System with Various Annealing Ambient, pp. 331-349, Ankara, Turkey
[9] P.M. Sarun, S. Vinu, R. Shabna, A. Biju, U. Syamaprasad, Microstructural and superconducting properties of Yb-substituted (Bi, Pb)-2212 superconductor sintered at different temperatures, J. Alloy. Compd. 472 (2009) 13–17.
[10] D. Marconi, G. Stiufiuc, A.V. Pop, Effect of partial substitution of Ca by 4f elements on dissipative processes in Bi:2223 superconductors, Journal of Physics Conference Series 153 (2009) 012022.
[11] R. Awad, A.I. Abou-Aly, M.M.H. Abdel Gawad, I. G-Eldeen, The influence of SnO_2 nano-particles addition on the vickers microhardness of (Bi, Pb)-2223 superconducting phase, J. Supercond. Nov. Magn. 25 (2012) 739–745.
[12] A. Ates, Zeminlerinin Sivilaşma Potansiyelinin Arazi Ve Laboratuvar Deneyleri Ile Araştirilmasi, Institution of Economic Development and Social Researches Publications, 1st Ed., 2020.
[13] M. Sahoo, D. Behera., Effect of Ti Doping on Structural and Superconducting Property of YBa2Cu3O7−y High Tc Superconductor J Supercond Nov Magn (2014) 27:83–93
[14] R. Shabna, P.M. Sarun, S. Vinu, U. Syamaprasad, Charge carrier localization and metal to insulator transition in cerium substituted (Bi,Pb)-2212 superconductor, J. Alloy. Compd. 493 (2010) 11–16.
[15] S. Vinu, P.M. Sarun, A. Biju, R. Shabna, P. Guruswamy, U. Syamaprasad, The effect of substitution of Eu on the critical current density and flux pinning properties of (Bi, Pb)-2212 superconductor, Supercond. Sci. Technol. 21 (2008) 045001–045005.

[16] Razia, S., Murikoli, S. P., Surendran, V., & Upendran, S. (2009). Doping dependent metal to insulator transition in the (Bi, Pb)-2212 system: The evolution of structural and electronic properties with europium substitution. *Chinese Physics B*, *18*(9), 4000.
[17] Erdem, U., Zalaoglu, Y., Ulgen, A. T., Turgay, T., & Yildirim, G. (2021). Role of trivalent Bi/Tm partial substitution on active operable slip systems in Bi-2212 crystal structure. Cryogenics, 113, 103212.

[18] D.M. Newns, P.C. Pattnaik, C.C. Tsuei, Role of van hove singularity in high-temperature superconductors: Mean field, Phys. Rev. B 43 (1991) 3075–3084.

[19] M.B. Turkoz, S. Nezir, C. Terzioglu, A. Varilci, G. Yildirim, Investigation of Lu effect on $YBa_2Cu_3O_{7-\gamma}$ superconducting compounds, J. Mater. Sci: Mater. El. 24 (2013) 896–905.
[20] M.B. Turkoz, S. Nezir, C. Terzioglu, A. Varilci, G. Yildirim, Investigation of Lu effect on $YBa_2Cu_3O_{7-\gamma}$ superconducting compounds, J. Mater. Sci: Mater. El. 24 (2013) 896–905.
[21] Y. Zalaoglu, G. Yildirim, H. Buyukuslu, N.K. Saritekin, A. Varilci, C. Terzioglu, O. Gorur, Important defeats on pinning of 2D pancake vortices in highly anisotropic Bi-2212 superconducting matrix with homovalent Bi/La substitution, J. Alloy. Compd. 631 (2015) 111–119.
[22] P.B. Allen, W.E. Pickett, H. Krakauer, Anisotropic normal-state transport-properties predicted and analyzed for high-Tc oxide superconductors, Phy. Rev. B 37 (1988) 7482–7490.
[23] A. Ianculescu, M. Gartner, B. Despax, V. Bley, Th Lebey, R. Gavrila, M. Modreanu, Optical characterization and microstructure of $BaTiO_{(3)}$ thin films obtained by RF-magnetron sputtering, Appl. Surf. Sci. 253 (2006) 344–348.
[24] J. Ekin, Experimental techniques for low-temperature measurements: cryostat design, material properties and superconductor critical-current testing, Oxford University Press, New York, (2006).
[25] M. Li, Y. Zhang, Y. Li, Y. Qi, Granular superconductivity in polycrystalline $Bi_2Sr_2CaCu_2O_{8+\gamma}$ by homovalent La substitution on Bi sites, J. Non-Cryst. Solids 356 (2010) 2831–2835.
[26] Kovac, P., Hušek, I., Pachla, W., Melišek, T., Diduszko, R., Fröhlich, K., ... & Machajdik, D. (2002). Structure, grain connectivity and pinning of as-deformed commercial MgB2 powder in Cu and Fe/Cu sheaths. *Superconductor Science and Technology*, *15*(7), 1127.

Chapter 5

CELL CULTURE ON POLYURETHANE NANOFIBROUS SCAFFOLD

Mustafa Özgür ÖTEYAKA [1]

1 Doç.DR.Mustafa Özgür ÖTEYAKA, *Eskişehir Osmangazi University, Eskişehir Vocational School, Department of Electronic and Automation,* moteyaka@ogu.edu.tr, ORCID: 0000-0002-1488-6098.

1. INTRODUCTION

In vitro cancer methods are indispensable methods for working adhesion, proliferation, migration, morphology and metastatic behavior and rapid response of anti-drug agents in cancer. In this manner, research of specific medical treatments can be made without the elaboration of using *in vivo*. In addition, 2D cell cultures on different materials are used to study cancer disease and drug release. But, recent developments showed that 3D environment was more representative compared to 2D (Aoudjit & Vuori, 2001; Celebi Saltik & Öteyaka, 2016; Çelebi-Saltik et al., 2021; Min et al., 2004; Smith & Ma, 2004; Yoshioto et al., 2003). The differences in cell culture between 2D and 3D systems are cell density, receptor expression, cell concentration, signaling between cells and functions of metabolics (Beningo et al., 2004; Knight et al., 2000; Ng et al., 2005; Rhodes et al., 2004). Nanofiber materials have been shown that it improves the cell culture compared to micro scaled fiber materials (Pattison et al., 2005).

Electrospinning technique favor manufacturing of different nanofiber type such as oriented or aligned nanofibers (Bhardwaj & Kundu, 2010; Oteyaka et al., 2014; Sheikh et al., 2011; H Zhuo et al., 2008). The advantage of this scaffold is that they had higher surface areas. These characteristics are particularly useful in biomedical applications as they mimic biological structure and function. Some examples of applications are vascular graft, wound dressing, drug delivery and tissue engineering (Chen et al., 2010).

In drug delivery systems, biocompatible and biodegradable polymers are mostly used to deliver therapeutic agents. They can release the drug in the affected area. Many studies showed that the drugs was enrobed with nanofiber to conduct the drug (Kenawy el et al., 2002; Verreck et al., 2003; Zeng et al., 2003) . For example, Zong et al. (Zong et al., 2002) showed *in vivo* the effectiveness of doped antibiotics (mefoxin) with bioabsorbable poly(L-lactide-co-glycolide) nanofibers (PLGA) in reducing post-surgery adhesion. After lung cancer, breast cancer is the next disease causing deaths in women. For tumor model, the 4T1 breast carcinoma cells were widely employed (Yerlikaya & Erin, 2008). Surgical technique plays an essential act in administration of breast cancer. Xie and Wang (Xie & Wang, 2006) showed the treatment of C6 glioma (brain tumor) using the delivery of an anti-cancer drug (paclitaxel) *in vitro* with micro and nanofiber PLGA. Polyvinyl alcohol (PVA), poly(lactic acid) (PLA) and PLGA are the main polymers tested in drug delivery systems because they are biodegradable and can be electrospun. Before testing a drug *in vivo*, PU nanofibers can be a candidate for rapid time response of anti-drug mechanisms in cancer cell. For this purpose, polyurethane (PU) was electrospun to produce a nanofibrous scaffold by electrospinning technique and systematically examined. To increase sensitivity, the surfaces of the

scaffolds were cleaned with ethanol before and after cell culture. Chemical analysis of nanofibers showed that polyurethane was mainly composed of Carbon (C) and Oxygen (O). X-ray diffraction (XRD) results suggested that PU nanofibers existed in a crystalline form. Morphology analysis by scanning electron microscopy (SEM) before cell culture confirmed that PU scaffolds consisted of nanofibers with diameters between 100 and 150nm and randomly oriented. Cell culture showed that cleaning the PU scaffold with or without ethanol affected adhesion, proliferation, migration and morphology of cancer cells, since a high density of 4T1 cells was observed on untreated material. The shape of cancer cells changed considerably with treatment of the surface; the untreated scaffold had more rounded cells compared to treated scaffolds. This preliminary study has demonstrated that PU scaffolds composed of nanofibers have a positive effect on 4T1 cell cultures and may be used for testing rapid response of anti-drug agents *in vitro*.

2. MATERIALS AND METHODS

2.1. Materials

PU solution was acquired from Inovenso (Innovative engineering solution). The solution was composed of 15% wt. polyurethane (PU) and 85% wt N,N-dimethylformamide (DMF). Breast cancer cells, 4T1, were obtained from the Biology Department of Dumlupınar University. RPMI-1640 cell culture media and fetal bovine serum (FBS) were acquired from Sigma-Aldrich Inc. (St. Louis, MO).

2.2 Scaffold preperation

The electrospinning method was done at ambient temperature. Using a syringe pump, a 5 ml of solution was delivered out of a 0.8 μm nozzle at a constant rate of 1.50 ml/h. The nozzle was arranged to keep at a distance of 15 cm from the collector. Using a higher power voltage supply, a 22kV was applied between the needle and the metal collector. The scaffold was obtained after a total of 2 hours (Figure 1). Afterwards, the samples were cut to a similar diameter of the flask ready to culture cells. To simplify the understanding of this study, ethanol-treated and untreated scaffold samples was demonstrated in Table 1.

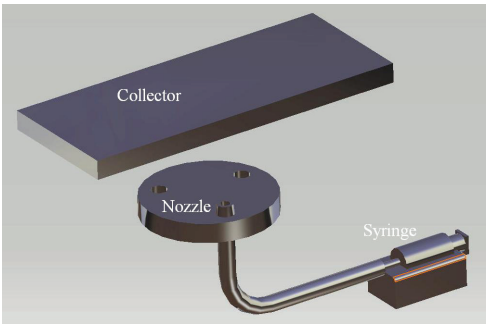

Figure 1: *Electrospinning method.*

Table 1*: Experimental sample tested.*

Scaffold	Before Cell Culture	After Cell Culture	Null Treatment
A			✓
B	✓		
C	✓	✓	

2.3 Cell Culture

4T1 cells were cultured in RPMI-1640 (plus 4.5 g/l glucose, 10 mM HEPES, 1 mM sodium pyruvate, 0.15% sodium bicarbonate, 100 µg/ml streptomycin and 100 U/ml penicillin) added with 10% FBS. Cells were incubated (HF90 incubator) in a humidified atmosphere at 37˚C with 5% CO_2. Experimental cultures were grown in 35x10 mm Corning plates. After aspiration of Corning plates and cleaning of cells with 1 ml of 0.25% trypsin, the cells were put in 2 ml of 0.25% trypsin in Corning flasks for 2 min. SEM images were acquired after 3 days of cell culture on scaffolds.

2.4 Characterization

Amorphous and crystalline phases of each scaffold were determined by an X-ray diffractometer (XRD, Rigaku-miniflex) using Cu K(α) radiation with a Ni filter between the range of 10 to 70°. The scanning speed was 2° min^{-1} with steps of 0.01°. Identification of the phases was achieved by comparing the experimental XRD patterns. The morphology of the scaffold was examined using JEOL 5600 LV scanning electron microscopy (SEM) at an accelerating voltage of 20kV with magnifications of ×12,000. The scaffold surfaces were gold-coated before SEM imaging. Afterwards, chemical compositions of the scaffolds were determined using energy dispersive X-ray spectroscopy (EDS). In addition, cell adhesion was driven using SEM. ImageJ software (Freeware provided by the NIH, Bethesda, MA, USA) was used to evaluate the mean fiber diameters and cell numbers.

3. RESULTS AND DISCUSSION

3.1 Characterization of nanofibers

Figure 2 shows SEM-EDS analysis of the scaffold (sample A) spun from PU/DMF solution. The SEM-EDX pattern presented three (3) main peaks: Aluminum (Al), Carbon (C) and Oxygen (O). In order, the relative percentages of these elements were: 29% wt Al, 57% wt C and 13% wt O. The highest intensity peak was assigned to Al due to the X-rays reaching the base of the scaffold that was made of aluminum folio. Nanofibers are mainly composed of C and O elements. Here, we should note that hydrogen was probably also present but we could not observe it because of the limited detection capability of the apparatus. Sheikh et al. (15) studied copper nanoparticles doped in PU nanofibers and found the same results in pristine nanofibers described above, the presence of C and O. As can be seen in Figure 2 the fibers are randomly oriented after electrospinning, with bead formation at some places. The average diameter of nanofibers was 0.09 μm (90 nm). Also, on the surface, we could observe different shaped bead formations, such as rounded or oval-like. The structure of fibers change with electrospinning parameters such as concentration, voltage and ffed rate. This behavior is explained well in the literature. Zhuo et al. (Haitao Zhuo et al., 2008) spun 5.0% wt PU/DMF solution with different voltages. They found that better nanofibers can be produced after 12.0 kV. In the same study, they observed the influence of feeding rate on nanofiber morphology for 5.0% wt PU/DMF solution. At a higher feeding rate, they found a larger fiber while at a lower feeding rate, they observed a smaller and uniform fiber.

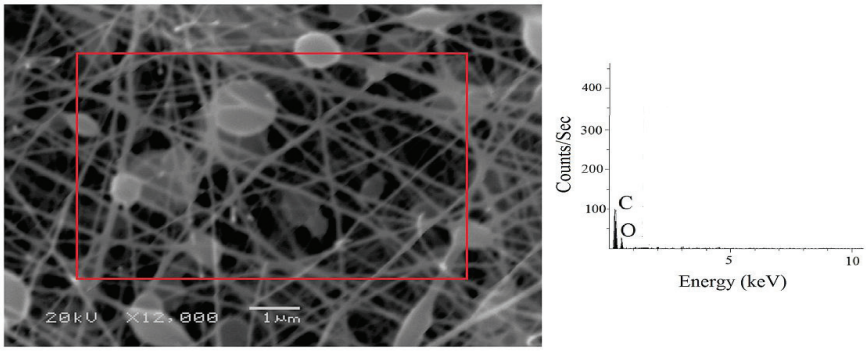

Figure 2. *SEM image of nanofibrous scaffold (at left) and EDS analysis of nanofibrous scaffold (at right).*

To determine the crystallography of nanofibers, X-ray diffraction (XRD) analysis was performed. The XRD pattern of scaffold A is presented in Figure 3. As shown in Figure 3, the XRD pattern showed two main peaks one at 2Θ= 45° and the second at 2Θ= 65°, respectively. These peaks were dedicated to the metal aluminum. As mentioned above, the folio is composed of aluminum. Therefore, this can be misleading about the crystalline or amorphous phase of the PU nanofiber. Normally, the spectrum of pure PU nanofibers displays an amorphous nature (Sheikh et al., 2011).

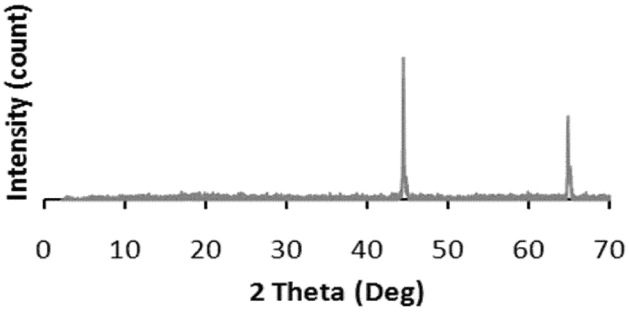

Figure 3: XRD result of scaffold A.

Figure 3. *XRD result of Scaffold A.*

The thermal analysis curves (TG) of both samples are presented in Figure 4. The TG results showed that the PU nanofibers were decomposed in two stages: (1) at approximately 286°C–496°C, with loss of approximately 62.2% weight; and (2) at 496°C–638°C, with loss of approximately 31% weight. The film showed a similar behavior but was slightly lower than the scaffold. This means that nanofibrous scaffold is more resistant than film.

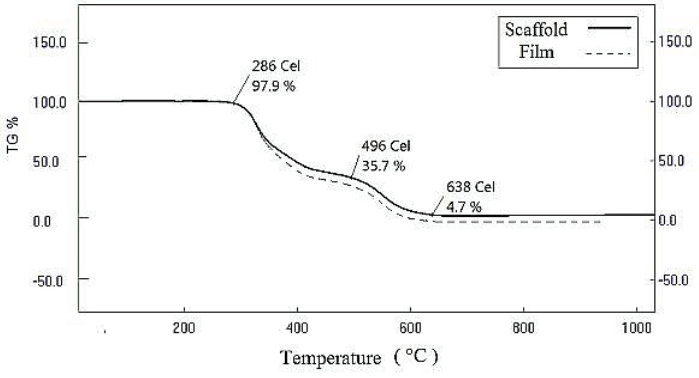

Figure 4. TG analysis of polyurethane scaffold and film.

3.2 Cell culture analysis

Referring to the SEM image in figure 2 the scaffold featured a highly porous structure composed of randomly oriented fibers. In this structure, breast cancer cells could successfully adhere to the surface within 24 hours and led to a thick cellular layer by day 3 for all specimens. In general, cells in matrices cover the entire surface with some noticeable crevices, as shown in Figures 5, 6 and 7. It is also noteworthy that the scaffold was compromised and did not disintegrate during incubation time.

This structural integrity is due to the high stability of PU, which provides sufficient mechanical support for the adhesion, proliferation and migration of breast cancer cells. Figures 5, 6 and 7 demonstrate that confluent cancer cells can be engineered on the scaffold within 3 days. The morphology and coverage revealed by SEM prove that this scaffold possesses necessary biochemical characteristics to involve cancer cells.

The surface of scaffold A was not treated with ethanol before and after cell culture. Figure 5a and 5b show regeneration of 4T1 cells on scaffold A. At first glance, we can observe a high density of cells on the surface with an extracellular matrix (ECM). The shape of the cells was rounded and there were approximately a total of 59 cells on the surface of scaffold A (figure 5a). At some parts, cells were located on each other. Proliferation of small spherical cells on large cancerous cells was also observed (Figure 5b).

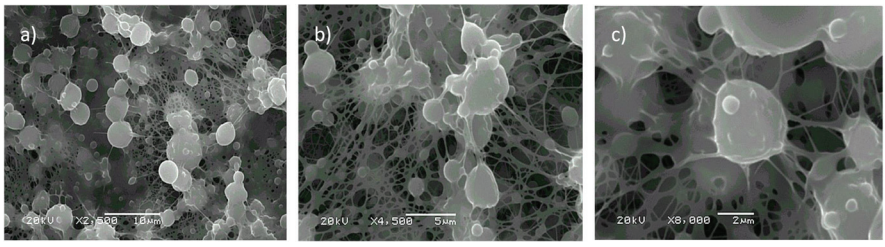

Figure 5. *SEM images of cell culture on polyurethane scaffold a) x2500 b) x4500 c) x8000.*

Degradation of the polymers is an important factor that influences the mechanical/biological interaction. To examine the sensitivity to anti-cancer drugs, cancer cells were cultured for at least 3 days. Biodegradation can be observed in some polymers through hydrolysis followed by bio assimilation. In our study, we did not expect any degradation of scaffold A, B and C during cell culture.

In Figure 6 cell adhesion, proliferation and migration on scaffold B is presented. This sample was only cleaned with ethanol before cell culture. The regeneration process on scaffold B is quite similar to that of A. In Figure 6, the direction of cell arms is more evident and they are oriented in different directions. The network communication between neighbors is shown in more detail in Figure 6b. Here, we can observe some arms oriented under matrices and probably proceeding through the pores. The total number of cells on the surface was about 34 on scaffold (figure 6a) and their shape were a mixture of round and hexagonal. Szot et al. (Szot et al., 2011) found that cancer cell HMEC-1 was not sensitive against to the materials.

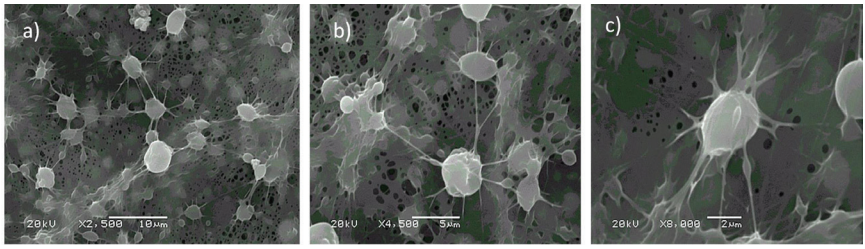

Figure 6. *SEM images of cell culture on polyurethane film a) X2500 b) X4500 c) 8000.*

In Figure 7 SEM images of scaffold C are presented with different magnifications. This scaffold was cleaned before and after cell culture with ethanol to prevent contamination. As observed in this figure, 4T1 cells successfully adhered to, grew and migrated on the materials. Szot et al. (Szot et al., 2011) did not observe HMEC-1 cell infiltration into the scaffold after 7 days. They explained that the density of the scaffold and absence of manufactured porosity hindered cell infiltration. Porosity of scaffold can be increased with modification of the electrospinning parameters. The communication between cells is mediated by their multiple arms (Figure 7b). Furthermore, the cells within this matrix covered the entire surface with some pores present at different locations. On the entire surface of scaffold C, the total of cells was about 40 (figure 7a). The shape of the cells depended on the size; the larger cells were more hexagonal while the smaller ones were more rounded.

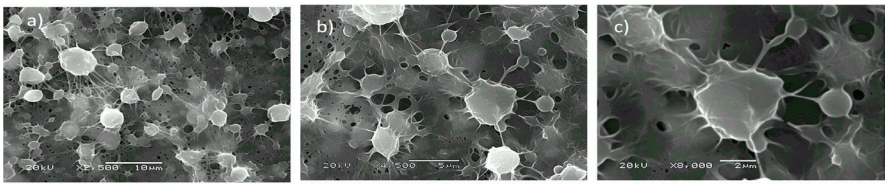

Figure 7. *SEM images of cell culture on cleaned polyurethane scaffold a) x2500 b) x4500 c) x8000.*

The images presented in Figures 5a, 6a and 7a were treated with software ImageJ. The color density of each image was extracted and is presented as a histogram in figure 8. This analysis is performed to show the distribution and density of cells on the surface of scaffolds. The main peaks were concentrated between blue and purple for all the scaffolds. These peaks corresponded to the matrices of the cells. More cells were present on the surfaces of scaffold A and C compared to scaffold B. PU nanofibers can be a candidate for use in investigating rapid time response of anti-drug mechanisms in cancer cells. Compared with conventional polymers, nanofibers can undergo structural modification easily and maintain integrity while facilitating molecular diffusion in cells, thus making them desired molecules.

4. Conclusion

The electrospinning technique enables the fabrication of a porous PU scaffold with fibers of an average 90 nm in diameter. Adhesion, proliferation and migration of 4T1 breast cancer cells were observed on the PU scaffold after 3 days of cell culture. Moreover, the morphology of the cells depended on the cleaning of the scaffold with ethanol, which mainly influenced cell shape and quantity. Untreated scaffold A had rounded cells while ethanol-treated scaffolds B and C had a mixture of hexagonal and rounded cells on their surfaces. Less contamination and higher cell growth were observed on scaffolds A and C compared to B. Preservation of 3D cancer (4T1) growth *in vitro* and partial cell infiltration was observed for all the scaffolds tested. These results strongly suggest the potential use of the PU scaffold for studying the mechanisms of cell culture in 3D and rapid responses of anti-drug agents. Further research and characterization of the scaffold will allow the determination of whether these scaffolds are convenient to attain this objective.

References

Aoudjit, F., & Vuori, K. (2001). Integrin signaling inhibits paclitaxel-induced apoptosis in breast cancer cells. *Oncogene 20*, 4995-5004.

Beningo, K., Dembo, M., & Wang, Y. (2004). Responses of fibroblasts to anchorage of dorsal extracellular matrix receptors *Proc.Natl. Acad. Sci. U.S.A.* , *101*(18024).

Bhardwaj, N., & Kundu, S. (2010). Electrospinning: a fascinating fiber fabrication technique *Biotechnology Advances*, *28*, 325-347.

Celebi Saltik, B., & Öteyaka, M. (2016). Cardiac patch design: Compatibility of nanofiber materials prepared by electrospinning method with stem cells. *TURKISH JOURNAL OF BIOLOGY*, *40*, 510-518. https://doi.org/10.3906/biy-1506-82

Chen, P., Wu, Q., Ding, Y., Chu, M., Huang, Z., & Hu, W. (2010). A controlled release system of titanocene dichloride by electrospun fiber and its antitumor activity in vitro *Eur.J. of Pharmaceutics and Biopharmaceutics*, *76* 413-420.

Çelebi-Saltik, B., Öteyaka, M. Ö., & Gökçinar-Yagci, B. (2021). Stem cell-based small-diameter vascular grafts in dynamic culture. *Connective Tissue Research*, *62*(2), 151-163. https://doi.org/10.1080/03008207.2019.1651848

Kenawy el, R., Bowlin, G. L., Mansfield, K., Layman, J., Simpson, D. G., Sanders, E. H., & Wnek, G. E. (2002). Release of tetracycline hydrochloride from electrospun poly(ethylene-co-vinylacetate), poly(lactic acid), and a blend. *J Control Release*, *81*(1-2), 57-64. https://doi.org/10.1016/s0168-3659(02)00041-x

Knight, B., Laukaitis, C., Akhtar, N., Hothcin, N., Edlund, M., & Horwitz, A. (2000). Visualizing muscle cell migration in situ. *Curr. Biol.*, *10*(576).

Min, B., Lee, G., Kim, S., Nam, Y., Lee, T., & Park, W. (2004). Electrospinning of silk fibroin nanofibers and its effect on the adhesion and spreading of normal human keratinocytes and fibroblasts in vitro. *Biomaterials 25*, 1289-1297.

Ng, K., Leong, D., & Hutmacher, D. (2005). The challenge to measure cell proliferation in two and three dimensions *Tissue Engineering*, *11*, 182.

Oteyaka, M., Ozel, E., & Yıldırım, M. (2014). Experimental Study on Relationship of Applied Power And Feeding Rate on Production of Polyurethane Nanofibre. *Gazi University Journal of Science 26*, 611-618

Pattison, M., Wurster, S., Webster, T., & Haberstroh, K. (2005). Three-dimensional, nano-structured PLGA scaffolds for bladder tissue replacement applications. *Biomaterials 26*, 2491.

Rhodes, N., Srivastava, J., Smith, R., & Longinotti, C. (2004). Heterogeneity in proliferative potential of ovine mesenchymal stem cell colonies *J.Mater. Sci.* , *15*, 397-402.

Sheikh, F., Kanjwal, M., Saran, S., Chung, W., & Kim, H. (2011). Polyurethan nanofibers containing copper nanoparticles as future materials. *Applied Surface Science 257*, 3020-3026.

Smith, L., & Ma, P. (2004). Nano-fibrous scaffolds for tissue engineering. *Colloids Surface B*, *39*, 125-131.

Szot, C., Buchanan, C., Gatenholm, P., Rylander, M., & Freeman, J. (2011). Investigation of Cancer Cell Behavior on Nanofibrous Scaffolds. *Materials Science and Engineering C*, *31*(37-42).

Verreck, G., Chun, I., Peeters, J., Rosenblatt, J., & Brewster, M. (2003). Preperation and Characterization of Nanofibers Containing Amorphous Drug Dispersions Generated by Electrotatic Spinning. *Pharm. Res.* , *20*, 810.

Xie, A., & Wang, C. (2006). Electrospun micro- and nanofibers for sustained delivery of paclitaxel to treat C6 gliaoma in vitro. *Pharm Res 23* (8), 1817–1826.

Yerlikaya, A., & Erin, N. (2008). Differential sensitivity of breast cancer and melanoma cells to proteasome inhibitor Velcade. *Int J Mol Med 22(6)*, 817-823.

Yoshioto, H., Shin, Y., Terai, H., & Vacanti, J. (2003). A biodegradable nanofiber scaffold by electrospinning and its potential for bone tissue engineering. *Biomaterials 24*, 2077-2082.

Zeng, J., Xu, X., Chen, X., Liang, Q., Bian, X., & Yang, X. (2003). Biodegradable electrospun fibers for drug delivery. *J. Control. Release 92* 227-231.

Zhuo, H., Hu, J., Chen, S., & Yeung, L. (2008). Preparation of Polyurethan Nanofibers by Electrospinning. *Journal of applied polymer science 109*, 406-411.

Zhuo, H., Hu, J., Chen, S., & Yeung, L. (2008). Preparation of polyurethane nanofibers by electrospinning [https://doi.org/10.1002/app.28067]. *Journal of applied polymer science*, *109*(1), 406-411. https://doi.org/https://doi.org/10.1002/app.28067

Zong, X., Fang, D., Kim, J., Cruz, S., Hsiao, B., & Chu, B. (2002). Structure and Process Relationships in Bioabsorbable Nanofiber Membranes by Electrospinning. *Polymer*, *43*(16), 4403-4312

Chapter 6

DESIGN AND ANALYSE OF ROBUST SWITCHED CONTROLLERS FOR A MAGNATIC LAVITATION SYSTEM

Emre KEMER[1]

Hasan BAŞAK[2]

1 Asst. Prof. Emre KEMER, Department of Electrical and Electronics Engineering, Faculty of Engineering, Uşak University, ORCID: 0000-0001-8716-1971

2 Asst. Prof. Hasan BAŞAK, Department of Electrical and Electronics Engineering, Faculty of Engineering, Artvin Çoruh University, ORCID: 0000-0002-3724-6819

INTRODUCTION

Magnetic levitation systems have become popular research platform because these systems have been employed in different applications such as magnetic levitation train (Mingda et al., 2019), microrobot actuation (Hagiwara et al., 2012) and wind turbines (Yu et al., 2017). Magnetic levitation systems have fast, unstable highly nonlinear dynamics. It is a challenging problem to find a stabilising controller that keeps the metal ball at a desired position from the coil with very small tracking error. Therefore, this study will address positioning problem of the magnetic levitation system.

Researchers have been developing control algorithms to improve the performance of magnetic levitation systems. Recently publications are reviewed to cite a few. For example, Ghosh et al. (2014) proposed two degree of freedom PID (Proportional-Integral -Derivative) controller for a magnetic levitation system that offers a robust performance in experimental results. Swain et al. (2017) proposed two-degree of freedom fractional order PID controller which provides better tracking and robustness compared with standard PID controller. PID controller has simplicity and model independent nature so it might be first method to employ in magnetic levitation system. To adjust PID control parameters online, extremum searching algorithm was proposed by Chen et al. (2017) for magnetic levitation systems. Furthermore, Yumuk at al. (2021) designed fractional order PI control using frequency domain settings to adjust controller parameters. On the other hand, nonlinear controller methods such as Backstepping, integral-backstepping and synergetic controllers were designed by Malik et al. (2019) to levitate the ball in air at desired distance from ground. Similarly, Yaseen et al. (2021) designed adaptive-terminal-sliding-mode, adaptive-backstepping-sliding mode and adaptive integral-backstepping-sliding-mode nonlinear controllers to achieve the desired ball distance from the coil. Performance of these controllers are analysed in the presence of varying parameters, noise and disturbance. Munna et al. (2018) developed robust H-infinity control scheme to stabilize the ball of a magnetic levitator in the presence of disturbances using a parallel distributed compensation concept. The tracking performance of a fuzzy logic controller was analysed in (Narayn et al., 2018). Nonsingular terminal-sliding mode controller with disturbance estimation was developed in

reference (Junxiao et al., 2020) which enhances capacity of the disturbance rejection in a magnetic levitation system. Vo et al. (2021) proposed a fixed time sliding mode controller with a disturbance observer to achieve a robust stability, very small tracking error of a magnetic levitation system in the presence of uncertainty.

In this study, two robust switched control methods have been developed to achieve a high tracking performance in the presence of mass parameter variation, additive noise and time-varying disturbance. The first robust switched control method was based on minimum dwell time constraint and the second switched control method utilises the minimum quadratic Lypunov function. The performances of those designed controllers will be compared and analysed to show their merits and disadvantages in nonlinear simulation using Simulink/MATLAB program.

ROBUST SWITCHED CONTROL METHODS

Robust switched control methods use more controllers to improve stability and desired requirements of the system instead of using one controller. Figure 1 illustrates a basic switching controller structure. It can be seen from this figure; the system consists of a several controllers and the switching signals decide to switch between controllers.

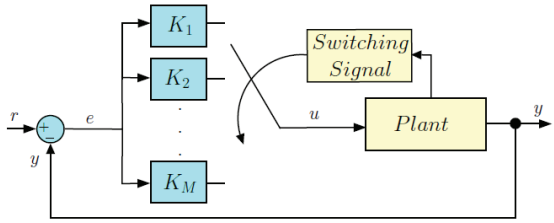

Figure 1: Switching controller structure

The switching signals have a crucial role on the switching controller methodologies. These signals can cause instability of the system even the controllers are individually stable. On the other hand, the switched system can be stable even the controllers individually unstable. These scenarios are illustrated on Figure 2. Therefore, the switched controller methodologies are built on choosing (deciding) the different switching signal strategies. The

minimum dwell time and the minimum switching methods used in this study are some of them (see (Liberzon, 2003; Lin and Antsaklis, 2009; Geromel and Colaneri 2006; Allerhand and Shaked 2012) for more details).

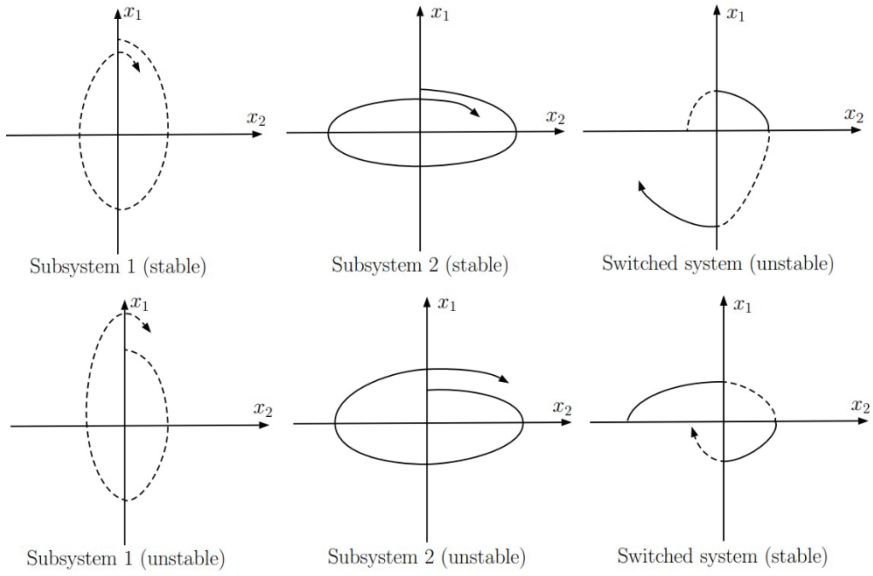

Figure 2: Switching scenarios

Minimum Dwell Time Method

Using this method, quadratic stability of the system is guaranteed by introducing a minimum time constraint between two consecutive switching instants (minimum dwell time, T > 0, see Figure 3). In other words, no switching occurs during the *minimum dwell time,* which eliminates unnecessary switching that force to the system instability.

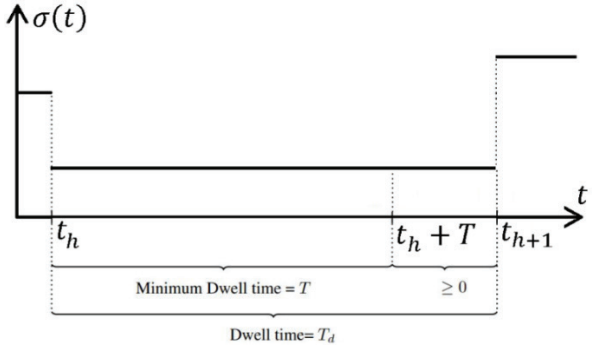

Figure 3: Description of the minimum dwell time

This switching method is based on the state of the system. Basically, the state space is divided into a finite number of regions that are overlapping each other. The switch happens the system trajectory hits the boundary of the related region. The regions and overlapping region are depicted in Figure 4, where solid and dash line respectively show Cell 1 and 2, and the shaded region shows overlapping. The vertices of each cell can be seen in Figure 4. The indexes of the cells and vertices are called respectively i and j in this part.

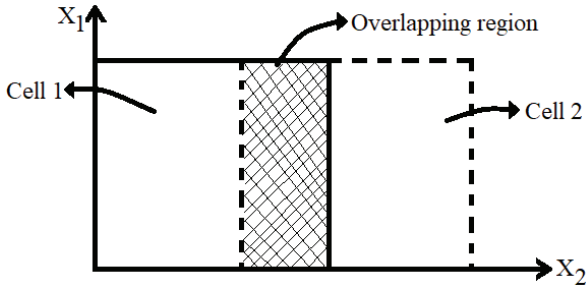

Figure 4: Dividing state space of the system to cell partitions.

Theorem 1 (Kemer et al., 2018)**:** For given scalars $\alpha > 0$ and $T > 0$, if the set of matrices S_i and Y_i are of compatible size and the collection of symmetric matrices Z and $Q_{i,h}^{j} > 0,\ i = 1, \dots, M,\ h = 0, \dots, H,\ j = 1, \dots, N$ satisfy the following LMIs for all $i = 1, \dots, M$ and $j = 1, \dots, N$:

$$\begin{bmatrix} Z & B_{w,i}^{j\ \prime} \\ * & Q_{i,h}^{j} \end{bmatrix} > 0, \qquad \forall\, h \in \{0, \dots, H\},$$

$$\begin{bmatrix} \varphi & \left(C_i^j S_i + D_{u,i}^j Y_i\right)' & Q_{i,h}^{j} - S_i' + \alpha A_i^j S_i + \alpha B_{u,i}^j Y_i \\ * & -I & \alpha\left(C_i^j S_i + D_{u,i}^j Y_i\right) \\ * & * & -\alpha(S_i' + S_i) \end{bmatrix} < 0$$

$$\begin{bmatrix} \varphi & \left(C_i^j S_i + D_{u,i}^j Y_i\right)' & Q_{i,h+1}^{j} - S_i' + \alpha A_i^j S_i + \alpha B_{u,i}^j Y_i \\ * & -I & \alpha\left(C_i^j S_i + D_{u,i}^j Y_i\right) \\ * & * & -\alpha(S_i' + S_i) \end{bmatrix} < 0$$

where $h = 0; \dots; H - 1$

$$\begin{bmatrix} \sigma & \left(C_i^j S_i + D_{u,i}^j Y_i\right)' & Q_{i,H}^j - S_{i,H}' + \alpha A_i^j S_i + \alpha B_{u,i}^j Y_i) \\ * & -I & \alpha\left(C_i^j S_i + D_{u,i}^j Y_i\right) \\ * & * & -\alpha(S_i' + S_i) \end{bmatrix} < 0$$

$$Q_{i,H}^j - Q_{s,0}^j \leq 0. \quad \forall s \in \{1, \dots, M\} \text{ and } s \neq i$$

here $\varphi = \frac{Q_{i,h}^j - Q_{i,h+1}^j}{T/H} + He\{A_i^j S_i' + B_{u,i}^j Y_i\}$, and $\sigma = He\{A_i^j S_i' + B_{u,i}^j Y_i\}$ then there exists a state-feedback controller defined as: $K_i = Y_i S_i^{-1}$, such that the closed-loop system is quadratically stable for any switching rule with a dwell-time that is greater than the minimum dwell-time, T and such that the H_2-gain from w to z is less than or equal to $\sqrt{Tr(Z)}$.

Minimum Switching Method

Minimum switching method depends on the Lyapunov energy function of the system. Hence that means the related controller is active as long as it has the minimum energy otherwise switching happens other controller, which has the minimum energy. This switching method assumes that the all states are measurable for feedback. Based on results of reference (Geromel and Colaneri, 2006) and using the parameter dependent Metzler matrix, the following theorem is derived in reference (Deaecto et al., 2013) for the time varying polytopic systems. Here, the aim is to compute a family of state feedback controllers and a minimum switching rule for that the control law $u(t) = K_{\sigma(x(t))}x(t)$ asymptotically stabilises the origin of the system and optimises the H_2 norm performance index.

Theorem 2 (Deaecto et al. 2013)**:** For all $i \in \mathbb{K}$, if symmetric positive-definite matrices X_i, matrices Y_i and positive scalar γ exist and hold the following linear matrix inequalities

$$\begin{bmatrix} He\{A_j X_i + B_j Y_i\} & X_i C_i' + Y_i' D_i' & \gamma X_i \\ * & -I & 0 \\ * & * & \gamma X_j \end{bmatrix} < 0, \ \forall\, i, j \in \mathbb{K} \times \mathbb{K},$$

then robust switched controller with $K_i = Y_i X_i^{-1}, \forall\, i \in \mathbb{K}$ and the minimum switching strategy

$$\sigma(x) = arg \min_{i \in \mathbb{K}} x' X_i^{-1} x$$

provide that the switching system is globally asymptotically stable and

$$J(K_1, \dots, K_N, \sigma) < \min_{i \in \mathbb{K}} Tr(H' X_i^{-1} H)$$

MAGNETIC LAVITATION MODEL

Magnetic levitation system comprises of a power supplier, an electromagnet, a metal ball, a position sensor and a controller (Yaseen et al. 2021). The electromagnet is made from ferromagnetic material. The current passes though the magnet, which produces electromagnetic force. The controller regulates the amount of the desired current and so the amount of the desired electromagnet force. The gap of between the center of coil and the ball is varied by changing electromagnetic force. The basic configuration of magnetic levitation system is given in Figure 5.

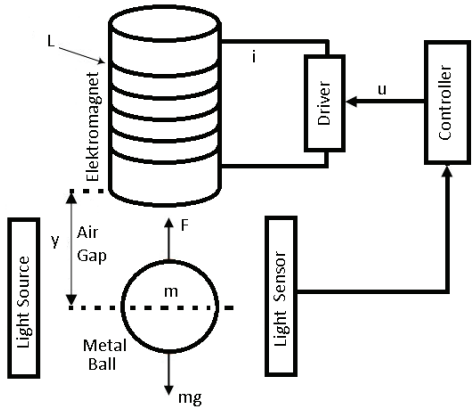

Figure 5: Basic configuration of magnetic levitation system (Marquez, 2003)

According to Newton's second law, all forces acting on the ball are taken into consideration the equation of the ball motion is

$$m\ddot{y} = -f_k + mg + F \qquad 1)$$

In which m is the ball mass, f_k is the friction force, g is the gravity acceleration and F is the electromagnetic force owing to the current. The stored energy in electromagnet is

$$E_0 = \frac{1}{2}Li^2 \tag{2}$$

here L is the electromagnet inductance. The inductance parameter varies based on the ball position. L is approximated as:

$$L = \frac{\lambda}{1+\mu y} \tag{3}$$

The fact is that when the ball approaches the electromagnet, the flux in the magmatic circuit leads to an increase of the value of the inductance. Thus, the force is

$$F(i,y) = -\frac{1}{2}\frac{\lambda\mu i^2}{(1+\mu y)^2} \tag{4}$$

Suppose that fraction force is

$$f_k = k\dot{y} \tag{5}$$

here $k > 0$ is the viscous friction coefficient and Equations (4) and (5) is substituted into Equation (1), then the equation of the ball motion is obtained as follows:

$$m\ddot{y} = -k\dot{y} + mg - \frac{1}{2}\frac{\lambda\mu i^2}{(1+\mu y)^2} \tag{6}$$

Defining state variables $x_1 = y,\ x_2 = \dot{y}$ and then the state space model is obtained as

$$\begin{aligned} \dot{x}_1 &= x_2 \\ \dot{x}_2 &= -\frac{k}{m}x_2 + g - \frac{1}{2m}\frac{\lambda\mu i^2}{(1+\mu x_1)^2} \end{aligned} \tag{7}$$

The main objective of this study is to design controllers which stabilise the ball at a desired position $x_1 = y_0$. Hence, for equation (7), the equilibrium point is $x_e = [x_{1e}\ x_{2e}]' = [y_0\ 0]'$ and equilibrium input from $\dot{x}_2 = 0$ and $i_e = \sqrt{\left(\frac{2mg}{\lambda\mu}\right)(1+\mu x_{1e})^2}$.

The system of (10) is linearized about the equilibrium point, x_e and for input, i_e as follows:

$$\begin{vmatrix} \dot{x}_1 \\ \dot{x}_2 \end{vmatrix} = \begin{vmatrix} 0 & 1 \\ \frac{2g\mu}{1+\mu x_{1e}} & -\frac{k}{m} \end{vmatrix} \begin{vmatrix} x_1 \\ x_2 \end{vmatrix} + \begin{vmatrix} 0 \\ -\frac{\sqrt{2\lambda\mu g}}{\sqrt{m}(1+\mu x_{1e})} \end{vmatrix} u \tag{8}$$

SIMULATION RESULTS AND ANALYSIS

Assuming that desired position of the system (8) is varying in the range of $0.04 \leq x_1 \leq 0.08$ and the mass is uncertain in the range of $0.02 \leq m \leq 0.08$. The switched linear system with poltyopic uncertainity can be given as:

$$\dot{x} = A_i^{\mathrm{j}}(m, x_1)x + B_i^{\mathrm{j}}(m, x_1)u$$
$$y = Cx = [1 \quad 0]x \tag{9}$$

Consider the parameter variation in (8); the state space of the levitation model is divided into two overlapped cells to solve Theorem 1. Then the following system matrices for the vertices of the polytope are computed for $i \in \{1,2\}, j \in \{1, \dots, 4\}$:

$$A_1^1 = \begin{vmatrix} 0 & 1 \\ 36.32 & -0.05 \end{vmatrix}, \qquad A_1^2 = \begin{vmatrix} 0 & 1 \\ 36.32 & -0.01 \end{vmatrix},$$
$$A_1^3 = \begin{vmatrix} 0 & 1 \\ 34.05 & -0.01 \end{vmatrix}, \qquad A_1^4 = \begin{vmatrix} 0 & 1 \\ 34.05 & -0.05 \end{vmatrix},$$
$$A_2^1 = \begin{vmatrix} 0 & 1 \\ 34.17 & -0.05 \end{vmatrix}, \qquad A_2^2 = \begin{vmatrix} 0 & 1 \\ 34.17 & -0.01 \end{vmatrix},$$
$$A_2^3 = \begin{vmatrix} 0 & 1 \\ 32.15 & -0.01 \end{vmatrix}, \qquad A_2^4 = \begin{vmatrix} 0 & 1 \\ 32.15 & -0.05 \end{vmatrix},$$

$$B_1^1 = \begin{vmatrix} 0 \\ -27.81 \end{vmatrix}, \; B_1^2 = \begin{vmatrix} 0 \\ -13.91 \end{vmatrix}, \; B_1^3 = \begin{vmatrix} 0 \\ -13.04 \end{vmatrix}, \; B_1^4 = \begin{vmatrix} 0 \\ -26.07 \end{vmatrix}$$
$$B_2^1 = \begin{vmatrix} 0 \\ -26.16 \end{vmatrix}, \; B_2^2 = \begin{vmatrix} 0 \\ -13.08 \end{vmatrix}, \; B_2^3 = \begin{vmatrix} 0 \\ -12.31 \end{vmatrix} \; B_2^4 = \begin{vmatrix} 0 \\ -24.62 \end{vmatrix}$$

In addition to this, if the centre of each polytope is taken into account to solve Theorem 2, then one can obtain the following matrices for the cells, $i \in \{1,2\}$:

$$A_1 = \begin{vmatrix} 0 & 1 \\ 35.1859 & -0.0313 \end{vmatrix}, \qquad B_1 = \begin{vmatrix} 0 \\ -20.2071 \end{vmatrix},$$
$$A_2 = \begin{vmatrix} 0 & 1 \\ 33.1612 & -0.0313 \end{vmatrix}, \qquad B_2 = \begin{vmatrix} 0 \\ -19.0443 \end{vmatrix}$$

The system in (12) is augmented with integral of the output tracking error vector $\mathrm{e_y}$ as follows:

$$\dot{x} = \bar{A}_i^j x + \bar{B}_i^j u \tag{10}$$

where

$$\bar{A}_i^j = \begin{vmatrix} A_i^j & 0 \\ -C & 0 \end{vmatrix}, \bar{B}_i^j = \begin{vmatrix} 0 \\ B_i^j \end{vmatrix}, \tag{11}$$

Based on the system (10), Theorem 1 is solved for $\alpha = 0.09$, $H = 1$, $T = 0.1$, then the controller gains are calculated as:

$$\begin{aligned} K_1 &= [-36.8516 \quad -2.9012 \quad 157.3624], \\ K_2 &= [-36.9476 \quad -2.9150 \quad 158.1176], \end{aligned} \tag{12}$$

Furthermore, Theorem 2 is solved based on the system (10), then the controller gains are found as follows:

$$\begin{aligned} K_1 &= [-64.8107 \quad -4.4324 \quad 429.7512], \\ K_2 &= [-23.4503 \quad -1.6402 \quad 143.7336] \end{aligned} \tag{13}$$

Using Simulink/MATLAB program, the model in Figure 6 is built for the levitation system given in the previous section. Moreover, four different scenarios with three different masses are taken into account to investigate the performance of switched controllers by found Theorems 1 and 2. These scenarios are listed as follows:

1. The levitation system without any noise and disturbance,
2. The levitation system with only white noise and without disturbance,
3. The levitation system with only disturbance and without noise,
4. The levitation system with both white noise and disturbance,

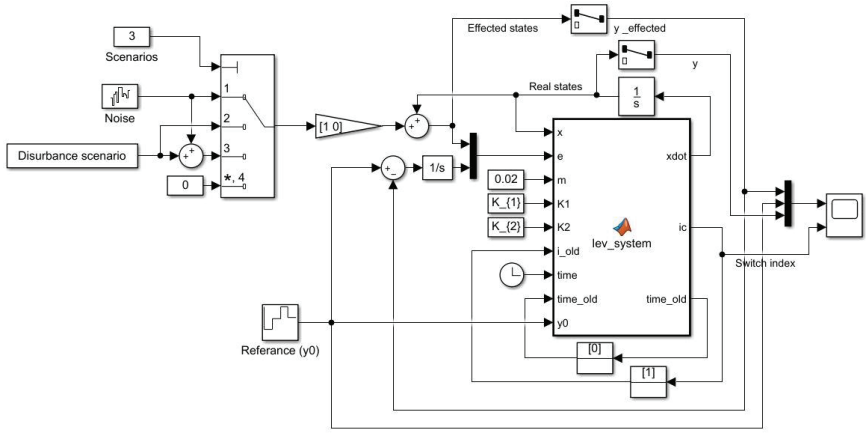

Figure 6: Simulink model of the levitation system

These four scenarios are simulated with the nonlinear magnetic levitation system and the gains of switched controllers given in (12)

and (13). The simulation results are given in Figures 7-14. Figures 7 and 8 show respectively the results of the minimum dwell time and minimum switching methods without any noise and disturbance. It can be seen that the switched controller found by Theorem 1 is more robust in the presence of mass variation. Overshoots can be seen in closed-loop response with the switched controller based on the minimum switching method. The switching frequency is shown in Figure 8. The controllers based on minimum switching method are switched very fast, which can damage the magnetic levitation system in the practice.

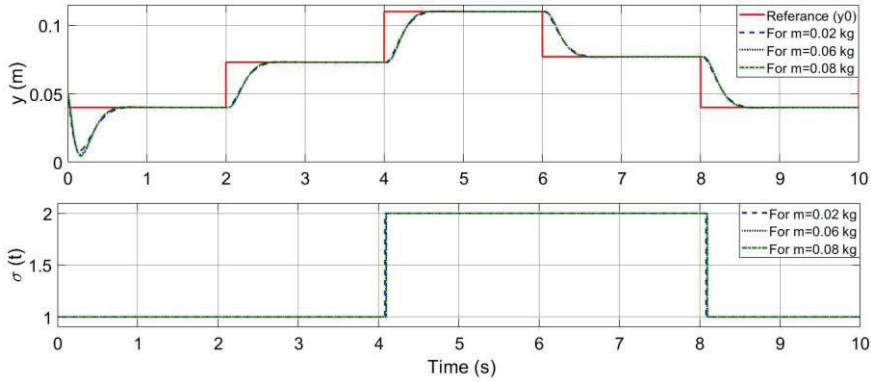

Figure 7: Results of the minimum dwell time method without any noise and disturbance

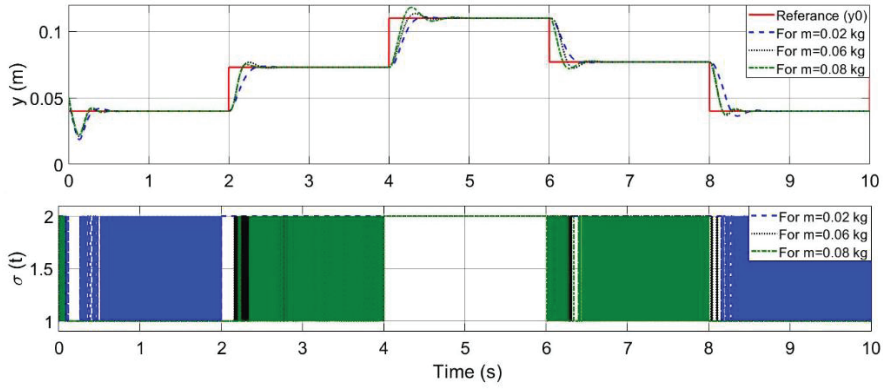

Figure 8: Results of the minimum switching method without any noise and disturbance

Figures 9 and 10 show respectively the results of the minimum dwell time and minimum switching methods with only white noise and in case of different mass scenario. It can be seen that both

controllers provide the satisfactory performance and eliminate the noise in closed-loop response.

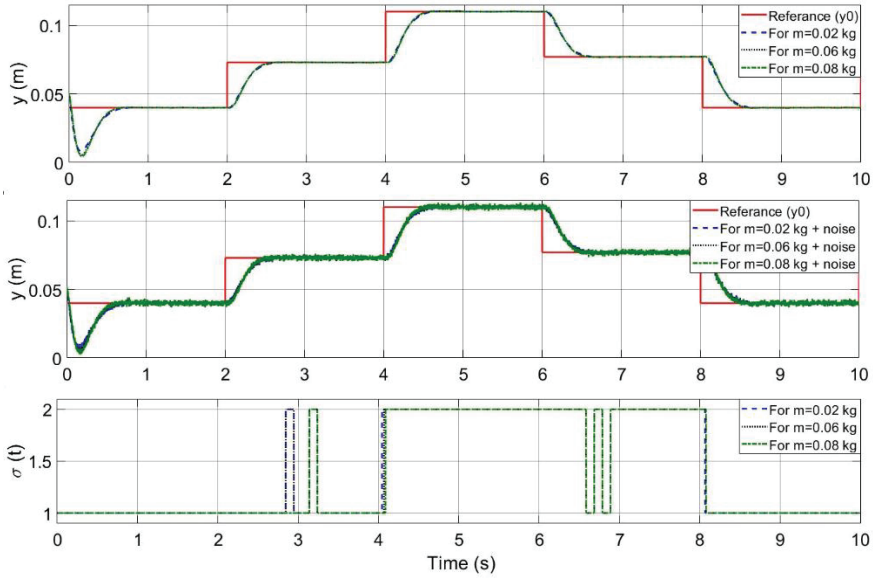

Figure 9: Results of the minimum dwell time method with white noise and without disturbance

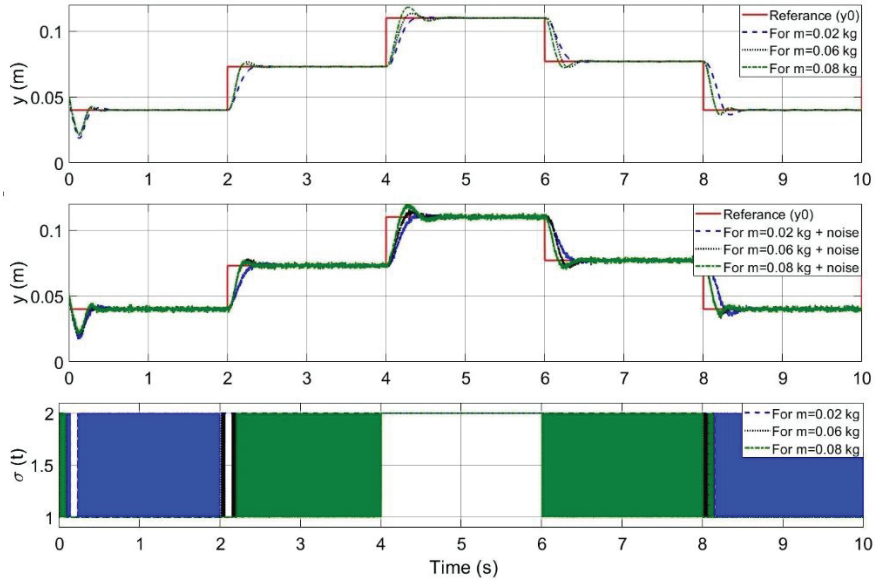

Figure 10: Results of the minimum switching method with white noise and without disturbance

For scenario 3, Figures 11 and 12 are given respectively to show disturbance rejection capacity of the switched controllers found by using the minimum dwell time and minimum switching methods. The switched controller based on dwell time rejects the disturbance on the ball position. One can see that the disturbance effects result in oscillatory response of the switched controller using the minimum switching method. Therefore, it can be said that the switched controller found by Theorem 2 has weak robustness against the disturbance on ball position. On the other hand, the switched controller based on dwell time is quite successful to reject the disturbance.

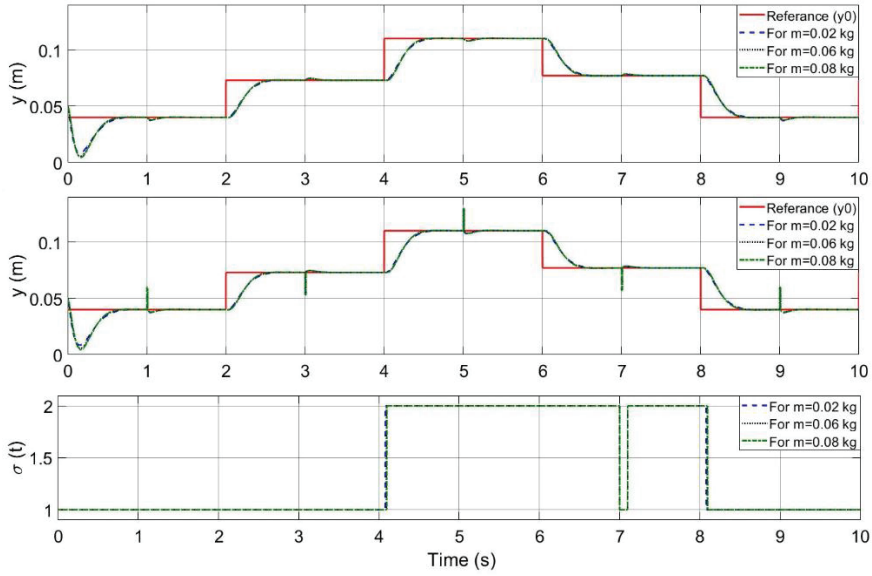

Figure 11: Results of the minimum dwell time method with disturbance and without white noise

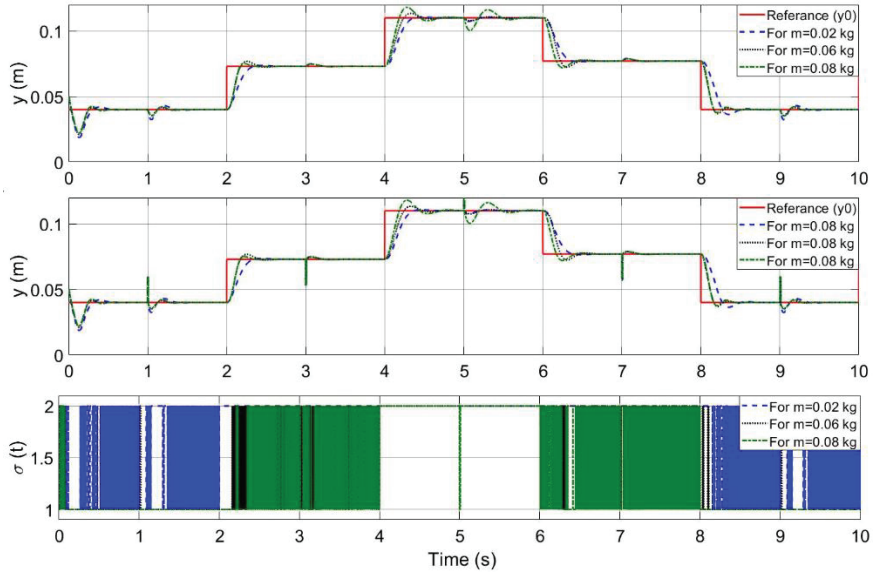

Figure 12: Results of the minimum switching method with disturbance and without white noise

For the last scenario, we analysed the performance of switched controllers in the case of the additive noise and disturbance. Here again we change the mass parameter before beginning the test. Figures 13 and 14 display respectively the results of the minimum dwell time and minimum switching methods with disturbance and white noise.

The switched controller computed by using Theorem 1 is very satisfactory. Again, the disturbance and a change of the mass worsen the response of the switched controller using the minimum switching method. Furthermore, the switching frequency of the switched controller based on minimum switching method is very fast in all scenarios and so this method has an implementation problem in the practice. The switched controller computed by using Theorem 2 should be designed considering reduction in switching actions. This study suggests the switched controller based on dwell time for the experimental implementation.

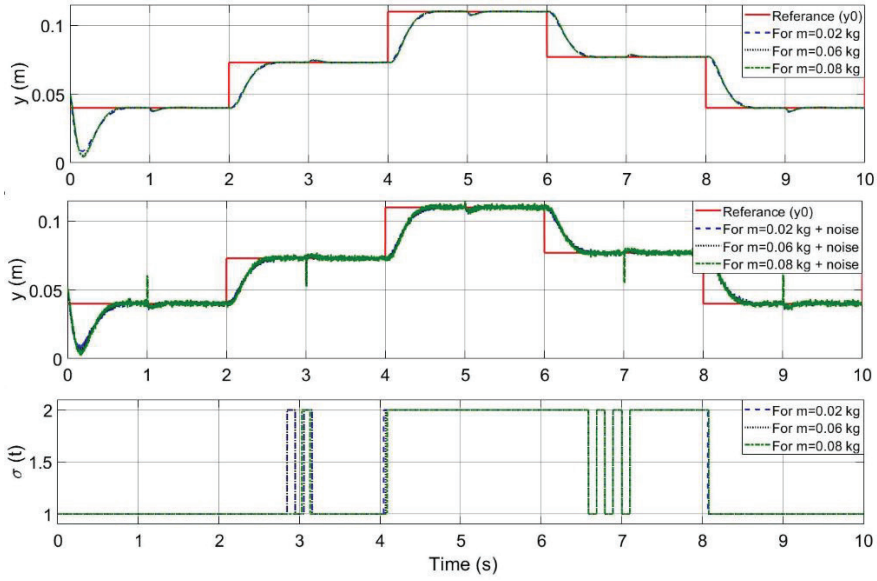

Figure 13: Results of the minimum dwell time method with white noise and disturbance

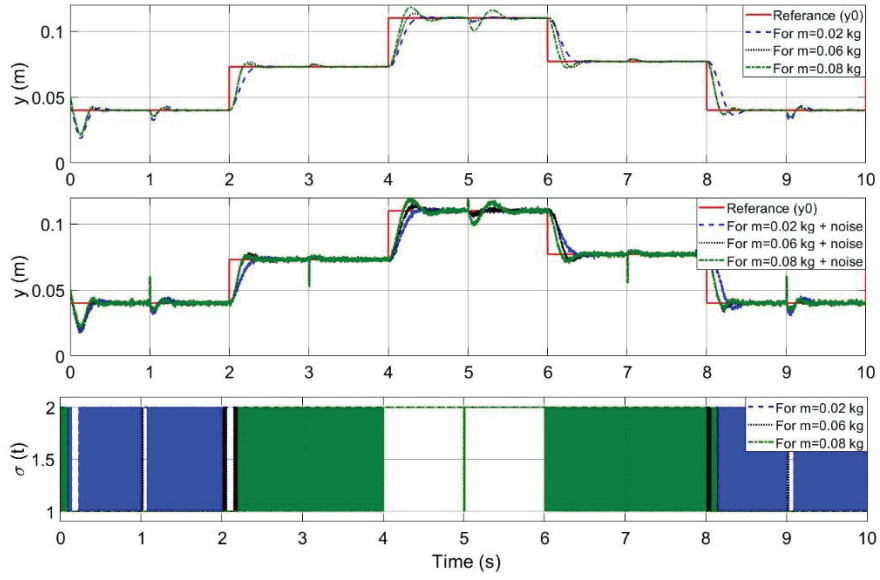

Figure 14: Results of the minimum switching method with white noise and disturbance

CONCLUSIONS

This study has presented designs of two robust switched controllers for magnetic levitation systems. The mathematical model of magnetic levitation system is given to develop robust switched controllers. Resulting controllers are applied to a magnetic levitation system in simulation using Simulink/MATLAB program. The performances of designed controllers are compared and analysed in case of different scenarios. Simulation results have demonstrated the efficiency of switched controllers in presence of mass variation, noise and time-varying disturbance.

REFERENCES

1. A. Ghosh, T. R. Krishnan, P. Tejaswy, A. Mandal, J. K. Pradhan, S. Ranasingh, "Design and implementation of a 2-DOF PID compensation for magnetic levitation systems.", *ISA transactions* 53.4 (2014): 1216-1222.
2. D. Liberzon, "Switching in systems and control", Springer Science & Business Media, 2003.
3. E. Kemer, H. Başak, E. Prempain, "Switched H 2-state-feedback control with application to a fighter aircraft", *Proceedings of the Institution of Mechanical Engineers, Part G: Journal of Aerospace Engineering* 233.14 (2019): 5428-5437,2019.
4. E. Yumuk, M. Güzelkaya, I. Eksin, "Application of fractional order PI controllers on a magnetic levitation system", *Turkish Journal of Electrical Engineering & Computer Sciences*, *29*(1), 98-109, 2021.
5. G. S. Deaecto, J. C. Geromel, J. Daafouz, "Switched state-feedback control for continuous time-varying polytopic systems", *International Journal of Control*, 84(9), 1500-1508, 2011.
6. H. J. Marquez, "Nonlinear Control Systems—Analysis and Design", JohnWiley & Sons, Hoboken, NJ, USA, 2003.
7. H. Lin, P. J. Antsaklis, "Stability and stabilizability of switched linear systems: a survey of recent results", *IEEE Transactions on Automatic control*, *54*(2), 308-322, 2009.
8. J. C. Geromel, P. Colaneri, "Stability and stabilization of continuous-time switched linear systems", *SIAM Journal on Control and Optimization*, *45*(5), 1915-1930, 2006.
9. K. Munna, A. S. Siddiqui, A. S. A. Mahmoud. "Robust H∞ control of magnetic levitation system based on parallel distributed compensator.", *Ain Shams Engineering Journal*, *9*(4), 1119-1129, 2018.
10. L. I. Allerhand, U. Shaked. "Robust control of linear systems via switching", *IEEE Transactions on Automatic Control*, 58(2), 506-512, 2012.
11. M. Hagiwara, T. Kawahara, T. Iijima, F. Arai, "High-speed magnetic microrobot actuation in a microfluidic chip by a fine V-groove surface", *IEEE Transactions on Robotics*, *29*(2), 363-372, 2012.
12. M. S. Yaseen, S. A. Siffat, I. Ahmad, A. S. Malik, "Nonlinear adaptive control of magnetic levitation system using terminal sliding mode and integral backstepping sliding mode controllers", *ISA transactions*, 2021.
13. Q. Chen, Y. Tan, J. Li, I. Mareels. "Decentralized PID control design for magnetic levitation systems using extremum seeking", *IEEE Access*, *6*, 3059-3067, 2017.
14. S. K. Swain, D. Sain, S. K. Mishra, S. Ghosh, "Real time implementation of fractional order PID controllers for a magnetic levitation plant", *AEU-International Journal of Electronics and Communications*, *78*, 141-156, 2017.
15. S. Malik, I. Ahmad, A. U. Rahman, Y. Islam, "Integral backstepping and synergetic control of magnetic levitation system", *IEEE Access*, *7*, 173230-173239, 2019.

16. S. Narayn, A. Tripathy, P. Sharma, "Single axis control of ball position in magnetic levitation system using fuzzy logic control." *IOP Conference Series: Materials Science and Engineering.* Vol. 323. No. 1. IOP Publishing, 2018.
17. T. Vo, T. N. Truong, H. J. Kang, "A Novel Fixed-Time Control Algorithm for Trajectory Tracking Control of Uncertain Magnetic Levitation Systems", *IEEE Access*, *9*, 47698-47712, 2021.
18. W. Junxiao, L. Zhao, L. Yu. "Adaptive terminal sliding mode control for magnetic levitation systems with enhanced disturbance compensation." *IEEE Transactions on Industrial Electronics,* 68(1), 756-766, 2020.
19. Y. Yu, X. Sun, W. Zhang, "Modeling and decoupling control for rotor system in magnetic levitation wind turbine" *IEEE Access*, *5*, 15516-15528, 2017.
20. Z. Mingda, Z. Long, X. Li. "A new strategy for improving the tracking performance of magnetic levitation system in maglev train.", *Symmetry*, *11*(8), 1053, 2019.

Chapter 7

COMPARING EXTREME LEARNING MACHINE AND ARIMA MODEL FOR FORECASTING COVID-19 TOTAL INFECTED CASES IN TURKEY

Pelin AKIN[1]

Tuba KOC[2]

1 Dr., Çankırı Karatekin University, Faculty of Science, Department of Statistics, Çankırı, Turkey, pelinakin@karatekin.edu.tr, ORCID ID: 0000-0003-3798-4827
2 Dr., Çankırı Karatekin University, Faculty of Science, Department of Statistics, Çankırı,Turkey, tubakoc@karatekin.edu.tr, ORCID ID: 0000-0001-5204-0846

1. INTRODUCTION

The COVID-19 virus, which emerged in Wuhan, China, spread worldwide quickly at the end of 2019. As a result of the spread of the virus worldwide, an increasing number of cases and deaths were declared a pandemic by World Health Organization (WHO) on 11th March 2020. This coronavirus was also named SARSCoV-2.

Social and economic life restrictions have begun in many countries with the pandemic. In particular, measures and prohibitions have been implemented to prevent people from collectively staying together. In many countries, education was suspended, and distance education was started. Domestic and international travel restrictions have been introduced. Concerts and sporting events have been postponed. Obligation to use masks and curfews has been introduced. Intensive research and development studies have emerged to develop a vaccine against this disease during the pandemic period. The human and economic impacts of COVID-19 have led to the evaluation of next-generation vaccine development technology platforms with a new paradigm to accelerate the vaccine development process [URL1].

The COVID-19 epidemic continues with unknown global effects. It cannot be argued that the coronavirus has essential social, economic, and financial impacts and its main impact areas such as illness and death. While scientists carry out drugs, vaccines, and similar research worldwide to solve the disease, academic research on the effects of COVID-19 continues in various branches of science. Machine learning models are used quite frequently in estimating the number of COVID-19 cases. Pinter et al. (2021) proposed a hybrid machine learning approach to predict COVID-19 in Hungary. Their study used hybrid machine learning methods of the adaptive network-based fuzzy inference system (ANFIS) and the multilayer perceptron-imperialist competitive algorithm (MLP-ICA) to predict infected individuals' time series and mortality. They predicted that the epidemic would decrease significantly by the end of May.

On the other hand, Khan et al. (2021) examined the deep extreme learning machine (DELM) method to predict the coronavirus epidemic. They used data samples of different characteristics to predict the coronavirus epidemic with deep learning in training and testing. Ardabili et al. (2020) presented a comparative analysis of machine learning models as alternatives to susceptible–infected–recovered (SIR) and susceptible-exposed-infectious-removed (SEIR) models to predict the COVID-19 pandemic and multilayer perceptron. MLP and adaptive network-based fuzzy inference systems have concluded that ANFIS

methods perform well. Vaid et al. (2020) developed a machine learning model to reveal hidden patterns and predict possible infections based on reported cases. Their study used an unbiased hierarchical Bayesian estimator approach to extract past infections from recent deaths. Kumar et al. (2020) forecasted the dynamics of the COVID-19 Pandemic in the Top 15 countries in April 2020 with ARIMA Model. Alzahrani et al. (2020) estimated the spread of the COVID-19 pandemic in Saudi Arabia using the ARIMA prediction model under current public health interventions. Kufel (2020) estimated the dynamics of verified COVID-19 cases for selected European countries using ARIMA models. Guleryuz (2021) used Box-Jenkins Methods (ARIMA), Brown's Exponential Correction model, and RNN-LSTM to estimate the number of COVID-19 cases in Turkey. Moftakhar et al. (2020) applied Artificial Neural Networks (ANN) and Automatic Regressive Integrated Moving Average (ARIMA) models to estimate the number of patients using the information of new cases observed in Iran. Both algorithms predicted an exponential increase in the number of newly infected patients. The model comparison confirmed that the ARIMA prediction is more accurate than ANN. Yousaf et al. (2020) applied the Auto-Regressive Integrated Moving Average Model (ARIMA) to the data obtained from the National Institute of Health (NIH)-Islamabad and obtained estimates of the number of confirmed cases, deaths, and recoveries of COVID-19 in Pakistan.

In this study, we used an extreme learning machine (ELM) and time series model to determine and predict COVID-19 total infected cases. The article is divided as follows: ELM models are defined in section 2, Autoregressive Integrated Moving Average (ARIMA). In section 3 are shown the results of the algorithms. Finally, a brief discussion is given in Section 4.

2. MATERIAL AND METHODS

2.1. Autoregressive Integrated Moving Average (ARIMA)

Different models are created by using different methods to forecast with time series. ARIMA models are the most widely known and widely used among these models. Autoregressive (AR), Moving Average (MA), Autoregressive Moving Average (ARMA), and Autoregressive Integrated Moving Average (ARIMA) are Box-Jenkins forecasting models (Box and Jenkins 1970). ARIMA model predicts a value in a response time series as a linear combination of past values, past errors, and current and past values of other time series (SAS, 2014). Real-life time series can be stationary as well as often non-stationary.

In general, the structure of the series, whose difference is taken d times to make it stationary, by the ARIMA (p,d,q) model is as given in the following equation.

$$\left(1 - \emptyset_1 B - \emptyset_2 B^2 - \cdots - \emptyset_p B^p\right)(1 - B)^d Y_t = \left(1 - \theta_1 B - \theta_2 B^2 - \cdots - \theta_q B^q\right) e_t$$

where Y_t is a real value at t-period and e_t is the error term. $\emptyset_i (i = 1,2, \dots, p)$ is AR parameters and $\theta_j (j = 1,2, \dots, q)$ is MA parameters. The values of p and q are integers and represent the degree of the model. $(1 - B)^d$ denotes dth degree difference operation. e_t assumed to be typically and independently distributed with mean zero and constant variance (Khashei and Bijari, 2010).

2.2. Extreme Learning Machine (ELM)

The extreme learning machine (ELM) model was proposed by Huang et al. in 2006 (Huang et al., 2006). The working principle of the ELM model and artificial neural networks are quite similar. However, the hidden layer w is determined randomly in the ELM model. In an ELM, let us say X_k is the input and Y_k is the output of the network. The mathematical expression of the network's output with a single hidden layer and M nodes in the hidden layer is defined as follows. (Suresh et al., 2010)

$$\sum_{i}^{M} \beta_i g(W_i X_k + b_i) = Y_k \quad , k = 1,2 \dots N$$

where β_i the output weight, W_i the input weight matrix, and the b_i the threshold values in the i. neuron.

The ELM algorithm can be summarized in three steps as follows. The first step is, input weight W_i and bias b_i is produced randomly with i =1,..., M. The second step is the output matrix of the hidden layer H calculated. The last step is the calculation of output weights (Liang et al., 2006). Nikolaos Kourentzes et al. have developed a newly introduced R package called nnfor to estimate and forecast ELM algorithms in time series data (Kourentzes, 2019).

3. APPLICATION

In this study, ELM and ARIMA methods have been applied to predicting the spread of the COVID-19 epidemic in Turkey. Time-series data from 11th March 2020 to 9th June 2021 of COVID-19 total infected cases from Turkey were collected from URL-1.

Firstly, The ELM model was applied to the COVID-19 data. The parameters in Table 1 were obtained as a result of the experiments.

Table 1. Parameters of the ELM learning algorithms

Layer Numbers	Input :30 Hidden Layer :40 Output Layer :1
Activation Functions	Linear
MSE	0.0001

A visual summary of the ELM model was given in Figure 1.

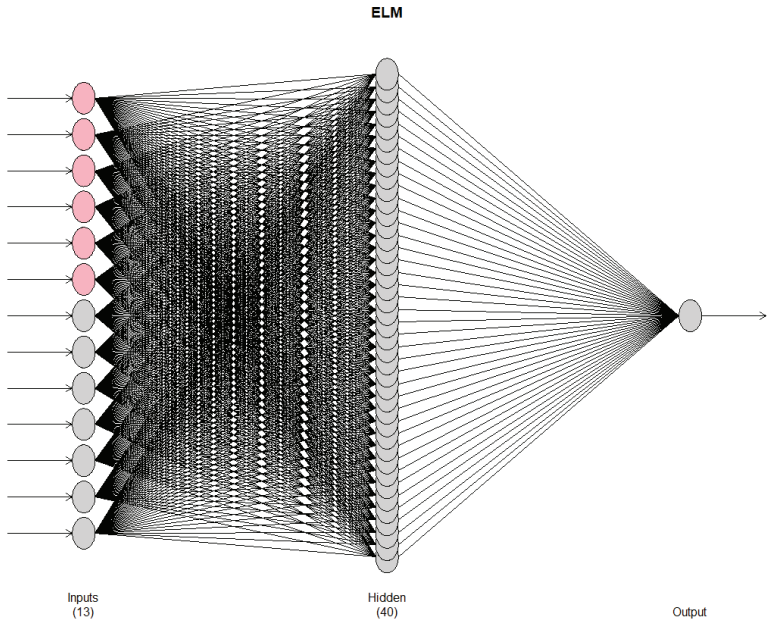

Figure 1. The structure of the ELM model

In Figure 1, the output indicates that the resulting network has 40 hidden nodes, it was trained 20 times, and the different values were combined using the median operator. Finally, the predicted value obtained from the ELM model and actual values were given in Figure 2.

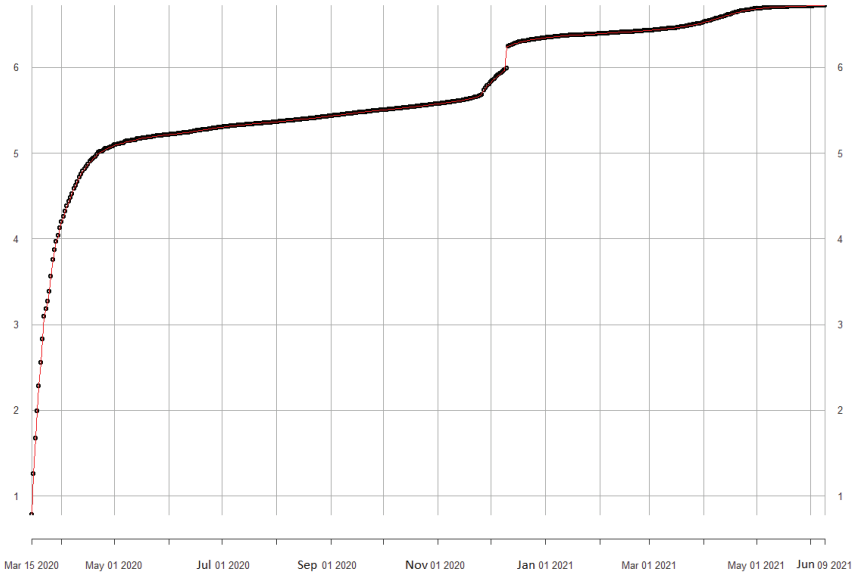

Figure 2. Comparison between the predicted value and actual value

It is seen in Figure 2 that the predicted values obtained from the ELM model and the actual values are very close. Secondly, the ARIMA model was applied to the COVID-19 data. In Figure 3, ACF and PACF graphs were given.

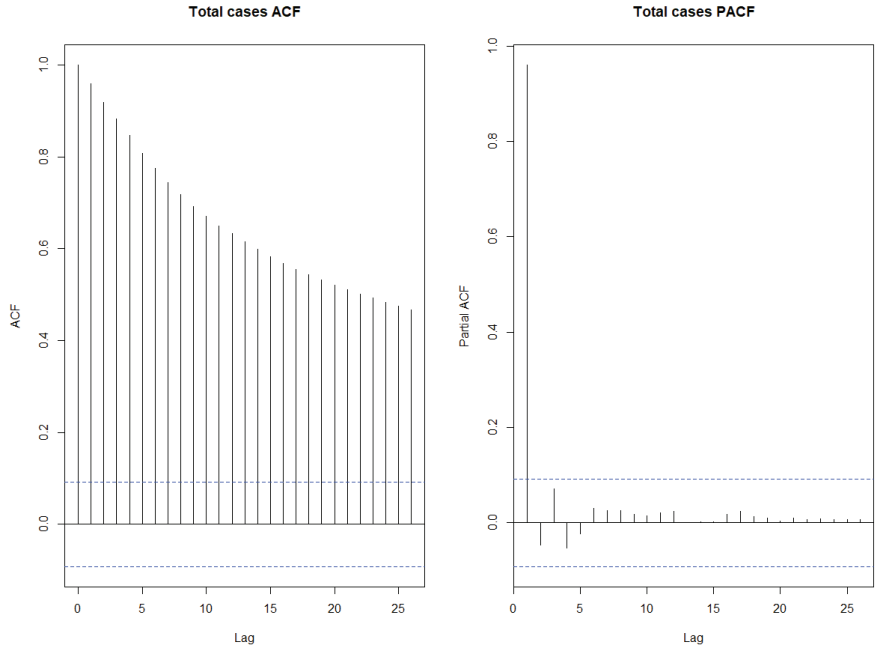

Figure 3. ACF and PACF plot

The ACF plot helps identify non-stationary time series. The ACF will drop to zero relatively quickly for a stationary time series, while the ACF of non-stationary data decreases slowly. Also, for non-stationary data, the value of lags is often large and positive. The process has not constant mean, and series look non-stationary consequently. Thus we need to take differences. Using Akaike Information Criteria (AIC), the best-fitted model has been identified out of the various competing models. The seasonal components (p,d,q) of best fit ARIMA models are (5,2,3) for total infected cases. The AIC value for the best fit ARIMA model is -1728.5. The predicted value obtained from the ARIMA model and actual values were given in Figure 4.

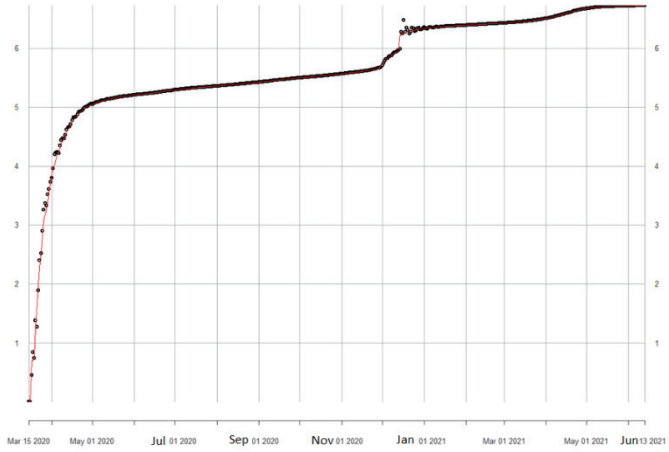

Figure 4. Comparison between the predicted value and actual value

Similar to the ELM model, the predicted values obtained from the ARIMA model and the actual values were found to be very close to each other. Evaluation metrics for ELM and ARIMA models were given in Table 2.

Table 2. Evaluation Metrics for ELM and ARIMA models

Model	MSE	RMSE	MAE
ELM	0.0001	0.0121	0.002
ARIMA	0.0012	0.035	0.0085

The ELM model was found to have smaller error metrics than the ARIMA model. Forecasts were computed for the next 90 days using these models.

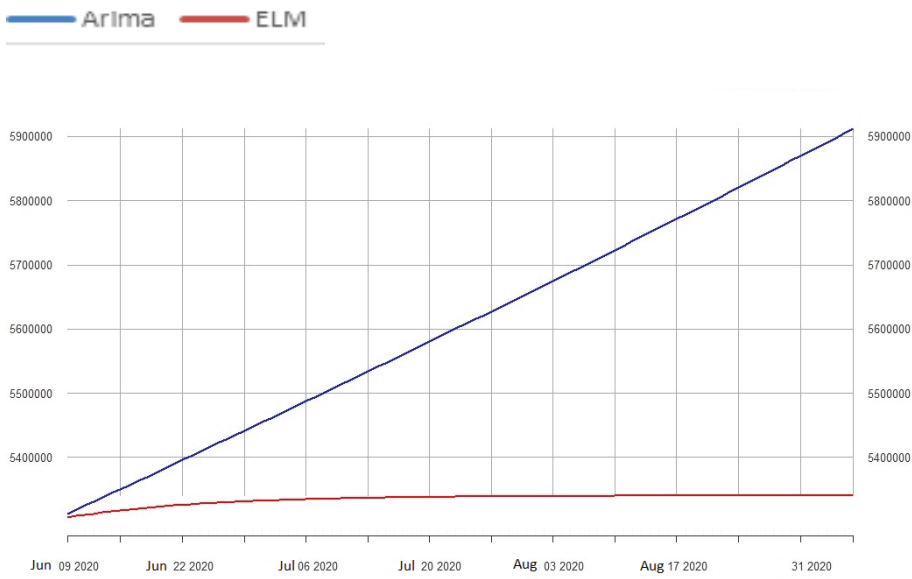

Figure 5. Forecasting result for ELM and ARIMA models

In Figure 5, while the total number of cases is expected to increase in the ARIMA model, it is expected to remain stable in the ELM model. The number of daily cases is obtained by subtracting the previous total case from the total number of cases. Therefore, a decrease in daily cases is expected for the ELM model.

4. CONCLUSION

In this study, ELM and ARIMA methods were applied to forecast the spread of the 90-day COVID-19 outbreak in Turkey. First, the optimal result was achieved when 30 inputs and 40 hidden layer parameters were used in the ELM model to the dataset. The predicted values obtained from the ELM model and the actual values are close. Secondly, the most suitable ARIMA model was selected by applying the ARIMA model. According to the AIC, ARIMA (5, 2, 3) was the best fit model for the total number of infected cases.

When the estimates were examined, it was seen that the results, such as the ELM model, were very close. Error measures were used to compare the ELM and ARIMA models. The ELM model has been shown to perform better (Karimuzzaman, 2020). When ARIMA forecasting is examined, the number of daily cases is 6000 for 90 days, while the number of daily cases is expected to decrease for 90 days according to the ELM model.

REFERENCES

Alzahrani, S. I., Aljamaan, I. A., & Al-Fakih, E. A. (2020). Forecasting the spread of the COVID-19 pandemic in Saudi Arabia using ARIMA prediction model under current public health interventions. Journal of infection and public health, 13(7), 914-919.

Ardabili, S. F., Mosavi, A., Ghamisi, P., Ferdinand, F., Varkonyi-Koczy, A. R., Reuter, U., & Atkinson, P. M. (2020). Covid-19 outbreak prediction with machine learning. Algorithms, 13(10), 249.

Box, G. E., Jenkins, G. M., & Reinsel, G. (1970). Time series analysis: forecasting and control Holden-day San Francisco. BoxTime Series Analysis: Forecasting and Control Holden Day1970.

Guleryuz, D. (2021). Forecasting outbreak of COVID-19 in Turkey; Comparison of Box–Jenkins, Brown's exponential smoothing and long short-term memory models. Process Safety And Environmental Protection, 149, 927-935.

Huang G-B, Zhu Q-Y, Siew C-K. Extreme learning machine: Theory and applications. Neurocomputing 2006; 70: 489–501.

Karimuzzaman, M., Afroz, S., Hossain, M. M., & Rahman, A. (2020). Forecasting the covid-19 pandemic with climate variables for top five burdening and three south asian countries. Medrxiv.

Khan, M. A., Abbas, S., Khan, K. M., Al Ghamdi, M. A., & Rehman, A. (2020). Intelligent forecasting model of COVID-19 novel coronavirus outbreak empowered with deep extreme learning machine. Computers, Materials & Continua, 64(3), 1329-1342.

Khashei, M. and Bijari M., An artificial neural network (p, d,q) model for time series forecasting, Expert Systems with Applications 37, 479–489, 2010.

Kourentzes, N., Barrow, D. K., & Crone, S. F. (2014). Neural network ensemble operators for time series forecasting. Expert Systems with Applications, 41(9), 4235-4244.

Kufel, T. (2020). ARIMA-based forecasting of the dynamics of confirmed Covid-19 cases for selected European countries. Equilibrium. Quarterly Journal of Economics and Economic Policy, 15(2), 181-204.

Kumar, P., Kalita, H., Patairiya, S., Sharma, Y. D., Nanda, C., Rani, M., ... & Bhagavathula, A. S. (2020). Forecasting the dynamics of COVID-19 pandemic in top 15 countries in April 2020: ARIMA model with machine learning approach. MedRxiv.

Liang, N. Y., Saratchandran, P., Huang, G. B., & Sundararajan, N. (2006). Classification of mental tasks from EEG signals using extreme learning machine. International journal of neural systems, 16(01), 29-38.

Moftakhar, L., Mozhgan, S. E. I. F., & Safe, M. S. (2020). Exponentially increasing trend of infected patients with COVID-19 in Iran: a comparison of neural network and ARIMA forecasting models. Iranian Journal of Public Health.

Pinter, G., Felde, I., Mosavi, A., Ghamisi, P., & Gloaguen, R. (2020). COVID-19 pandemic prediction for Hungary; a hybrid machine learning approach. Mathematics, 8(6), 890.

SAS Institute Inc. 2014. SAS/ETS® 13.2 User's Guide. Cary, NC: SAS Institute Inc.

Suresh, S., Saraswathi, S., & Sundararajan, N. (2010). Performance enhancement of extreme learning machine for multi-category sparse data classification problems. Engineering Applications of Artificial Intelligence, 23(7), 1149-1157.

URL-[1] (https://covid19.tubitak.gov.tr/covid19).

Vaid, S., Cakan, C., & Bhandari, M. (2020). Using machine learning to estimate unobserved COVID-19 infections in North America. The Journal of bone and joint surgery. American volume.

Yousaf, M., Zahir, S., Riaz, M., Hussain, S. M., & Shah, K. (2020). Statistical analysis of forecasting COVID-19 for upcoming month in Pakistan. Chaos, Solitons & Fractals, 138, 109926.

Chapter 8

AN OVERVIEW OF IMPACT OF INDUSTRY 4.0 TECHNOLOGIES ON MAINTENANCE, REPAIR AND OVERHAUL AND OTHER CIVIL AVIATION ACTIVITIES

Mecit ÖGE[1]

Tuba ÖZDEMİR ÖGE[2]

1 Faculty of Engineering, Architecture and Design, Department of Mechanical Engineering, Bartın University, Kutlubey-Yazıcılar Campus, 74100 Bartın, Turkey; ORCID ID, https://orcid.org/0000-0001-5243-0828

2 Vocational School of Health Services, Bartın University, 74100 Bartın, Turkey; ORCID ID, https://orcid.org/0000-0001-6690-7199

1. MRO Activities in Civil Aviation, Global MRO Market and Projections

In aviation, maintenance, repair and overhaul (MRO) activities stand for the tasks that should be fulfilled in accordance with airworthiness directives issued by certain national and international organizations, to ensure continued airworthiness of aircrafts or aircraft components. Harsh service environments in which turbine engine components operate, the impact of meteorological conditions, airborne substances and aerodynamic forces continuously exerted on the aircraft frame, coupled with the innately complex electro-mechanic control systems required to safely operate an aircraft are only a few of the considerations that fall within the scope of MRO activities. The complexity and importance of these tasks necessitate periodic maintenance checks for aircraft components after certain flight or usage periods, intervals of which are also specified by airworthiness authorities. These tasks and their intervals are generally organized and optimized so as to minimize the ground time spent for maintenance. These maintenance activities, often called by airline companies or airworthiness authorities as "checks", are categorized based on the activity's extent and termed accordingly as A, B, C or D checks; "A" standing for the lightest and "D" standing for the heaviest check. Lighter checks can be performed at operators' own premises, whereas heavier checks are often performed at the maintenance sites or the hangars of MRO companies or organizations as per Continuous Airworthiness Maintenance Programs (CAMPs) prepared by operators and supervised by airworthiness authorities (Lufthansa Technik, 2021; Aviation Week Network, 2021; Kinnison & Siddiqui, 2013; Qantasnewsroom, 2021). The airworthiness of a commercial aircraft depends on strict compliance to a set of technical and legal regulations, issued by local or national airworthiness authorities which are coordinated under International Civil Aviation Organization (ICAO) (Coutu & Ops, 2014). The maintenance tasks, workforce and inspection systems of public or private operators and MRO organizations are thus continuously supervised in a hierarchical manner.

Between years 2008 and 2019, until the outbreak of coronavirus (COVID-19) disease, the aviation industry experienced an unparalleled growth due to the rising global population coupled with a high economic growth rate, consequently leading to record annual growth levels for in-service global fleet (Mordor Intelligence, 2021; Oliverwyman, 2021). However, as of year 2019, commercial aviation industry has become one of the foremost sectors to confront the global economic impact of the COVID-19 pandemic due to the travel restrictions imposed by governments and consequent suspension of flights by operators as a measure to minimize the spread of the coronavirus (Researchandmarkets, 2021). This has led to

a sharp downturn in global traffic and revenues which forced worldwide operators to shift from their expanding business policies through new aircraft procurements, to maintaining the airworthiness of their existing fleets by focusing on MRO activities. In some of the countries, MRO activities have now been encouraged by governmental initiatives as well, to ensure that adequate MRO sites have been established near the airports. In the light of such developments, the global commercial MRO market has been valued at 33 billion USD for year 2021 and estimated to reach 34 billion USD by year 2026, corresponding to a compound annual growth rate (CAGR) higher than 1% in this forecast period (Mordor Intelligence, 2021). A ten-year MRO market forecast for 2019-2029 period also states that, Asian developing countries, particularly China and India, will be the center of growth for aviation industry, which will certainly affect the share of these countries in the global MRO market (Oliverwyman, 2021). Aside from these projections, MRO companies are yet to face another challenge brought about by the recent emergence of Industry 4.0 and the vast number of opportunities it offers. Technology-driven preventive maintenance plays a key role in the future of MRO organizations. Such that, many of the MRO companies' survival in the near future may depend on their success in achieving a full-scale integration of their preventive maintenance operations with innovative Industry 4.0 technologies; otherwise, they will likely fail to keep up with the competitiveness that these technologies offer for their rivals.

2. Industry 4.0 and Related Technologies

The concept of Industry 4.0 has emerged as an extension of the three industrial revolutions which shaped the world of industry, transportation, communication and all related sectors. The first industrial revolution emerged with the rise of steam power and transition from hand production to mechanized manufacturing in the 19th century. The second industrial revolution, also referred to as the "Technological Revolution" emerged in the late 19th and early 20th century as a result of the technological developments in key sectors such as steel production, and adoption of assembly line production process. The Third Industrial Revolution or Digital Revolution began in the late 20th century as computers and electronics took over the manufacturing world through digitization and automation. So far, all emerging industrial revolutions seem to have overshadowed the previous one's impact on industrial world and human life. Therefore, it will not be an overestimation to relate the existing sectors' future with their ability to adopt the newly emerging Industry 4.0 concepts in all aspects of their business.

Industry 4.0 relates to the use of innovative information, communication and data technologies such as cloud, big data, internet

of things (IoT), augmented reality, machine learning, etc. to enhance machine-machine and machine-human communication and interaction in all sectors that have been already digitized by Industry 3.0. Achievement of Industry 4.0 revolution is expected to boost the speed of globalization through a better control over product life cycles and transition from conventional to cyber-physical supply chains for all kinds of products and services, which means shortened times for all stages and processes in manufacturing, logistics and transportation. It can be stated based on the evolution of the four industrial revolutions that, all industrial processes including manufacturing, logistics, supply chains, marketing, inventory management, etc. became more controllable through evolution of smart technologies, which serves to the ultimate goal of reducing the process times required for all aspects of product/service lifetimes and supply chains. The real-time and dynamic monitoring and analysis of data flow in any industrial process, provided by Industry 4.0 enablers, paves the way for decentralized decision making, thus liberating virtually all aspects of an organization from the cumbersome functioning of conventional centralized systems. Higher levels of responsiveness can thus be obtained via smart processes such as predictive manufacturing, predictive maintenance or any other kind of predictive process which is enabled through the use of smart hardware, information technologies, energy saving, and efficient use of resources (Karnik et al., 2021). In this regard, the competitiveness of manufacturers or service providers relies highly on their capability to adapt to smart technologies, also referred to as Industry 4.0 enablers which have been divided into two categories as organizational enablers, relating to organizational operability; and technological enablers comprising of digital/physical process (additive manufacturing, smart robots), digital/physical interface (cyber-physical systems, augmented reality, internet of things, data processing (machine learning, artificial intelligence, big data analysis) and network (cloud computing, blockchain) technologies (Karnik et al., 2021).

3. The Impact of Industry 4.0 Technologies on Civil Aviation and MRO Activities

The highest and the most imminent impact of the fourth industrial revolution will likely be on the sectors for which time losses in product-life management incur the biggest financial losses, such as maintenance, repair and overhaul (MRO) sector in civil aviation. In civil aviation, minimization of the ground time of aircrafts for MRO activities is crucial and a huge amount of expense is at stake through MRO-related downtimes. It can be further postulated that, this is one of the foremost sectors that is influenced by the tiniest innovation to the greatest extent, as airline companies persistently push for lower MRO costs and higher incomes

through quick troubleshooting, reduced downtimes, optimized scheduling and parts management. In this regard, several attempts have been made so far to enhance MRO activities through smart technologies which is also facilitated by the fact that MRO activities can be integrated with almost all industry 4.0 enablers. In the following sub-sections, the impact of these Industry 4.0 technologies on civil aviation and mostly on MRO activities are discussed.

3.1. Additive Manufacturing (AM)

Additive manufacturing, also referred to as 3D printing, is distinguished from the other manufacturing methods as it involves no subtractive or formative methodologies, such as machining or metal forming. According to the International Standards Organization (ISO), with additive manufacturing (AM) technology, material joining is achieved through layer-by-layer material deposition by which 3D components with desired geometries are obtained (Altıparmak & Xiao, 2021; ASTM, 2021). Although the process was initially applied for 3D manufacturing of plastic materials, it has now been applied on a variety of materials including metallic materials, ceramics, bio-materials, composites and even concrete (Pelleg, 2020). In the process, the 3D layer-by-layer material printing is assisted by CAD/CAM software to transfer the digital information related to the design and manufacturing processes to the 3D printing device. ASTM also divides the process into seven categories based on the material joining or solidification method that is used (ASTM, 2021):

(1) In *vat photo-polymerization*, used in the production of high-performance ceramic components, the desired model is built with high accuracy by utilizing a vat of liquid polymer resin, surface of which is cured by a light source (Andreu et al., 2021; Camargo et al., 2021).

(2) Material jetting, also known as direct inkjet printing, involves selective deposition and subsequent curing of liquid photopolymer droplets, enabling higher product output rates on larger surfaces compared to vat photo-polymerization (Dilag et al., 2019).

(3) In *binder jetting* process, the target part is produced in two steps; a low temperature green part formation step, and a sintering step through which the green parts are consolidated (Li et al., 2021). This process is favored in deposition of specific materials which require low processing temperatures.

(4) The *material extrusion* process is widely used in 3D printing of viscoelastic materials such as ceramic pastes and thermosets which behave differently when the applied load is under and below their yield stress. The process is either “wet-on-dry printing”, when the previously deposited

layer is solidified; or "wet-on-wet printing" if it is still deformable (Mollah et al., 2021).

(5) In *Sheet lamination* the target part is built through lamination of thin material sheets where lamination is achieved through ultrasonic welding, bonding or brazing. Achieving the part's final shape requires using subtractive methods such as laser-cutting or machining (Friel, 2022).

(6) Powder bed fusion technique involves the use of various types of granular materials including ceramics, polymers and metals which are layer-by-layer sintered or molten by use of laser or another energy source (Soundararajan et al., 2021).

(7) (Laser based) direct energy deposition has been increasingly applied to deposit functionally graded materials. In this method, the feedstock material in powder or wire form is melted by a laser source, and upon solidification, a metallurgical bond is obtained between the substrate and the subject material (Hotz et al., 2021).

From the MRO point of view, additive manufacturing technologies has a high potential to be effective in the inventory management of low-volume spare parts that have long and unpredictable lead-times (Chen et al., 2019). Although, the cost-benefit ratio of 3D printing of most of the aircraft components cannot compare with that of conventional manufacturing methods, long lead times of some of the key components from original equipment manufacturers (OEMs) are likely to incur significant losses due to the extended MRO-related downtimes and associated expenses, which can be effectively avoided by on-site 3D printing processes. However, the strict requirements imposed by the national and international aviation authorities as to the certification and approval of each individual component used on the airplane restrict the extensive use of this technology (Novák et al., 2020), which brings about the necessity to establish new certification protocols and procedures related to the integration of this technology in the aviation industry. The MRO side of aviation industry thus has a long way to go in terms of full adoption of this manufacturing technology. However, the OEM side has been drawing on the benefits of this technology to a quite larger extent as it provides manufacturing engineers with high flexibility during the design process. Also, the components built with lattice structures as a merit of AM provide significant weight reduction without having to compromise material properties. This consequently leads to reduced environmental footprints via significantly reduced amount of energy requirement and CO_2 emission, along with the intrinsic waste-free nature of additive manufacturing (Altıparmak & Xiao, 2021; Kreiger & Pearce, 2013; Plocher & Panesar, 2019; Shapiro et al., 2016). The environmental impact of the use of additive manufacturing technologies by aviation actors

such as OEMs and MRO companies is likely to be even more pronounced than its cost-benefit impact, since the use of environmental-friendly and energy efficient technologies may become a requisite rather than being an option for an industry. This is because the aviation sector is liable for 2% of annual CO_2 output of human activities (Aviationbenefits, 2021).

3.2. Internet of Things (IoT)

Internet of things is one of the key enablers of Industry 4.0 which paves the way for digitization of the physical world and its integration into a world of cyber-systems. It is defined as the network of all kinds of smart objects which are equipped with hardware and software that enable collection and exchange of data with other smart objects or with their environment (Munirathinam, 2020). Smart devices equipped with sensors, actuators and microcontrollers can be remotely controlled, communicate with their environment or other smart devices through an internet connection, or autonomously react to the changes in their environment by means of a decision-making algorithm assisted by data processing technologies such as machine learning. Decentralized cyber-physical structures enabled by IoT and other enablers of Industry 4.0 thus facilitates all kinds of decision-making processes, leading to significantly shorter product/service life cycles and supply chains in all fields of industry when compared to conventional centralized physical systems. As a result of the reduced process times and the vast number of other possibilities that IoT offers, the number of IoT-compatible objects increases each year and is estimated to reach 500 billion by year 2030 (Cisco, 2021; Khalil et al., 2020). In the particular case of aviation industry, in which flight safety and airworthiness hold utmost importance, IoT-based applications and approaches have found wide usage as a result of the efforts to draw on the merits of this technology. In one of these efforts by Wang et al. (2020), the failure data received from 28 components of a certain airplane type in China, which showed the highest failure rate for a period of ten years, were used to assess the failure distributions that each component obey. The motivation of the authors was to achieve an accurate reliability estimation for maintenance and management of flight equipment by use of an objective Bayesian Markov chain Monte Carlo (MCMC) approach to tackle small sample problems and random right censoring characteristics of the failure data that reliability engineers often encounter. In aviation industry, spare parts inventory management also holds critical importance for MRO operations and in terms of profitability. The fact that 89% of aircraft parts and components are subject to unscheduled maintenance (Keivanpour & Kadi, 2019; Kinnison & Siddiqui, 2013; Reliabilityweb, 2021) renders the management of aircraft spare parts a difficult task. Keivanpour and Kadi (2019) state that, spare parts management, carried out for improving the

availability of spare components for maintenance and repair activities, minimizing the maintenance-related costs as well as the environmental issues, can be optimized by employing real-time condition monitoring which can be achieved through IoT compatible systems (Keivanpour & Kadi, 2019). Despite these merits on the MRO side, adoption of IoT based systems in aviation pose inevitable cyber-security challenges as well. As in all other fields, digitization of aviation sector via the increased use of wireless technologies by use of IoT compatible systems, render the aviation ecosystem components such as communication, navigation and surveillance (CNS) systems increasingly more vulnerable to cyber-attacks and malicious attempts (Dave et al., 2022). Recently, this issue has been the subject of various research studies that attempt to classify these threats and propose solutions for tackling the attacks on wireless aviation systems (Dave et al., 2022). It can be accordingly stated that, given the delicacy of the matter particularly in the aviation industry, cyber-security related studies should be performed at an even pace with those related the use of IoT based wireless technologies in the aviation sector.

3.3. Big Data Analytics

The substantial increase in bandwidth speeds brought about by each subsequent cellular network technology (Intel, 2021) and the resulting enhanced network capacities have led to the generation of substantial amount of data in various formats from diverse channels, also referred to as the big data (Chung et al., 2020). The emergence of big data, named after the amount of data which is considered too big for conventional means of data storage (Chung et al., 2020) has also led to new applications and fields of study in areas where the generated data holds critical importance, such as the aviation sector. In the MRO side of aviation sector, the challenging task of capacity planning due to the uncertainty in maintenance workloads was addressed by Dinis et al. (2019). They proposed the use of Bayesian Networks (BNs) as a tool for big data and predictive analysis (BDPA) in transforming raw MRO data into useful information for capacity planning tasks. They used real MRO data received from a MRO company to develop Bayesian Networks to demonstrate the developed BNs' superior applicability compared to other approaches (Dinis et al., 2019). The increased complexity of aviation data particularly after the accelerated integration of IoT with conventional aviation systems have rendered the conventional statistical and data analysis methods obsolete and inadequate, leading to the application of topological methods such as topological data analysis and persistent homology (TDA/PH) (Li et al., 2019) to deal with such complex aviation data sets. Li et al. (2019) introduced a numerical case study to justify the applicability of TDA/PH as a newly emerging era in applied mathematics to deal with complex aviation data sets and to show

this topological method's superiority in revealing the interactions underlying aviation data sets (Li et al., 2019). In another attempt to transform aviation-based big data into useful information, Pretto et al. (2019) proposed a way to harness the large amount of aviation data generated by websites and other sources to identify flight events and compute flight paths as a means for estimating aircraft noise levels from commercial air traffic (Pretto et al., 2019). Reportedly, their method can be used by aviation policy makers to minimize the detrimental environmental effect of commercial air traffic induced by aircraft and airport noise (Pretto et al., 2019). As indicated by these and many other works related to the exploitation of big data generated by aviation activities, there is a huge potential for the concept of big data, data science and related fields to enhance the profitability and efficiency of aviation operations and to minimize their impact on the environment as a result of the intrinsic power and potential of data which is regarded as the new fuel of the 21th century (Wired, 2021).

3.4. Augmented Reality (AR) and Digital Twin (DT)

Augmented reality and digital twin are the two important enablers of Industry 4.0 which have direct compliance with aviation operations, in particular with MRO activities. Although the two concepts resemble each other as they are both based on virtual reality, they differentiate from each other in some aspects. Augmented reality relates to overlaying digital environment on real-world environment (Fernández Del Amo et al., 2018), thus providing an improved sense of reality enriched by digital content, which has proven to be effective in a variety of fields involving healthcare (Asadzadeh et al., 2021; Herath et al., 2021; Jung et al., 2021; Sumdani et al., 2021; Venkatesan et al., 2021), education (Faqih & Jaradat, 2021; Kaur et al., 2020; Law & Heintz, 2021; Roopa et al., 2021; Theodoropoulos & Lepouras, 2021), training in diverse fields (D'Anniballe et al., 2020; Herbert et al., 2021; Mitsuhara et al., 2021; Tai et al., 2021), maintenance activities (Ceruti et al., 2019; Eschen et al., 2018; Ramirez et al., 2013; Webel et al., 2013), and industrial applications (Lambrecht et al., 2021; Ong et al., 2020; Suárez-Warden et al., 2015; Tatić & Tešić, 2017). The emergence and application of augmented reality dates back to early 1990s with the first AR system "Virtual Fixtures" developed by the Armstrong Laboratory of U.S. Air Force (Rosenberg, 1992). For commercial purposes, the technology was initially applied in gaming and entertainment businesses (Rosenberg, 2021). Augmented reality is distinguished from the older virtual reality techniques as it can be connected to the real world via mobile devices with digital symbols superimposed onto the real-world environment (Ceruti et al., 2019). In virtual reality, on the other hand, the user can only experience a computer generated (or artificial) environment (Whatistechtarget, 2021). Digital twin is a much newer concept than both virtual reality and

augmented reality and it delivers artificial or virtual twins of real entities, such as industrial products, infrastructures or systems. It resembles virtual reality rather than its successor augmented reality by providing a digital environment. However, it is differentiated from the both concepts through a direct connection between the real and digital counterparts, that enables simultaneously adjusting the digital twin to the changes on the real side. Increasing number of studies have been published related to the use of AR and DT in aviation and MRO sectors which are prone to adopt any technology related to the exploitation of data and digitization of real environments. Ceruti et al. (2019) attempted to demonstrate the viability of AR and AM technologies as a tool in aviation MRO activities and drew attention to the challenge of establishing regulatory frameworks before these technologies are fully adopted by the aviation sector. They further proposed that, AR technology can assist MRO operators with user-friendly manuals through enrichment of real environment with digital models and MRO instructions (Ceruti et al., 2019). Mourtzis et al. (2020) proposed a framework for AR-based MRO instructions using convolutional Neural Networks (Mourtzis et al., 2020). They reported that, AR reduced the mean time to repair to a considerable extent and further stated on the basis of their experiments that, their framework can reduce the AR-based instruction preparation time and improve the user experience (Mourtzis et al., 2020). Abramovici et al. (2017) proposed an approach to facilitate the collaboration between practitioners of different MRO tasks by use of AR-based collaboration assisting systems (Abramovici et al., 2017). Amo et al. (2018) also proposed a framework to identify the types and formats of information for AR for improving the maintenance efficiency of complex systems (Fernández Del Amo et al., 2018). Eschen et al. (2018) applied their mixed reality (MR) concept on four different cases in the aviation sector to facilitate the selection of the appropriate MR technology, such as AR and VR for a given case. They based their methodology on the classification of human/non-human-asset interactions (Eschen et al., 2018). As a comparatively novel technology, DT has also attracted considerable interest as a facilitator for maintenance activities. Apostolidis (2021) proposed a concept for an artificial intelligence (AI) based DT of the Power Electronics Cooling System (PECS) of an aircraft as a means for improving the MRO operations of this system (Apostolidis & Stamoulis, 2021). They proposed a way to redesign the mentioned system so as to build its digital twin that can be used for data analysis using AI (Apostolidis & Stamoulis, 2021). Laukotka (2021) proposed a combined approach of DT, product family design and model-based systems engineering (MBSE) approach for aircraft cabins to reduce failures and improve operational efficiency (Laukotka et al., 2021).

4. Concluding Remarks

The present work provides an overview of the global Maintenance, Repair and Overhaul (MRO) market in the aviation sector and the progress of its integration with Industry 4.0 enablers such as Additive Manufacturing (AM), Internet of Things (IoT), Big Data Analytics (BDA), Augmented Reality (AR) and Digital Twin (DT). It is highlighted that, the aviation sector is highly prone to exploit the merits of Industry 4.0 technologies as almost all operations ranging from original equipment manufacturing to MRO, from business management to capacity planning are data driven. Moreover, the global aviation sector has been forced to exploit the merits of Industry 4.0 technologies to the highest extent as a result of the significant impact of COVID-19 outbreak on all aspects of the sector. Coupled with the negative impact of the pandemic, the increased competitiveness also renders the adoption of such technologies a priority for operators and MRO companies. The main limitation for the actors of the industry has been the requirement for establishment of new legislative frameworks to adopt these new concepts and technologies as the sector is subject to strict rules imposed by local and international airworthiness authorities. Despite the legislative limitations, recent works on adaptation of Industry 4.0 technologies by aviation sector show that, there is virtually unlimited potential for exploitation of Industry 4.0 enablers by the aviation sector. The adoption of these technologies by the sector will likely be facilitated by the consequences of COVID-19 pandemic which have already resulted in radical changes in almost all governments of the world.

References

Abramovici, M., Wolf, M., Adwernat, S., & Neges, M. (2017). Context-aware Maintenance Support for Augmented Reality Assistance and Synchronous Multi-user Collaboration. *Procedia CIRP*, *59*, 18–22. https://doi.org/10.1016/J.PROCIR.2016.09.042

Aircraft Maintenance - Overhaul and Maintenance | Lufthansa Technik. Retrieved December 10, 2021, from https://www.lufthansa-technik.com/aircraft-maintenance

Altıparmak, S. C., & Xiao, B. (2021). A market assessment of additive manufacturing potential for the aerospace industry. *Journal of Manufacturing Processes*, *68*, 728–738. https://doi.org/10.1016/J.JMAPRO.2021.05.072

Andreu, A., Su, P. C., Kim, J. H., Siang, C., Kim, S., Kim, I., Lee, J., Noh, J., Suriya, A., & Yoon, Y. J. (2021). 4D printing materials for vat photopolymerization. *Additive Manufacturing*, *44*, 102024. https://doi.org/10.1016/J.ADDMA.2021.102024

Apostolidis, A., & Stamoulis, K. P. (2021). An AI-based Digital Twin Case Study in the MRO Sector. *Transportation Research Procedia*, *56*, 55–62. https://doi.org/10.1016/J.TRPRO.2021.09.007

Asadzadeh, A., Samad-Soltani, T., & Rezaei-Hachesu, P. (2021). Applications of virtual and augmented reality in infectious disease epidemics with a focus on the COVID-19 outbreak. *Informatics in Medicine Unlocked*, *24*, 100579. https://doi.org/10.1016/J.IMU.2021.100579

Aviation's impact on the environment : Aviation: Benefits Beyond Borders. . Retrieved December 10, 2021, from https://aviationbenefits.org/environmental-efficiency/aviations-impact-on-the-environment/

Benefits of 5G Technology: 5g Features and Advantages | Intel. Retrieved December 10, 2021, from https://www.intel.com/content/www/us/en/wireless-network/5g-benefits-features.html

Camargo, I. L. de, Morais, M. M., Fortulan, C. A., & Branciforti, M. C. (2021). A review on the rheological behavior and formulations of ceramic suspensions for vat photopolymerization. *Ceramics International*, *47*(9), 11906–11921. https://doi.org/10.1016/J.CERAMINT.2021.01.031

Ceruti, A., Marzocca, P., Liverani, A., & Bil, C. (2019). Maintenance in aeronautics in an Industry 4.0 context: The role of Augmented Reality and Additive Manufacturing. *Journal of Computational Design and Engineering*, *6*(4), 516–526. https://doi.org/10.1016/J.JCDE.2019.02.001

Chen, J., Gusikhin, O., Finkenstaedt, W., & Liu, Y. N. (2019). Maintenance, Repair, and Operations Parts Inventory Management in the Era of Industry 4.0. *IFAC-PapersOnLine*, *52*(13), 171–176. https://doi.org/10.1016/J.IFACOL.2019.11.171

Chung, S. H., Ma, H. L., Hansen, M., & Choi, T. M. (2020). Data science and analytics in aviation. *Transportation Research Part E: Logistics and Transportation Review*, *134*, 101837. https://doi.org/10.1016/J.TRE.2020.101837

Commercial Aircraft Maintenance, Repair, and Overhaul (MRO) Market - Growth, Trends, COVID-19 Impact, and Forecasts (2021 - 2026). (n.d.). Retrieved December 10, 2021, from https://www.researchandmarkets.com/reports/4515623/commercial-aircraft-maintenance-repair-and

Commercial Aircraft MRO Market | 2021 - 26 | Industry Share, Size, Growth - Mordor Intelligence. Retrieved December 10, 2021, from https://www.mordorintelligence.com/industry-reports/global-aircraft-maintenance-repair-and-overhaul-market-industry

Coutu, A., & Ops, A. (2014). *ICAO Doc 9760 (Airworthiness Manual) 3rd Edition-2014*.

D'Anniballe, A., Silva, J., Marzocca, P., & Ceruti, A. (2020). The role of augmented reality in air accident investigation and practitioner training. *Reliability Engineering & System Safety*, *204*, 107149. https://doi.org/10.1016/J.RESS.2020.107149

Data Is the New Oil of the Digital Economy | WIRED. Retrieved December 10, 2021, from https://www.wired.com/insights/2014/07/data-new-oil-digital-economy/

Dave, G., Choudhary, G., Sihag, V., You, I., & Choo, K.-K. R. (2022). Cyber security challenges in aviation communication, navigation, and surveillance. *Computers & Security*, *112*, 102516. https://doi.org/10.1016/J.COSE.2021.102516

Dilag, J., Chen, T., Li, S., & Bateman, S. A. (2019). Design and direct additive manufacturing of three-dimensional surface micro-structures using material jetting technologies. *Additive Manufacturing*, *27*, 167–174. https://doi.org/10.1016/J.ADDMA.2019.01.009

Dinis, D., Barbosa-Póvoa, A., & Teixeira, Â. P. (2019). Valuing data in aircraft maintenance through big data analytics: A probabilistic approach for capacity planning using Bayesian networks. *Computers & Industrial Engineering*, *128*, 920–936. https://doi.org/10.1016/J.CIE.2018.10.015

Eschen, H., Kötter, T., Rodeck, R., Harnisch, M., & Schüppstuhl, T. (2018). Augmented and Virtual Reality for Inspection and Maintenance Processes in the Aviation Industry. *Procedia Manufacturing*, *19*, 156–163. https://doi.org/10.1016/J.PROMFG.2018.01.022

Faqih, K. M. S., & Jaradat, M. I. R. M. (2021). Integrating TTF and UTAUT2 theories to investigate the adoption of augmented reality technology in education: Perspective from a developing country. *Technology in Society*, *67*, 101787. https://doi.org/10.1016/J.TECHSOC.2021.101787

Fernández Del Amo, I., Erkoyuncu, J. A., Roy, R., & Wilding, S. (2018). Augmented Reality in Maintenance: An information-centred design fra-

mework. *Procedia Manufacturing*, *19*, 148–155. https://doi.org/10.1016/J.PROMFG.2018.01.021

Friel, R. J. (2022). Metal Sheet Lamination – Ultrasonic. *Encyclopedia of Materials: Metals and Alloys*, 134–140. https://doi.org/10.1016/B978-0-12-819726-4.00120-4

Global Fleet & MRO Market Forecast Commentary 2019-2029. (n.d.). Retrieved December 10, 2021, from https://www.oliverwyman.com/our-expertise/insights/2019/jan/global-fleet-mro-market-forecast-commentary-2019-2029.html

Herath, S., Yau, C. D., Hoh, P. C., Liew, O. W., & Ng, T. W. (2021). An Augmented Reality tourniquet tightening trainer for peripheral venepuncture. *Sensors and Actuators A: Physical*, *332*, 113202. https://doi.org/10.1016/J.SNA.2021.113202

Herbert, B., Wigley, G., Ens, B., & Billinghurst, M. (2021). Cognitive load considerations for Augmented Reality in network security training. *Computers & Graphics*. https://doi.org/10.1016/J.CAG.2021.09.001

Hotz, H., Zimmermann, M., Greco, S., Kirsch, B., & Aurich, J. C. (2021). Additive manufacturing of functionally graded Ti-Al structures by laser-based direct energy deposition. *Journal of Manufacturing Processes*, *68*, 1524–1534. https://doi.org/10.1016/J.JMAPRO.2021.06.068

Internet of Things at a Glance | Cisco . Retrieved December 10, 2021, from https://www.cisco.com/c/dam/en/us/products/collateral/se/internet-of-things/at-a-glance-c45-731471.pdf

Jung, C., Wolff, G., Wernly, B., Bruno, R. R., Franz, M., Schulze, P. C., Silva, J. N. A., Silva, J. R., Bhatt, D. L., & Kelm, M. (2021). Virtual and Augmented Reality in Cardiovascular Care: State-of-the-Art and Future Perspectives. *JACC: Cardiovascular Imaging*. https://doi.org/10.1016/J.JCMG.2021.08.017

Karnik, N., Bora, U., Bhadri, K., Kadambi, P., & Dhatrak, P. (2021). A comprehensive study on current and future trends towards the characteristics and enablers of industry 4.0. *Journal of Industrial Information Integration*, 100294. https://doi.org/10.1016/J.JII.2021.100294

Kaur, D. P., Mantri, A., & Horan, B. (2020). Enhancing Student Motivation with use of Augmented Reality for Interactive Learning in Engineering Education. *Procedia Computer Science*, *172*, 881–885. https://doi.org/10.1016/J.PROCS.2020.05.127

Keivanpour, S., & Kadi, D. A. (2019). The Effect of "Internet of Things" on Aircraft Spare Parts Inventory Management. *IFAC-PapersOnLine*, *52*(13), 2343–2347. https://doi.org/10.1016/J.IFACOL.2019.11.556

Khalil, K., Elgazzar, K., Seliem, M., & Bayoumi, M. (2020). Resource discovery techniques in the internet of things: A review. *Internet of Things*, *12*, 100293. https://doi.org/10.1016/J.IOT.2020.100293

Kinnison, H. A., & Siddiqui, T. (2013). *Aviation Maintenance Management*. 318. https://www.accessengineeringlibrary.com/content/book/9780071805025

Kreiger, M., & Pearce, J. M. (2013). Environmental Life Cycle Analysis of Distributed Three-Dimensional Printing and Conventional Manufacturing of Polymer Products. *ACS Sustainable Chemistry and Engineering*, *1*(12), 1511–1519. https://doi.org/10.1021/SC400093K

Lambrecht, J., Kästner, L., Guhl, J., & Krüger, J. (2021). Towards commissioning, resilience and added value of Augmented Reality in robotics: Overcoming technical obstacles to industrial applicability. *Robotics and Computer-Integrated Manufacturing*, *71*, 102178. https://doi.org/10.1016/J.RCIM.2021.102178

Laukotka, F., Hanna, M., & Krause, D. (2021). Digital twins of product families in aviation based on an MBSE-assisted approach. *Procedia CIRP*, *100*, 684–689. https://doi.org/10.1016/J.PROCIR.2021.05.144

Law, E. L. C., & Heintz, M. (2021). Augmented reality applications for K-12 education: A systematic review from the usability and user experience perspective. *International Journal of Child-Computer Interaction*, *30*, 100321. https://doi.org/10.1016/J.IJCCI.2021.100321

Li, M., Huang, J., Fang, A., Mansoor, B., Pei, Z., & Ma, C. (2021). Binder jetting additive manufacturing of copper/diamond composites: An experimental study. *Journal of Manufacturing Processes*, *70*, 205–213. https://doi.org/10.1016/J.JMAPRO.2021.08.041

Li, M. Z., Ryerson, M. S., & Balakrishnan, H. (2019). Topological data analysis for aviation applications. *Transportation Research Part E: Logistics and Transportation Review*, *128*, 149–174. https://doi.org/10.1016/J.TRE.2019.05.017

Major Maintenance Due For Airbus A380s | Aviation Week Network. (n.d.). Retrieved December 10, 2021, from https://aviationweek.com/mro/major-maintenance-due-airbus-a380s

Mitsuhara, H., Tanimura, C., Nemoto, J., & Shishibori, M. (2021). Expressing Disaster Situations for Evacuation Training Using Markerless Augmented Reality. *Procedia Computer Science*, *192*, 2105–2114. https://doi.org/10.1016/J.PROCS.2021.08.218

Mollah, M. T., Comminal, R., Serdeczny, M. P., Pedersen, D. B., & Spangenberg, J. (2021). Stability and deformations of deposited layers in material extrusion additive manufacturing. *Additive Manufacturing*, *46*, 102193. https://doi.org/10.1016/J.ADDMA.2021.102193

Mourtzis, D., Angelopoulos, J., & Panopoulos, N. (2020). A framework for automatic generation of augmented reality maintenance & repair instructions based on convolutional Neural networks. *Procedia CIRP*, *93*, 977–982. https://doi.org/10.1016/J.PROCIR.2020.04.130

Munirathinam, S. (2020). Industry 4.0: Industrial Internet of Things (IIOT). *Advances in Computers*, *117*(1), 129–164. https://doi.org/10.1016/BS.ADCOM.2019.10.010

Novák, A., Sedlácková, A. N., Bugaj, M., Kandera, B., & Lusiak, T. (2020). Use of Unmanned Aerial Vehicles in Aircraft Maintenance. *Transportation Research Procedia*, *51*, 160–170. https://doi.org/10.1016/J.TRPRO.2020.11.018

Ong, S. K., Yew, A. W. W., Thanigaivel, N. K., & Nee, A. Y. C. (2020). Augmented reality-assisted robot programming system for industrial applications. *Robotics and Computer-Integrated Manufacturing*, *61*. https://doi.org/10.1016/J.RCIM.2019.101820

Pelleg, J. (2020). *Additive and traditionally manufactured components : a comparative analysis of mechanical properties*. Elsevier., https://doi.org/10.1016/C2019-0-04180-5

Plocher, J., & Panesar, A. (2019). Review on design and structural optimisation in additive manufacturing: Towards next-generation lightweight structures. *Materials & Design*, *183*, 108164. https://doi.org/10.1016/J.MATDES.2019.108164

Pretto, M., Giannattasio, P., De Gennaro, M., Zanon, A., & Kühnelt, H. (2019). Web data for computing real-world noise from civil aviation. *Transportation Research Part D: Transport and Environment*, *69*, 224–249. https://doi.org/10.1016/J.TRD.2019.01.022

Ramirez, H., Mendivil, E. G., Flores, P. R., & Gonzalez, M. C. (2013). Authoring Software for Augmented Reality Applications for the Use of Maintenance and Training Process. *Procedia Computer Science*, *25*, 189–193. https://doi.org/10.1016/J.PROCS.2013.11.023

Reliability Centered Maintenance report by F Stanley Nowlan and Howard F Heap - Reliabilityweb: A Culture of Reliability. Retrieved December 10, 2021, from https://reliabilityweb.com/articles/entry/reliability_centered_maintenance_report_by_f_stanley_nowlan_and_howard/

Roopa, D., Prabha, R., & Senthil, G. A. (2021). Revolutionizing education system with interactive augmented reality for quality education. *Materials Today: Proceedings*, *46*, 3860–3863. https://doi.org/10.1016/J.MATPR.2021.02.294

Rosenberg, L. B. (1992). *The Use of Virtual Fixtures as Perceptual Overlays to Enhance Operator Performance in Remote Environments.* https://apps.dtic.mil/sti/citations/ADA292450

Rosenberg, L. B. (2021). *Augmented Reality: Reflections at Thirty Years*. 1–11. https://doi.org/10.1007/978-3-030-89906-6_1

Shapiro, A. A., Borgonia, J. P., Chen, Q. N., Dillon, R. P., McEnerney, B., Polit-Casillas, R., & Soloway, L. (2016). Additive Manufacturing for Ae-

rospace Flight Applications. *Https://Doi.Org/10.2514/1.A33544*, *53*(5), 952–959. https://doi.org/10.2514/1.A33544

Soundararajan, B., Sofia, D., Barletta, D., & Poletto, M. (2021). Review on modeling techniques for powder bed fusion processes based on physical principles. *Additive Manufacturing*, *47*, 102336. https://doi.org/10.1016/J.ADDMA.2021.102336

Standard Terminology for Additive Manufacturing – General Principles – Terminology. Retrieved December 11, 2021, from https://www.astm.org/f3177-15.html

Suárez-Warden, F., Mendívil, E. G., Rodríguez, C. A., & Garcia-Lumbreras, S. (2015). Assembly Operations Aided by Augmented Reality: An Endeavour toward a Comparative Analysis. *Procedia Computer Science*, *75*, 281–290. https://doi.org/10.1016/J.PROCS.2015.12.249

Sumdani, H., Aguilar-Salinas, P., Avila, M. J., Barber, S. R., & Dumont, T. M. (2021). Utility of Augmented Reality and Virtual Reality in Spine Surgery: A Systematic Review of the Literature. *World Neurosurgery*. https://doi.org/10.1016/J.WNEU.2021.08.002

Tai, Y., Shi, J., Pan, J., Hao, A., & Chang, V. (2021). Augmented reality-based visual-haptic modeling for thoracoscopic surgery training systems. *Virtual Reality & Intelligent Hardware*, *3*(4), 274–286. https://doi.org/10.1016/J.VRIH.2021.08.002

Tatić, D., & Tešić, B. (2017). The application of augmented reality technologies for the improvement of occupational safety in an industrial environment. *Computers in Industry*, *85*, 1–10. https://doi.org/10.1016/J.COMPIND.2016.11.004

The A, C and D of aircraft maintenance. Retrieved December 10, 2021, from https://www.qantasnewsroom.com.au/roo-tales/the-a-c-and-d-of-aircraft-maintenance/

Theodoropoulos, A., & Lepouras, G. (2021). Augmented Reality and programming education: A systematic review. *International Journal of Child-Computer Interaction*, *30*, 100335. https://doi.org/10.1016/J.IJCCI.2021.100335

Venkatesan, M., Mohan, H., Ryan, J. R., Schürch, C. M., Nolan, G. P., Frakes, D. H., & Coskun, A. F. (2021). Virtual and augmented reality for biomedical applications. *Cell Reports Medicine*, *2*(7), 100348. https://doi.org/10.1016/J.XCRM.2021.100348

Wang, C., Guo, J., & Shen, A. (2020). Sensitivity analysis of censoring data from component failure analysis and reliability evaluation for the aviation internet of things. *Computer Communications*, *157*, 28–37. https://doi.org/10.1016/J.COMCOM.2020.04.003

Webel, S., Bockholt, U., Engelke, T., Gavish, N., Olbrich, M., & Preusche, C. (2013). An augmented reality training platform for assembly and mainte-

nance skills. *Robotics and Autonomous Systems*, *61*(4), 398–403. https://doi.org/10.1016/J.ROBOT.2012.09.013

What is virtual reality? - Definition from WhatIs.com. Retrieved December 10, 2021, from https://whatis.techtarget.com/definition/virtual-reality

Chapter 9

SOLUTION PLASMA PROCESSING AND ITS APPLICATIONS

Zehra Nur OZER[1]
Mehmet OZKAN[2]

1 Assoc.Prof.Dr. Zehra Nur OZER, Afyon Kocatepe University,Orcid no: 0000-0002-5887-4486
2 Assist.Prof.Dr. Mehmet OZKAN, Afyon Kocatepe University, Orcid no: 0000-0001-8346-1459

Plasma is aforementioned as the fourth state of the matter with respect to a scheme defining an increase in the energy level from solid to liquid to gas, and finally to an ionized state of the gas plasma that shows original features. For formation of the plasma, energy that can ionize a gas is applied. Plasma is formed by several excited atomic, molecular, ionic species with the inclusion of electrons, positive and negative ions, free radicals, gas atoms, molecules in the ground or excited state and also quanta of electromagnetic radiation (Misra et al. 2016). Plasma is not also electrically conductive but also interactive and sensitive to electromagnetic fields.

Plasma can be classified as thermal and non-thermal equilibrium plasma (Horikoshi and Serpone 2017, Yui et al. 2017). In thermal equilibrium plasma the gas and electron temperatures are almost equal and plasma is generated by a strong electrical power under gas pressure. Non-thermal equilibrium plasma can be obtained with adequate energy under vacuum or in atmospheric pressure by electrostatic discharge. It is very important for plasma technology to provide wide range of operating pressures and also temperatures. Thus, non-thermal equilibrium plasma is preferred for applications. Different gases are used for the generation of plasma for different purposes.

Plasma can be obtained by electric current through a gas in a laboratory environment and inducing it with high power radio waves or micro electromagnetic waves. Plasma is used in many areas in technology. It has many applications in optoelectronic devices, photovoltoic batteries, thin film production, surface treatment, chemical industry and medicine.

The usage areas of plasma in technology have generally appeared in the form of systems working under vacuum until the 2000s. This technology is still widely used. At the beginning of the century we live in, atmospheric plasma sources also had application areas in technology. Atmospheric pressure plasma systems have started to be used for sterilization purposes, especially in the health and food sectors. On the other hand, plasma can be created in liquid phase by obtaining sufficient electric field on the electrodes. This type of plasmas is specifically used for water purification, for induce reactive species such as hydroxyl radical, superoxide anion and hydrogen peroxide. In addition to this, it became possible to synthesis of various materials, such as nanoparticles by liquid phase plasma (Hieda et al. 2008). In 2008, the solution plasma system, which is an atmospheric plasma system in liquid, was started to be used for the first time as a work of Takai and his friends in 2008.

SOLUTION PLASMA PROCESS (SPP)

Plasma methods include solid-phase, liquid-phase and gas-phase. SPP is known as atmospheric pressure plasma at room temperature (Takai 2008). In this process, different solutions are used to induce chemical reactions. Being a useful tool for nanomaterial synthesis, SPP is glow discharge in the liquid phase. This method defined as a balanced non-thermal electrohydraulic discharge with electron and ion exchange between the non-thermal liquid phase and the gas phase in aqueous solution (Tong et al., 2012). Since the molecular density is higher in liquid phase plasma compared to gas phase, higher reaction is expected at lower temperatures (Saito and Akiyama, 2015). SPP provides high mass transfer and low electrode damage.

The characteristic regions for solution plasma are gas phase, liquid phase, interface between gas and liquid and interface between electrode surface and gas plasma (Nagai, 2013). Figure 1 shows solution plasma model. In the center plasma is exist and it is encircled with gas phase that is surrounded by liquid phase.

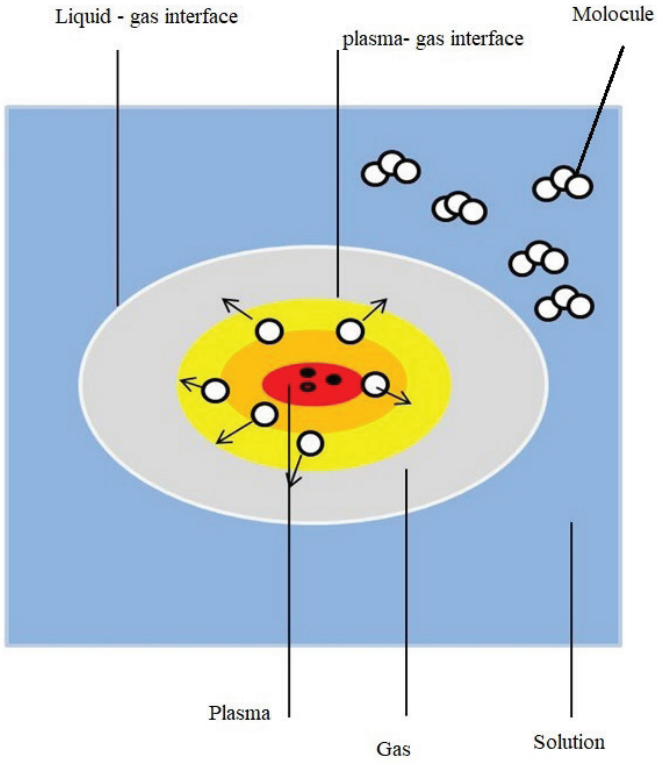

Figure 1. *Solution plasma model (Takai 2014).*

By using activated radicals too fast reactions are maintained in SPP. In comparison to chemical methods, SPP for nanoparticle synthesis results in a short time ranges. In addition, it can be prepared in room conditions within low energy plasma. However, it works in glow discharge parameters and this presents a suitable medium for controlling the chemical reactions in the solution.

Solution plasma studies are more advantageous than the low pressure plasma method. Therefore, the solution plasma system has gained importance for the development of the industrial field. Studies on the applications of SPP in nanomaterial technology are recently presented in literature from surface modification, decomposition, synthesis process to sterilization. Using this process, many nanometarials are synthesized such as metallic, metallic oxide and carbon based nanoparticles. Also, metal oxide composites, polymer treatment and polymer polymerization, water treatment and fuel gas production studies are presented in the literature (Mizutani et al. 2015, Pootawang et al. 2010-2011, Lee et al. 2014, Nakasugi et al. 2015, Saito et al. 2014, Panomsuwan et al. 2015, Janpetch et al. 2016, Pornsunthorntawee et al. 2014, Locke et al. 2006, Nomura et al. 2006).

GENERATION OF SOLUTION PLASMA AND EXPERIMENTAL SETUP

The geometric design and phase patterns can be categorized (Chokradjaroen 2021). Here we will describe direct discharge between in liquid phase in the manner of SPP. In this process, plasma is obtained by discharge between two electrodes mounted in liquid. SPP was firstly proposed by the group of Takai and Saito's group as mentioned above. The electrodes are normally placed in short distances between 0.3mm-2 mm to obtain effective results.

The set up consist of a DC pulsed power supply, reaction cell, optic emission spectrophotometer, PH meter, thermometer (Figure 2). For solution plasma generation, a typical power supply that works in bipolar pulse type with 0-4 kV voltage ranges. Pulse width can be changed in between 0-10 μs including a variable repetition frequency of 0-30 kHz.

The system can be designed in different ways. For example, the electrodes can be placed vertically or horizontally in the reaction cell. In addition to the figure 2, examples of different designs of the experimental system are given in the figure 3 and figure 4. Effects of the placement of the electrodes on the material formation and plasma will be examined in the post-processing studies.

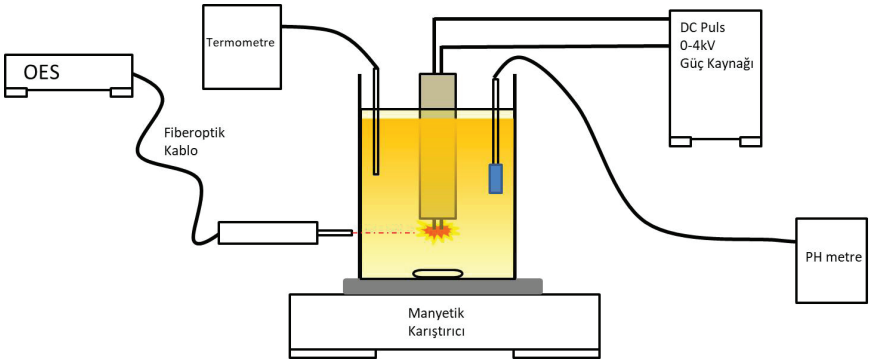

Figure 2. *SP generation setup.*

The voltage, pulse width and frequency applied during operation can be adjusted at the desired level. Since it is a high voltage power source, an additional circuit connected to a multimeter is normally used to measure the applied voltage before the discharge during the experiment. Different volumes of reaction cells are used in which the solution suitable for the metallic nanoparticle to be synthesized is placed. All chemical and physical reactions take place in this reaction cell during the experiment. The reaction cell consists of a cylindrical ceramic coated rod with two tungsten (W) electrodes of different thicknesses at certain distances between them. During the experiment, the voltage provided from the DC power source is given to the tungsten electrodes, and an electrical discharge is created in the solution, thus a chemical reduction process is provided in the solution.

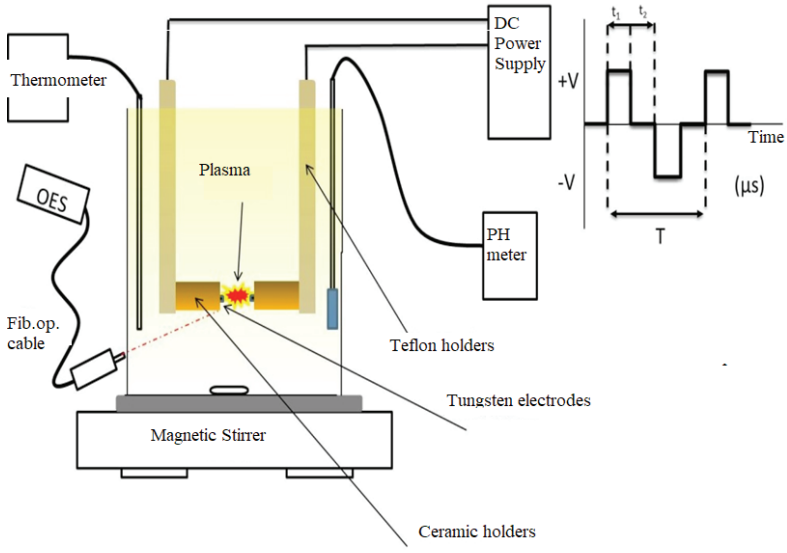

Figure 3. *Alternative design for SP generation setup.*

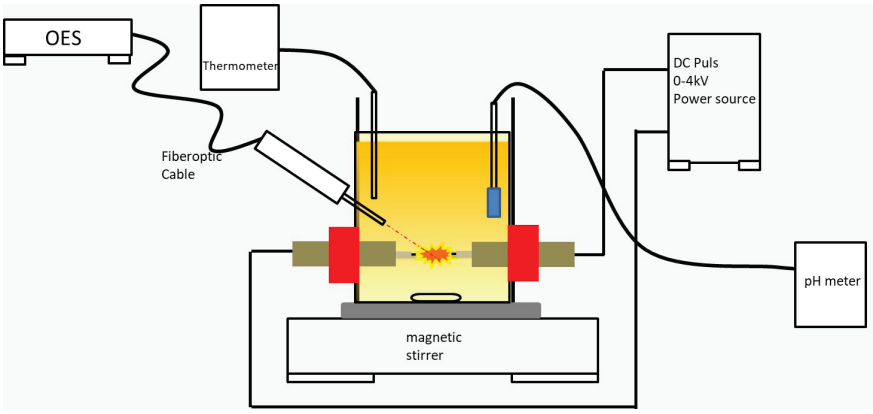

Figure 4. *Alternative design for SP generation setup.*

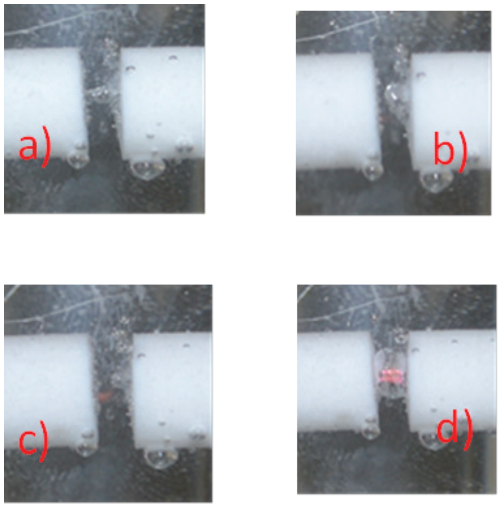

Figure 5. *Phases of discharge formation, between electrodes during operation of the solution plasma system a) beginning of discharge, b,c) development of discharge, d) stabilization of discharge.*

In figure 5, discharge steps are seen during the work performed with a voltage of 1500V, frequency of 15 kHz, pulse width of 2 µs and distance between electrodes of 1 mm. Small bubbles form at first, they become larger, and the discharge becomes more pronounced.

Optic emission spectrophotometer is a device that we can obtain a graph of the intensity and wavelength of the light emitted by the environment or any light source. It consists of two main parts, a fiber optic cable and an electronic circuit where data is transferred to the computer environment. It enables us to determine the radicals formed during the discharge in the solution by analyzing the wavelengths of the rays coming from the plasma

formed in the solution with the help of fiber optic cable. Figures 6 and 7 show optical emission spectra before and after plasma formation. The formation of hydrogen (H_α 655nm, $H\beta$ 480 nm, 435nm), Oxygen (775-845 nm), OH (306 nm) and H_2 (545 nm) radicals by the decomposition of water in the plasma process is clearly visible in the spectrum.

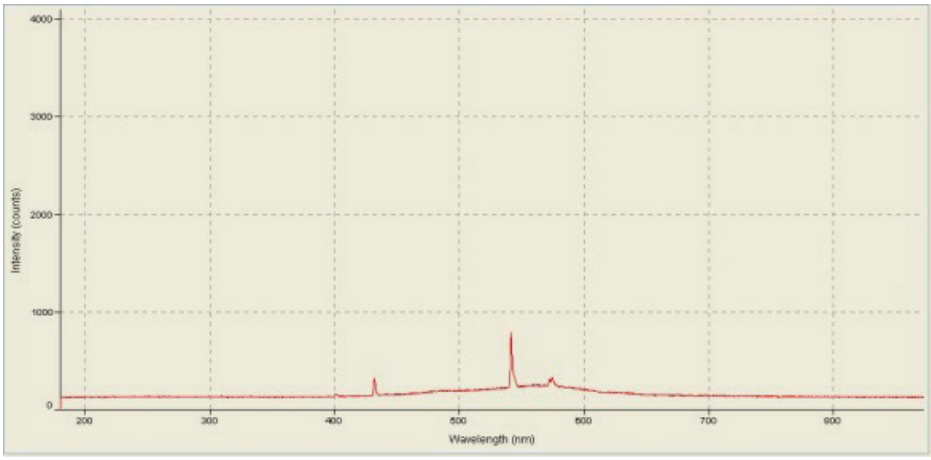

Figure 6. *An example of optical emission spectrum before experiment.*

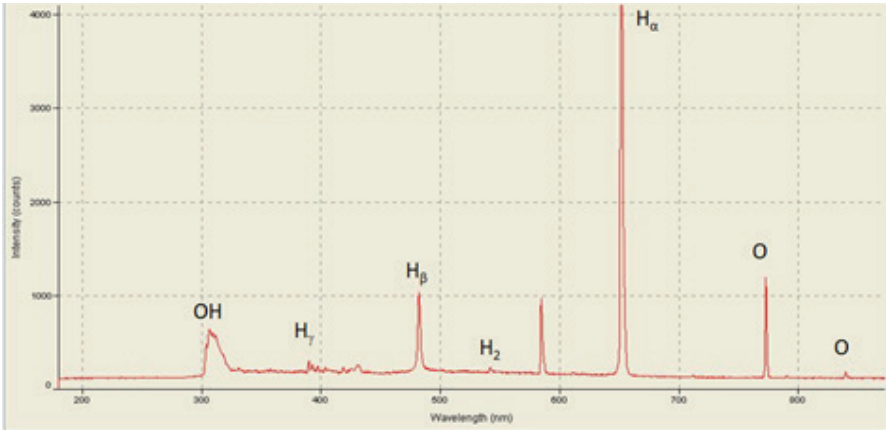

Figure 7. *Optical emission spectrun during the experiment. (Akyüz et al., 2019).*

In nanoparticle synthesis formed by discharge in aqueous solutions, initially dissolved particles in water are reduced and nanoparticles are synthesized simultaneously during discharge. In this process, the core reaction continues continuously in the formation of nanoparticles (Figure 8).

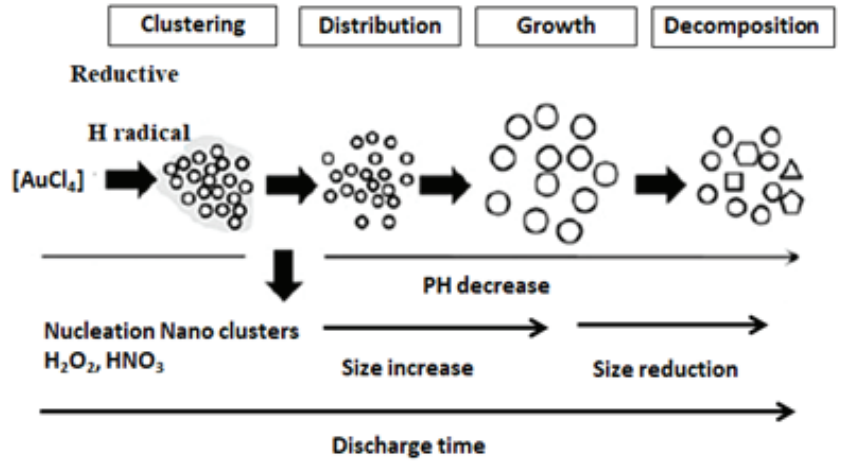

Figure 8. *Mechanism of nanoparticle formation in solution.*

The PH meter is used to measure the working temperature and PH value of the solution during operation. The nanoparticles formed are composed of nanoclusters smaller than 1 nm. As the discharge time increases, the pH of the solution decreases, and the nanoparticles dissolve and decrease in size. Thus, the reduction rate of the ions decreased. While the dissolved anisotropic (direction-dependent atomic arrangement) nanoparticles derived from the ion grow at low speed, the spherical nanoparticles continue to dissociate.

Depending on the type of solution liquid, its absorbance is expected to decrease during the experiment. In figure 9, absorbance graph for three silver samples (Ozkan and Sakarya 2019).

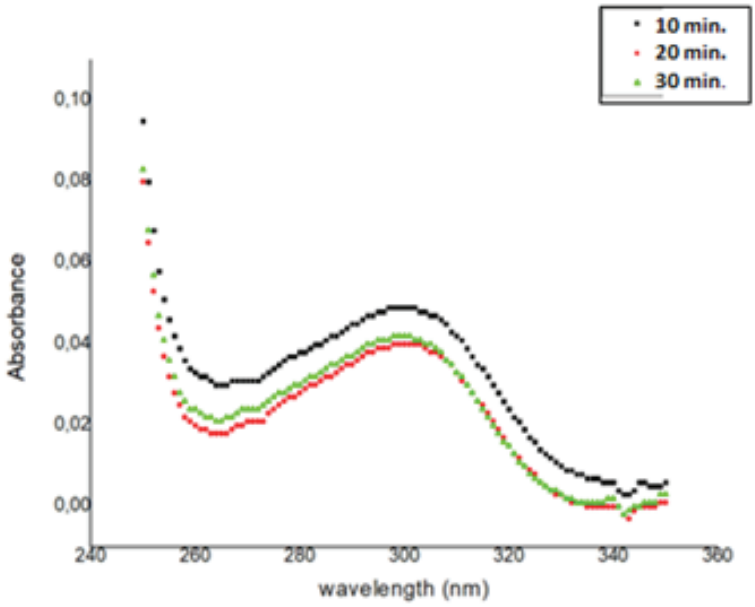

Figure 9. *Absorbance graph of samples taken under 0.5 kV for every ten minutes.*

The change in absorbance of the samples was investigated by UV visible spectrophotometer in the 600 nm wavelength. From figure 9, it is observed that the absorbance value of the solution decreased with the increase of the plasma time.

In SPP, there is no need for a reducer. Particle synthesis by reduction of hydrogen radicals and ions without adding any reducing agents using the solution plasma method has been shown to be a very effective process due to the rapid formation (Jin et al., 2014). During discharge in solution, various active species such as H^-, O^{-2}, OH^-, HO_2, high-energy electrons, UV radiation and shock waves are physically formed (Heo and Lee, 2011). In table 1, we present the possible formation reactions that consist radicals during SPP is given.

Plasma Phase	Liquid Phase
$H_2O \rightarrow H^* + OH^*$	$H^* + H2O \rightarrow H^* + OH^* + O^*$
$2H_2O \rightarrow 2H_2 + O_2$	
$2OH^* \rightarrow H_2O_2$	
$H_2O \rightarrow H^* + OH^*$	

Table 1. *Possible formation of radicals in SPP (Akyüz et. al., 2019).*

In SPP, the geometry of electrodes and the inputs in the power system effects the formation of radicals and excited atoms or molecules. There are typical regions for the process which are glow discharge, corona discharge and pre-breakdown regimes. In the glow discharge regime the peak voltage is more than 2 kV and the space between electrodes is smaller than 2mm. When the distance between electrodes are increased and high voltage peak is high then corona discharge regime is exist. In the pre-breakdown regime the electrochemical reactions have control over.

Another important factor in the process is to control the solution plasma stability. PH and the conductivity of the prepared solution are important to determine the operation regime for solution plasma. It is shown that if the solution conductivity is high than the ionic current is high for the same input electrical power and also instable plasma exists. Also by the increment of the pulse width, electrical power increases. In this case, high conductivity and stable glow discharge can be obtained (Takai 2014). Also, polishing or sharpening electrodes is another way to obtain high stability of plasma as stated in ref (Yui et al. 2017).

In literature it is mentioned that electrode types influence the electrical breakdown and radical generation in the SPP (Miron et al. 2010). Studies on tantalum and tungsten electrodes are done in comparison for SPP. It is found that, higher energy is needed for tantalum electrodes for electrical breakdown. In another study on tungsten and lanthanum hexaboride are compared in terms of electrical breakdown by Miron et al. 2011. As a result it is found that lower electric field is needed for tungsten electrodes. In addition to that according to melting points of these materials, under plasma conditions existence of different reactive species are thought to be observed.

Injected gases can be also used in plasma. The most common gases used in these type systems are O_2,CO_2, N_2 and Ar. The electron density is increased via injection of gases cause of the generation of electron increase the collisions between ions (Banno et al 2016).

APPLICATIONS OF SPP

SPP is a straightforward process for synthesis of metal nanoparticles in the manner of offering fast reactions in non-equilibrium plasma and being discharge plasma at atmospheric pressure. From the studies in literature we know that there are different sizes, shapes and compositions can be obtained via SPP (Saito et al. 2018). Because of its advantages, SPP has become an interdisciplinary working area. Its potential application field examples except nanomaterial syntheses can be expressed as the following: surface modification, water treatment, sterilization, recycling rare metals and decomposition of toxic compounds (Takai et al. 2014).

CONCLUSION

SPP is presented as ecologically friendly, fast and effective process for nanomaterial synthesis and has a wide range of applications in the literature.

In this chapter, the advantages of SPP, its generation including characteristic features and parameters and applications are presented.

SPP offers promising studies of synthesis of nanomaterials, surface treatment and dispersion of nanoparticles, high-speed processing, water and waste treatment and sterilization for the technology of near future (Takai 2014).

REFERENCES

Misra, N. N., Pankaj, S. K., Segat, A., Ishikawa, K. (2016). Cold plasma interactions with enzymes in foods and model systems. Trends in Food Science & Technology, 55, 39-47.

Horikoshi, S., Serpone, N. (2017). In-liquid plasma: A novel tool in the fabrication of nanomaterials and in the treatment of wastewaters. RSC advances, 7(75), 47196-47218.

Yui, K., Tanuma, N., Yamada, H., Kawasaki, Y. (2017). Reduced endogenous urinary total antioxidant power and its relation of plasma antioxidant activity of superoxide dismutase in individuals with autism spectrum disorder. International Journal of Developmental Neuroscience, 60, 70-77.

Hieda, J., Saito, N., Takai, O. (2008). Exotic shapes of gold nanoparticles synthesized using plasma in aqueous solution. Journal of Vacuum Science & Technology A: Vacuum, Surfaces, and Films, 26(4), 854-856.

Takai, O. (2008). Solution plasma processing (SPP). Pure and Applied Chemistry, 80(9), 2003-2011.

Tong, D. G., Wu, P., Su, P. K., Wang, D. Q., Tian, H. Y. (2012). Preparation of zinc oxide nanospheres by solution plasma process and their optical property, photocatalytic and antibacterial activities. Materials Letters, 70, 94-97.

Saito, G., Akiyama, T. (2015). Nanomaterial synthesis using plasma generation in liquid. Journal of Nanomaterials, 2015.

Takai, O. (2014). Fundamentals and applications of solution plasma. Journal of Photopolymer Science and Technology, 27(3), 379-384.

Chokradjaroen, C., Niu, J., Panomsuwan, G., Saito, N. (2021). Insight on Solution Plasma in Aqueous Solution and Their Application in Modification of Chitin and Chitosan. International Journal of Molecular Sciences, 22(9), 4308.

Akyüz, A. Ö., Özkan, M., Ağar, Ö. (2019). Çözelti Plazma Tekniği ile Polimer Degradasyonu: Viskozitenin Online İzlenmesi. Teknik Bilimler Dergisi, 6(2).

Özkan, M., Sakarya, A. (2019). Çözelti Plazması Yöntemiyle Sentezlenen Gümüş Nanoparçacık Boyutuna Voltaj ve Çalışma Süresinin Etkisi. El-Cezeri Journal of Science and Engineering, 6(3), 606-612.

Jin, S. H., Kim, S. M., Lee, S. Y., Kim, J. W. (2014). Synthesis and characterization of silver nanoparticles using a solution plasma process. Journal of nanoscience and nanotechnology, 14(10), 8094-8097.

Heo, Y. K., Lee, S. Y. (2011). Effects of the gap distance on the characteristics of gold nanoparticles in nanofluids synthesized using solution plasma processing. Metals and Materials International, 17(3), 431-434.

Miron, C., Bratescu, M. A., Saito, N., Takai, O. (2010). Time-resolved optical emission spectroscopy in water electrical discharges. Plasma Chemistry and Plasma Processing, 30(5), 619-631.

Miron, C., Bratescu, M. A., Saito, N., Takai, O. (2011). Optical diagnostic of bipolar electrical discharges in HCl, KCl, and KOH solutions. Journal of Applied Physics, 109(12), 123301.

Banno, M., Kanno, K., Yui, H. (2016). Development of direct gas injection system for atmospheric-pressure in-solution discharge plasma for plasma degradation and material syntheses. RSC advances, 6(19), 16030-16036.

Saito, G., Sasaki, H., Takahashi, H., Sakaguchi, N. (2018). Solution-plasma-mediated synthesis of Si nanoparticles for anode material of lithium-ion batteries. Nanomaterials, 8(5), 286.

Mizutani, T., Ogawa, S., Murai, T., Nameki, H., Yoshida, T., & Yagi, S. (2015). In situ UV–vis investigation of growth of gold nanoparticles prepared by solution plasma sputtering in NaCl solution. Applied Surface Science, 354, 397-400.

Pootawang, P., Saito, N., Takai, O. (2011). Ag nanoparticle incorporation in mesoporous silica synthesized by solution plasma and their catalysis for oleic acid hydrogenation. Materials Letters, 65(6), 1037-1040.

Lee, Y. J., Kim, S. M., Kim, J. W., Lee, S. Y. (2014). The characterization and electrocatalytic activities of carbon-supported Pt nanoparticles synthesized by the solution plasma process. Materials Letters, 123, 184-186.

Nakasugi, Y., Saito, G., Yamashita, T., Sakaguchi, N., & Akiyama, T. (2015). Solution plasma synthesis of Au nanoparticles for coating titanium dioxide to enhance its photocatalytic activity. Thin Solid Films, 583, 135-141.

Horiguchi, G., Chikaoka, Y., Shiroishi, H., Kosaka, S., Saito, M., Kameta, N., & Matsuda, N. (2018). Synthesis of Pt nanoparticles as catalysts of oxygen reduction with microbubble-assisted low-voltage and low-frequency solution plasma processing. Journal of Power Sources, 382, 69-76.

Saito, G., Nakasugi, Y., Yamashita, T., & Akiyama, T. (2014). Solution plasma synthesis of ZnO flowers and their photoluminescence properties. Applied surface science, 290, 419-424.

Pootawang, P., Saito, N., Takai, O. (2010). Solution plasma process for template removal in mesoporous silica synthesis. Japanese Journal of Applied Physics, 49(12R), 126202.

Panomsuwan, G., Saito, N., Ishizaki, T. (2015). Electrocatalytic oxygen reduction activity of boron-doped carbon nanoparticles synthesized via solution plasma process. Electrochemistry Communications, 59, 81-85.

Panomsuwan, G., Saito, N., & Ishizaki, T. (2015). Electrocatalytic oxygen reduction activity of boron-doped carbon nanoparticles synthesized via solution plasma process. Electrochemistry Communications, 59, 81-85.

Janpetch, N., Saito, N., Rujiravanit, R. (2016). Fabrication of bacterial cellulose-ZnO composite via solution plasma process for antibacterial applications. Carbohydrate polymers, 148, 335-344.

Pornsunthorntawee, O., Katepetch, C., Vanichvattanadecha, C., Saito, N., & Rujiravanit, R. (2014). Depolymerization of chitosan–metal complexes via a solution plasma technique. Carbohydrate polymers, 102, 504-512.

Locke, B. R., Sato, M., Sunka, P., Hoffmann, M. R., Chang, J. S. (2006). Electrohydraulic discharge and nonthermal plasma for water treatment. Industrial & engineering chemistry research, 45(3), 882-905.

Nomura, S., Toyota, H., Tawara, M., Yamashita, H., Matsumoto, K. (2006). Fuel gas production by microwave plasma in liquid. Applied physics letters, 88(23), 231502.

Chapter 10

EXPERIMENTAL INVESTIGATION OF THE USE OF NEW TYPE TURBULATOR IN A DOUBLE PİPE HEAT EXCHANGER

*Hakan KARAKAYA**
*Hacire DEVİREN***

1 * Assoc. Prof. Dr. Hakan KARAKAYA, Batman University, Batman University Faculty of Engineering and Architecture Department of Mechanical Engineering, ORCID:0000-0001-9242-6233,hakan.karakaya@batman.edu.tr.

** Hacire DEVİREN, Batman University, Batman University Faculty of Engineering and Architecture Department of Mechanical Engineering, ORCID:0000-0003-1285-740X, devirenhacire10@gmail.com.

1. INTRODUCTION

Energy is the name that is given to an object's or system's ability to work. Energy sources can be classified into two groups as nonrenewable and renewable energy sources. Scientific findings reveal the fact that the unconsciously use of nonrenewable energy sources from the industrial revolution to the modern-day will cause an energy shortage in the immediate future.

The demand for energy that is now the most important component of the industry and people is increasing while energy sources under the sun will deplete fast. Energy consumption in Turkey has increased based on technological advancements and population growth; this situation causes natural sources to be consumed in an unconscious manner. There have conducted studies toward increasing the use of alternative energy sources besides conventional energy sources to provide a sustainable energy balance.

Efforts to save energy by increasing heat transfer in the energy sector are quite high recently. The issues of increasing the heat transfer and using the energy efficiently, economically, and effectively are emphasized in the studies on energy saving in the systems used today.

Heat transfer takes place between fluids at different temperatures and is separated from each other by a solid wall. Heat exchangers are used to transferring heat. Heat exchangers have a wide range of uses.

Heat exchangers can be classified based on the type of heat exchange, surface area density, number of fluids, heat transfer mechanism, design (construction) features, and flow patterns. The construction materials of the heat exchanger, performance parameters (fluid inlet and outlet temperatures, flow rates, and pressure drops), types of fluids, fluid phases, economic factors, heat transfer mechanism, size of the heat exchanger, pollution tendencies should be known in terms of evaluating the design and performance of heat exchangers. Factors such as fluid temperature, pressure, corrosion, resistance to working conditions in acid and alkaline environments should be taken considered while choosing the material in the heat exchanger design. Moreover, physical properties such as density, heat transfer coefficient, heat dissipation coefficient should also be taken into account.

Low heat transfer coefficient in the heat exchangers significantly reduces the surface heat transfer; this is because a high heat transfer coefficient is desirable. High-pressure gases are passed through the surface of the inner pipe in heat exchangers while lower pressure gases are passed through the outer surface of the pipes. Thus, the heat transfer coefficient

on the inner pipe surface becomes greater than the heat transfer coefficient on the outer surface of the pipe. Crossflow can be applied to the pipe to increase the heat transfer coefficient on the outer surface of the pipe.

Several methods are utilized to increase the amount of heat transfer in heat exchangers. These can be divided into two groups as active method and passive method. It is called the active method if the heat transfer is increased by giving energy to the fluid and the environment. Mixing the fluid using mixers, using mechanical elements, rotating the surface, creating electrostatic fields in the flow area can be given as examples for the active method. It is called the passive method if the heat transfer is increased without energizing the fluid and the environment. The passive method can be exampled as enlarged surfaces, finned surfaces, turbulators placed in the pipe to give the fluid rotational motion, and turbulence-enhancing rough surfaces (Balbay, 2001; Karali, 2002; Yakut, 2006; Genceli, 1983).

This study aimed to improve heat transfer by using one of the passive methods which is one of the heat transfer improvement techniques in a concentric tube heat exchanger. In the experiments, turbulators in different positions and numbers were placed in the heat exchanger in order to activate the heat transfer from the hot fluid to the cold fluid. An experimental set was set up to carry out experimental studies. Parameters such as temperature, pressure loss, and velocity in the flow in the heat exchanger were determined by measuring devices with turbulators placed in nested cylinders with constant surface temperature boundary conditions. Thermal efficiency, pressure loss, and friction factor are calculated with the help of parameters and presented as a comparative graphic (Deviren, 2019).

2. TURBULATORS

Turbulators are elements placed inside the pipe to increase the heat transfer and the amount of turbulence of the flow. Usage purposes of turbulators are as follows:

- Turbulators in the flow medium ensure the boundary layers to break down and be regenerated.
- They increase the amount of heat transfer.
- They increase the amount of turbulence of the flow.
- They lengthen the current path.
- They impart rotary motion to the flowing fluid.

Heat exchangers are the systems used in many industrial applications. Literature has several studies on increasing the thermal efficiency of these systems. Relevant studies target to increase the thermal efficiency and thus

the energy efficiency in heat exchangers.

Bilen et al. (2001) formed a finned heating surface in a rectangular channel in which air is used as the fluid at constant surface temperature (45 ºC) to experimentally analyze its effect on heat transfer and friction loss properties. Cylindrical blades were placed on the surface regularly and irregularly. The Reynolds number was chosen for the study in the range of 3,700-30,000. According to the results, the amount of heat transfer in irregularly placed fins increases up to 33%.

Durmuş (2004) surveyed to review the effect of conical turbulators in the heat exchanger tube on the heat transfer rates. Experiments were performed in the range of $15{,}000 \leq Re < 60{,}000$. The results obtained were compared with each other after heat transfer, pressure loss, and exergy analyses were performed for conditions with turbulator and without turbulator.

Akpınar et al. (2006) placed helical (arc-shaped) wires of different distances and different diameters inside a double-pipe heat exchanger. They used air as the hot fluid and water as the cold fluid. Reynolds numbers in the range of 6,500 to 13,000 were used for both reverse and parallel flow modes of fluids. 2.64 Times increase in Nusselt number and 2.74 times increase in friction factor were seen compared to the empty pipe in the helical system.

Promvonge et al. (2006) experimentally researched the effects of two different types of turbulators inside the pipe on the heat transfer and friction properties. Measurements were made depending on the number of steps of the turbulators for Reynolds number in the range of 8,000–18,000. Conditions with turbulator and without turbulator were compared with each other. For observations, the Reynolds number, Nusselt, and friction factor increased in the turbulator condition.

Another study was conducted by Kurtbaş et al. (2007). They calculated the efficiency, entropy ratio, and NTU values of their fin-type turbulators. It was observed that the Nusselt number increased from 95 to 354, the exergy loss ratio increased from 0.04 to 0.2, and the heat exchanger efficiency changed between 0.17 and 0.72 based on blade angle, placement distance of turbulators, and blade diameter in Reynolds number in the range of $104 \leq Re < 3x104$.

Yıldız (2007) used a double-pipe coaxial heat exchanger to review the effect of turbulators, which are formed by placing springs of different diameters in the pipe in different numbers and sequences, on the heat transfer. He conducted experiments on Reynolds numbers in the range of $2{,}500 \leq Re \leq 12{,}000$. Conditions with turbulator and without turbulator

were compared with each other by using the data obtained as the result of the experiments.

Promvange (2008) analyzed the effects of square cross-section wires on heat transfer and turbulent flow friction properties. Experiments were carried out for Reynolds numbers ranging from 5,000 to 25,000; two different springs were used at the same time. Results were compared with the use of both straight pipe and crimped circular wire. For findings, the use of square-section springs provides higher heat transfer than the empty pipe.

Fan et al. (2011) placed inclined conical turbulators inside the pipe and examined them with numerical simulation. Inclination angle and the distance between the turbulators were considered. According to the calculation results, the Nusselt number increased 5 times compared to the empty pipe values while the friction factor increased 10 times.

Turgut et al. (2012) used the Taguchi method to determine optimum design parameters with injection-type turbulators in the heat exchanger. They analyzed the effects of injector-type turbulators of different diameters, angles, and numbers on heat transfer and pressure loss. They also endeavored to optimize Nu and f values.

Karakaya and Durmuş (2013) experimentally investigated the effects of conical spring turbulators placed in the pipe at 30 ºC, 45 ºC, and 60 ºC angles on heat transfer and pressure decrease. Measurements were made with the Reynolds number varying between 10,000-34,000. Heat transfer, pressure loss, and exergy analyses were conducted and data were compared for conditions with turbulator and without turbulator.

The effects of a conical and a quarter of a cone on flow were investigated experimentally by Guo et al. (2013). Conical turbulators were placed parallel to the flow direction. Conical parts were placed inclined at the top and bottom of the bar passing through the middle of the pipe. After all, conical turbulators cause more heat transfer increase than conical part turbulators.

Mohammmed et al. (2013) numerically investigated the effect of curved rod-shaped turbulators in the heat exchanger on the flow. Different slope angles, lengths, and positions were used for these turbulators. As result, these turbulators increased the heat transfer; the Nusselt number increased by up to 400% compared to the empty pipe.

Bisetto et al (2015) made experimental and numerical analyses for zigzag-shaped turbulators in the heat exchanger. For their findings, the turbulators increase the Nusselt number, and the thermal efficiency of the system increases between 3-10%.

Rao et al. (2015) made an experimental and numerical study by opening spherical pits and teardrop-shaped pits into the pipe to review their effect. They observed considering the Reynolds number between 8,500-60,000 that teardrop-shaped pits have the highest heat transfer performance compared to spherical pits.

Pourahmad et al. (2016) made NTU analyses of turbulators made of 1 mm thick galvanized plates in the form of wavy strips at different angles in the straight pipe. Experiments were presented with the variation of Reynolds numbers in the turbulent flow regime. According to the results, heat transfer increased with increasing Reynolds number and decreasing wavy strip angle. NTU analyzes compared conditions with and without wavy bands at different angles. Turbulators in the form of wavy strips with an angle of 45º also reached the highest value of NTU.

First of all, perforated disc-shaped turbulators in the pipe, which are in full contact with the wall, were investigated via the Taguchi-Gri relational analysis method by Chamoli et al. (2016). They used parameters such as Reynolds number, step ratio, diameter ratio in analyses. Characteristic features of these parameters were specified.

Acır et al. (2017) endeavored to find the parameter that affects exergy and energy efficiency for solar air heaters in their study. Gray relational analysis method was used in their study.

Muthusamy et al. (2017) developed a desalination system and added turbulators to their systems to obtain maximum efficiency from the experimental set. A significant saving in energy and exergy efficiency were observed due to this system they developed.

Experimental and numerical analyzes were performed by placing rectangular turbulators and twisted turbulators in a pipe and on a rod in the middle of the pipe by Nanan et al. (2017). Relevant turbulators were placed at various intervals in the form of a horizontal, a horizontal-a vertical, and cross. They observed at the end of the study that there was an increase in the number of Nusselts compared to the straight pipe.

Yang et al. (2017) placed rectangular turbulators on the top and bottom of a flow channel, opposite and diagonally. According to their results, the Nusselt number increases as the Reynolds increases.

Liu et al. (2017) drilled a triangular cavity in the bottom of the pipe and experimentally and numerically analyzed the effect of this cavity on heat transfer and flow.

Xie et al. (2017) made a series of simulations with various turbulence models to find the best numerical model. They performed the numerical

analysis of turbulators in the form of a straight rod and a convex rod in the direction of the flow, which is intertwined in the form of a crescent. Crescent-shaped rods displayed better performance compared to flat rods regarding heat transfer performance. The rods placed intertwined in the flow direction in the shape of a crescent increased the heat transfer between 21-38% compared to the flat rods and caused a pressure decrease of 15-39%. It was also observed that the rods placed in a crescent shape in the opposite direction of the flow increased the heat transfer between 16-41% compared to the flat rods and caused a pressure decrease of 44-80%.

Another study that was carried out by Zheng et al. (2017) numerically investigated the effects of spherical pits in a rectangular air duct with a 2:1 aspect ratio on heat transfer, flow properties, and entropy. It was seen at the end of the study that as heat transfer increases, Reynolds number increases at the same time. Moreover, the heat transfer increased with the increase in the diameter of the pit.

Manjunath et al. (2017) investigated the effect of thermal efficiency and thermohydraulic performance of spherical turbulators in rectangular channels with 3D CFD analysis. After the evaluation of the results, it was observed that spherical turbulators cause flow disturbances. At the same time, the thermal efficiency and Nusselt number increased with the increase of the sphere diameter.

Liu et al. (2018) reviewed the conical turbulators placed in the flow. They placed conical segments on a rod in the middle of the pipe and investigated the effects of conical segments, center angle, inclination angle, and pitch distance. They concluded that increasing the number of conical parts and the center angle increase both the heat transfer rate and the flow resistance, and then they decrease as the oblique angle increases.

Rashidi et al. (2018) placed turbulators in the flow and performed their experimental and numerical analysis. The surface that it hits with the flow in the same direction is changed by bending a rectangular piece at different rates. At the same time, the amount of turbulence in the flow increased significantly.

Çelik et al. (2018) examined zigzag turbulators placed in the flow by utilizing the Taguchi-Gri relational analysis method. The distance between the turbulator was used as the parameter. The researchers determined the parameters and performance characteristics with this method.

Baykara (2019) analyzed the effects of conical turbulators in the inner tube of a double-pipe heat exchanger on heat transfer, pressure loss, efficiency, exergy loss, and thermal performance. Diameter, cone type, and several steps were used as parameters in the experiments. Experiments

were made with Reynolds numbers varying between 18,000 and 37,000. As Re value increased, Nu number, entropy production rate increased, friction factor and thermal performance value decreased at the same time.

Erzincanlı (2019) made a survey and examined the effects of turbulators with 3 different diameters, in which single-phase flows were placed, on heat transfer, Nu number, and friction factor. The highest Nu value was obtained in the smallest diameter turbulator. The highest friction factor was obtained in parallel with the Nu number.

3.MATERIAL AND METHOD

3.1. Introduction of the Experimental Setup

We performed this study in the experimental setup of the turbulator heat exchanger established in the Energy Laboratory of the Faculty of Technology of Batman University. Figure 1. shows the schematic representation of the experimental setup.

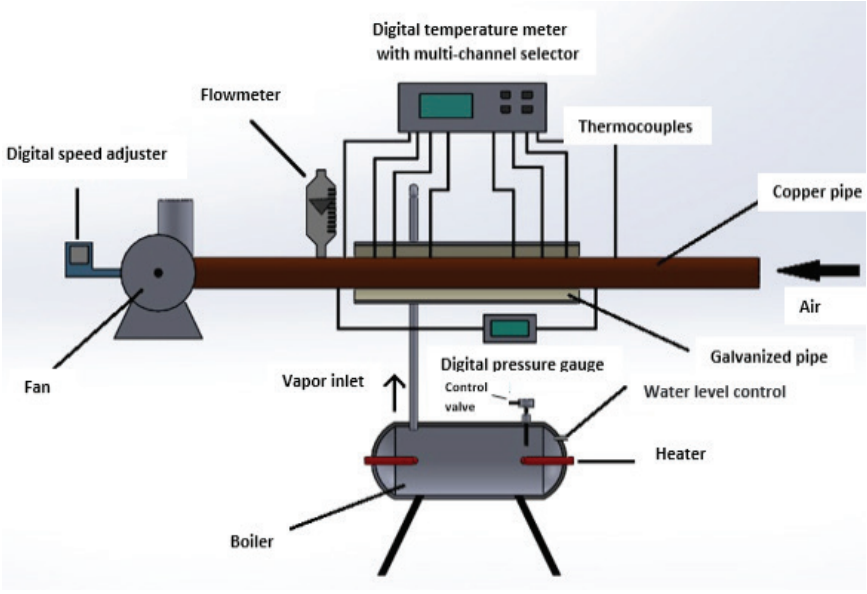

Fig. 1. Schematic Representation of the Experiment Set

The experimental setup consists of following elements: boiler that allows the evaporation of water, nested coaxial double pipe heat exchanger, thermocouples measuring the inlet and outlet temperatures in the pipe wall, data collector in which the measurement values are transferred to the computer environment, digital manometer that measures pressure and finally, the flow meter used to measure the flow rate.

There is a a copper pipe with an inner pipe length of 1600 mm, an inner

diameter of 65 mm and an outer diameter of 68 mm in the nested coaxial, double-pipe heat exchanger. It is made of galvanized sheet with an outer pipe length of 800 mm, an inner diameter of 100 mm and a thickness of 1.0 mm. A glass wool insulation is made around the outer pipe to prevent heat loss. The outer tube is in contact with the outer surface of the inner tube and contains water vapor from the boiler.

The steam, which is in contact with the outer surface of the inner pipe, is discharged through a channel to prevent a pressure of more than 1 atm. So, a constant temperature boundary condition at 100ºC is provided on the outer surface of the inner pipe.

T-type Nickel-Chrome thermocouples with a diameter of 0.5 mm make temperature measurements. Thermocouples help to observe that a constant temperature was maintained on the outer surface of the inner tube. One end of the thermocouples, which are produced resistant to high temperatures that are not affected by steam is fixed by passing through the holes drilled on the outer surface of the inner tube. Two thermocouples are placed to measure the inlet and outlet temperature of the fluid. One more thermocouple that continuously measures the temperature of the environment is used. The other end of the thermocouples is connected to the data collector which is connected to the computer. The temperature values measured with thermocouples are continuously recorded on the computer. The thermocouples can measure the temperature between -200 ºC and +400 ºC, with 0.1 K stability and ±0.1% error.

A 32-channel ELİMKO E-680 brand digital scanner was used for temperature measurements. Measurements can be collected and saved on a central computer with the RS-485 connector. Pressure changes during the experiment were measured in mbar with a digital manometer of the brand Cem DT-8890.

A 1.1 kW AC motor and a fan operating at 2500 rpm provided the air flow passing through the inner pipe during the experiment. The flow occurring in the fan at different speeds is regulated by the EKAMAT A-200 model digital speed controller. Flow at various speeds was created by the digital speed controller. The average velocity of the current passing through the pipe at each flow rate setting was measured in m/h with the KIMO-MP 210 Anemometer device.

The star type turbulators are positioned at the inlet (x=0), in the middle (at x=40 cm) and at the end (at x=60 cm) in the inner part of the inner tube in the heat exchanger consisting of two nested pipes. At the same time, these turbulators are adjusted to be 3, 4, 5 pieces at different speeds and the distance between them is 1.5 cm, 3 cm and 4.5 cm. Figure 2. shows the geometry of the turbulator used in the experiments and the arrangement

of the turbulators. The position of x=0 cm is named as the entrance, the position of x=40 cm as the middle, and the position of x=60 cm as the end regarding graphics.

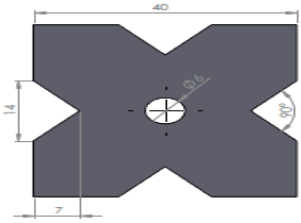

a)

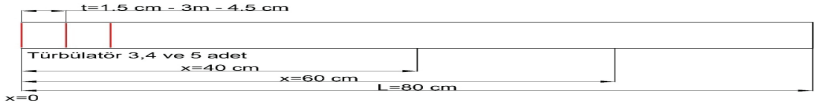

b)

Fig. 2. a)Turbulator geometry

b)The situation where the turbulators are at the pipe

The experiments were performed under steady-state conditions. The steam boiler was operated and the water was evaporated at first. Steam passed through the annular cavity of the heat exchanger and brought the outer surface of the inner tube to a constant temperature. Steam was sent for approximately 120 minutes in each experiment to ensure a constant temperature condition over the entire surface. The fan was started when the temperatures at the surface became stable. It was ensured that the flow was fully developed throughout the experimental region. The fan speed adjustment was carried out by adjusting the volumetric flow from the flow meter according to the desired Reynolds number value. The current was passed through the inner pipe at the desired flow rate and the temperature change on the surface was monitored. The temperatures at the inlet and outlet of the pipe were also measured. The pressure difference was measured as long as the current was sent with the digital manometer connection placed at the pipe inlet and outlet.

3.2. Method of Calculation

3.2.1. Determination of Reynolds Number

Reynolds number that we used as a parameter in experiments was measured by measuring the air velocity passing from the fan into the inner pipe.

$$Re = \frac{V d_i}{v} \quad (1)$$

Hereby v is kinematic viscosity of air, V is average velecity of fluid while d_i is inner diameter of inner tube.

3.2.2. Determination of Nusselt number

ΔT_{lm} logarithmic mean temperature difference needs to be calculated for convection heat transfer in a circular tube in heat exchangers. The difference between the inlet temperature (T_i) and outlet temperatures (T_o) of the wall temperature (T_w) must be known regarding logarithmic temperature difference. T_w was obtained by taking the averages of the temperatures measured at the wall. Namely, following equations can be written;

$$\Delta T_1 = T_w - T_i$$

$$\Delta T_2 = T_w - T_o$$

Thus, the log mean temperature difference is computed by equation (2).

$$\Delta T_{lm} = \frac{\Delta T1 - \Delta T2}{ln(\frac{\Delta T1}{\Delta T2})} \quad (2)$$

The h heat convection number is calculated for Nu number. The h_m can be found as a result of equalizing the heat transferred by convection in the circular pipe to the heat stored by the fluid between the inlet and outlet temperature in the system.

$$Q_{real} = Q_{convection}$$

That is to say,

$$(\rho . V A_c) . c_p . (T_o - T_i) = h_m . A_s . \Delta T_{lm} \quad (3)$$

ρ is the density of the fluid, A_c is the cross-sectional area of the inner pipe, V is the average velocity of the fluid, c_p is the specific heat of the fluid, T_o and T_i are the inlet and outlet temperatures of the fluid, h is heat convection number, A_s is the lateral surface of the inner pipe, and ΔT_{lm} is the logarithmic mean temperature difference.

Below equation is found if h_m is written as formula:

$$h = \frac{(\frac{\rho V.\pi.d_i^2}{4}).c_p.(To-Ti)}{\pi.d_i.L.\Delta T_{lm}} \quad (4)$$

Thus, Nusselt number is computed as follows:

$$Nu = \frac{h\ d_i}{k} \quad (5)$$

k is coefficient of thermal conductivity of air.

3.2.3. Calculation of pressure loss and friction factor

The friction factor was calculated by substituting the pressure difference measured by the manometer placed at the pipe inlet and outlet in the Darcy equation.

$$\Delta P = f \frac{L}{D_i} \rho \frac{V^2}{2} \quad (6)$$

3.2.4. Empirical Relations used in Empty Pipe

Experiments were first made in an empty pipe, then experiments with turbulators started. Nusselt numbers obtained from equation (7) are compared by calculating with the below equation accepted for empty pipe in the literature for both the validity of the experiments and the comparison with the situation with turbulator.

$$Nu = 0.023 \times (\mathrm{Re})^{0.8} \times (\mathrm{Pr})^{0.4} \quad (7)$$

The friction factor values were also compared with the friction factor accepted in the literature and its validity was examined (Incopera , F. and DeWitt , D. 2001).

$$f = (0.790 \ln \mathrm{Re}_D - 1{,}64)^{-2} \quad (8)$$

$3000 \leq \mathrm{Re}_D \leq 5\mathrm{x}10^6$

4. RESEARCH FINDINGS AND DISCUSSION

Data arising from the computed findings can be seen by graphic method below.

4.1. Nusselt Number–Reynolds Number Change

Graphs showing the variation of the Nusselt number concerning the Reynolds number were drawn for the case where the turbulators were spaced 1.5 cm – 3 cm – 4.5 cm in the system where turbulators are located

at the entrance, middle, and end and placed as 3, 4 and 5 pieces. Theoretical and experimental values in the empty tube are also shown on the graph for comparison. Regarding graphics, the Nusselt numbers increased with increasing Reynolds numbers. The heat transfer increased with the increase of the Nusselt number.

Figure 3. graphically gives the variation of Nusselt number concerning Reynold number when turbulators are placed in a row as 3, 4, and 5 at the entrance. According to graphic data, the highest Nusselt value is obtained when there are 5 turbulators when we made a Nusselt numbers comparison. This is followed by 4 and 3 turbulators, respectively. It is observed that the Nusselt number increased with the increase in the distance between the turbulators. As is understood from the graphic, the maximum Nusselt value is 208.589 in 30,000 Reynolds numbers with 5 turbulators and 4.5 cm spacing while the minimum Nusselt value is 40.141 in 5,000 Reynolds numbers with 3 turbulators and 1.5 cm spacing.

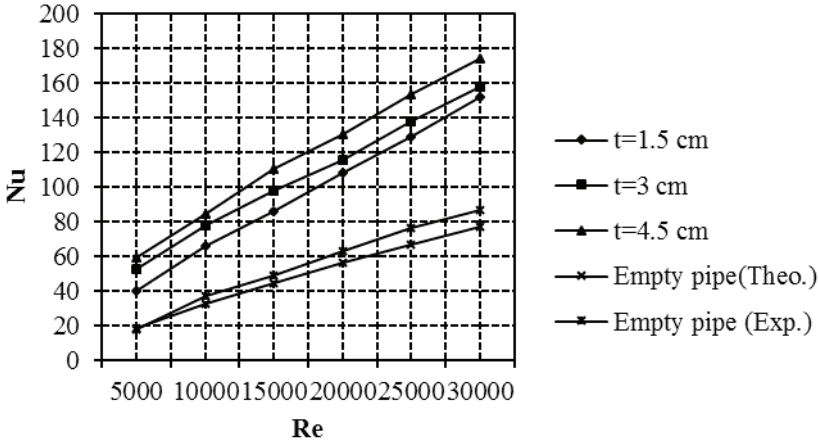

a)

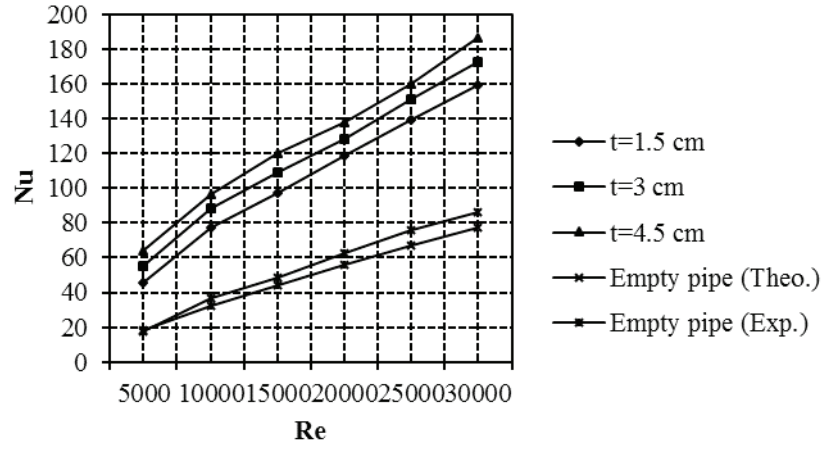

b)

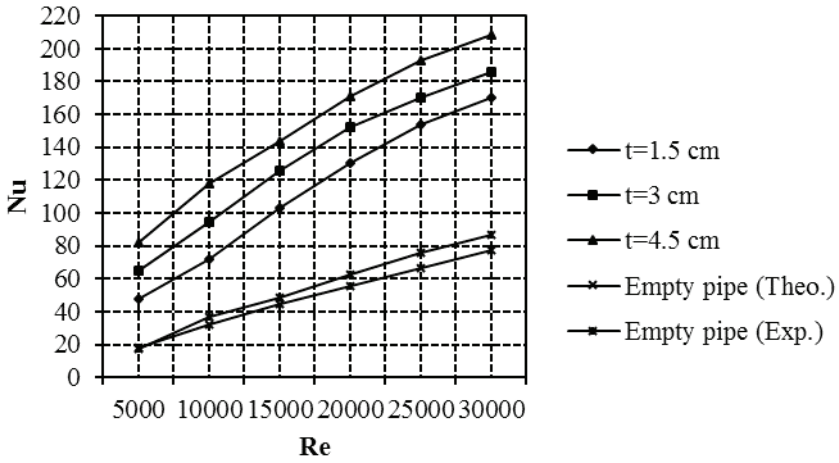

c)

Fig. 3. Reynolds Number -Nusselt Number in case of turbulators at the entrance

a)3 pcs b) 4 pcs c) 5 pcs

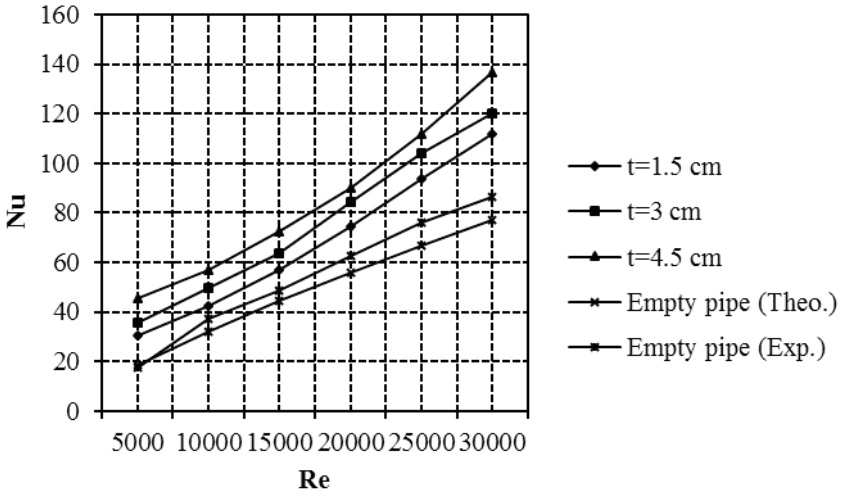
160
140
120
100
80
60
40
20
0
Nu
5000 10000 15000 20000 25000 30000
Re
t=1.5 cm
t=3 cm
t=4.5 cm
Empty pipe (Theo.)
Empty pipe (Exp.)

a)

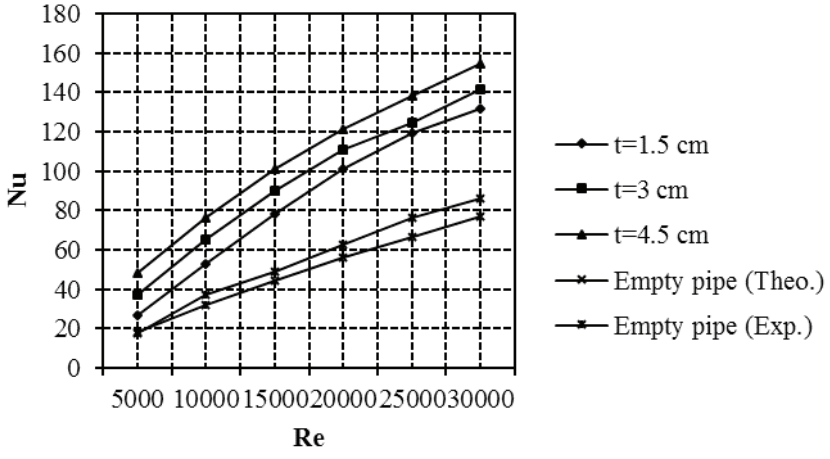
180
160
140
120
100
80
60
40
20
0
Nu
5000 10000 15000 20000 2500 30000
Re
t=1.5 cm
t=3 cm
t=4.5 cm
Empty pipe (Theo.)
Empty pipe (Exp.)

b)

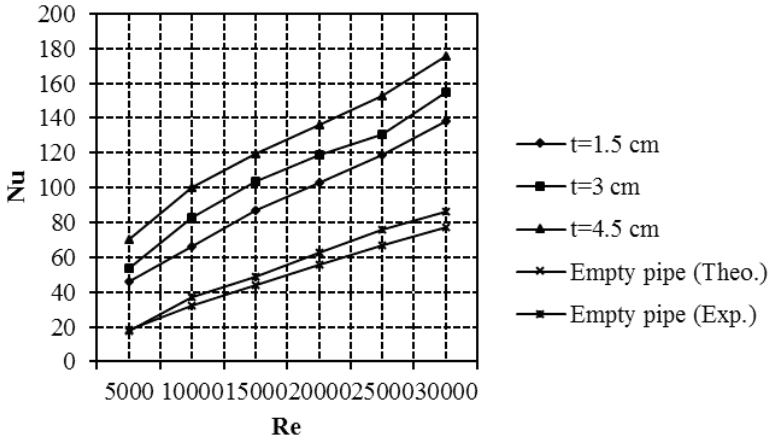

c)

Fig. 4. Reynolds Number-Nusselt Number in case of turbulators at the middle

a)3 pcs b) 4 pcs c) 5 pcs

Figure 4. graphically shows the variation of the Nusselt number concerning the Reynold number when the turbulators are placed in a row with 3, 4, and 5 in the middle. According to graphic data, the highest Nusselt value was found when there were 5 turbulators. This is followed by 4 and 3 turbulators, respectively. The Nusselt number increased with the increase in the distance between the turbulators. As is understood from the graphic, the highest Nusselt value is 175.418 in 30,000 Reynolds number with 5 turbulators and 4.5 cm spacing while the minimum Nusselt number is 30.215 in 5,000 Reynolds number with 3 turbulators and 1.5 cm spacing.

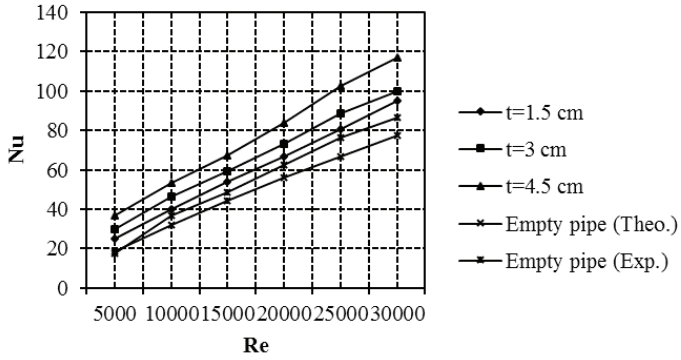

a)

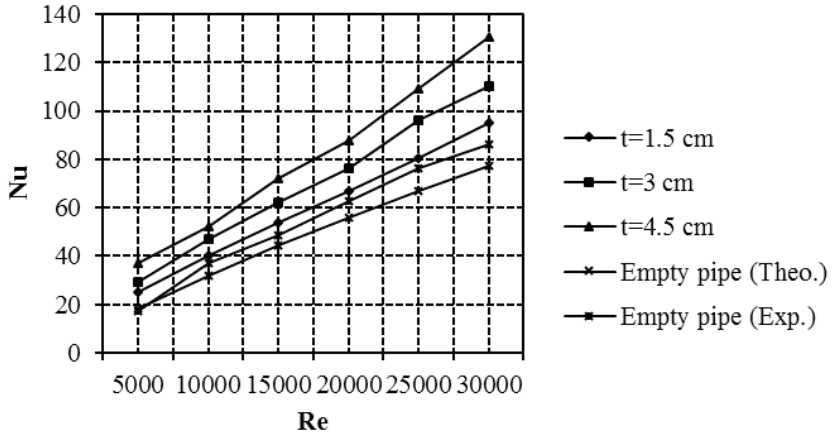

b)

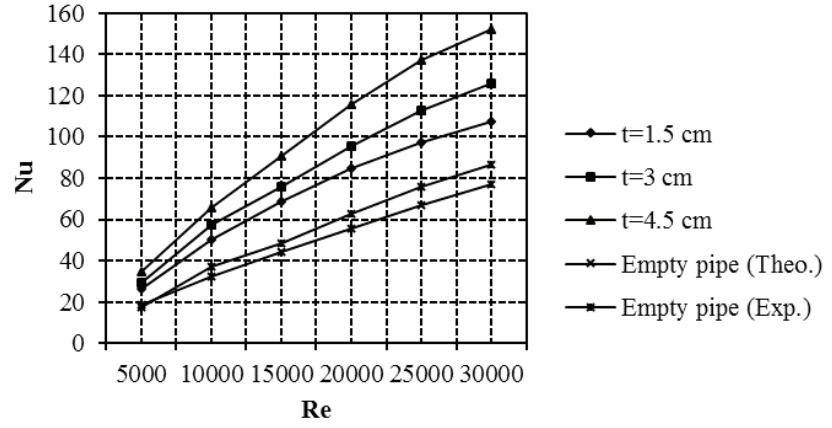

c)

Fig. 5. Reynolds Number-Nusselt Number in case of turbulators at the end

a)3 pcs b) 4 pcs c) 5 pcs

Figure 5. graphically shows the variation of the Nusselt number concerning the Reynold number when the turbulators are placed in a row with 3, 4, and 5 at the end. According to graphic data, the highest Nusselt value is found when there are 5 turbulators. This is followed by 4 and 3 turbulators, respectively. The Nusselt number increased with the increase in the distance between the turbulators. As is understood from the graphic, the highest Nusselt value is 152.039 in 30,000 Reynolds numbers with 5

turbulators and 4.5 cm spacing while the minimum Nusselt value is 25.043 in 5,000 Reynolds numbers with 3 turbulators and 1.5 cm spacing.

The highest Nusselt numbers were compared to the empty pipe without a turbulator. So, there was seen an increase of 101% in the 3-row turbulator arrangement, 115% in the 4-row turbulator arrangement, and 141% in the 5-row turbulator arrangement.

4.2. Pressure Loss-Reynolds Number Change

Graphs giving the pressure loss variation-Reynolds number variation were drawn for the 1.5 cm – 3 cm – 4.5 cm intervals of the turbulators in the system where turbulators are located at the entrance, middle, and end and placed as 3, 4, and 5 pieces. The theoretical and experimental values are also shown on the graphic for comparison in the case of using an empty pipe. We can when the graphics are reviewed that the pressure loss increased with increasing Reynolds numbers.

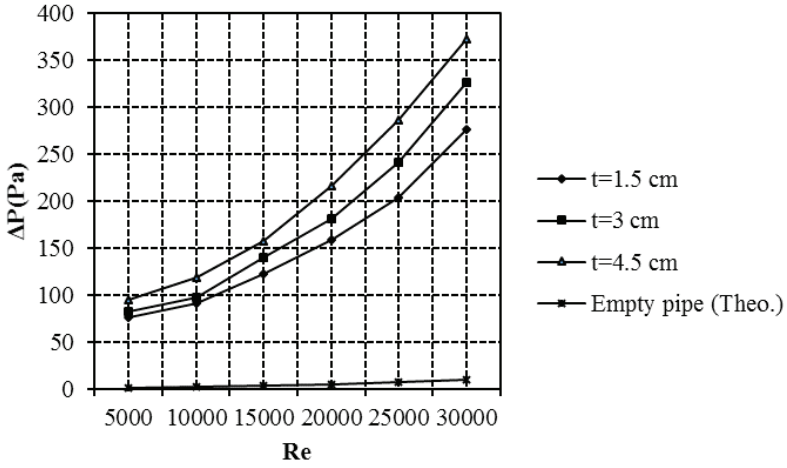

a)

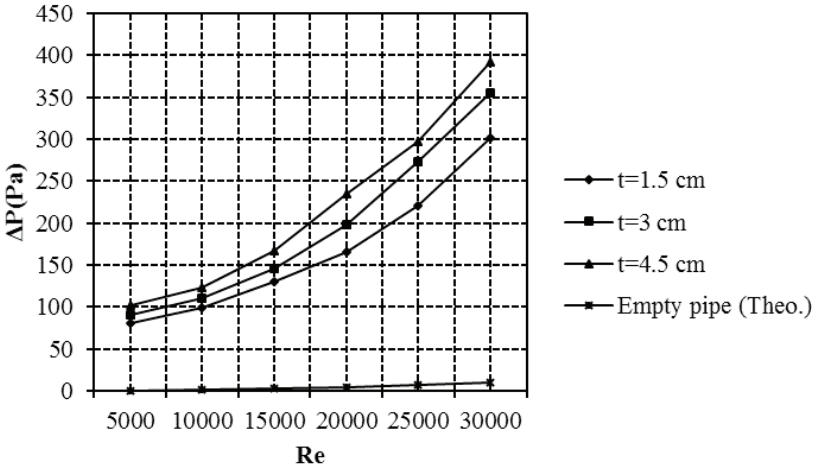

b)

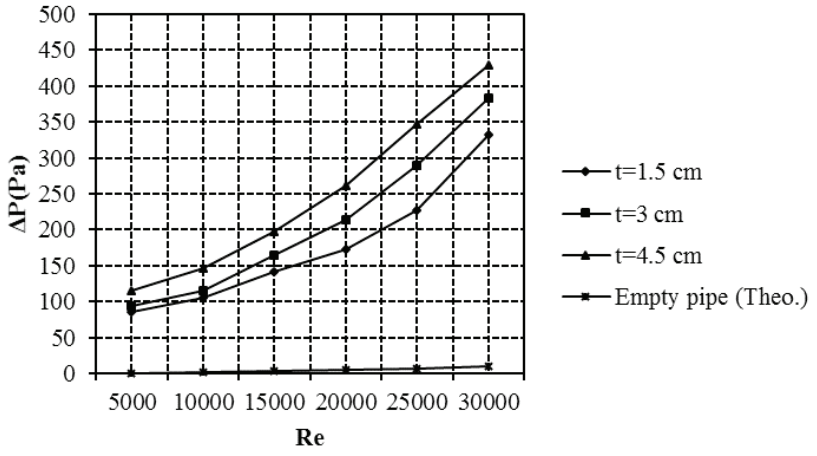

c)

Fig. 6. Reynolds Number-Pressure Loss element in case of turbulators at the entrance

a)3 pcs b) 4 pcs c) 5 pcs

Figure 6. shows the graphs of the pressure loss values according to the change in Reynolds number when the turbulators are placed in a row as 3, 4, and 5 at the inlet. According to the graphic data, the highest value is seen when there are 5 turbulators. This is followed by 4 and 3 turbulators, respectively. The pressure loss increased with the increase in the distance between the turbulators. As is understood from the graphic, the highest pressure loss is 429.476 in 30,000 Reynolds numbers for 5 turbulators and

4.5 cm spacing while the lowest pressure loss is 76,117 in 5,000 Reynolds numbers with 3 turbulators and 1.5 cm spacing.

Figure 7. shows the graphs of the pressure loss values according to the change in the Reynolds number when the turbulators are placed in a row with 3, 4, and 5 in the middle. This is followed by 4 and 3 turbulators, respectively. The pressure loss increased with the increase in the distance between the turbulators. As is understood from the graphic, the highest pressure loss is 412.900 in 30,000 Reynolds numbers with 5 turbulators and 4.5 cm spacing while the lowest pressure loss is 71.218 in 5,000 Reynolds numbers with 3 turbulators and 1.5 cm spacing.

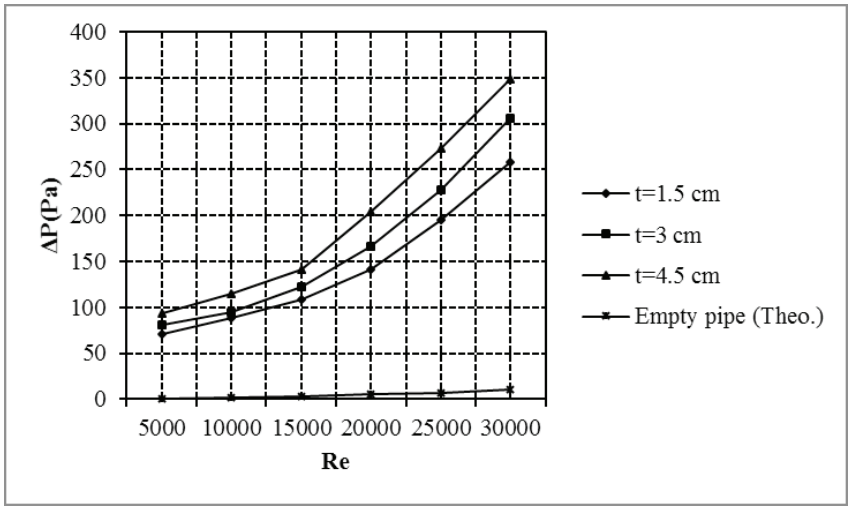

a)

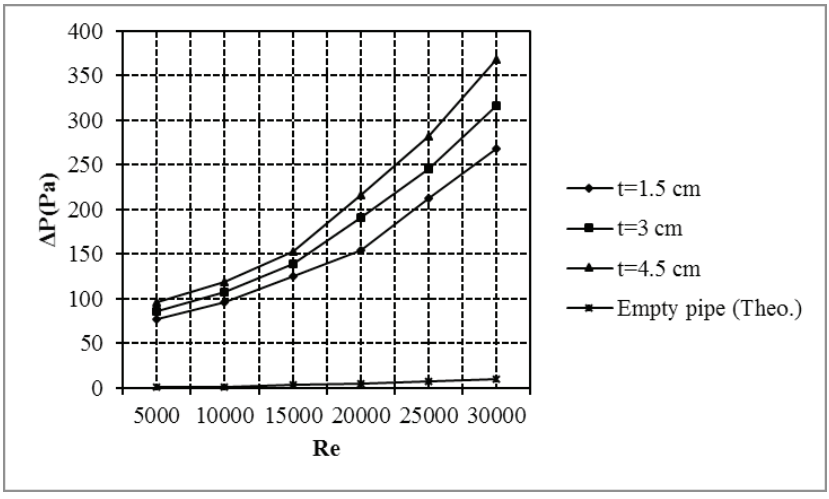

b)

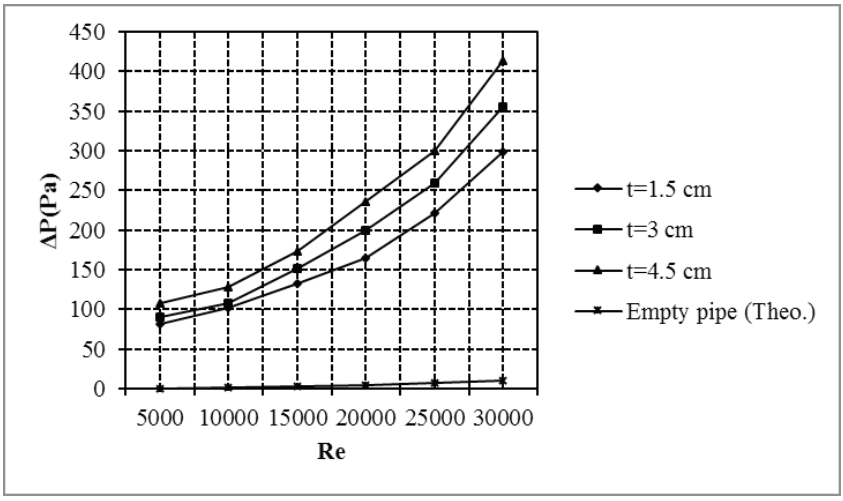

c)

Fig. 7. Reynolds Number-Pressure Loss element in case of turbulators at the middle

a)3 pcs b) 4 pcs c) 5 pcs

Figure 8. shows the graphs of the pressure loss values according to the change in Reynolds number when the turbulators are placed in a row with 3, 4, and 5 at the end. The highest value is seen when there are 5 turbulators when we compared pressure losses based on graphic data. This is followed by 4 and 3 turbulators, respectively. The pressure loss increased with the increase in the distance between the turbulators. As is understood from the graphic, the highest pressure loss is 377.345 in 30,000 Reynolds numbers with 5 turbulators and 4.5 cm spacing while the lowest pressure loss is 68.514 in 5,000 Reynolds numbers with 3 turbulators and 1.5 cm spacing.

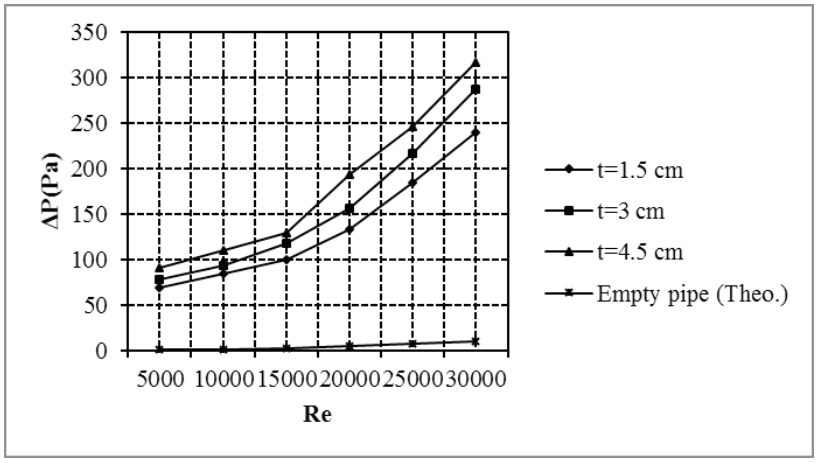
350
300
250
200
150
100
50
0
ΔP(Pa)
5000 10000 15000 20000 25000 30000
Re
t=1.5 cm
t=3 cm
t=4.5 cm
Empty pipe (Theo.)

a)

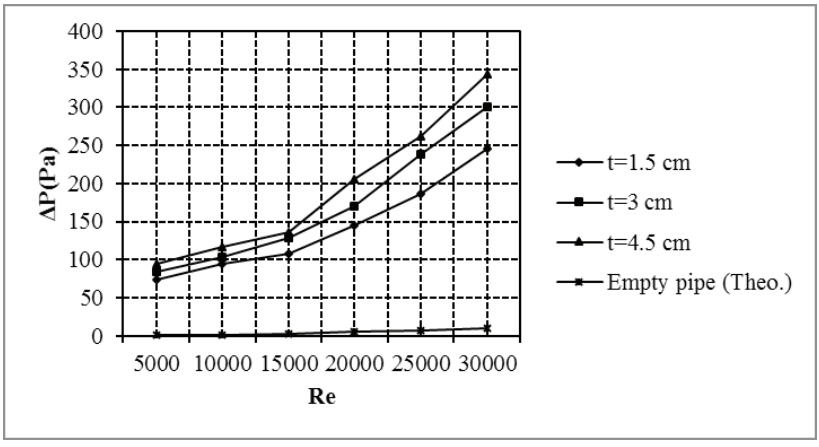
400
350
300
250
200
150
100
50
0
ΔP(Pa)
5000 10000 15000 20000 25000 30000
Re
t=1.5 cm
t=3 cm
t=4.5 cm
Empty pipe (Theo.)

b)

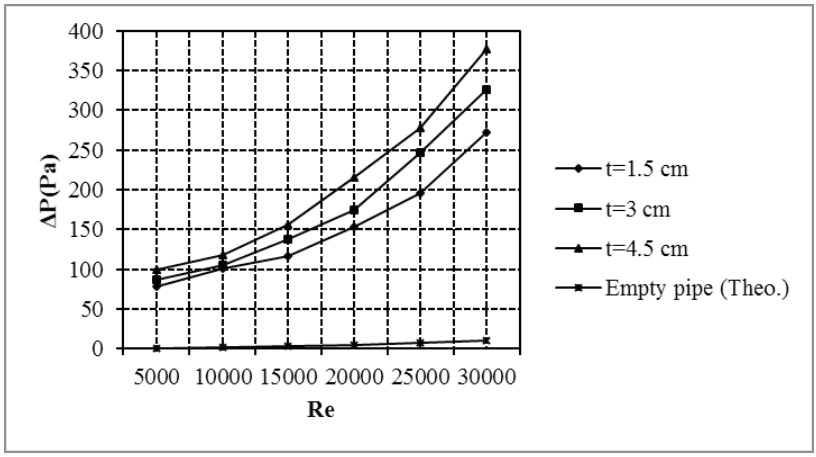
400
350
300
250
200
150
100
50
0
ΔP(Pa)
5000 10000 15000 20000 25000 30000
Re
t=1.5 cm
t=3 cm
t=4.5 cm
Empty pipe (Theo.)

c)

Fig. 8. Reynolds Number-Pressure Loss element in case of turbulators at the end

a)3 pcs b) 4 pcsc) 5 pcs

It is highlighted when the highest pressure losses are compared with the empty pipe without a turbulator that there is a 37-fold increase in the 3-row turbulator arrangement, a 41-fold increase in the 4-row turbulator arrangement, and a 43-fold increase in the 5-row turbulator arrangement.

4.3. Friction Factor - Reynolds Number Change

Graphs giving the variation of the friction factor according to the Reynolds number were drawn for 1.5 cm - 3 cm - 4.5 cm intervals in the system where turbulators are located at the entrance, middle, and end and placed as 3, 4, and 5 pieces. Based on the empty pipe state, the theoretical and experimental values are also shown on the graph for comparison. According to the results, the Friction Factor decreased with increasing Reynolds numbers.

Figure 9. graphically shows the variation of the friction factor according to the Reynolds number when the turbulators are arranged as 3, 4, and 5 at the inlet. The highest value is seen when there are turbulators when we compared the friction factors based on graphic data. The friction factor increased with the increase in the distance between the turbulators. As is understood from the graphic, the highest friction factor is 5.650 in 5,000 Reynolds numbers with 5 turbulators and 4.5 cm spacing while the lowest friction factor is 0.569 in 30,000 Reynolds numbers with 3 turbulators and 1.5 cm spacing.

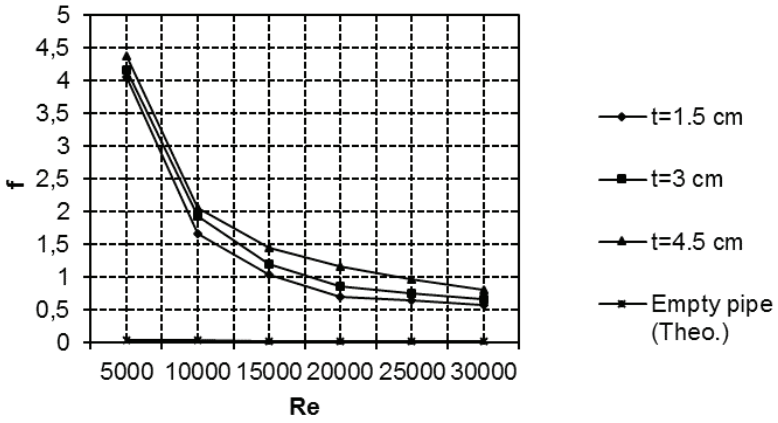

a)

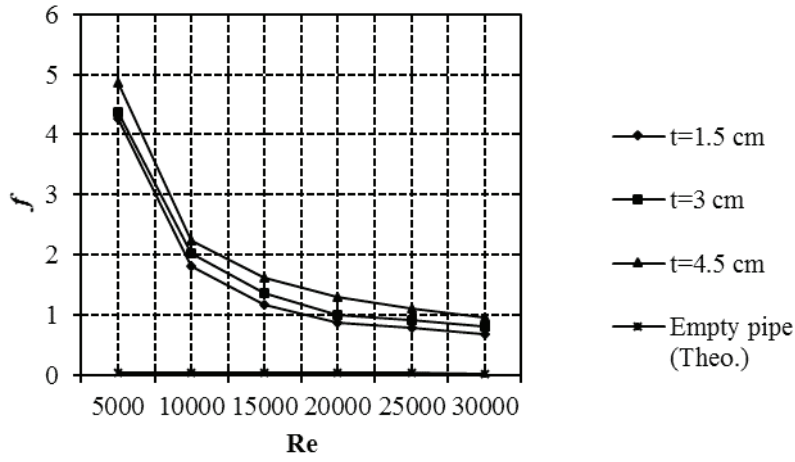

b)

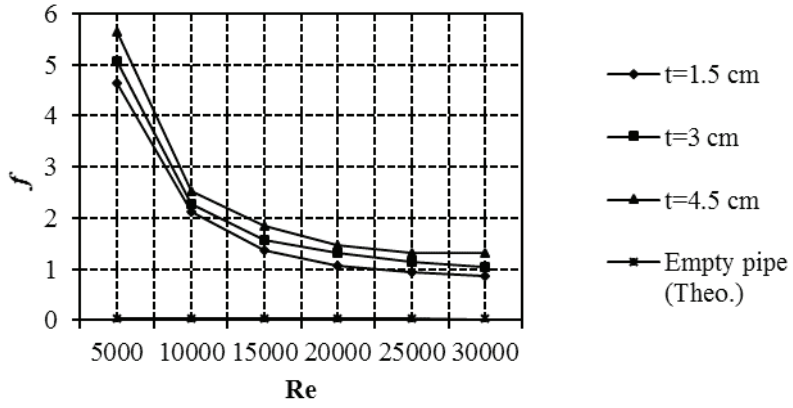

c)

Fig. 9 Reynolds Number-Friction Factor in case of turbulators at the entrance

a)3 pcs b) 4 pcs c) 5 pcs

Figure 10. graphically shows the variation of the friction factor according to the Reynolds number when the turbulators are arranged as 3, 4, and 5 in the middle. The highest value is seen when there are 5 turbulators when we compared friction factors based on graphic data. This is followed by 4 and 3 turbulators, respectively. The friction factor increased with the increase in the distance between the turbulators. As is understood from the graphic, the highest friction factor is 5.427 in 5,000 Reynolds numbers with 5 turbulators and 4.5 cm spacing while the lowest friction factor is 0.498 in 30,000 Reynolds numbers with 3 turbulators and 1.5 cm spacing.

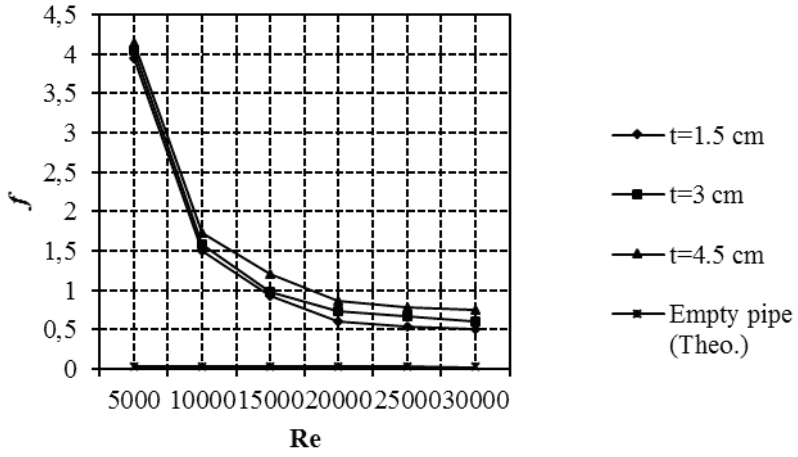
4,5
4
3,5
3
2,5
2
1,5
1
0,5
0
f
5000 10000 15000 20000 25000 30000
Re
t=1.5 cm
t=3 cm
t=4.5 cm
Empty pipe (Theo.)

a)

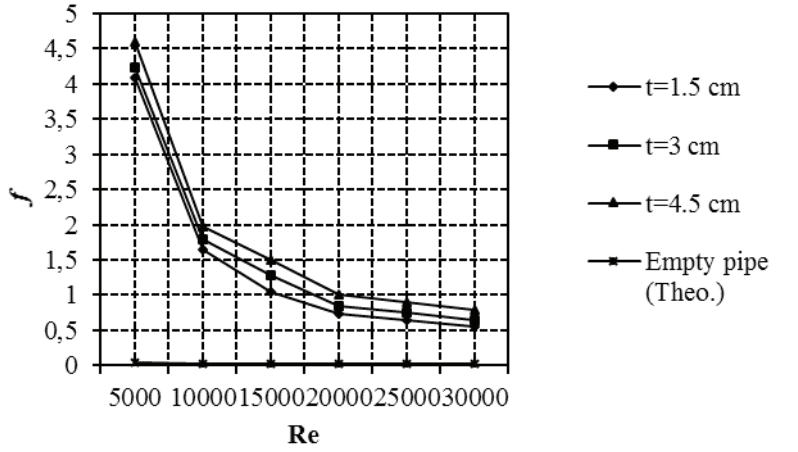
5
4,5
4
3,5
3
2,5
2
1,5
1
0,5
0
f
5000 10000 15000 20000 25000 30000
Re
t=1.5 cm
t=3 cm
t=4.5 cm
Empty pipe (Theo.)

b)

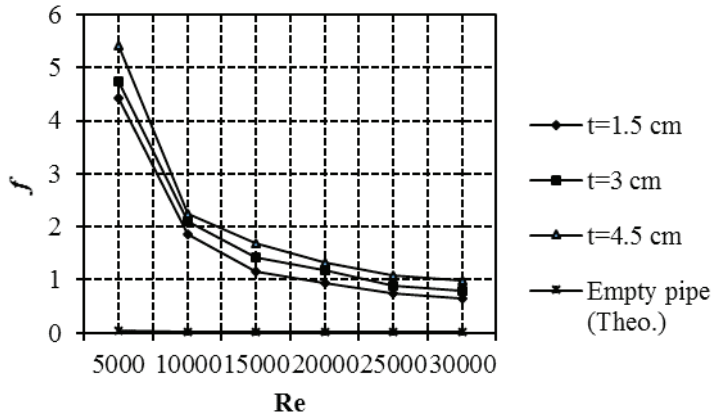

c)

Fig. 10. Reynolds Number-Friction Factor in case of turbulators at the middle

a)3 pcs b) 4 pcs c) 5 pcs

Figure 11. graphically shows the variation of the friction factor according to the Reynolds number when the turbulators are arranged as 3, 4, and 5 at the end. The highest friction factor is seen when there are 5 turbulators based on friction factor comparison. This is followed by 4 and 3 turbulators, respectively. The friction factor increased with the increase in the distance between the turbulators. As is understood from the graphic, the highest friction factor is 4.850 in 5,000 Reynolds numbers with 5 turbulators and 4.5 cm spacing while the lowest friction factor is 0.364 in 30,000 Reynolds numbers with 3 turbulators and 1.5 cm spacing.

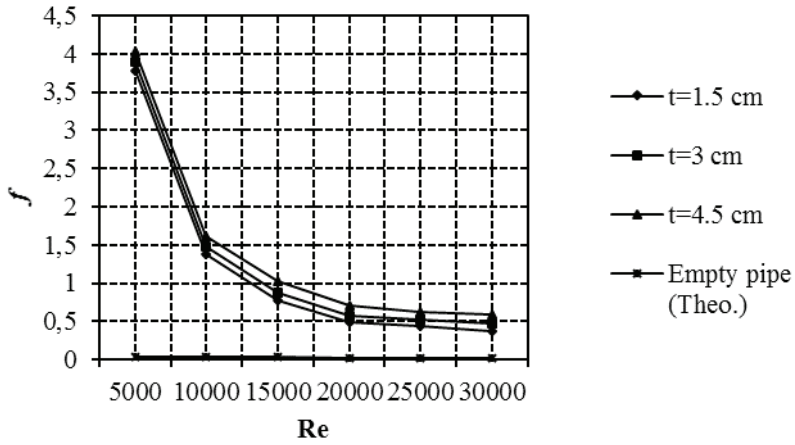

a)

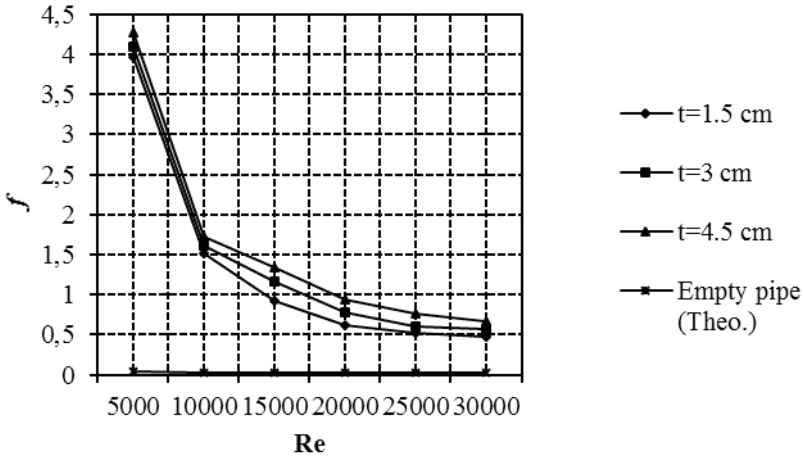

b)

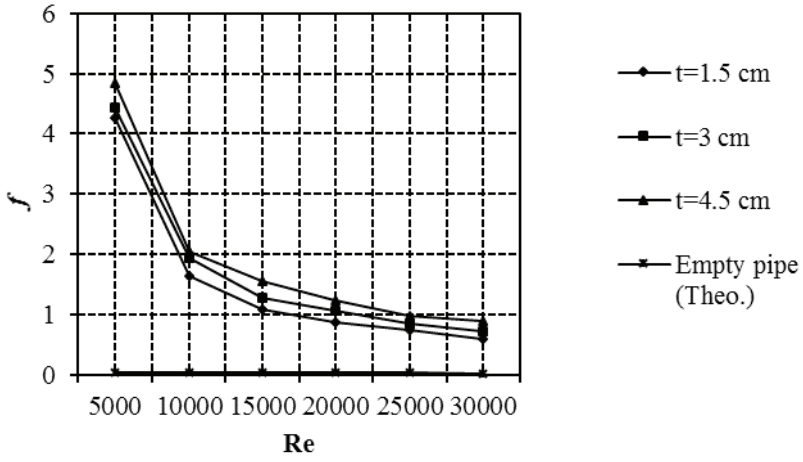

c)

Fig. 11. Reynolds Number-Friction Factor in case of turbulators (5 pieces) at the end

a) 3 pcs b)4 pcs c)5 pcs

It is highlighted when the highest friction factors are compared with the empty pipe without a turbulator that there is a 115-fold increase in the 3-row turbulator arrangement, a 128-fold increase in the 4-row turbulator arrangement, and a 148-fold increase in the 5-row turbulator arrangement.

5. CONCLUSION AND RECOMMENDATIONS

This experimental study researched the effects of turbulators placed in the tube in a double-pipe heat exchanger on the flow. 3, 4, and 5 turbulators at the entrance, middle, and end were placed at intervals of 1.5 cm - 3 cm - 4.5 cm. The effects on heat transfer, pressure loss, friction factor were analyzed with the data obtained as a result of experiments and calculations. Values were calculated based on Reynolds number and the number of heat transfer units. Results arising from the study are summarized as follows:

- As the Re value increases, the Nu number increases at the same time. Moreover, the Nu number increases as the heat transfer increases.
- For observations, the Nusselt number increased with the increase in the number of turbulators and the distance between the turbulators. At the entrance, middle, and end, the highest Nu value was achieved with 5 turbulators at 4.5 cm intervals, while the lowest Nu value was achieved at 1.5 cm intervals with 3 turbulators.
- Nusselt numbers were compared with an empty pipe without a turbulator; there was an increase of 101% in the 3-row turbulator arrangement, 115% in the 4-row turbulator arrangement, and 141% in the 5-row turbulator arrangement.
- Increases in Re value caused increases in pressure losses.
- While the highest pressure loss at the inlet, middle, and end was achieved with 5 turbulators at 4.5 cm intervals, the lowest pressure loss was provided with 3 turbulators at 1.5 cm intervals.
- Pressure Losses were compared to the empty pipe without turbulator; according to the results, there was a 37-fold increase in the 3-row turbulator arrangement, a 41-fold increase in the 4-row turbulator arrangement, and a 43-fold increase in the 5-row turbulator arrangement.
- An increase in Re value caused a decrease in the friction factor.
- It was observed that the friction ratio increased with the increase in the number of turbulators and the distance between the turbulators. The highest friction factor was achieved with 5 turbulators at 4.5 cm intervals at the inlet, middle and end while the lowest friction factor was observed with 3 turbulators at 1.5 cm intervals.
- The highest friction factors were compared with the empty pipe without a turbulator; according to the results, there was an increase of 115 times in the 3-row turbulator arrangement, 128 fold in the

4-row turbulator arrangement, and 148 fold in the 5-row turbulator arrangement.

The use of turbulators in heat exchangers provides an improvement in heat transfer. However, improvements in heat transfer were observed while increases in pressure loss were also observed. Since the increase in pressure loss in the system requires the fluid movement to be provided by a more powerful fan, there occurs an extra cost. Therefore, an optimum solution needs to be developed and the appropriate turbulator type, number, and arrangement should be determined considering the heat transfer and pressure loss. The use of turbulators in heat exchangers with the optimum solution provides important contributions in terms of energy efficiency.

6. KAYNAKLAR

Acır, A., Canlı, M.E., Ata, G. and Çakıroglu, R. (2017). Parametric optimization of energy and exergy analyses of a novel solar air heater with grey relational analysis. *Applied Thermal Engineering*. 122, 330-338.

Akpinar, E.K. (2006). Evaluation of heat transfer and exergy loss in a concentric double pipe exchanger equipped with helical wires, *Energy Conversion and Management*, 47, 3473-3486.

Balbay, A. (2001). *Computer aided design for shell and tube heat exchangers* (Unpublished Master's thesis). Fırat University Graduate School of Natural and Applied Sciences, Elazig.

Baykara, Ş. (2019). *Investigation of the effect of conical type turbulators in a heat exchanger on heat transfer and pressure loss* (Master thesis). Republic of Turkey Higher Education Council National Thesis Center (Thesis No: 572539).

Bilen, K., Akyol, U., Yapici, S. (2001). Heat Transfer and Friction Correlations and Thermal Performance Analysis for a Finned Surface. *Energy Conversion and Management*. 42, 1071-1083.

Bisetto, A., Col, D.D. and Schievano, M. (2015). Fire tube heat generators: Experimental analysis and modeling. *Applied Thermal Engineering*, 78, 236-247.

Chamoli, S., Yu, P. and Kumar, A. (2016). Multi-response optimization of geometric and flow parameters in a heat exchanger tube with perforated disk inserts by Taguchi grey relational analysis. *Applied Thermal Engineering*. 103, 1339-1350.

Celik, N., Pusat, G. and Turgut, E. (2018). Application of Taguchi method and grey relational analysis on a turbulated heat exchanger. *International Journal of Thermal Sciences*. 124, 85-97.

Deviren, H. (2019*). Experimental investigation of the effect of newly developed turbulators on heat efficiency and pressure loss in heat exchangers* (Master's thesis). Republic of Turkey Higher Education Council National Thesis Center (Thesis No: 606867).

Durmus, A. (2004). Heat Transfer and Exergy Loss in Cut out Conical Turbulators. *Energy Conversion and Management*. 45, 785–796.

Erzincanlı, S. (2019), *Experimental investigation of heat transfer performance of wave turbulators in pipes* (Master's thesis). Republic of Turkey Higher Education Council National Thesis Center (Thesis No: 568943).

Fan, A., Deng, J., Guo, J. and Liu, W. (2011). A numerical study on thermo-hydraulic characteristics of turbulent flow in a circular tube fitted with conical strip inserts. *Applied Thermal Engineering*. 31, 2819-2828.

Genceli, O.F. (1983). *Heat Exchangers Lecture Notes*, Istanbul Technical University Mechanical Engineering Department, Istanbul

Guo, J., Yan, Y., Liu, W., Jiang, F. and Fan, A. (2013). Effects of upwind area of tube inserts on heat transfer and flow resistance characteristics of turbulent flow. *Experimental Thermal and Fluid Science*. 48, 147-155.

Inropera, F. DeWitt, D., 2001. Fundamentals of Heat and Mass Transfer, 4th edition, Wiley & Sons, Incorporated.

Karakaya, H. and Durmus, A. (2013). Heat transfer and exergy loss in conical spring turbulators,. *International Journal of Heat and Mass Transfer*. 60, 756-762.

Karali, R., 2002, *Computer aided optimization of heat exchangers* (Unpublished master's thesis)., Mustafa Kemal University Graduate School of Natural and Applied Sciences, Hatay.

Kurtbaş, İ., Durmuş, A., Eren, H. and Turgut, E. (2007). Effect of propeller type swirl generators on the entropy generation and efficiency of heat exchangers. *International Journal of Thermal Sciences*, 46, 300-307.

Liu, J., Hussain, S., Wang, L., Xie, G. and Sundén, B. (2017). Heat transfer and turbulent flow characteristics over pocket cavity in the junction part of an outlet guide vane in a gas turbine. *Applied Thermal Engineering*. 124, 831-843.

Liu, P., Zheng, N., Shan, F., Liu, Z. and Liu, W. (2018). An experimental and numerical study on the laminar heat transfer and flow characteristics of a circular tube fitted with multiple conical strips inserts. *International Journal of Heat and Mass Transfer*. 117, 691-709.

Manjunath, M.S., Karanth, K.V. and Sharma, N.Y. (2017). Numerical analysis of the influence of spherical turbulence generators on heat transfer enhancement of flat plate solar air heater. *Energy*. 121, 616-630.

Mohammed, H.A., Hasan, H.A. and Wahid, M.A. (2013). Heat transfer enhancement of nanofluids in a double pipe heat exchanger with louvered strip inserts. *International Communications in Heat and Mass Transfer*. 40, 36-40.

Muthusamy, C. and Srithar, K. (2017). Energy saving potential in humidification-dehumidification desalination system. *Energy*. 118, 729-741.

Nanan, K., Thianpong, C., Pimsarn, M., Chuwattanakul, V. and Eiamsa-ard, S. (2017). Flow and thermal mechanisms in a heat exchanger tube inserted with twisted cross-baffle turbulators. *Applied Thermal Engineering*. 114, 130-147.

Pourahmad, S. and Pesteei, S.M. (2016). Effectiveness-NTU analyses in a double tube heat exchanger equipped with wavy strip considering various angles. *Energy Conversion and Management*. 123, 462-469.

Promvonge, P. and Eiamsa-ard S. (2006). Heat transfer and turbulent flow friction in a circular tube fitted with conical-nozzle turbulators. *International Communications in Heat and Mass Transfer*, 34, 72-82.

Promvonge, P. (2008). Thermal Performance in Circular Tube Fitted with Coiled Square Wires. *Energy Conversion and Management*. 495, 980–987.

Rao, Y., Li, B. and Feng, Y. (2015). Heat transfer of turbulent flow over surfaces with spherical dimples and teardrop dimples. *Experimental Thermal and Fluid Science*. 61, 201-209.

Rashidi, S., Akbarzadeh, M., Karimi, N. and Masoodi, R. 2018. Combined effects of nanofluid and transverse twisted-baffles on the flow structures, heat transfer and irreversibilities inside a square duct – A numerical study. *Applied Thermal Engineering*. 130, 135-148.

Turgut, E., Cakmak, G. and Yıldız, C. (2012). Optimization of the concentric heat exchanger with injector turbulators by Taguchi method. *Energy Conversion and Management*. 53, 268-275.

Xie, G., Liu, X., Yan, H. and Qin, J. (2017). Turbulent flow characteristics and heat transfer enhancement in a square channel with various crescent ribs on one wall. *International Journal of Heat and Mass Transfer*. 115, 283-295.

Yakut, G. (2006). *Theoretical and experimental investigation of shell and tube heat exchanger* (Master's thesis). Republic of Turkey Higher Education Council National Thesis Center (Thesis No: 200541).

Yang, W., Xue, S., He, Y. and Li, W. (2017) Experimental study on the heat transfer characteristics of high blockage ribs channel. *Experimental Thermal and Fluid Science*. 83, 248-259.

Yıldız, Ş. (2007). *The Effects Of Sprıng Turbulators In The Annular Heat Exchangers On The Heat Transfer And Pressure Losses* (Master Thesis). Republic of Turkey Higher Education Council National Thesis Center (Thesis No: 212135).

Zheng, L., Xie, Y. And Zhang, D. (2017). Numerical investigation on heat transfer performance and flow characteristics in a rectangular air cooling channel (AR = 2) with ridged dimples. *International Journal of Heat and Mass Transfer*. 107, 403-417.

Chapter 11

ENVIRONMENTAL IMPACTS OF LARGE DAMS: YUSUFELI DAM/TURKEY

Ayla BILGIN[1]

1 * Corresponding author: Doç.Dr., Artvin Coruh University, Engineering Faculty, Department of Environmental, Engineering, 08100, Artvin/ Turkey Tel: +90(466)2151040 /4669 Fax: +90(466)2151057,E-mail:ayla.bilgin@gmail.com, ayla.bilgin@artvin.edu.tr, Orcid number: 0000-0002-1873-6038, Artvin Coruh University, Department of Environmental Engineering, Artvin/Turkey

INTRODUCTION

Water dams have been built for more than 5000 years, but the first large ones have emerged in Europe and North America in the 19th century. In the 20th century, its construction increased in developed countries (for example, during the "big dams" in the United States). In the 1980s and later, the most suitable areas were used in developing countries. Dams have been promoted as an important tool for meeting water and energy needs, and some as a long-term, strategic investment capable of providing a large number of benefits typical of all major infrastructure projects. Large dams are constructed with the aim of establishing an industrial base with regional development, employment creation and export capacity (WCR 2001).

Large dams play an important role in meeting people's water and energy needs. There have been important developments in dam construction from past to present.The World Commission on Dams 2000 report, an independent assessment based on case studies from around the world, showed that many dams underperformed in terms of intended benefits and service delivery. In addition, the negative environmental and social impacts of large dams were largely unexpected or minor. The construction of dams causes physical, chemical and biological changes in natural ecosystems. It has been established within the framework of legal regulations that measures should be taken to reduce these effects.(McCartney, Sullivan, and Acreman 2000). Today, environmental problems such as economic and technical problems are taken into consideration in the design of dams (Satoshi et al. 2003).

The environmental, social and health-related consequences of large dam projects are internationally remarkable (Baviskar and Singh 1994). Although dams are important for water and energy supply, flood management and irrigation, millions of people are often exposed to negative health and social impacts in less developed countries (Goldsmith and Hildyard 1984).

Environmental Impacts of Big Dams

The establishment of a large dam with high savings capacity may have multilateral and significant impacts. These effects can be classified as physical, biological, social, economic, political and ecological effects. In general, the environmental impact of the dam lake can be examined as "negative and destructive environmental effects of dams" (Karimi Jashni and Chamanchi 2007).

Dams have positive and negative effects on ecosystems. In order to investigate these effects, it is necessary to conduct research with many

disciplines. To assess the impact of a dam on the ecosystem; Knowledge of the hydrology of the river, its hydraulic properties, water physical, chemical biological properties, geomorphological characteristics, aquatic biota and habitat requirements, coastal vegetation and direct use of the river's related resources by the local population is required. (Dynesius and Nilsson 1994).

Rivers are natural corridors that are important for the flow of energy, matter and species. Therefore, it plays an important role in landscape studies, regulation and maintenance of biodiversity. Changes caused by dams directly and indirectly affect the heterogeneity of habitats and ultimately the ecological integrity of river ecosystems. Dams cause changes in the natural flows of river systems. The most obvious effect of storage reservoirs is the permanent destruction of ecosystems by land. The most common downstream effect of large dams is a reduced variation in water discharge throughout the year. Total discharge can be reduced if evaporation rates are high and/or water is removed directly from the reservoir. (Ward and Stanford 1995). In many countries resettlement is being carried out due to the large dam construction (Table 1).

While evaluating the environmental risks of dams, they are evaluated under four main headings (Muhlbauer 2004);

- Physicochemical risks
- Biological Risks
- Economic, social and cultural risks
- Health and safety risks

These risks are also considered as sub-headings and are given in Figure 1.

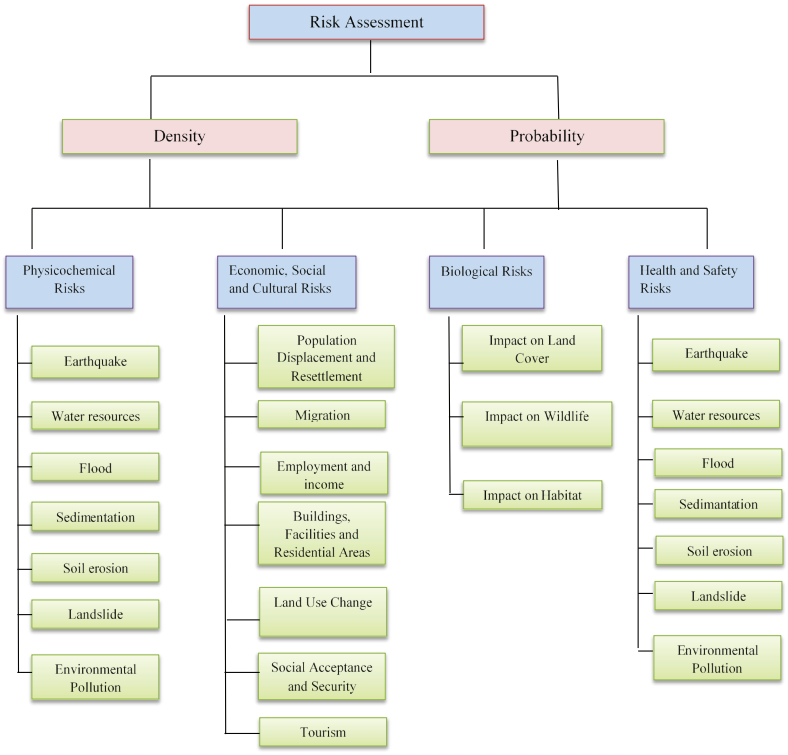

Fig. 1. *Environmental risk assessment of dams (Muhlbauer 2004)*

Table 1. *Countries and number of people who are resettled due to large dams in the world (Bilgin 2015)*

Dams	Country	Resettlement
Three Gorges China	China	1,250,000
Upper Krishna II	India	220,000

Sardar Sarovar	India	127,000
Aswan High Dam	Egypt	100,000
Kossou Ivory	Coast	85,000
Akosombo	Ghana	84,000
Longtan	China	73,000
Mahaweli I–IV	China	60,000
Kariba	Zambia and Zimbabwe	57,000
Sobradhino	Brazil	55,000

3.Impact on Ecosystem

It is necessary to assessment both the abiotic and biotic components together to evaluate the effects of dams on ecosystems (Table2) (McCartney et al. 2000).

Table 2. *Evaluation of the impact of large dams on ecosystems (McCartney et al. 2000).*

Data	Evaluation
Aquatic	
Hydrological	Flow volumes and flow regime due to river water retention (eg flood peaks and flow time)
Hydraulic characteristics	Water velocity and river stage
Water Quality	To evaluate change water characteristics (eg. Dssoved oxygen, temperature, electrical conductivity, etc.)
Geomorphological characteristics	Channel bed erosion and accretion, river bank erosion and delta erosion
Biotic	
Aquatic biota	Mammals, birds, reptiles, fish, amphibians, molluscs, macro-invertebrates,aquatic macrophytes, and plankton
Habitat requirements	Macro-invertebrates and fish
Riparian vegetation	To evaluate the changes in vegetation on the river bank as a result of river water retention.
Riparian fauna	To evaluate impacts of dams on communities of riparian vegetation.
Socio-Economic	
Number of people living in the flooded valley	To evaluate the number of persons who will be resettlement
Cultural importance of rivers and resources	To determine the loss of important cultural or archaeological sites.

4. Evaluation of Yusufeli Dam

The Yusufeli Dam is built on the Coruh River. The height of the dam body is 270 meters and it will be the 7th in the world's highest dams list. The Yusufeli Dam will have 540 MWe installed power and is planned to produce 1 billion 888 million kilowatt hours of electricity annually. This amount corresponds to the production of 7 thousand in Turkey's electricity consumption. The Yusufeli Dam, which has a storage capacity of 2 billion 130 million m^3, has the highest storage capacity among the Hydroelectric Power Plant (HEPP) to be established and operated on the Coruh River. The storage capacity of the dam corresponds to approximately 30% of the annual flow of the Coruh River (URL-1 n.d.).

Initial work for the Yusufeli Project, a part of the Coruh River Hydroelectric Development Master Plan, was launched in 1970, but the tender for the dam project was made in 2010. According to State Water Works data ; the project will cover 0.6% of Turkey's annual energy needs. When the Yusufeli Dam, which is a large-scaled dam, is completed, an area of 3,241 hectares will be under the water. The project will cause Yusufeli district center and 3 villages to be completely , and 16 villages and land to be partially under the water (KD 2011).

Dam and HEPP projects are evaluated within the scope of EIA Regulation according to their capacities. However, since the Yusufeli Dam Project was included in the investment program prior to 1997, it was exempted from the EIA within the scope of the EIA Regulation under the title of 'Legal Excluded Projects. Therefore, an "Environmental Impact Assessment" report has not been prepared. In 2006, an environmental impact assessment report was prepared by a company to meet the requirements of international credit institutions involved in project finance.

Fig 2. *Yusufeli Dam /Turkey*

CONCLUSION

Along with the developing technology, the damage in the environment is increasing. However, it has harmful effects on environment and human life during dam construction phase. Environmental impact assessment studies are required before starting dam construction and other investment studies. The construction of the dam in accordance with environmental legislation is necessary for a planned environmental management. Taking the results of environmental assessment seriously and using them in practice can reduce some of destructive effects.

References

Baviskar, Amita, and Arun Kumar Singh. 1994. "Malignant Growth: The Sardar Sarovar Dam and Its Impact on Public Health." *Environmental Impact Assessment Review* 14(5–6):349–58.

Bilgin, A. 2015. "Yusufeli Barajı Çevresel Risk Değerlendirmesi, Yusufeli Barajının İlçeye Etkileri, Türker Matbaacılık (in Turkish)."

Dynesius, M., and C. Nilsson. 1994. "Ecological Effects of River Regulation on Mammals and Birds: A Review."

Goldsmith, E., and N. Hildyard. 1984. "The Social and Environmental Impact of Large Dams. Wadebridge: Wadebridge Ecological Centre."

Karimi Jashni, A., and M. Chamanchi. 2007. "Comparing the Destructive Environmental Impacts of Dams with Using Veten-Verau Matrix. The First Specialized Dam and Environment Workshop."

KD. 2011. "Kaçkar Dağları ve Yusufeli Bölgesi Yönetim Planı, (in Turkish)."

McCartney, MP, C. Sullivan, and MC Acreman. 2000. "Ecosystem Impacts of Large Dams. UNEP."

Muhlbauer, WK. 2004. "Pipeline Risk Management Manual: Ideas, Techniques and Resources. 3rd Edit. Gulf Professional Publishing, Elsevier, Oxford, UK."

Satoshi, Ishida, Kotoku Motoi, Abe Eiichi, M.A.Fazal, Tsuchihara Takeo, and Imaizumi Masayuki. 2003. "Construction of Subsurface Dams and These Impact on the Environment." *RMZ – Materials and Geoenvironment* 50(June 2017):149–52.

URL-1. n.d. "Https://Www.Enerjiatlasi.Com/Hidroelektrik/Borcka-Baraji.Html."

Ward, J. V., and J. A. Stanford. 1995. "Ecological Connectivity in Alluvial River Ecosystems and Its Disruption by Flow Regulation." *Regulated Rivers: Research & Management* 11(1):105–19.

WCR. 2001. *World Commission Report, Dams and Development: A New Framework for Decision-Making*.

Chapter 12

NANO ANTIFOULING COATING APPROACHES IN THE MARINE INDUSTRY

Ayfer ERGİN [1]

M.Fatih ERGİN[2]

1 Asist. Prof. Dr. Ayfer ERGİN, İstanbul University - Cerrahpaşa, Engineering Faculty, Maritime Transportation Management Engineering, ayfersan@iuc.edu.tr, Orcid number: 0000-0002-6276-4001

2 Dr.M.Fatih ERGİN, İstanbul University - Cerrahpaşa, Engineering Faculty, Chemical Engineering, mfergin@iuc.edu.tr, Orcid number: 0000-0003-4158-368X

1 Introduction

The undesired collection of bacteria, algae, and animals on structures submerged in seawater is known as marine biofouling. Ships, drilling rigs, mooring lines, etc., many structures are seriously affected by this event. (Hellio & Yebra, 2009; Hu, Xie, Ma, & Zhang, 2020). After hours, a layer of slime consisting of microscopic organisms (bacteria and algae) develops on the submerged parts of these structures (Zobell & Allen, 1935). This layer simplifies the placement and attachment of macro-organisms (Zobell & Allen, 1935). This event has been a source of contention for the marine industry for many years, and it has also resulted in several environmental and economic consequences.

Nowadays, maritime transport has an important place in international trade. It is responsible for more than 80% of international trade (Yasa, Ergin, Ergin, & Alkan, 2016). In addition, more than 70% of cargo value transported to international trade is carried by ships (UNCTAD, 2017). Maritime shipping has made a rapid development over time, from 4 billion tons in 1990 to 11 billion tons in 2020 (Ergin & Ergin, 2021; UNCTAD, 2020). It has grown by almost 3 times since 1990. This situation has also increased the effects of maritime activities on the environment. Although maritime transport is the most environmentally friendly among other modes of transport (Ergin & Ergin, 2018), it is responsible for 1.8% of global greenhouse gases (Crippa et al., 2019). Ensuring fuel efficiency on ships is of vital importance for the environment. One of the factors affecting fuel efficiency on ships is marine biofouling.

High frictional resistance occurs due to the growth of organisms in a ship's hull, namely, the roughness produced (Barlas, 2019; K. A. Dafforn, J. A. Lewis, & E. L. Johnston, 2011a; Gu et al., 2015; M. P. Schultz, 2007; Yebra, Kiil, & Dam-Johansen, 2004). This results in weight gain on the ship hull as well as potential speed reduction, and loss of maneuverability. To compensate for this, the ship uses more power, that is, consumes more fuel, resulting in more emissions (Abbott, Abel, Arnold, & Milne, 2000) (Yebra et al., 2004) (Dafforn et al., 2011a). This may lead to an increase in fuel consumption of up to 40% (Champ, 2000). The increase in fuel consumption can cause the total trip cost to increase by up to 77% (Abbott et al., 2000). Marine biofouling gives rise to an increase in the frequency of dry-docking operations. In other words, when corrective measures are implemented, it induces time loss and freight penalties. In addition, a large amount of toxic waste is produced during these applications (Abbott et al., 2000). Marine biofouling, deterioration of ship coating, and leads to corrosion (Yebra et al., 2004). In a different problem, the introduction of species that cling to ships to environments where they do not naturally exist may give rise to the deterioration of the ecosystem (Dafforn et al.,

2011a) (Reise, Gollasch, & Wolff, 1998; Yebra et al., 2004). To overcome these problems, the use of antifouling coating on ship hulls is the most preferred measure.

Antifouling can be defined as the process of eliminating or preventing the accumulation and growth of organisms (Zhou, 2014). Tributyltin self-polishing copolymer coating (TBT-SPC paints) has been the most effective antifouling coating, although different solution methods have been used throughout maritime history in the fight against marine biofouling (Abbott et al., 2000; Yebra et al., 2004). In studies conducted over time, it has been determined that TBT-SPC systems adversely affect the environment. Especially harmful effects on sea creatures have been determined (Evans, Leksono, & McKinnell, 1995). For this reason, the International Maritime Organization (IMO) introduced prohibitions on the use of TBT in 2001. IMO has banned the application of TBT-based toxic antifouling coating since 2003. It also stated that as of 2008, such paints should not be present on the ships' surface (Champ, 2001). This situation has created the need to develop new, economical, and more environmentally friendly antifouling products.

It would not be wrong to define nanotechnology as a discipline that combines many branches of science by building on each other. If the properties of atoms at the nano level are studied using physics and chemistry, only a part of the picture can be seen. However, looking at the processing and application of molecules and even their effects on the human body from the perspective of biology will lead to a more accurate interpretation of the picture (Ergin M. F. , 2020).

2. Economic and Ecological Effects of Marine Biofouling

Marine biofouling causes billions of dollars of damage every year for many sectors, especially the maritime sector as seen in Figure 1. This pollution leads to great economic damage not only to ship hulls but also to moorings, submerged man-made surfaces, oil and gas platforms, aquaculture, pipelines, and many other structures. Shipping trade is one of the most important components of global trade with its nearly 90% volume. As a result of adhering marine biofouling organisms to ships, roughness forms on ship surfaces. This results in a reduction in the speed (Hu et al., 2020; Stupak, García, & Pérez, 2003; Yebra et al., 2004; Zhou, 2014) and maneuverability of the ship (Stupak et al., 2003). The loss of maneuverability leads to increased fuel consumption and delays in arriving and departing from the port (Ergin & Ergin, 2021). This is especially vital for ships with frequent port loading and unloading, such as ro-ro and container ships. This decrease in maneuverability ensures the transit times lengthen and causes extra freight penalties. Alternatively, maneuverability

can be increased by using tugboats at port entrances and exits. In this way, the total operating cost increases (Abbott et al., 2000).

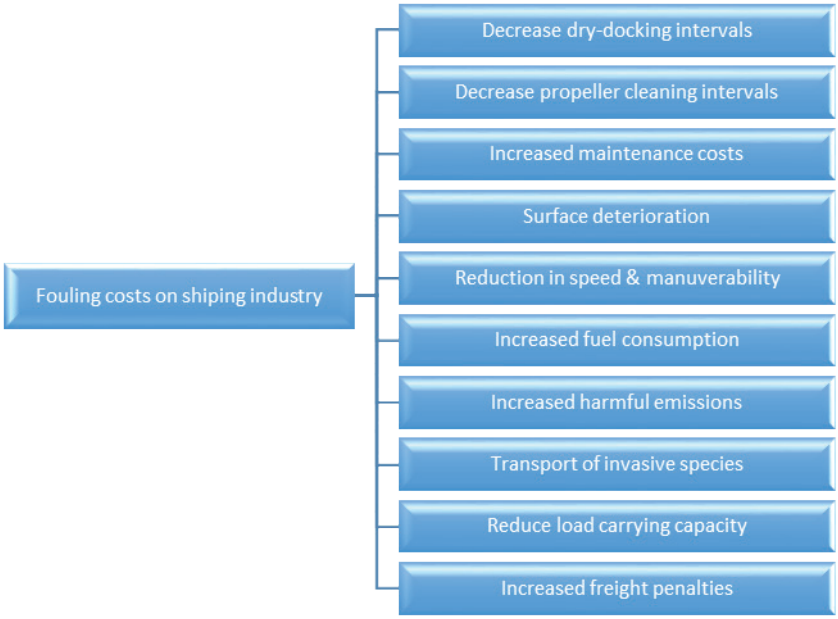

Figure 1. Fouling costs on shipping industry (Modified Y. Gu et al.)

As a result of biological contamination in ships, surface roughness increases and as a consequence of increased frictional resistance causes enhance in fuel consumption (Hu et al., 2020; Kempf, 1937; M. Schultz, Bendick, Holm, & Hertel, 2011; M. P. Schultz, 2007; Yebra et al., 2004). Haslbeck stated that biofilms attached to the hull alone increase fuel consumption between 8 % and 12 %. He also determined that normal propeller pollution increases fuel consumption by 6% to 14% (Haslbeck, 2003). Townsin examined the economic effects of marine biofouling on shipping. He stated that the antifouling coating will reduce fuel consumption by 4% (Townsin, 2003). Schultz and et al studied the costs associated with US Navy mid-sized surface combatant body contamination and calculated that their total annual cost was 56 million dollars (M. Schultz et al., 2011). Increased friction from marine pollution induces a decrease in ship speed and provides the transit time extended. This situation creates freight penalties for shipowners. To overcome this, ships can increase ship speed by consuming more fuel. The increase in fuel consumption leads to the operating costs of the ship to increase. Townsin has noted that organisms adhering to ships not using antifouling can increase the weight of the ship by up to 150 kg per m^2 (Townsin, 2003). This increased weight brings about the ship to carry less cargo and freight penalties.

Hull and propeller pollution on ships is one of the reasons for the increase in ship-sourced greenhouse gas GHG emissions (Buhaug, 2005). (Hellio & Yebra, 2009). Farkas et al. studied the effect of antifouling coating on fuel consumption in crude oil and bulk carriers. In their studies, they have shown that the crude oil carrier can be made with a fuel saving of 138 tons per route and a reduction in carbon dioxide emissions of up to 430 tons. In addition, it has been found that 20.4 tons of fuel-savings per route can be achieved with a reduction in carbon dioxide emissions up to 63.6 tons for the bulk carrier examined (Farkas, Degiuli, Martić, & Vujanović, 2021). Despite the greenhouse emission reduction effect of antifouling on ships, it should be kept in mind that the solvents found in these coatings are released into the sea (Ergin & Ergin, 2021).

Shipowners had dry-docking operations made to protect their ships from the negative effects of marine biofouling. This is a significant operating cost. Dry-dock operation is usually done once every 5 years. However, this operation can be done every 2½ to 3 years depending on the ship type, ship speed, seawater temperature, salinity, pH, trade area. In the process of dry-docking operations, a lot of waste material is formed in the shipyards. This generated waste is extremely important for the environment (Champ, 2003). Hull cleaning ranges from 10,000 to 30,000 dollars, depending on the part of the hull being cleaned and the cleaning technique used, and can take between one and three days in port. Propeller cleaning costs vary between 2000 and 5000 dollars and can be done in one day (Hellio & Yebra, 2009).

Marine biofouling easily colonizes ships as well as constructed underwater structures and accelerates the formation of corrosion (Little, Lee, & Ray, 2008). (Hu et al., 2020) (Abioye, Loto, & Fayomi, 2019). Marine biofouling and corrosion cause thinning of the hull surface and significantly reduce the strength of materials (Ilhan-Sungur, Cansever, & Cotuk, 2007) (Duan et al., 2008). Contaminated organisms can penetrate protective coatings and expose the underlying metal, inducing subsequent corrosion (Blackwood, Lim, Teo, Hu ve Pang, 2017). Cleaning on the hull surface corrosion requires high maintenance costs.

In marine aquaculture, infrastructure as well as target culture species are severely affected by biofouling. Biological pollution-related costs in marine aquaculture are 5 – 10 % of production costs (Lane & Willemsen, 2004). This corresponds to approximately 1.5 to 3 billion dollars per year (Fitridge, Dempster, Guenther, & De Nys, 2012). However, the aquaculture industry's ongoing growth, as well as stricter legislation for biocides in food production, necessitate the development of more environmentally friendly antifouling coatings.

Anti-fouling methods also limit the rate of invasive microorganism introduction. Ballast water treatment is primarily aimed at reducing/ preventing the spread of invasive microorganisms. Additional costs are incurred as a result of additional efforts to minimize the transmission of invasive microorganisms in ballast water and sediments. The estimated operating cost of invasive microorganisms mitigation measures may represent 1.6% to 4% of the annual operating cost for a ship operating in European seas, and smaller ships may have higher proportional costs. These invasive microorganisms have the potential to alter the structure and function of marine ecosystems, resulting in social and economic ramifications (Perrings, Mooney, & Williamson, 2009) (Pimentel, Zuniga, & Morrison, 2005) (Rilov & Crooks, 2009). It shows that species polluting invasive microorganisms have a higher impact on fuel consumption than native species (Fernandes et al., 2016). Migration of invasive species due to marine biofouling may result in loss of native species (S. A. Kumar, 2017) (Reise et al., 1998).

3. Antifouling Solutions With Nanotechnology

On the effectiveness of anti-poison coatings; three different basic working strategies were determined as Fouling-Resistant, Fouling-Degrading, and Fouling-Release (see Figure 2). Fouling-Resistant uses hydrated structures to prevent contaminants such as proteins, algae, or bacteria from adhering to surfaces(Thérien-Aubin, Chen, & Ober, 2011). Fouling-Release coatings, on the other hand, allow surfaces to be cleaned by an external force such as water . The strategy used in both of these coatings is to give the surface a hydrophilic character and remove the contaminants from the environment (Chen, Li, Zhao, & Zheng, 2010; Damodaran & Murthy, 2016). In fouling-degrading, another method, coatings use the method of decomposing bacteria and microorganisms by oxidation (Sakala & Reches, 2018).

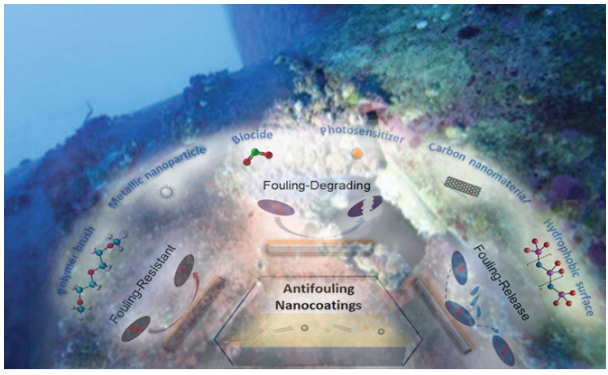

Figure 2. Coating strategies and active substances used for antifouling.

3.1. Antifouling Biocides

Antifouling biocides are chemical substances that provide biofouling-derived micro-organisms harmless on the surface they come into contact with. Since July 2010, tri-substituted organostannic compounds commonly used in antifouling coatings have been banned in the EU Commission Regulation (in 2010) (Merenyi, 2012) due to their leaching into the marine environment and toxic effects on marine life. However, copper antifouling coatings, which are more effective against biocides produced by hard-shelled organisms such as mussels, have been used for a long time. The most preferred copper compounds for antifouling coatings are copper oxide, copper thiocyanate, and copper flake. However, as a result of such use of copper, it has been determined that the copper leaking from the antifouling coatings affects seawater and living things. Because of this, the use of copper paints on boats is prohibited in Washington, USA (Zhang & Singhasemanon, 2014). In addition, the European Union warned the countries to be sensitive about this issue. Therefore, it has been determined that some biocides used in antifouling coatings have continuous leaching characteristics. These biocides cause accumulation in marine organisms, develop antibiotic resistance in humans, and pose a potential threat to the aquatic environment. Therefore, pollution-free and environmentally friendly antifouling coatings are needed to prevent pollution in the seas.

3.2. Polymer-Based Antifouling Coatings

One of the notable studies to prevent the adhesion of proteins to surfaces is the grafting of polyethylene glycol (PEG) polymer onto polyaniline (PANI) nanofibers (Li et al., 2019). Thus, new composite nanofibers belonging to PEG brushes are formed on the surface (Hui, Sun, Niu, Luo, & interfaces, 2017). Also, the reaction of PEG with proteins containing amino groups of aldehyde finite chains causes oxidative degradation (Chen et al., 2010). This resulted in it having short-term stability. In addition, due to their hydrated structure, PEG coatings lose their strength as a result of swelling. In order to produce the nanostructure, alternative studies have been carried out using different materials such as polyoxazoline, polyglycerol dendrons, polysaccharides, and zwitterionic polymers (Chen et al., 2010; Divandari et al., 2017; Knowles et al., 2017; Li et al., 2019; Lin et al., 2011; Liu, Singh, Lalani, & Liu, 2012; Rendueles, Kaplan, & Ghigo, 2013; Wyszogrodzka & Haag, 2009). In addition, ring nanostructures that are more resistant to proteins have been obtained by using poly (2-alkyl-2-oxazolines) (Wang et al., 2019).

Poly (dimethylsiloxane) (PDMS) coatings that have low surface energy represent another type of antifouling system with the ability to fouling-release (K. A. Dafforn, J. A. Lewis, & E. L. J. M. P. B. Johnston,

2011b). In addition, the insertion of silicone oils into the nanocomposite structure increases the lubricity of the coating surface. So, it prevents the adhesion of crustaceans such as mussels on the surface and significantly reduces pollution. To further improve the hydrophobicity of the coating surface, polystyrene beads are added to the PDMS structure. In addition, the addition of silicone oils to them improves the lubricity of the coating surface. Since the surface of PS sphere-coated PDMS has fewer spots where polluting organisms will cling, pollutants can't hold, and the adherents can be easily cleaned by external effects such as water (Figure 3).

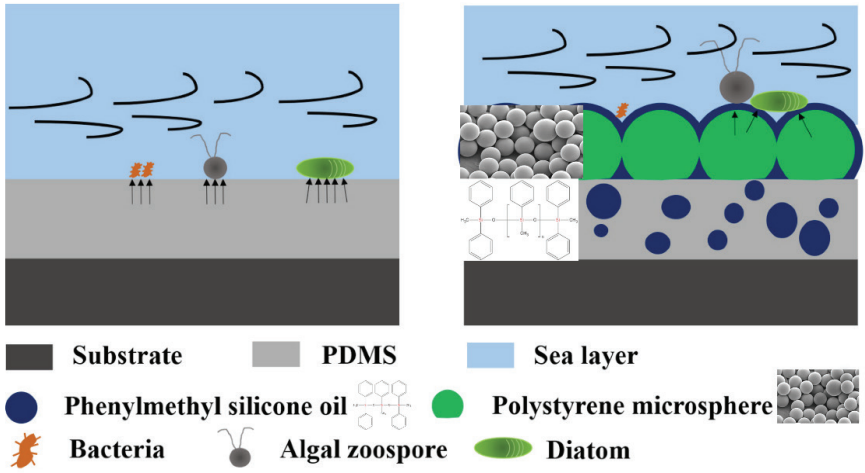

Figure 3. Synergistic defense of PSO (phenylmethylsilicone oil)/PDMS (polydimethylsiloxane)-PS (polystyrene) coating against biofoulings (Modified from Ref. (Mo et al., 2021))

3.3. Hydrogel Coatings for Antifouling

Hydrogels are polymer networks that contain approximately 80 to 90% water in their structure. It is not a highly preferred material because of the adhesion problem as a surface coating of hydrogel structures. However, it is an interesting property that they can release marine organisms due to their antifouling properties due to their super hydrophilicity and their elastic modularity (Brady Jr & Singer, 2000). Different studies have been carried out to improve the adhesion properties of hydrogels so that they can be used as antifouling coatings. The reasons why the hydrogel coating is preferred are that it is easy to apply, easily copolymerized with molecules containing silanes or hydroxyl, and can be applied when powdered and mixed with water again (Gao et al., 2020).

3.4. Inorganic Content-Based Coatings for Biofouling Prevention

Antifouling coatings containing nanomaterials reveal hydrophobicity,

water repellency, non-stickiness, microbial resistance, and anti-corrosion properties (Callow & Callow, 2011; Yebra, Kiil, Weinell, & Dam-Johansen, 2006). Thanks to these remarkable features, it is thought that it will help to eliminate many problems encountered in the maritime sector (Lakhotia, Mukhopadhyay, Kumari, & Reviews, 2018). Silver nanoparticles (S. Kumar, Bhattacharya, Singh, Halder, & Mitra, 2017) are also widely used in the production of nanomaterials for antifouling paints, carbon nanostructures such as carbon nanotubes (CNTs) and graphene. In addition, various metal oxides such as titanium dioxide (TiO2) (Kim et al., 2016) and zinc oxide (ZnO) (Al-Naamani, Dobretsov, Dutta, & Burgess, 2017) nanoparticles have been used as nanocomposites in formulations showing antifouling activities . In the literature, studies on antifouling - nanomaterials have focused especially on ZnO and TiO_2. However, in the study, we examined the effect of nano-silver, nano-carbon, and other nano-metal oxides on antifouling coatings.

3.4.1. Silver Nanoparticles

Silver ions impart antibacterial, fungistatic/fungicide and algiostatic/algicide properties to the structure in which it is used (DeVasConCellos, Bose, Beyenal, Bandyopadhyay, & Zirkle, 2012). In addition, silver has an inhibitory effect against different microorganisms (Goswami, Sahareen, Singh, Kumar, & Chemistry, 2015). Nano-sized silver particles have found many applications as antimicrobial agents due to their high surface-to-volume ratio and increased surface reactivity. Especially, this metal is often used in the manufacture of medicinal products(Durán et al., 2016). The antibacterial property of nano-sized silver has been reported in the literature that it can be used in antifouling coatings against microfouling. In addition, there are not many studies in the literature on nano-sized silver antifouling coatings against macrofouling (DeVasConCellos et al., 2012). In one study, it was reported that the coating containing silver nanoparticles prevented the adhesion of marine and freshwater algae, while in another it was reported that it prevented the settlement of mussels. However, the effect of nano-sized silver particles on antifouling coatings has not been fully elucidated.

3.4.2. Graphene and Carbon Nanotube

In the honeycomb crystal structure, sp2 hybridizing graphite is the main building block of nanotube and C60 (Figure 4). Graphene is one of the important nanomaterials used for applications such as energy production and storage (Ozer et al., 2017; Sun et al., 2015). Carbon nanotubes (CNTs) consist of hollow, cylindrical structures of varying diameters and lengths. Carbon nanotubes are divided into three groups: single-walled (SWCNT), double-walled (DWCNT) and multi-walled (MWCNT). The use of CNTs

in antifouling coatings includes fouling release activities for the biocidal properties of surfaces (Dasgupta, Rajukumar, Rotella, Lei, & Terrones, 2017; Upadhyayula & Gadhamshetty, 2010).

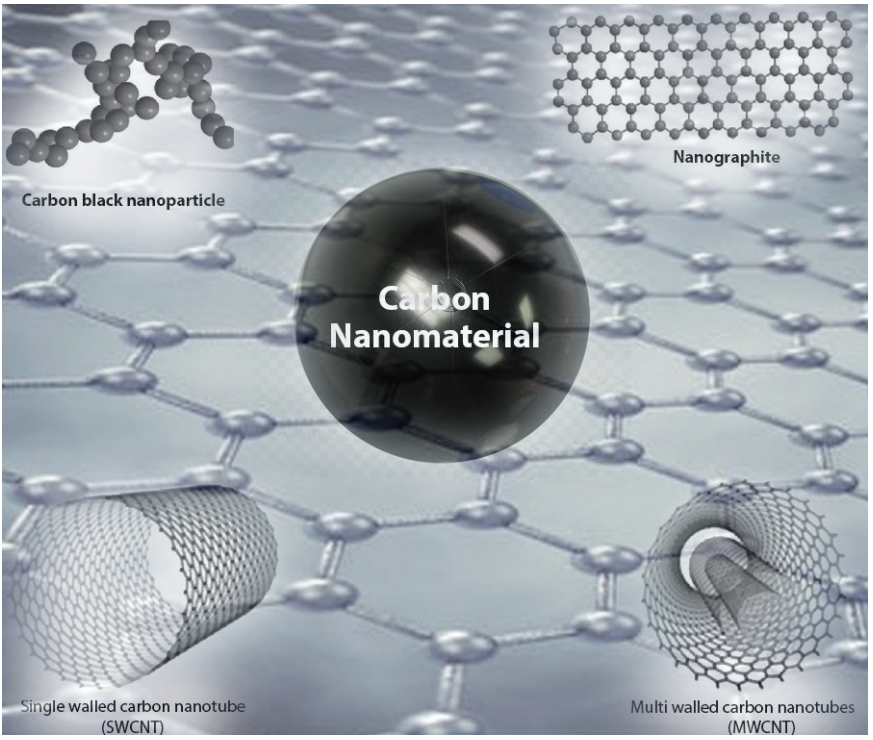

Figure 4. Various carbon-based nanomaterials.

The first CNT-based antifouling coating was obtained in 2008 by treating synthetic multi-walled CNTs with silicone (Beigbeder et al., 2008). Today, CNT-based coatings have become one of the important nanomaterials applied as a toxic and anti-corrosion marine coating in marine and freshwaters (Dustebek, Kandemir-Cavas, Nitodas, & Cavas, 2016). In order for CNTs to be applied in antifouling coatings, they must be added to a polymer matrix (Deng et al., 2015; Jin, Li, Park, & Chemistry, 2015). Different types of carbon nanotubes and epoxy resins are used together. CNTs with large surface areas work as an effective adsorbent due to the π-bonds on their surface and their layered and hollow structure. In addition to these properties, they have remarkable high tensile strength and modulus of elasticity values. When CNT (Figure 5) is added as an additive to the coating matrix, the coatings show much better mechanical properties. In a study, the effect of the increase in the amount of MWCNT on the antifouling coating was investigated. In addition, it was determined that the increase in the amount of MWCNT showed an improvement

in the mechanical strength of the coating. This work was supported by another study examining the effect of MWCNT and graphene oxide (GO) supplements on the mechanical properties of PDMS coatings (Dustebek et al., 2016). The inclusion of MWCNT in nanocomposite formulations revealed highly positive effects on the tensile strength and percent elongation of PDMS coatings. These studies reveal that in addition to their antifouling properties, CNT and graphene oxide have very good effects on mechanical properties in nanocomposite coatings.

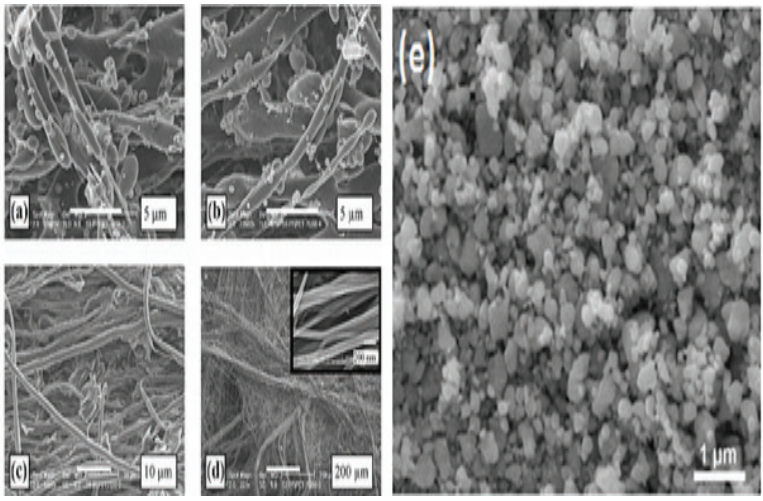

Figure 5. Figure 7a. SEM micrograph (a) - at the beginning of draw (b) - at low draw ratios, (c) - at high draw ratios, (d) - CNT at highest draw ratios

In a different study, it was revealed that CNT and graphene oxide may have different antifouling mechanisms in antifouling coatings. First, CNT and graphene oxide are toxic to macro-fouling organisms. Secondly, it has been stated that it can prevent larvae settlement in a non-toxic way by preventing attachment and adhesion of larvae (Mesarič et al., 2013).

3.4.3. Metal Oxides and Metal/Metal Oxide Hybrid Nanostructure

Antimicrobial metal oxide nanoparticles (TiO2, SnO2, and ZnO) have anti-corrosion, self-cleaning and healing properties. These are frequently used in antifouling applications. Generally, in the literature, researchers have investigated the relationship between nanoparticles obtained from metal oxides and antifouling paints (Naskar et al., 2018). Hybrid metal-metal oxide and hybrid carbon-metal oxide and ZnO and TiO2 nanoparticles are the most important nanostructures used in the prevention of biological pollution. ZnO nanoparticles are preferred more than other metal oxides due to their cheapness and easy production. In addition, ZnO has been determined as a safe material by the FDA (Food and Drug Administration,

United States). TiO2 is used in coatings and paints due to its self-cleaning feature. However, since TiO2 requires activation with UV light, they are often applied outdoors. Silver nanoparticles are one of the non-toxic antimicrobial agents synthesized by environmentally friendly methods. Also, it is used with TiO2 to further improve the functional properties of silver nanoparticles. Yee et al., 2017, carried out a 2-step hydrothermal synthesis of silver-titanium nanotube composite using nano-Ag and nano TiO2 structures in their study. The nanomaterial obtained in their study reduces the biofilm formation of marine bacteria by 98% compared to nanotubes.

The coating consisting of triple superhydrophobic nanocomposite was obtained by solution casting method using graphene oxide suspended in PDMS and alumina nanorods. The obtained results showed that the triple superhydrophobic nanocomposite hybrid layers have positive effects on the contact angle, surface free energy and micro-nano roughness of the coatings. In their study, they showed that the developed nanocomposite material is a very promising antifouling coating for the maritime world.

Aluminum oxides are one of the most preferred inorganic materials due to their cheapness, non-toxicity, and very stable inorganic materials in nanomaterial construction. Boehmite is an aluminum oxide hydroxide (γ-AlO(OH)) mineral that is a component of aluminum ore bauxite. Boehmite nanoparticles with extra hydroxyl groups on their surface can improve the hydrophilic and surface properties of the membrane they are used in. Therefore, it is stated that it will prevent the contamination of the membranes (Farjami, Moghadassi, & Vatanpour, 2021; Vatanpour, Madaeni, Rajabi, Zinadini, & Derakhshan, 2012).

While ZnO and TiO2 are widely used in nanocomposite production, Cu2O, CuO, and Al2O3 are also included in nanocomposite coatings (Baniamerian et al., 2018). PDMS, which has a hydrophobic feature, is a preferred material as a coating because of this feature. It is especially applied in antifouling paint applications. Biopolymers such as chitosan are preferred to develop environmentally friendly nanocomposites. It has been determined that chitosan and ZnO or TiO2 based nanocomposite coatings are effective against biofilm-forming bacteria and various marine microorganisms. Metal oxides have photocatalytic properties that prevent biofouling in light, while the addition of chitosan improves antifouling properties in dark conditions. Most of the nanocomposite antifouling coating studies using ZnO nanoparticles or nanorods have been carried out under laboratory conditions. There are many different types of organisms that cause biological pollution in real environments such as the sea. Therefore, it is very important to test and prove the anti-toxicity activities of coatings exposed to different physical and biological factors.

4. Results

One of the biggest problems of the shipping industry almost everywhere in the world; is marine biofouling that naturally clings to marine vehicles.

Different antifouling coatings are applied to the surfaces of marine vehicles in contact with the sea in order to prevent biofouling. Since these applied coatings have antimicrobial activity, it is expected to prevent micro and macro contamination. Many applied coatings formulations use substances, such as copper or isothiazolinone, which will remove or destroy the contaminating organisms. However, the effects of these chemicals not only affect unwanted organisms but also almost all sea creatures. Therefore, the International Maritime Organization (IMO) removed the antifouling agent called triorganotin from use in 2008 due to its effect. However, non-toxic coating methods used today are both costly and not as effective as old solutions. For this reason, it seems appropriate to use nanotechnological coatings that are as environmentally friendly as possible, non-toxic to sea creatures, or have as few toxic properties as possible.

Today, shipowners receive support from companies that require hydrodynamic and statistical expertise to examine the effect of hull and propeller cleaning on fuel performance. In this way, when the ship performance drops below a certain level as a result of biofouling, maintenance is done and fuel-saving is provided. Therefore, biofouling reduction costs can be considered an investment to reduce fuel consumption.

One of the inferences from the research conducted in the study is related to TBT. The use of TBT-based antifouling paints on ships has been banned since 2003. However, before 2003, that is, about 80% of ships aged 18 years or more had TBT-based antifouling coatings. About half of the antifouling coatings remain on the ship's surface (Abbott et al., 2000). This means that serious TBT pollution will occur during ship recycling operations. For example, a 33-year-old ship may have had a TBT-based antifouling coating 3 times when it came to the ship recycling stage. A very high rate of toxic substances is released during the ship recycling stage. In 2020, 9.2% of the world's ship recycling industry was realized in Turkey (UNCTAD, 2021). This shows that seriously toxic substances are released in our shipyards. Considering that most Turkish shipyards are located in the Sea of Marmara, the effect of the ship recycling industry on the mucilage in the Marmara Sea in 2021 should be investigated. It is extremely important to use more environmentally friendly nano antifouling coatings on routes where maritime trade and cruise tourism are intense and especially in marine aquaculture, both for the protection of marine ecology and for less toxic waste in shipyards.

REFERENCES

Abbott, A., Abel, P., Arnold, D., & Milne, A. (2000). Cost–benefit analysis of the use of TBT: the case for a treatment approach. *Science of the total environment, 258*(1-2), 5-19.

Abioye, O. P., Loto, C., & Fayomi, O. (2019). Evaluation of anti-biofouling progresses in marine application. *Journal of Bio-and Tribo-Corrosion, 5*(1), 22.

Al-Naamani, L., Dobretsov, S., Dutta, J., & Burgess, J. G. (2017). Chitosan-zinc oxide nanocomposite coatings for the prevention of marine biofouling. *Chemosphere, 168*, 408-417.

Baniamerian, H., Safavi, M., Alvarado-Morales, M., Tsapekos, P., Angelidaki, I., & Shokrollahzadeh, S. J. E. r. (2018). Photocatalytic inactivation of Vibrio fischeri using Fe2O3-TiO2-based nanoparticles. *166*, 497-506.

Barlas, B. (2019). Antifouling Boyaların Hidrodinamik Özellikleri Üzerine Bir HAD Çalışması. *Journal of ETA Maritime Science, 7*(4), 318-331.

Beigbeder, A., Degee, P., Conlan, S. L., Mutton, R. J., Clare, A. S., Pettitt, M. E.,Dubois, P. (2008). Preparation and characterisation of silicone-based coatings filled with carbon nanotubes and natural sepiolite and their application as marine fouling-release coatings. *Biofouling, 24*(4), 291-302.

Brady Jr, R. F., & Singer, I. L. (2000). Mechanical factors favoring release from fouling release coatings. *Biofouling, 15*(1-3), 73-81.

Callow, J. A., & Callow, M. E. (2011). Trends in the development of environmentally friendly fouling-resistant marine coatings. *Nature communications, 2*(1), 1-10.

Champ, M. A. (2000). A review of organotin regulatory strategies, pending actions, related costs and benefits. *Science of the total environment, 258*(1-2), 21-71.

Champ, M. A. (2001). *The status of the treaty to ban TBT in marine antifouling paints and alternatives.* Paper presented at the Proceedings of the 24th UJNR (US/Japan) Marine Facilities Panel Meeting, Hawaii.

Champ, M. A. (2003). Economic and environmental impacts on ports and harbors from the convention to ban harmful marine anti-fouling systems. *Marine Pollution Bulletin, 46*(8), 935-940.

Chen, S., Li, L., Zhao, C., & Zheng, J. J. P. (2010). Surface hydration: Principles and applications toward low-fouling/nonfouling biomaterials. *51*(23), 5283-5293.

Crippa, M., Oreggioni, G., Guizzardi, D., Muntean, M., Schaaf, E., Lo Vullo, E.,-Vignati, E. (2019). Fossil CO2 and GHG emissions of all world countries. *Luxemburg: Publication Office of the European Union*.

Dafforn, K. A., Lewis, J. A., & Johnston, E. L. (2011a). Antifouling strategies: history and regulation, ecological impacts and mitigation. *Marine Pollution Bulletin, 62*(3), 453-465.

Dafforn, K. A., Lewis, J. A., & Johnston, E. L. J. M. P. B. (2011b). Antifouling strategies: history and regulation, ecological impacts and mitigation. *62*(3), 453-465.

Damodaran, V. B., & Murthy, N. S. J. B. r. (2016). Bio-inspired strategies for designing antifouling biomaterials. *20*(1), 1-11.

Dasgupta, A., Rajukumar, L. P., Rotella, C., Lei, Y., & Terrones, M. (2017). Covalent three-dimensional networks of graphene and carbon nanotubes: synthesis and environmental applications. *Nano Today, 12*, 116-135.

Deng, C., Jiang, J., Liu, F., Fang, L., Wang, J., Li, D., & Wu, J. (2015). Influence of carbon nanotubes coatings onto carbon fiber by oxidative treatments combined with electrophoretic deposition on interfacial properties of carbon fiber composite. *Applied Surface Science, 357*, 1274-1280.

DeVasConCellos, P., Bose, S., Beyenal, H., Bandyopadhyay, A., & Zirkle, L. G. (2012). Antimicrobial particulate silver coatings on stainless steel implants for fracture management. *Materials Science Engineering: C, 32*(5), 1112-1120.

Divandari, M., Morgese, G., Trachsel, L., Romio, M., Dehghani, E. S., Rosenboom, J.-G., Benetti, E. M. (2017). Topology effects on the structural and physicochemical properties of polymer brushes. *Macromolecules, 50*(19), 7760-7769.

Duan, J., Wu, S., Zhang, X., Huang, G., Du, M., & Hou, B. (2008). Corrosion of carbon steel influenced by anaerobic biofilm in natural seawater. *Electrochimica Acta, 54*(1), 22-28.

Durán, N., Durán, M., De Jesus, M. B., Seabra, A. B., Fávaro, W. J., Nakazato, G. J. N. n., biology, & medicine. (2016). Silver nanoparticles: A new view on mechanistic aspects on antimicrobial activity. *12*(3), 789-799.

Dustebek, J., Kandemir-Cavas, C., Nitodas, S. F., & Cavas, L. J. P. i. O. C. (2016). Effects of carbon nanotubes on the mechanical strength of self-polishing antifouling paints. *98*, 18-27.

Ergin, A., & Ergin, M. F. (2018). Reduction of Ship Based CO2 Emissions from Container Transportation. *International Journal of Computational and Experimental Science and Engineering, 4*(3), 1-4.

Ergin, A., & Ergin, M. F. (2021). THE ROLE OF ANTIFOULING COATING IN THE MARINE INDUSTRY. *Research & Reviews in Engineering*, 53.

Ergin M. F. , Ü. B. (2020). YANGIN VE PATLAMA OLAYLARINDA NANOTEKNOLOJİNİN KULLANIMI. In F.ASICIOGLU&S.MERCAN (Ed.), *YANGINVEPATLAMANINADLİBİLİMLERYÖNÜNDENDEĞERLENDİRİLMESİ* (pp. 187-191). İstanbul: Nobel Yayınevi.

Evans, S., Leksono, T., & McKinnell, P. (1995). Tributyltin pollution: a diminishing problem following legislation limiting the use of TBT-based anti-fouling paints. *Marine Pollution Bulletin, 30*(1), 14-21.

Farjami, M., Moghadassi, A., & Vatanpour, V. (2021). Influence of solvent type on the ability and properties of the boehmite nanoparticles embedded emulsion polyvinyl chloride nanocomposite ultrafiltration membranes. *Iranian Polymer Journal*, 1-15.

Farkas, A., Degiuli, N., Martić, I., & Vujanović, M. (2021). Greenhouse gas emissions reduction potential by using antifouling coatings in a maritime transport industry. *Journal of Cleaner Production, 295*, 126428.

Fernandes, J. A., Santos, L., Vance, T., Fileman, T., Smith, D., Bishop, J. D., . . . Buisman, E. (2016). Costs and benefits to European shipping of ballast-water and hull-fouling treatment: Impacts of native and non-indigenous species. *Marine Policy, 64*, 148-155.

Fitridge, I., Dempster, T., Guenther, J., & De Nys, R. (2012). The impact and control of biofouling in marine aquaculture: a review. *Biofouling, 28*(7), 649-669.

Gao, L., Ma, S., Ma, Z., Zheng, Z., Zhou, F., & Liang, Y. (2020). In situ covalent bonding in polymerization to construct robust hydrogel lubrication coating on surface of silicone elastomer. *Colloids Surfaces A: Physicochemical Engineering Aspects, 599*, 124753.

Goswami, S., Sahareen, T., Singh, M., Kumar, S. J. J. o. I., & Chemistry, E. (2015). Role of biogenic silver nanoparticles in disruption of cell–cell adhesion in Staphylococcus aureus and Escherichia coli biofilm. *26*, 73-80.

Gu, Y.-Q., Mou, J.-G., Zheng, S.-H., Jiang, L.-F., Wu, D.-H., Ren, Y., & Liu, F.-Q. (2015). Characteristics on drag reduction of bionic jet surface based on earthworm's back orifice jet. *Acta Physica Sinica, 64*(2), 024701.

Hellio, C., & Yebra, D. (2009). *Advances in marine antifouling coatings and technologies*: Elsevier.

Hu, P., Xie, Q., Ma, C., & Zhang, G. (2020). Silicone-based fouling-release coatings for marine antifouling. *Langmuir, 36*(9), 2170-2183.

Hui, N., Sun, X., Niu, S., Luo, X. J. A. a. m., & interfaces. (2017). PEGylated polyaniline nanofibers: antifouling and conducting biomaterial for electrochemical DNA sensing. *9*(3), 2914-2923.

Ilhan-Sungur, E., Cansever, N., & Cotuk, A. (2007). Microbial corrosion of galvanized steel by a freshwater strain of sulphate reducing bacteria (Desulfovibrio sp.). *Corrosion Science, 49*(3), 1097-1109.

Jin, F.-L., Li, X., Park, S.-J. J. J. o. I., & Chemistry, E. (2015). Synthesis and application of epoxy resins: A review. *29*, 1-11.

Kempf, G. (1937). On the effect of roughness on the resistance of ships. *Trans INA, 79*, 109-119.

Kim, J., Baek, Y., Hong, S. P., Yoon, H., Kim, S., Kim, C., Yoon, J. (2016). Evaluation of thin-film nanocomposite RO membranes using TiO2 nanotubes and TiO2 nanoparticles: a comparative study. *Desalination Water Treatment, 57*(51), 24674-24681.

Knowles, B. R., Wagner, P., Maclaughlin, S., Higgins, M. J., Molino, P. J. J. A. a. m., & interfaces. (2017). Silica nanoparticles functionalized with zwitterionic sulfobetaine siloxane for application as a versatile antifouling coating system. *9*(22), 18584-18594.

Kumar, S., Bhattacharya, W., Singh, M., Halder, D., & Mitra, A. (2017). Plant latex capped colloidal silver nanoparticles: a potent anti-biofilm and fungicidal formulation. *Journal of Molecular Liquids, 230*, 705-713.

Kumar, S. A. (2017). *Eco-friendly nano-hybrid materials for advanced engineering applications*: CRC Press.

Lakhotia, S. R., Mukhopadhyay, M., Kumari, P. J. S., & Reviews, P. (2018). Surface-modified nanocomposite membranes. *47*(4), 288-305.

Lane, A., & Willemsen, P. (2004). Collaborative effort looks into biofouling. *Fish Farming Int, 44*, 34-35.

Li, B., Jain, P., Ma, J., Smith, J. K., Yuan, Z., Hung, H.-C., Pfaendtner, J. (2019). Trimethylamine N-oxide–derived zwitterionic polymers: A new class of ultralow fouling bioinspired materials. *Science advances, 5*(6), eaaw9562.

Lin, S., Zhang, B., Skoumal, M. J., Ramunno, B., Li, X., Wesdemiotis, C., Jia, L. J. B. (2011). Antifouling poly (β-peptoid) s. *12*(7), 2573-2582.

Little, B. J., Lee, J. S., & Ray, R. I. (2008). The influence of marine biofilms on corrosion: a concise review. *Electrochimica Acta, 54*(1), 2-7.

Liu, Q., Singh, A., Lalani, R., & Liu, L. (2012). Ultralow fouling polyacrylamide on gold surfaces via surface-initiated atom transfer radical polymerization. *Biomacromolecules, 13*(4), 1086-1092.

Merenyi, S. (2012). REACH: Regulation (EC) No 1907/2006. In: CSL, Consolidated Substances Legislation.

Mesarič, T., Sepčič, K., Piazza, V., Gambardella, C., Garaventa, F., Drobne, D., & Faimali, M. (2013). Effects of nano carbon black and single-layer graphene oxide on settlement, survival and swimming behaviour of Amphibalanus amphitrite larvae. *Chemistry Ecology, 29*(7), 643-652.

Mo, Y., Xue, P., Yang, Q., Liu, H., Zhao, X., Wang, J., Qi, Y. J. P. (2021). Composite slow-release fouling release coating inspired by synergistic anti-fouling effect of scaly fish. *13*(16), 2602.

Naskar, A., Khan, H., Sarkar, R., Kumar, S., Halder, D., & Jana, S. (2018). Anti-biofilm activity and food packaging application of room temperature solution process based polyethylene glycol capped Ag-ZnO-graphene nanocomposite. *Materials Science Engineering: C, 91*, 743-753.

Ozer, L. Y., Garlisi, C., Oladipo, H., Pagliaro, M., Sharief, S. A., Yusuf, A.,Palmisano, G. (2017). Inorganic semiconductors-graphene composites in photo (electro) catalysis: Synthetic strategies, interaction mechanisms and applications. *Journal of Photochemistry Photobiology C: Photochemistry Reviews, 33*, 132-164.

Perrings, C., Mooney, H., & Williamson, M. (2009). *Bioinvasions and globalization: ecology, economics, management, and policy*: OUP Oxford.

Pimentel, D., Zuniga, R., & Morrison, D. (2005). Update on the environmental and economic costs associated with alien-invasive species in the United States. *Ecological economics, 52*(3), 273-288.

Reise, K., Gollasch, S., & Wolff, W. J. (1998). Introduced marine species of the North Sea coasts. *Helgoländer Meeresuntersuchungen, 52*(3), 219-234.

Rendueles, O., Kaplan, J. B., & Ghigo, J. M. J. E. m. (2013). Antibiofilm polysaccharides. *15*(2), 334-346.

Rilov, G., & Crooks, J. A. (2009). Biological invasions in marine ecosystems. *Ecological, Management and Geographic Perspectives*.

Sakala, G. P., & Reches, M. J. A. M. I. (2018). Peptide-based approaches to fight biofouling. *5*(18), 1800073.

Schultz, M., Bendick, J., Holm, E., & Hertel, W. (2011). Economic impact of biofouling on a naval surface ship. *Biofouling, 27*(1), 87-98.

Schultz, M. P. (2007). Effects of coating roughness and biofouling on ship resistance and powering. *Biofouling, 23*(5), 331-341.

Stupak, M. E., García, M. T., & Pérez, M. C. (2003). Non-toxic alternative compounds for marine antifouling paints. *International biodeterioration & biodegradation, 52*(1), 49-52.

Sun, X.-F., Qin, J., Xia, P.-F., Guo, B.-B., Yang, C.-M., Song, C., & Wang, S.-G. (2015). Graphene oxide–silver nanoparticle membrane for biofouling control and water purification. *Chemical Engineering Journal, 281*, 53-59.

Thérien-Aubin, H., Chen, L., & Ober, C. K. J. P. (2011). Fouling-resistant polymer brush coatings. *52*(24), 5419-5425.

Townsin, R. (2003). The ship hull fouling penalty. *Biofouling, 19*(S1), 9-15.

UNCTAD. (2017). *Review of Maritime Transport 2017*. Retrieved from

UNCTAD. (2020). *Review of Maritime Transport, 2020*. Retrieved from

UNCTAD. (2021). *Review of Maritime Transport 2021*. Retrieved from United Nations Conference on Trade and Development:

Upadhyayula, V. K., & Gadhamshetty, V. (2010). Appreciating the role of carbon nanotube composites in preventing biofouling and promoting biofilms on material surfaces in environmental engineering: a review. *J Biotechnology advances, 28*(6), 802-816.

Vatanpour, V., Madaeni, S. S., Rajabi, L., Zinadini, S., & Derakhshan, A. A. (2012). Boehmite nanoparticles as a new nanofiller for preparation of antifouling mixed matrix membranes. *Journal of Membrane Science, 401*, 132-143.

Wang, P., Dong, Y., Zhang, S., Liu, W., Wu, Z., & Chen, H. (2019). Protein-resistant properties of poly (N-vinylpyrrolidone)-modified gold surfaces: The advantage of bottle-brushes over linear brushes. *Colloids Surfaces, 177*, 448-453.

Wyszogrodzka, M., & Haag, R. (2009). Synthesis and characterization of glycerol dendrons, self-assembled monolayers on gold: a detailed study of their protein resistance. *Biomacromolecules, 10*(5), 1043-1054.

Yasa, H., Ergin, M. F., Ergin, A., & Alkan, G. (2016). Importance of Inert Gases for Chemical Transportation. *PROCEEDINGS BOOK*, 825.

Yebra, D. M., Kiil, S., & Dam-Johansen, K. (2004). Antifouling technology—past, present and future steps towards efficient and environmentally friendly antifouling coatings. *Progress in organic coatings, 50*(2), 75-104.

Yebra, D. M., Kiil, S., Weinell, C. E., & Dam-Johansen, K. (2006). Effects of marine microbial biofilms on the biocide release rate from antifouling paints—A model-based analysis. *Progress in organic coatings, 57*(1), 56-66.

Zhang, X., & Singhasemanon, N. (2014). Sacramento, California 95812.

Zhou, F. (2014). *Antifouling Surfaces and Materials: from land to marine environment*: Springer.

Zobell, C. E., & Allen, E. C. (1935). The significance of marine bacteria in the fouling of submerged surfaces. *Journal of bacteriology, 29*(3), 239-251.

Chapter 13

PERFORMING AN EXAMPLE FORKLIFT DESIGN AND A SIMULATION WITH PID CONTROLLER

Çağatay ERSİN[1*]
Ali ÖZ[2]

1 * Çankırı Karatekin Üniversitesi, Meslek Yüksekokulu, Elektronik ve Otomasyon Bölümü, Çankırı, Türkiye. cagatayersin@karatekin.edu.tr ORCID ID: 0000-0001-5018-9313
2 Mehmet Akif Ersoy Üniversitesi, Teknik Bilimler Meslek Yüksekokulu, Motorlu Araçlar Ve Ulaştırma Teknolojileri Bölümü, Burdur, Türkiye. alioz@mehmetakif.edu.tr ORCID ID: 0000-0002-0814-4020

INTRODUCTİON

Active use of warehouses in enterprises; It is important to keep the raw material stocks adequately before the production of the product and to keep the product from the production stage until the distribution stage. Forklifts are frequently used in warehouses to lift the weights that are not sufficient for human power and to use the shelves at a height that people cannot reach. The storage method has an important role in procurement processes. In this respect, the selection of forklifts used in warehouses is important in terms of cost, ensuring the continuity of the work, occupational safety, and efficient use of the working area (Sarıçalı, Kundakçı, 2017). A conventional forklift requires a large amount of space during manoeuvring. This causes a decrease in the area used for stacking and a loss of efficiency. The multi-directional forklift is designed for more efficient use of areas in businesses (China, 2015). forklifts; They are dangerous vehicles because they have a high mass, are of solid and durable construction, and often operate close to pedestrians. In addition, loads are usually carried by simply being supported on the forks (ie not directly fixed on the vehicle) (Aslan, 2018). In recent years, the use of forklifts has started to increase in many industrial business and transportation operations. Forklifts have become the main vehicle used in material handling, as well as being a flexible transport vehicle that can perform many tasks. In our country, forklift production about stacking machines dates back to the 1970s. Today, an average of 10 thousand construction equipment and 10 thousand forklifts are produced and offered for sale every year (Eren, 2015). The material used in the creation of the forklift and the control algorithm of the forklift's carrying end come to the fore in product transportation. The structure of the material created also plays an important role in determining and estimating the service life of materials (Karhan, Çakır, Arslan, 2021). Designing and controlling technological systems is essential for these systems to work in a balanced way (Ersin, Yaz, Karhan, 2019). The analysis and design of the controller/controller circuits that enable the systems to operate in the desired properties are among the main areas of control theory. In this area, controllers with different structures and characteristics have been developed. One of them is the most widely used basic PID (proportional-integral-derivative) controller structure for industrial purposes. This type of controller, which provides the control of the systems by taking the ratio-integral-derivative values of the input and/or their combinations, are generally used as P, PI, PD and PID. The parameters of PID controllers can be obtained both experimentally and analytically. In addition, the design stages do not include many processes. Therefore, they are widely used in industrial applications (Vatansever, Deniz, 2013). PID controller is also known as the proportional-integral-derivative controller. The PID control

provides the control using e(t)=r(t)-y(t) the error between the reference signal r(t) and the output value y(t). The output u(t) of the PID control is the sum of the error multiplied by the proportional coefficient, its integral and its derivative. (Üstüner, Taşkın, 2015). The block diagram of the PID controller is shown in figure 1.

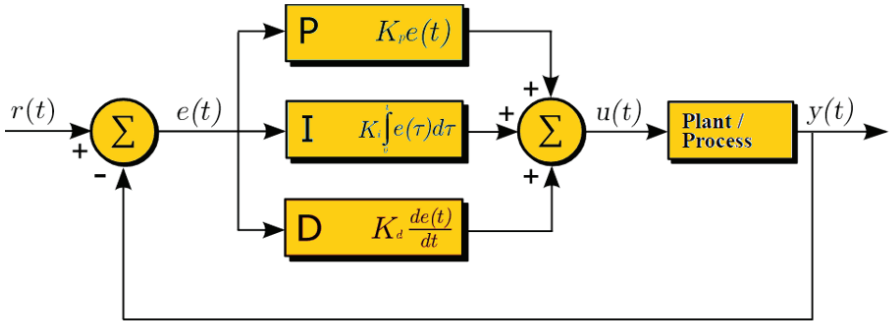

Figure 1. *PID controller block diagram*

PID is a control feedback mechanism. This mechanism is a method that uses the amount of error, the rate of change in the error and the cumulative error made to bring the error of the system relative to the reference signal closer to zero. Certain coefficients are used to control the effect of these values. PID controllers consist of three terms as Proportional, Sum and Derivative (Arıkan, etc, 2019). In a system design and control algorithm implementation, simulation must be performed first. The simulation is done to see the operating characteristics of the system before real-time operation. For this, before performing stable simulation, the behaviour of the system under operating conditions should be examined and appropriate data should comply with a certain rule (Çakır, Karhan, 2020). In this study, the material handling control of the forklift was carried out in the simulation environment. Before performing the simulation, a detailed literature review about the forklift was made and a real forklift was examined.

1. MATERIALS AND METHOD

1.1. System Design

Forklift use has continued to increase in many industrial and transportation operations in recent years. Today, forklifts have become an essential device for material handling as well as a flexible means of transport for a multitude of tasks. Forklifts provide many benefits in the industry, such as increasing efficiency or reducing manual handling (Horberry, etc., 2004). In this study, material handling control of forklifts was carried out.

Forklifts were examined and designed in SolidWorks 3D CAD software. The transport end view of the forklift designed in SolidWorks software is shown in figure 2.

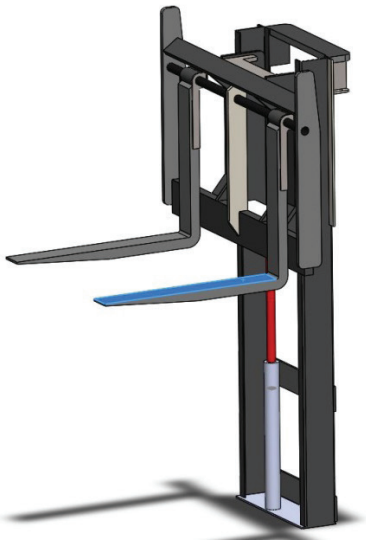

Figure 2: *Transport end view of the designed forklift*

Forklifts are used in the industry for material handling. A linear motor has been added to the system for material handling of the forklift designed in the SolidWorks program. The system provides the material to be transported upwards with the linear motor. The designed forklift tip was meshed with the "Simscape Multibody" extension added to the SolidWorks CAD program and transferred to Simulink software. The block diagram of the forklift tip designed in Simulink software is drawn.

1.2. Simulation of the System

Continuous control types are P-controller, I-controller, D-controller, and a few of these controls come together to form PI-controller, PD-controller and PID-controller control bodies. The PID control method includes three separate parameters. P (proportional), I (integral) and D (derivative) parameters are available. A PID controller compares the input (reference) signal with the feedback from the output and an error occurs due to the difference. According to this error, the PID controller makes an effect by trying to minimize the error and sends it to the output. In this way, errors are detected by continuous feedback from output to input until the error is minimized, and the controller reduces the error by sending its effect to the output. In this study, the forklift handling end was designed and

exported to Simulink software for simulation and control in Solidworks CAD software. For the control of the exported system, the PID controller block, which is widely used in control studies today, has been added. The block diagram of the PID controller is shown in figure 3.

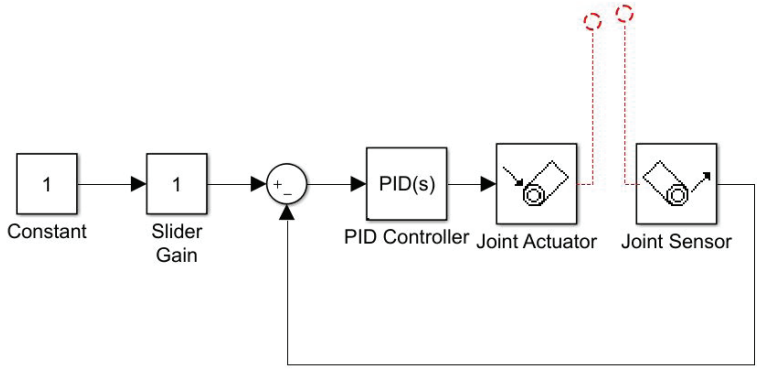

Figure 3: *PID block image added to the simulation*

The system with the PID block prepared is added to the prismatic block of the exported system, where the linear motor is, and feedback is obtained. Thanks to the PID block, mobility and control of these movements are provided to the system. When Prismatic blocks are exported, input will be output as in figure 4. To control the block, the number of inputs and outputs of the prismatic blocks in the system has been increased to 2 and PID control blocks have been connected here. The Simulink model of the system whose PID control blocks are connected is shown in figure 4.

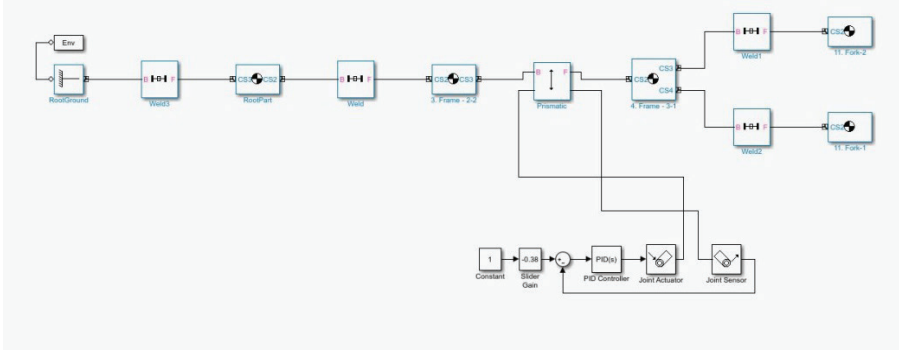

Figure 4: *Image of the system with the PID block added*

The P, I, D and N values of the PID controller under the control of the prismatic block of the exported system are set graphically. The graph that emerged in the formation of these values is shown in figure 5.

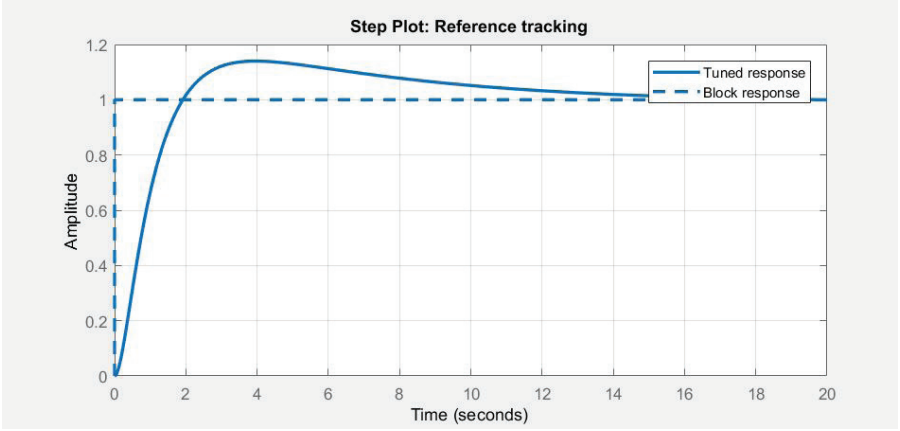

Şekil 5: *PID değerlerinin grafiksel görüntüsü*

The simulation image of the system, whose design, simulation and PID values are entered, is shown in Figure 6.

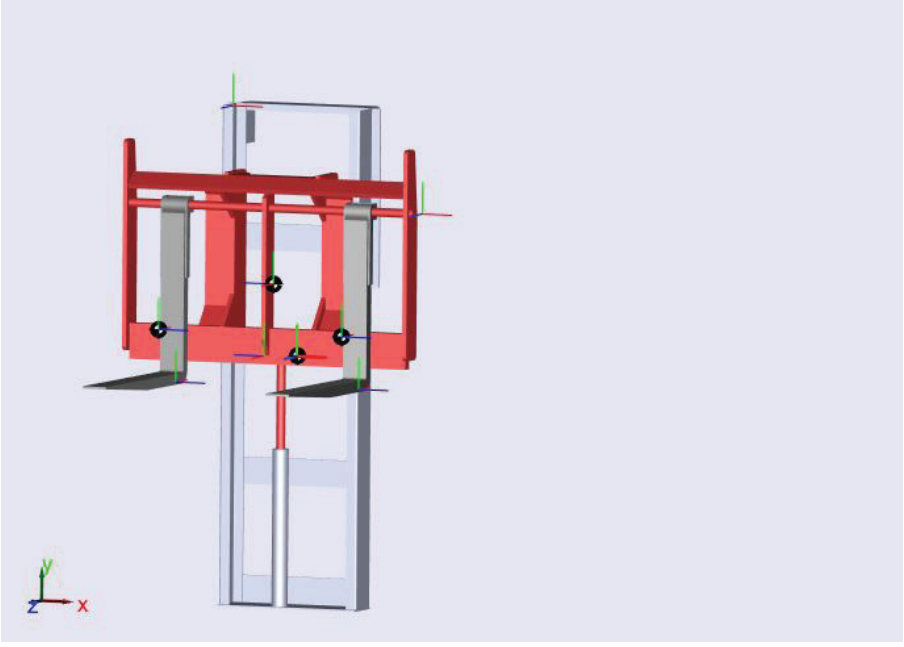

Şekil 6: *Simülasyonu gerçekleştirilen sistemin görüntüsü*

In this study, the system was controlled with a PID controller for the forklift tip to work stably without shaking the material. The constant block in the PID block added to the Simulink model is used to assign a constant value and to extract a matrix with the same dimensions as the constant value. The 'sum' block is preferred for the system to provide feedback. The PID block is connected to the prismatic block, which is the export state of the linear moving forklift tip. For PID control, P-value, I value and D value is entered in the PID block of the prismatic block. For the PID control block, the response time of the system and the reference tracks are set on the graphic and the values of the PID control unit are assigned according to this reference graphic. System feedback and PID control 'joint actuator' and 'joint sensor' have been added. The joint actuator is used to drive torque or linear/angular position, velocity and acceleration motion signals. The base follower array and joint axis determine the sign of forwarding movement. The 'joint sensor' also measures the linear/angular position, speed, acceleration, calculated force/torque and reaction force, the torque of the system. The base follower array and joint axis determine the sign of forwarding motion. The outputs in the system are Simulink signals. It can combine multiple output signals into a single signal.

The 'slider gain' block, which is in the system and used by fixing the motion control with certain angle values, has been added to the prismatic block. After the simulation of the system, the error values were taken to the optimum level with the PID control and the movements were provided by entering the gain values with the slider gain.

RESULT

Due to the increasing population and material requirements, the use of forklifts has become widespread. When transporting materials with forklifts, control of the forklift end is necessary. In this study, the forklift handling end was designed in Solidwork CAD software and this design was controlled with a PID controller. Stable movement of forklift load-carrying end with minimum vibration has been carried out. The simulation of the designed system is provided with a PID controller. PID control and feedback blocks for vertical movement were added to the prismatic block of the system whose block diagram was drawn in Simulink software. P-value entered in Simulink program for stable operation of the system: 1.71e+17

I value: 98.02e+23

D value: 8987800561.44

Filter Coefficient: 545397025.42.

It has been observed that the system works stably in the simulation with these values.

REFERENCES

Arıkan, A., Kayaduman, A., Polat, S., Şimşek, Y., Dikmen, İ. C., Gökhan, H.,. & Abbasov, T. Otonom Araçlar İçin Kontrol Yöntemi Simülasyonu Ve Uygulaması Control Method Simulation And Application For Autonomous Vehicles.

Aslan, A. (2018). Forklift Kazalarını Önlemek İçin Bir Risk Algılama Sistemi Tasarımı Ve Bir Uygulama (Master's Thesis, Fen Bilimleri Enstitüsü).

Çakır M. F. Ve Karhan M.,(2020). "Ndfeb Mıknatısların Üretimine Yönelik Sanal Platform Modeli", Politeknik Dergisi, 23(3): 763-770.

Çin, E. (2015). Çok Yönlü Hareket Edebilen Forklift Prototipi İmalatı (Master's Thesis, Hitit Üniversitesi Fen Bilimleri Enstitüsü).

Erel, F., (2015) Forkliftlerle Güvenli Çalışma, İş Sağlığı Ve Güvenliği Uzmanlık Tez, Ankara.

Ersin, Ç., Mustafa, Y. A. Z., & Karhan, M. Savunma Sanayi İçin Örnek Bir Iot Uygulaması. Electronic Letters On Science And Engineering, 15(3), 66-73.

Horberry, T., Larsson, T. J., Johnston, I., & Lambert, J. (2004). Forklift Safety, Traffic Engineering And İntelligent Transport Systems: A Case Study. Applied Ergonomics, 35(6), 575-581.

Karhan, M., Çakır, M. F., & Arslan, Ö. (2021). Investigation Of The Effect Of Roughness Value On The Wettability Behavior Under Electric Field İn Xlpe Materials Used İn Medium And High Voltage Applications. Electrical Engineering, 1-14.

Sarıçalı, G., & Kundakcı, N. (2017). Forklift Alternatiflerinin Kemıra-M Yöntemi İle Değerlendirilmesi. Optimum Ekonomi Ve Yönetim Bilimleri Dergisi, 4(1), 35-53.

Üstüner, M. A., & Taşkın, S. Bir Süreç Kontrol Sisteminde Bulanık-PID Ayarı İle Etkileşimin Yok Edilmesi Decoupling İn A Process Control Systems With Fuzzy-Pıd Tuning.

Vatansever, F., & Deniz, S. (2013). Genetik Algoritma Tabanlı PID Kontrolör Simülatörü Tasarımı. Uludağ University Journal Of The Faculty Of Engineering, 18(2), 7-18.

Chapter 14

KONYA BICYCLE ROUTES IMPROVEMENT STUDIES AND EVALUATION OF BICYCLE ROADS WITH GEOGRAPHICAL INFORMATION SYSTEM (GIS) TECHNOLOGY

Hatice Canan GUNGOR[1]

1 Necmettin Erbakan Üniversitesi, Meram Meslek Yüksekokulu, Mülkiyet Koruma ve Güvenlik Bölümü, Türkiye, Konya. cgungor@erbakan.edu.tr ORCID: https://orcid.org/0000-0002-5563-9552

1. Introduction

The city of Konya is one of the cities where bicycle use is most common in our country. Another issue as important as widespread use is that the people of Konya primarily use bicycles as a means of transportation. Despite the development of public transportation opportunities, it is observed that a significant number of bicycle users prefer bicycles to reach different parts of the city. Sustainable bicycle path studies aiming to increase the use of bicycle as a means of transportation in Konya continue under the leadership of Konya Metropolitan Municipality (KMM).

In order to provide a sustainable and uninterrupted bicycle path transportation, Konya bicycle paths have been examined. However, it has been observed as a result of various field studies that there are some deficiencies.. Some of the bicycle path design criteria has been classified and analysed. Geographical Information Systems (GIS) may provide an improvement in the redesigned of the route studies. At the same time, future bicycle path routes can be proposed with GIS.

In this study, 550 questionnaires regarding the existence and use of existing bicycle paths on the public were targeted. The new bicycle path targets will be determined with the evaluation that will emerge as a result of the survey analysis and the city's suitable routes. It is thought that the study will contribute to both the city of Konya and public health in terms of sports transportation.

It is useful to underline that bicycle transportation, which has led to the differences in the usual transportation preferences, especially with the 2019 covid-19 pandemic, is on the agenda nowadays.

Today, it is a known fact that individual transportation needs and public transportation needs are mostly provided by motor vehicles. However, over time, due to the main reasons such as the stress of city life, noise and air pollution, it has been observed that some changes have occurred in the transportation needs of city residents in many developed and developing cities of the world. In order to meet this need, people have started to turn to transportation vehicles that are healthier, noiseless and have minimal damage to the environment. At this point, we come across the concept of bicycle, an ancient means of transportation whose first invention dates back to 1645 (Suher, 1996).

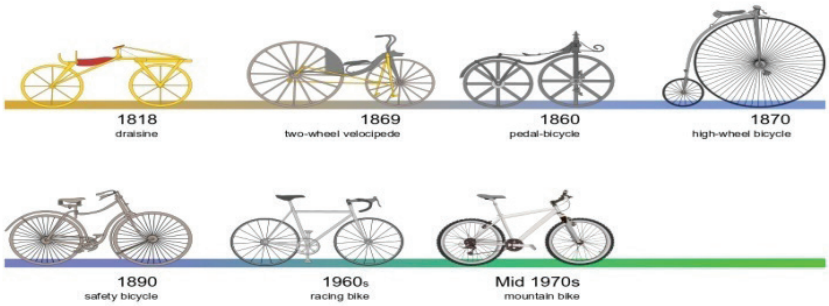

Figure 1.1 The development process of the bicycle (Url-1)

Cycling as an individual means of transport; It is a means of transportation that provides its movement and balance on two wheels, is based on mechanical power and moves with the pedaling of this power (Küçükpehlivan ve Doğru, 2017).

Konya is one of the cities where bicycle use is most common in our country. When Konya bicycle paths are examined in order to ensure a sustainable and uninterrupted bicycle path transportation, it is inevitable to improve the studies with Geographic Information System (GIS) technology. GIS processes the data in a short time in spatial studies and brings the authorities to the right conclusion. In this study, 550 surveys were conducted on the existence and use of existing bicycle paths among the public. As a result of the survey analysis, suitable routes of the city and new bike path targets were determined. It was underlined that bicycle transportation, which is the prominent difference in conventional transportation preferences, especially with the 2019 Covid-19 pandemic, is on the agenda today.

1.1 Cycling Road in Konya

Sustainable bicycle path studies aiming to increase the use of bicycles as a means of transportation in Konya continue under the leadership of KMM. The amount of bicycle paths, which have been under construction since 2005, according to years are given in Table 1.1 and their graphical distribution is given in Figure 1.2.

According to the data shared by Konya Metropolitan Municipality(KMM), the amount of bicycle paths built by the end of 2016 reached 350 km. There are bicycle paths in the three central districts of the city, Selçuklu, Meram and Karatay. However, as of 2014, bicycle path works continue in districts such as Çumra, Seydişehir and Beyşehir, which are connected to the center by the Metropolitan law. (Konya Homepage, 2018).

Table 1.1 *The amount of bicycle paths built by years (KMM, 2016)*

2005	2006	2007	2008	2009	2010	2011	2012	2013	2014	2015	2016
12 km	20km	27 km	25 km	14 km	19,5 km	28,5 km	49 km	45 km	40 km	40 km	30 km

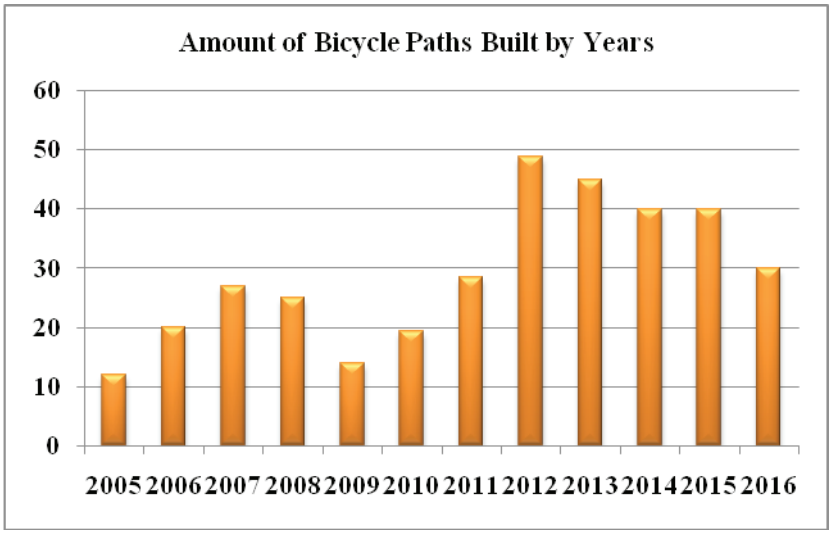

Figure 1.2 Graphical distribution of bicycle paths by years (KMM, 2016)

2. The Concept of Sustainability and Konya Cycling Road Route Improvement Studies

The concept of sustainability brings with it an understanding of urbanism. Therefore, it is important to consider the concept of sustainability when making transportation decisions in city planning (Beatley, 2000). The construction of bicycle lanes, encouraging their use and making them a part of uninterrupted transportation is necessary in terms of sustainability, especially in the province of Konya, generally in our country. When Konya bicycle paths are examined in order to provide a sustainable and uninterrupted bicycle path transportation, it has been observed as a result of various field researches that there are some deficiencies that need to be eliminated despite many useful studies.

It is worth noting that for sustainable transportation to be successful, it must be examined in terms of environmental, social and economic aspects.

3. Material Methods

Bicycle path design criteria are classified as road width, longitudinal

slope, design speed, visibility distance, horizontal curve value, vegetation, barrier effect, continuity and safety.(Köseoğlu ve Guler, 2017)

Road widths are recommended as a minimum of 1.50 meters and a maximum of 2.40 meters in one direction. The longitudinal slope is between 5% and 11% in the short distance and 005% in the long distance. Design speed should be between 30 and 50 km/h. Visibility is variable. (Pinici, 2019)

3.1 Konya Selcuklu Bicycle Road – School Route Connection Improvement Work

With reference to the sustainability principle and the specified design principles, the continuous bicycle paths along the Istanbul Road and Beyşehir Road in Konya Province Selcuklu District were discussed and it was researched how various public and private schools on these bicycle paths could be connected to the existing bicycle path and suggestions were presented. The main reason why schools are preferred is the widespread use of bicycles among students. Many bicycle routes have been examined in Selçuklu and examples were presented below.

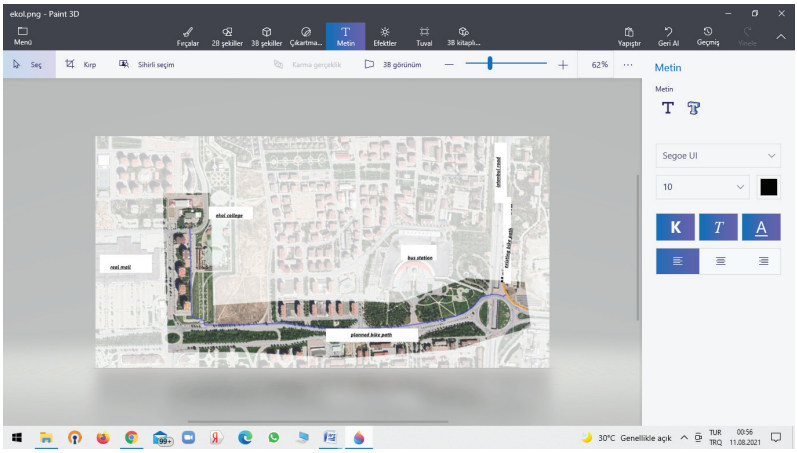

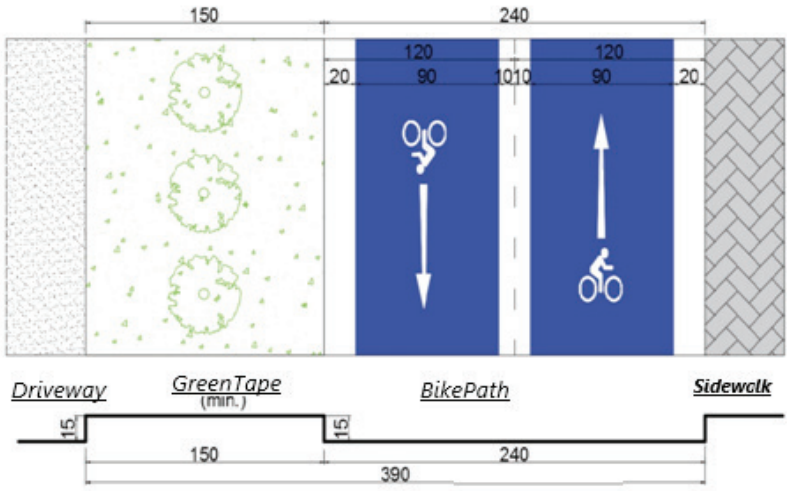

Figure 3.1 *The proposed bike path line between Ekol College and Yeni Istanbul*

Street

(Bicycle path plan proposed between Ekol College and Yeni Istanbul Street

(Environment and Urban Ministry, 2017)

The bicycle path that will connect Ekol college, Real AVM, Ecdad Park and residences with high numbers of cyclists to Yeni Istanbul Street should be planned at the pavement level, in two dir1ctions and with a width of 2.40 m. The proposed bike path lane for the planned line is shown in Figure 2.1 in the plan view. According to the state of the road lane in planning, the green band can be drawn up to 1m.

In addition, the bicycle path connection to be made between Türmak High School and Istanbul Road and also between Cumhuriyet Mahallesi Schools District - New Istanbul Street Connection has been examined and alternative routes have been suggested.

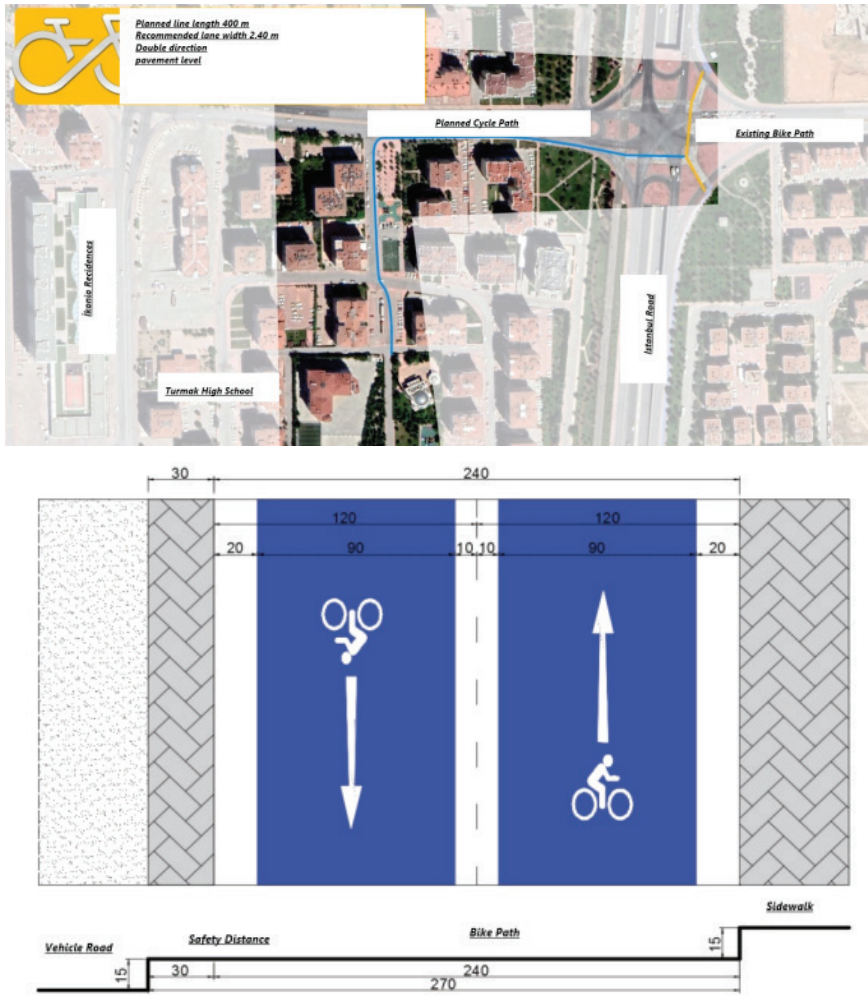

Figure 3.2 Türmak High School – Yeni Istanbul Street Connection

Thanks to the bicycle path connection to be made between Türmak High School and Istanbul Road, the discontinuity between many residences on and around the road and the main bicycle path will be eliminated.

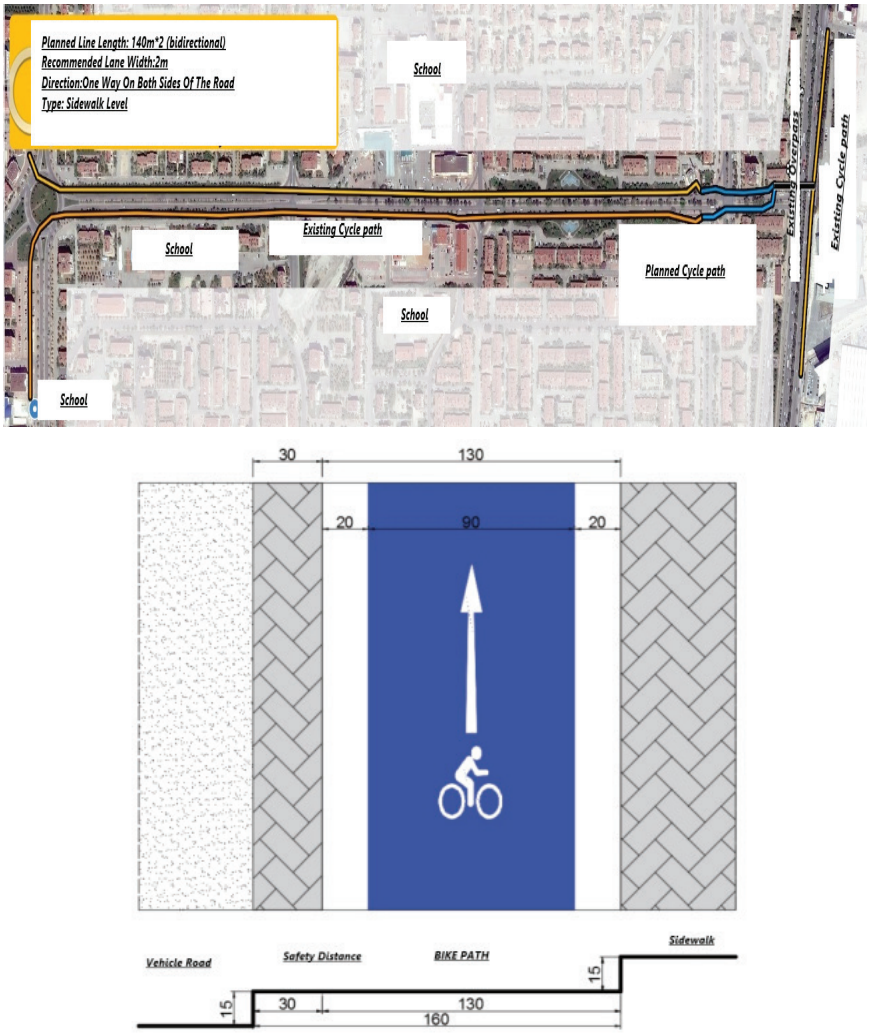

Figure 3.3 *Cumhuriyet Mahallesi Schools District – New Istanbul Street Connection*

(Environment and Urban Ministry, 2017)

There are over ten schools together with the schools in the neighborhood, 4 of which are on the side of the street. In addition, it is seen that there are many shopping centers and residential buildings on Eyüp Sultan Street. In addition, it is seen that there is a serious demand for bicycle travel from Cumhuriyet Mahallesi to the Sanayi side of Yeni Istanbul Street. Continuing the bicycle path from Eyüp Sultan Street on both sides of the road to Yeni Istanbul Street in the same way stands out as the most practical and easy solution.

4. Selcuklu District Cycling Road Survey and Evaluation

"We asked 550 people" survey conducted on different ages and working groups A survey was conducted on 550 different people for Konya Province. In the survey, in which the majority (422 people) were students, adults (128 people) participated in the survey at a certain rate. The survey consists of 13 questions in total. The main purpose of the survey was to get an idea about the view of the bicycle path in Selçuklu District, where the rate of bicycle use and the length of bicycle paths are the highest. In this way, it was revealed what efficiency could not be obtained from the studies on the bicycle path network, and it was possible to see the deficiencies, if any, according to the survey data obtained.

With reference to the sustainability principle and design principles, the bicycle paths between Konya Province Selçuklu District Istanbul Road and Beyşehir Road were discussed, and it was researched how various public and private schools on these bicycle paths could be connected to the existing bicycle path and suggestions were presented. The questionnaire consisting of 13 questions was asked to 550 people.

1. In which district of Konya do you live? A-Selçuklu B- Meram C- Karatay D- Other Districts

2. How often do you use the bicycle as a means of transportation? A- I do not prefer B- Occasionally C- Frequently

3. Do you prefer existing bike paths when cycling? A- Occasionally B- I don't prefer C- Frequently

4. Are there bicycle parking areas in your city? A-Yes B- No C- Insufficient

5. To what extent would the more widespread use of bicycle lanes affect your frequency of cycling as a means of transportation? A- Does not affect B- Effects

6. Are there blue bike lanes in your city? If yes, what do you think about these roads? A- Its current state should be preserved B- It should be improved C- It should be removed

7. What do you think about the relationship of existing bicycle lanes with vehicular traffic, roads/pedestrian traffic and roads? If you have any suggestions or complaints, write them in question 13. A- The bike path must be close to both roads B- the path must be far from both roads C- It doesn't matter

8. Do you think that the police/police control is sufficient for the inspection of bicycle paths? A- Insufficient B- Medium C- Sufficient

9. What are your thoughts on direction and information signs/signs on bicycle paths? A-Increased B-Insufficient C-Sufficient

10. Are the bike paths wide enough? A-Insufficient B- moderate C-Sufficient

11. Please indicate which of the following bicycle routes is more suitable for you A- Routes passing through green areas B- Routes parallel to the existing vehicular traffic C- Routes passing through the existing pedestrian traffic

12. Would you like a safe connection road between the bicycle path and schools/bus, tram stops? A- No B-Yes

13. In the last part of the questionnaire, people were given the opportunity to write their thoughts, criticisms and suggestions, if any.

Table4. Survey Results

	A(%)	B(%)	C(%)	D(%)
1.	51,91	25,96	18,98	3,14
2.	35	46,07	18,85	
3.		14,59	60,14	
4.		19,44	57,62	
5.		75,92		
6.		81,34	0,53	
7.		55,95	21,31	
8.		19,26	6,54	
9.		32,04	15,92	
10.		54,08	24,47	
11.	51	39,53	9,31	
12.		91,83		
13.		FREE		

51.92% of the survey participants stated that they reside in Selçuklu District. While the rate of participants residing in Meram was 25.96%, the number of participants from Karatay was determined as 18.99%. The rate of participants living in rural areas remained at the rate of 3.14% (Bicycle road works continue in Çumra, Seydişehir and Ereğli districts).

While the rate of those who frequently use the bicycle as a means of transportation remained at 18.85%, the rate of those who did not prefer it

was determined as 35.08%. As a result of the survey, it was determined that 46.07% of the people use the bicycle occasionally. These data show that the majority of people are inclined to use the bicycle as a leisure and hobby in their spare time of life. The rate of people using bicycles as a means of transportation to use existing bicycle paths was recorded as 60.14%. It is seen that 25.27% of them prefer bicycle paths from time to time. The rate of those who did not prefer the bike paths while cycling was determined as 14.59%. It is not possible to attribute the reasons for these rates to a single cause. However, when the comments in the survey are taken into account, the issue that people generally complain about is that pedestrians use the existing bicycle paths for walking more than people who use bicycles as a means of transportation, and that people with vehicles use them for parking. Are there bicycle parking areas in your city? More than half of the respondents (57.62%) answered the survey question that there is more parking space, but insufficient. To what extent would the more widespread use of bicycle lanes affect how often you use the bicycle as a means of transportation? The rate of those who answered "positive increase" to the survey question was determined as 75.92%. 24.08% of the segment said, "It does not affect. There would be no change." It is seen that they replied. In the answers given to the last question of the survey, it was noted that 91.83% of the majority of the people supported the construction of a safe connection road between school - bus & tram lines.

5. Conclusion

In this study, firstly, the concepts of bicycle and bicycle path were tried to be explained. In the continuation of the study, the bicycle path data of Konya Metropolitan Municipality are given on the basis of kilometers by years and general information about the bicycle path, bicycle park and bicycle overpass works of the municipality are given.

Within the framework of the sustainability principle, determinations were made on some pilot areas, connection routes were shown and proposed bicycle path plans compatible with the existing road/pavement axes were presented in order to rehabilitate the bicycle paths and use them more effectively.

An attempt was made to measure the heart rate of the city's residents with a general state-of-the-art survey on bicycle lanes. Thus, it was possible to obtain statistical data that will shed light on the impact of the services provided and the studies to be carried out.

As a result of the survey, it was concluded that some additional measures should be taken in order to ensure the continuity of the roads, vehicle-pedestrian occupations and road safety, together with the satisfaction of the bicycle paths.

The bicycle, which has become a necessity with the Covid 19 pandemic, has been accepted in many developed countries as a means of transportation. Considering the inactivity of people, which has been created with mechanization in our age, the bicycle provides both the movement for a healthy life and the social distance in the epidemic period and most importantly, the environmental pollution.

References

Beatley, T. (2000). Green Urbanism: Learning from the European Cities (Washington, DC: Island).

KMM. (2016). Konya Metropolitan Municipality in-house evaluation presentation.

Köseoğlu, Z. T., & Güler, H. (2017, September). Determination of Bicycle Routes and Capacity Analysis. In 5th International Symposium on Innovative Technologies in Engineering and Science 29-30 September 2017 (ISITES2017 Baku-Azerbaijan).

Kuyumcu, Y. (2017). Bicycle as a Means of Transportation and Bicycle Path Proposal for Urban Transportation in Çorum, Master Thesis, Bahçeşehir University.

KÜÇÜKPEHLİVAN, G., & Doğru, A. Ö. (2017). User-Focused Determination of Bicycle Path Routes with AHY. Map Magazine, 157, 1-8.

MoEU., 2017., (Ministry of Environment and Urbanization), Urban Bicycle Routes Guide.

Pinici, F. (2019). *Eskişehir bisiklet yollarının analizi ve planlanması* (Master's thesis, Sakarya Üniversitesi).

Suher, H.(1996). Urbanism, Istanbul: Istanbul Technical University Faculty of Architecture Publications.

Konya Homepage, *http://www.konya.bel.tr/haberayrinti.php?haberID=6197*, last accessed 2019/11/07.

Url1. https://upload.wikimedia.org/wikipedia/commons/a/af/Bicycle_evolution-tr.svg last accessed 2021/11/07